Novel transient flow methods for the investigation of chemical reactions

Linden Robert McCabe Schrecker

Supervisors: Prof. King Kuok (Mimi) Hii and Prof. Klaus Hellgardt

Imperial College London
Department of Chemistry, Department of Chemical Engineering

PhD Thesis
2023

Statement of originality

I declare that the work enclosed in this thesis is wholly my own work. All information derived from the work of others, published or unpublished, has been cited accordingly and can be found in the reference section.

Linden Schrecker

November 2023

Copyright Declaration

The copyright of this thesis rests with the author. Unless otherwise indicated, its contents are licensed under a Creative Commons Attribution-Non Commercial 4.0 International Licence (CC BY-NC).

Under this licence, you may copy and redistribute the material in any medium or format. You may also create and distribute modified versions of the work. This is on the condition that: you credit the author and do not use it, or any derivative works, for a commercial purpose.

When reusing or sharing this work, ensure you make the licence terms clear to others by naming the licence and linking to the licence text. Where a work has been adapted, you should indicate that the work has been changed and describe those changes.

Please seek permission from the copyright holder for uses of this work that are not included in this licence or permitted under UK Copyright Law.

Acknowledgements

The most important acknowledgement of my PhD is to my primary supervisor Mimi Hii. Her unflappable belief, encouragement, useful advice both in chemistry and beyond, openness to new ideas, and “no bs” frankness were central to my growth into the researcher I am and the enjoyment I had in my PhD. I can’t thank her enough.

I would also like to wholeheartedly thank my other supervisors, both academic and industrial Klaus Hellgardt, Philipp Staehle, Marcel Vranceanu, and Andy Wieja for opening my eyes to the wonders of chemical engineering and automation, and for putting up with my chemist’s brain in the early stages. For this I am very thankful, and without which my science would be unrecognisable. I must also thank many others at BASF who made these four years as good as they were, especially to Christian Holtze for his constant encouragement and unrelenting enthusiasm, and to Joachim Dickhaut to whom I feel as familial as if my adopted German sister really were my sister. Thanks also to Robin Attrill, who I can always rely on for a friendly pair of eyes for proofing anything and a good conversation.

I would be amiss not to thank members of ROAR both past and present: Ben Deadman, Paola Ferrini, Elenita Sanna, and Chris ‘Big Fridge’ Roberts. You all made lab life enjoyable and taught me many valuable things. Similarly, I must thank all the members of the KKH group, especially Matt my BASF brother-in-arms, Mel for constant coffee breaks, Oliver for paving the way in the KKH group, and Marvin Alberts and Daniel Dalland for putting up with my teaching and teaching me things. Also thanks to Pete and Stuart in NMR for their support. Beyond the lab, thanks to Aatikah, Bel, Hannah, Josh, Molly, and Sean for all the fun, and many other friends on the CDT, in Imperial, in music, and beyond.

My final thanks to my parents, Honey and David, my brother Rowan, and Aria for everything you have all given me. Life would not be the same without you all.

Abstract

Reaction data is important to collect not only for theoretically understanding chemistry better, but also for mass producing chemicals for medicine, agriculture, and society in general. The development of transient flow adds an efficient tool by which reactions can be studied.

In this thesis, the first comprehensive review of transient flow has been compiled, a foundational step in the establishment of any field. This review reveals the growth of the field over the past 12 years, although also shed light on areas in which further development is needed. Transient flow methods for collection of time series data are the most ubiquitous techniques, however justification of which method to use to collect such data is scarce. A comparison of different cumulative flow rate step and ramp methods on three reactions demonstrates the 'reverse push-out' step method as an accurate method, easy to implement by those inexperienced in flow chemistry.

Focus was then placed on developing novel transient flow methods in the investigation of the kinetics of the Knorr pyrazole synthesis. A novel reactant stoichiometry ramp and a related multivariate ramp were developed and utilised in this investigation. A microkinetic model was constructed for the reaction revealing unusual complex kinetic pathways, unlike previously simple proposed pathways.

Transient flow methods for the investigation of traditionally discrete reaction parameters were developed to further the efficiency of diverse data collection. The aromatic Claisen rearrangement was investigated to better understand the effect of substituent and solvent on the rate of reaction. Novel methods were developed: a 'one-pot' method by which six substituted reactions could be investigated simultaneously; and a solvent ramping method transforming solvents from a discrete reaction parameter into continuous parameters, which could be efficiently assessed. Access to such reaction data allows robust predictive models to be constructed and fundamental chemical insights to be obtained.

Table of Contents

Table of Acronyms **10**
Chapter 1: Introduction to transient flow **13**
1 Background 14
1.1 How do we collect chemical reaction data? 14
1.1.1 Reaction data collection in batch 15
1.1.2 Reaction data collection in flow 16
1.2 What is transient flow? 17
1.3 What do we need for transient flow? 19
1.3.1 Fluid dynamics 19
1.3.2 Reaction condition control 21
1.3.3 Analytical tools 21
1.4 Types of transient flow parameter 26
2 Reaction time transience 27
2.1 Varying active reactor volume 28
2.1.1 Energy source switch on methods 28
2.1.2 Change in reactor volume methods 30
2.2 Changing cumulative flow rate 32
2.2.1 Flow rate step change methods 33
2.2.2 Flow rate ramp methods 38
2.3 Best practice 44
3 Reaction temperature transience 45
3.1 Transient temperature ramps in flow 46
3.2 Bi-variate flow rate-temperature ramps 48
3.3 Potential effect of ramp direction 51
4 Other transient parameters 51
5 Conclusions 56
6 Aim and objectives 58
Chapter 2: Comparison of time series data collection in continuous flow **60**
1 Introduction 61
1.1 Aim and objectives 61
1.2 Background 61
1.3 Mathematical deconvolution 63
1.3.1 Flow rate step changes 65
1.3.2 Linear flow rate ramps 67
2 Method 72
2.1 Example chemical reactions 72
2.1.1 Acetic anhydride hydrolysis 72

2.1.2 Knorr pyrazole synthesis 73
2.1.3 Aromatic Claisen rearrangement 73
2.2 Flow system: Configuration 1 (ReactIR) 74
2.2.1 System development and construction 74
2.2.2 ReactIR methods 75
2.2.3 Residence time distribution study 78
2.3 Flow system: Configuration 2 (on-line HPLC) 80
2.3.1 System development 80
2.3.2 On-line HPLC methods 81
3 Results and discussion 82
3.1 Acetic anhydride hydrolysis 82
3.1.1 Steady state and small step changes 83
3.1.2 Full step change comparison 84
3.1.3 Linear flow rate ramp comparisons 85
3.1.4 Error analysis 86
3.2 Knorr pyrazole synthesis 88
3.2.1 Steady state and step change comparison 88
3.2.2 Flow rate ramp comparison with previous methods 89
3.2.3 Error analysis 90
3.3 Aromatic Claisen rearrangement 93
3.3.1 Solvent expansion 93
3.3.2 Method comparison 94
4 Conclusions 97
Chapter 3: Discovery of an unexpectedly complex mechanism for the Knorr pyrazole synthesis 99
1 Introduction 100
1.1 Aim and objectives 100
1.2 The Knorr pyrazole reaction 101
1.3 Transient flow methods 103
2 Different excess residence time transience 105
2.1 Batch experimentation 105
2.2 Initial transient flow experiments 107
2.3 ‘Different excess’ experiments 108
2.4 ‘Same excess’ and ‘doping’ experiments 110
2.5 Diethyl pyrazole **3.4b** kinetic data 111
3 Reactant stoichiometry and additive transience 113
3.1 Reactant stoichiometry method 113
3.2 Multivariate residence time-reactant stoichiometry ramps 116
3.3 Additive concentration ramps 118

4 Intermediate analysis 120
4.1 Off-line HPLC-MS analysis 120
4.2 *In-situ* ^{1}H and ^{13}C NMR analysis 121
4.3 Other symmetric substrates 123
5 Microkinetic modelling 125
5.1 Reaction data used for model fitting 125
5.2 Microkinetic modelling setup 126
5.3 Iterative development of microkinetic model 127
5.4 Final microkinetic model 132
5.5 Components not included in microkinetic model 135
5.6 Comparison of microkinetic model surface to other transient reaction data 136
6 Unsymmetric methyl-ethyl diketone 138
7 Conclusions 141
Chapter 4: Investigation of traditionally discrete reaction parameters 143
1 Introduction 144
1.1 Aim and objectives 144
1.2 The aromatic Claisen rearrangement 146
1.3 One-pot methods 147
2 Substrate synthesis and HPLC method development 148
2.1 Parallel synthesis of reactants 148
2.2 HPLC method development 149
2.3 HPLC calibration methods 152
3 Individual substrate transient flow 154
3.1 Solvent expansion effects 154
3.2 Residence time ramps 155
3.3 Temperature ramps 157
4 'One-pot' transient flow 160
4.1 Residence time ramps 160
4.2 Temperature ramps 161
4.3 Mass balance 162
4.4 Hammett plots 163
5 Applications: thermodynamics and predictive model 166
5.1 Thermodynamics 166
5.2 Predictive model 169
5.3 Test substrates 171
5.4 *para*-Bromine side reaction 173
6 Solvent ramping 175
6.1 Premise 175

6.2 Reaction in DMF 177
6.3 Solvent ramps 178
6.4 Initial analysis 185
6.5 Ethanol-water ramp and deuterated ramp 187
6.6 'One-pot' solvent ramp 189
7 Conclusions 192
Chapter 5: Conclusions and future work 194
Chapter 6: Experimental 199
1 Introduction 200
2 Comparison of time series data collection in continuous flow 200
2.1 Flow system configuration 1 200
2.1.1 Flow system overview 200
2.1.2 Pumps 201
2.1.3 Tubing and fittings 202
2.1.4 Heating and cooling 202
2.1.5 *In-line* FTIR 203
2.1.6 System pressure 203
2.2 Flow system configuration 2 204
2.2.1 Flow system overview 204
2.2.2 Heating and cooling 205
2.2.3 On-line HPLC 205
2.2.4 On-line HPLC method for aromatic Claisen rearrangement of **2.6/4.1a** 205
2.3 Standard transient residence time experiments 207
2.3.1 Reverse Push Out step change (RPO step) 207
2.3.2 Push Out step change (PO step) 207
2.3.3 Linear Reverse Push Out flow rate ramp (RPO ramp) 208
2.3.4 Linear Push Out flow rate ramp (PO ramp) 209
2.4 Compound synthesises and characterisation 209
3 Discovery of an unexpectedly complex mechanism for the Knorr pyrazole synthesis 210
3.1 General compound synthesis and characterisation 210
3.1.1 3,5-dimethyl-1-phenyl-*1H*-pyrazole (**2.5/3.4a**) 210
3.1.2 3,5-diethyl-1-phenyl-*1H*-pyrazole (**3.4b**) 211
3.1.3 2,8-dimethylnonane-4,6-dione (**3.1d**) 211
3.1.4 Regioisomeric mixture of 5-ethyl-3-methyl-1-phenyl-*1H*-pyrazole (**3.4f**) and 5-methyl-3-ethyl-1-phenyl-*1H*-pyrazole (**3.4f'**) 213
3.2 Flow experiments 215
3.2.1 General flow experiment setup 215
3.2.2 Standard transient residence time ramp experiment (General Method A) 215
3.2.3 Standard transient reactant stoichiometry ramp experiment (General Method B) 217

3.2.4 Standard transient bi-variate ramp experiment (General Method C) 218
3.2.5 Standard transient additive ramp experiment (General Method D) 219
3.3 Combined experimental runs 220
3.3.1 Experimental run 1 220
3.3.2 Experimental run 2 220
3.3.3 Experimental run 3 221
3.3.4 Experimental run 4 222
3.3.5 Experimental run 5 224
3.3.6 Experimental run 6 225
3.3.7 Experimental run 7 226
3.4 HPLC-MS methods and experiments 227
3.4.1 Initial intermediate identification method for R = Me 227
3.4.2 Method for identification of unsymmetric diketone reaction intermediates 228
3.4.3 Intermediate identification method for range of alkyl substituents 229
3.5 NMR experiments 231
3.5.1 Lack of interaction between diketone **3.1a** and pyrazole **3.4a** 231
3.5.2 Major regioisomer identification 231
3.6 MATLAB Surface plotting 233
4 Investigation of traditionally discrete reaction parameters 237
4.1 Synthesis methods and characterisation 237
4.1.1 General Methods 237
4.1.2 Synthesis of 4-methoxy phenyl ally ether (**2.6/4.1a**) 237
4.1.3 Synthesis of starting materials in medium throughput (**4.1b, 4.1c, 4.1e-h**) 238
4.1.4 Synthesis of 2-allyl-4-methoxy phenol (**2.7/4.2a**) 240
4.1.5 Synthesis of other aromatic Claisen products (**4.2b-h**) 241
4.2 On-line HPLC methods 244
4.2.1 Method 1: analysis of the reaction of **2.6/4.1a** 244
4.2.2 Method 2: analysis method for ‘one-pot’ method 244
4.2.3 Method 3: analysis method for reaction of **4.1d** for solvent ramps 246
4.3 Transient flow experimental work 247
4.3.1 Solution preparation for flow experiments 247
4.3.2 Transient temperature ramp method 248
4.4 Solvent ramping method 249
4.4.1 Solvent ramping method: single substrate 249
4.4.2 Solvent ramping method for one-pot 250
References 252

Table of Acronyms

%w/v	percentage weight by volume
$\Delta H^{\ddagger}$	enthalpy of activation
$\Delta S^{\ddagger}$	entropy of activation
A	pre-exponential factor
Ac	acetyl
APCI	atmospheric pressure chemical ionization
Ar	aryl
ATR	attenuated total reflectance
AU	absorption units
BM	Berkeley Madonna
Boc	tert-butyloxycarbonyl
BPR	back pressure regulator
Bu	butyl
CSTR	continuously stirred tank reactor
D	mass diffusion coefficient
DAD	diode array detector
DBU	1,8-diazabicyclo[5.4. 0]undec-7-ene
DCM	dichloromethane
DEPT	distortionless enhancement by polarization transfer
DFT	density functional theory
DIPEA	diisopropylethylamine
DMA	dimethyl acetamide
DMF	dimethyl formamide
DMSO	dimethyl sulfoxide
DoE	design of experiments
E	bulk modulus of elasticity
E_a	activation energy
ECD	electron capture detector
EIC	extracted ion chromatogram
ELSD	evaporative light scattering detector
EPA	Environmental Protection Agency
ES-API	electrospray-atmospheric pressure ionisation
ESI	electrospray ionisation
Et	ethyl
$E_T(30)$	Reichardt polarity metric
FID	flame ionisation detector
FTIR	Fourier transform infrared spectroscopy
GC	gas chromatography
GPC	gel permeation chromatography
GSIOC	Gilson serial input output channel
h	Planck's constant
HFIP	hexafluoro isopropanol
HPLC	high performance liquid chromatography
HRMS	high resolution mass spectrometry
HTE	high throughput experimentation
ID	internal diameter
IPA	isopropanol
IR	infrared

IS	individual substrate
k	reaction rate constant
K	equilibrium constant
k_B	Boltzmann constant
L	characteristic length
LC	liquid chromatography
LiHDMS	lithium hexamethyldisilazide
m/z	mass to charge ratio
MAE	mean absolute error
MBDoE	model based design of experiments
Me	methyl
ML	machine learning
MOCCA	multivariate online contextual chromatographic analysis
MS	mass spectrometry
MSA	methanesulfonic acid
NMP	N-methyl pyrrolidine
NMR	nuclear magnetic resonance
nOe	nuclear Overhauser effect
NSA	nitro salicylic acid
OD	outer diameter
ODE	ordinary differential equation
OP	one-pot
P	pressure
PAT	process analytical technology
Pe	Péclet number
PFR	plug flow reactor
Ph	phenyl
PID	proportional-integral-differential
PO	push-out
ppm	parts per million
ppy	2-phenylpyridine
Pr	propyl
PTFE	polytetrafluoroethylene
Q	cumulative flow rate
Q_0	initial cumulative flow rate
Q_{end}	final cumulative flow rate
R	molar gas constant
RAFT	reversible addition-fragmentation chain-transfer
REACH	Registration, Evaluation, Authorisation and Restriction of Chemicals
RI	refractive index
RMSE	root mean squared error
RPO	reverse push-out
rt	room temperature
RTD	residence time distribution
SA	salicylic acid
S_NAr	nucleophilic aromatic substitution
SS	steady state
T	temperature
TEA	triethyl amine
t_{end}	flow rate ramp end time
TF	transient flow
t_f	exit time

TFA	trifluoroacetic acid
THF	tetrahydrofuran
t_i	initial time
TIC	total ion chromatogram
TLC	thin-layer chromatography
t_m	measurement time
TMS	tetramethylsilane
TRAILS	time resolved actinometry in large systems
u	local flow velocity
UPLC	ultra performance liquid chromatography
UV/Vis	ultra-violet/visible
V	volume
V_D	dead volume
V_R	active reactor volume
VTNA	variable time normalisation analysis
β	volumetric expansion coefficient or isokinetic temperature
θ	normalised residence time
κ	transmission coefficient
ρ	flow rate ramp rate or density or Hammett plot gradient
σ	Hammett parameter
τ	residence time

Chapter 1: Introduction to transient flow

In this Chapter, first the background to transient flow as a field is discussed (Section 1) followed by a comprehensive review of transient flow methods applied to chemical reactions, until October 2023. This review begins with the use of transient flow to collect residence time data (Section 2), separated by the method by which the time-series data is generated. Research investigating the effect of reaction temperature with transient flow is then discussed (Section 3), first with temperature ramps and then more complex residence time-reaction temperature multivariate methods. The penultimate section (Section 4) covers transient flow approaches to other reaction parameters and further multivariate methods, before a summary of the research to date to identify areas where there is significant potential for further research (Section 5).

1 Background

1.1 How do we collect chemical reaction data?

In science, collection of good data underpins the development of knowledge.[1] Chemists collect data of various forms which can be categorised into data on the properties of molecules or materials (physical data) and data on chemical reactions (reaction data). For small organic molecules, physical data (such as melting point or molecular structure) is generally easier to model and collect efficiently. Reaction data, however, has generally been more challenging to record, due to its temporal, transitory nature, and less well curated due to challenges in measuring and reporting all influencing parameters, such as the room temperature, the exact experimental setup, and work-up procedure. Reaction data is collected by monitoring reaction outputs (conversion, yields, product structure, heats of reaction, *etc*.) under different reaction conditions. These reaction conditions include different parameters which affect the reaction outcome, which can be discrete (such as catalyst, base, or solvent) or continuous (such as reaction time, temperature, or concentration) parameters. Reaction data is used for a variety of applications, such as optimising reaction yields, informing reaction mechanism, and kinetic modelling (Fig. 1.1).

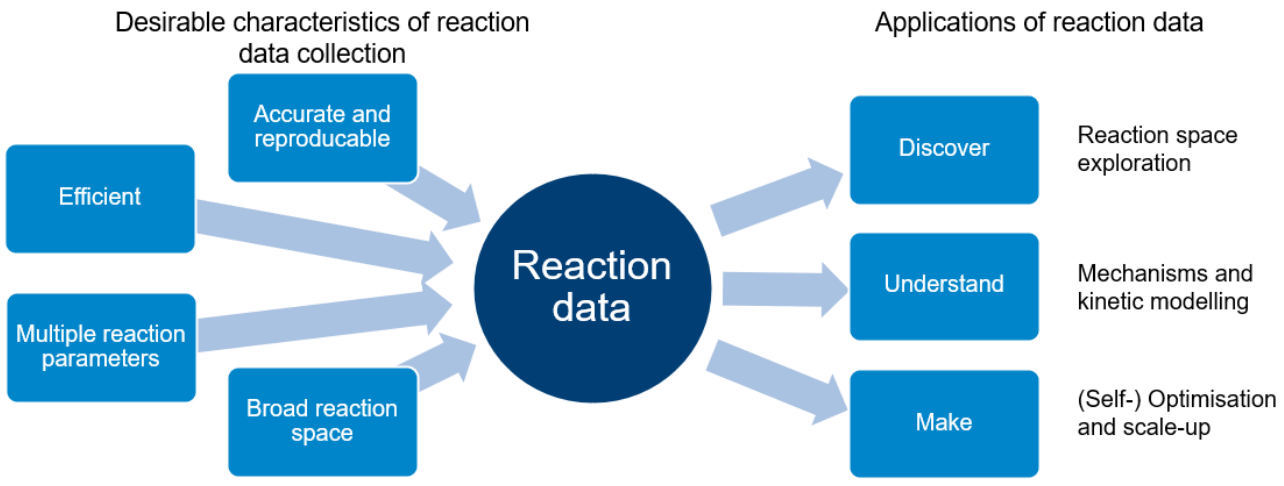


Figure 1.1. Diagrammatic view of the desired characteristics of reaction data collection and some uses of the uses of reaction data.

The different uses of reaction data have different prioritisation of requirements of the data, but the ideals of data collection remain broadly the same (Fig. 1.1). It is generally desirable to collect accurate and

reproducible reaction data efficiently while varying multiple reaction parameters (time, temperature, catalysts, *etc.*) over a broad reaction space (*e.g.* very high to low temperatures). Within synthetic organic chemical reactions, almost all reaction data collection falls short on at least one if not multiple of these ideals.

1.1.1 Reaction data collection in batch

The most ubiquitous technique for reaction data collection is by monitoring a reaction in a batch vessel. Traditionally, the reaction mixture was analysed by an *ex situ* analysis method at the end point of the reaction or by qualitative techniques from extracted reaction aliquots, such as thin-layer chromatography (TLC). Over recent decades, however, the development of user-friendly and commercially available analytical tools has facilitated analysis of multiple time points from a batch reactor during the reaction (*in situ*) and under realistic reaction conditions (*operando*), thus producing multiple quantifiable time data points per reaction. The availability of *in situ* analytical tools has allowed time-series data to be collected in a more data dense manner and with greater ease.[2] For example, implementation of *in situ* Attenuated Total Reflectance Fourier Transform Infrared Spectroscopy (ATR FTIR) allows a data point to be collected every 15 seconds with no human intervention. However, expedient collection of time-series data is no guarantee that the data is accurate or repeatable.

High throughput experimentation (HTE) allows multiple reactions to be performed in parallel, generally in a multiwell plate.[3] This method is very effective for screening categorical variables such as substrates, additives, or catalysts but is inefficient at screening continuous variables such as reaction temperature. Time-series data can be challenging to collect from multiwell plates, as extracting aliquots multiple times reduces the reaction volume and can cause solvent evaporation. The common setup of a multiwell plate also prohibits certain continuous parameters, such as temperature and pressure to be screened, requiring further reaction plates to be set up, giving no efficiency gain.

Batch experimentation can have inaccurate mixing and poor heat transfer due to the standard mixing capabilities of batch reactors and the inherent small surface area to volume ratio. Additionally, although batch vessels with *in situ* analytical tools allow time-series data to be collected, collecting diverse data on other reaction parameters such as temperature, initial concentrations, or substrate is still arduous. However, in other aspects batch has fundamental advantages such as the capability to easily handle solid forming reactions, more widely available equipment and know how, and the facile collection of kinetic time-series data.

1.1.2 Reaction data collection in flow

Flow chemistry can alleviate some of the issues with reaction data collection from batch reactors while introducing other problems (Table 1.1).[4] Generally, flow offers better initial mixing to homogenise the reaction mixture, providing more accurate reaction times, and faster heat transfer due to the increased surface area to volume ratio.[5] Flow chemistry also lends itself to more accurately and safely screening a broader reaction space such as higher temperatures through safe application of pressure and short reaction times *via* fast flow rates. Analytical tools can easily be implemented into flow systems either *ex situ* (off-line or at-line) or *in situ* (on-line or in-line) providing data on the chemical reaction performed. The good mass and heat transfer of flow systems allows this data to more easily be used to inform scale up as the fundamental kinetics of the reaction are more directly studied than in batch vessels.[6] However, there are several important limitations of flow chemistry to consider such as the difficulty in handling solids, the more specialised equipment and skill set needed to perform flow experiments, and the single point nature of traditional steady state flow chemistry data.

Table 1.1. Qualitative comparison of batch, steady state flow, and transient flow methods for data collection.

	Batch	Steady state flow	Transient flow
Accurate mixing	Poorly defined	Well defined	Well defined
Temperature control	Poor heat transfer	Fast heat transfer	Fast heat transfer
Reaction space	Limited	Larger	Larger
Solids handling	Easy	Challenging	Challenging
Initial set up	Standard	Specialised	Specialised
Experimental downtime	High	High	Low
Collection of time-series data	Easy	Slow	Easy
Collection of other variable series data	Slow or challenging[7,8]	Slow	Concentrations, temperature

1.2 What is transient flow?

In traditional flow chemistry it is necessary to reach steady state (consistent output) before an accurate measurement can be collected. It is considered necessary for the system to be in equilibrium, often requiring as a rule of thumb 1.5 to 4 reactor volumes,[9,10] to ensure that the conditions experienced by every part of the reaction solution are known and constant. This means that collection of reaction data over a range of initial conditions can be a slow process and large quantity of material are needed. In contrast, transient flow begins by setting steady state conditions, and then varying a reaction condition in a controlled manner before allowing the system to equilibrate to another steady state (Figure 1.2). During the process, the output of the reactor can be continuously monitored, and the conditions experienced by each part of the reaction stream can be deconvoluted. This allows continuous series of data to be collected over a range of reaction conditions in an efficient manner. (see Section 2 – 4 for comprehensive examples). In previously published work, transient flow has also been referred to as dynamic flow and non-steady state flow. Throughout this thesis the term ‘transient flow’ has been used, defined as a flow stream containing a reaction or process in which one or more reaction or process condition variable is varied in a continuous manner, usually analysed to provide a data series.

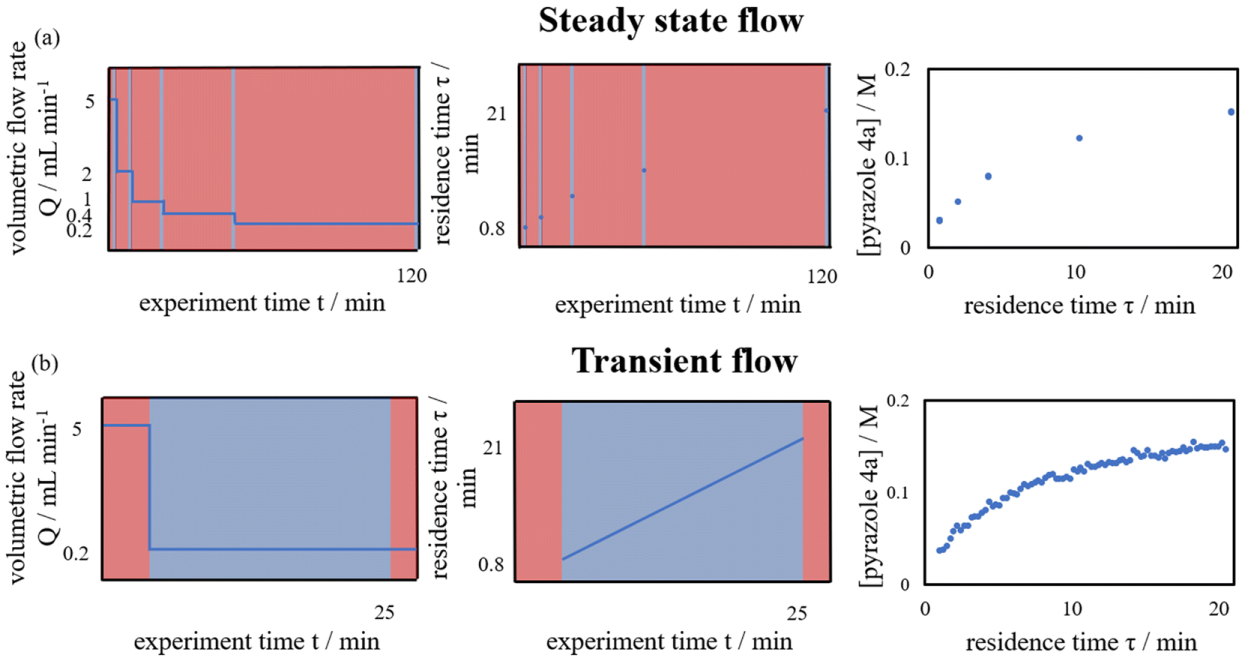


Figure 1.2. Comparisons of kinetic data collected in flow using: (a) steady state flow for five time points; and (b) residence time transient flow (see section 2). Blue areas indicating regions where useful reaction data are collected.

The methods of transient flow have their foundations in three known techniques: stopped flow, perturbation theory, and analytical chromatography. Stopped flow techniques utilise in-line analytical tools to monitor the reaction, and flow to provide good initial mixing and control of reaction conditions, improving the study of fast reactions.[11] Although the active reaction itself is monitored in a batch setting, flow is utilised to improve the accuracy of the reaction initialisation and thus the accuracy of the reaction data collected. Perturbation theory gives the foundation for performing a change to a process parameter in a well-defined manner and monitoring the result of the change as a continuous data series.[12,13] Analytical chromatography has been widely used as a flow analysis method in which a process parameter (such as flow rate or temperature) is continuously changed to affect the separation of chemical compounds.[14] HPLC and GC utilise equipment, such as pumps and ovens, which can accurately change parameters, such as flow rates and temperature, in an accurate automated manner, whilst the output is monitored continuously by in-line or on-line analytical tools. Combination of the ideas of reaction monitoring from stopped flow, the fluid dynamic mathematics of perturbation theory, and methods and equipment of analytical chromatography, and applying the result to a reaction yields the field of transient flow.

1.3 What do we need for transient flow?

In order to best implement transient flow methodology, the flow system used should meet three main requirements: a well-defined residence time distribution/fluid dynamic, the capability to accurately and rapidly control reaction conditions, and an analytical tool with suitable sampling frequency relative to the rate of transient parameter ramping. Although not all are necessary for the use of transient flow, all three bring significant enhancements to the implementation.

1.3.1 Fluid dynamics

Fluid dynamics describe how the mass transfer processes, or 'mixing', in a reactor take place. The most important features for transient flow systems are good initial mixing so that the reaction mixture is homogenous, with well-defined reaction stoichiometry, and that the residence time distribution (RTD) is well understood, preferably under a plug flow regime. A plug flow regime is one in which the amount of axial dispersion is negligible over the length of the reactor and thus each differential length element of the reactor has a narrow and symmetric residence time distribution, *i.e.* not mixing much with the reaction solution upstream or downstream from it. This is important for transient flow methods because if under the assumptions of ideal plug flow, each section of reaction mixture can be assumed to be independent from those around it and the system can be considered as a continuous series of infinitesimally small and well-mixed batch reactions.

The residence time distribution can be studied through determining the dimensionless Péclet number of the reactor system (Eq. 1.1). This is a dimensionless number used to define the proportional amount of axial dispersion within the system. This can be determined either by an injection of a tracer into the system, or *via* a step change in tracer concentration utilising equation 1.2.

$$Pe = \frac{L\,u}{D} \qquad \text{[Eq. 1.1]}$$

where Pe = Péclet number (dimensionless), L = characteristic length (m), u = local flow velocity (m s^{-1}), and D = mass diffusion coefficient (m^2 s^{-1}).

$$\frac{dF}{d\theta} = \frac{e^{-\frac{Pe(1-\theta)^2}{4}}}{\sqrt{12.566/Pe}} \qquad \text{[Eq. 1.2]}$$

where F = normalised tracer concentration response to a step change in tracer concentration, θ = normalised residence time, and Pe = Péclet number.

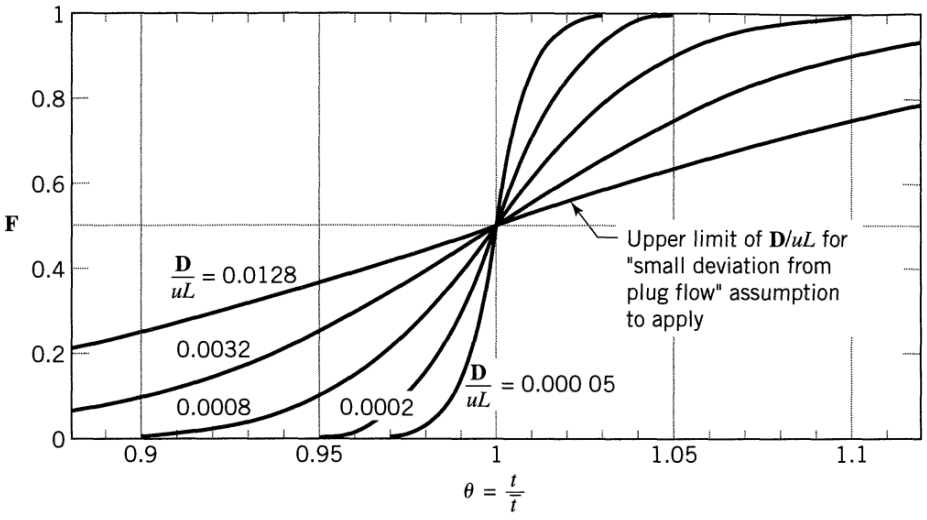


Figure 1.3. Residence time distribution step response curves for small deviations from plug flow known as an "F curve". F is the normalised tracer concentration response from a step change in tracer concentration or the cumulative tracer concentration response to a tracer injection. F is plotted against the normalised residence time (residence time over mean residence time) (figure reproduced from Levenspiel[12]).

Figure 1.3 shows the residence time distribution step response curves from a step change in tracer concentration for a range of different Péclet number values. Such plots can be analysed through integrating and fitting equation 1.2 to determine the Péclet number by fitting the normalised concentration curve monitored after a step change in tracer concentration. Temperature, flow rate, pressure, and solvent can all affect viscosity and dispersion rates that have an effect on the Péclet number. Generally, if a Péclet number is greater than 100 (D/uL<0.01) then it is considered to have minimal

deviations from plug flow and thus any dispersion effects can be considered negligible (*i.e.* well defined infinitely narrow residence time distribution).[12] Conversely, if a Péclet number is less than 100, the rate of diffusion compared to the advective transport rate (*i.e.* the active flow rate along the reactor length) is considered to have a residence time distribution too broad to be modelled as a plug flow reactor.

1.3.2 Reaction condition control

Accurate and rapid control of reaction conditions is essential to allow transient flow experiments to deliver more efficient and higher quality data than steady state methods or batch experiments. For example, if the reactor can only be heated slowly relative to the sampling time of the analytical tool, then the transient approach has no advantage over a steady state approach. Similarly, if a reagent's concentration cannot be accurately modulated in a continuous manner, then the system may produce less useful, less accurate reaction data. The increased efficiency gained from accurate and rapid control of reaction parameters can be further enhanced by utilising automated equipment to minimise operator interaction. As chromatographic equipment, such as HPLC pumps and GC ovens, are designed to perform rapid accurate gradient methods, this equipment is often useful when constructing a transient flow system in which ramping of reaction parameters accurately and automatically is desired.

However, a flow system has theoretical limits to how fast certain parameters may be ramped while maintaining well-defined fluid dynamics.[15] At low ramping rates below this theoretical limit in a reactor with minimal deviation from a plug flow reactor, each differential volume element of the reaction stream can be assumed to be at pseudo-steady state. Above this limit, reaction data may still be collected but the result must be treated with more caution, as it is more likely to deviate from steady state data.

1.3.3 Analytical tools

The availability and choice of analytical tools are critical to all kinetic experiments, determining the type of data and rate of data acquisition, and transient flow experiments are no exception. If an analytical tool

has poor time resolution (*i.e.* not many data points produced per unit time), fewer data points will be collected over a transient flow experiment of the same length. In such a case, rapidly ramping reaction conditions will lead to a broader range of conditions analysed, but only very few data points will be collected. Consequently, this can limit the benefits offered by transient flow over steady state methods. For example, if we have a transient flow ramp which takes an hour to scan through a wide range of conditions, but we have an analytical tool which takes half an hour to collect a data point, only two data points will be collected within the parameter series despite examining all the space. Therefore, choosing a suitable analytical tool is important to performing transient flow experiments.

The implementation of analytical tools in batch chemistry can be described as '*in situ*' or '*ex situ*' dependent on whether the tool analyses the active reaction directly ('*in situ*'), or a sample or end point of the reaction ('*ex situ*'). In contrast flow chemistry can be categorised into four groups: in-line, on-line, at-line and off-line (Figure 1.4).[16] These terms are sometimes used interchangeably in literature and can become confused. In the interest of clarity, a definition of these terms are given below:

'In-line': the whole process stream flows through the analysis window and is analysed without being removed. Note: this does not necessarily mean that the measurement is continuous.

'On-line': a portion of the process stream is diverted through the analysis window and analysed automatically.

'At-line': the reaction mixture is analysed by an instrument which is dedicated to the process, *i.e*. not in a separate place for performing analysis. There can be a degree of manual interaction.

'Off-line': a sample is collected from the reaction at any point and then is manually transferred to the analytical tool, often a non-dedicated instrument in a different location, where it is analysed.

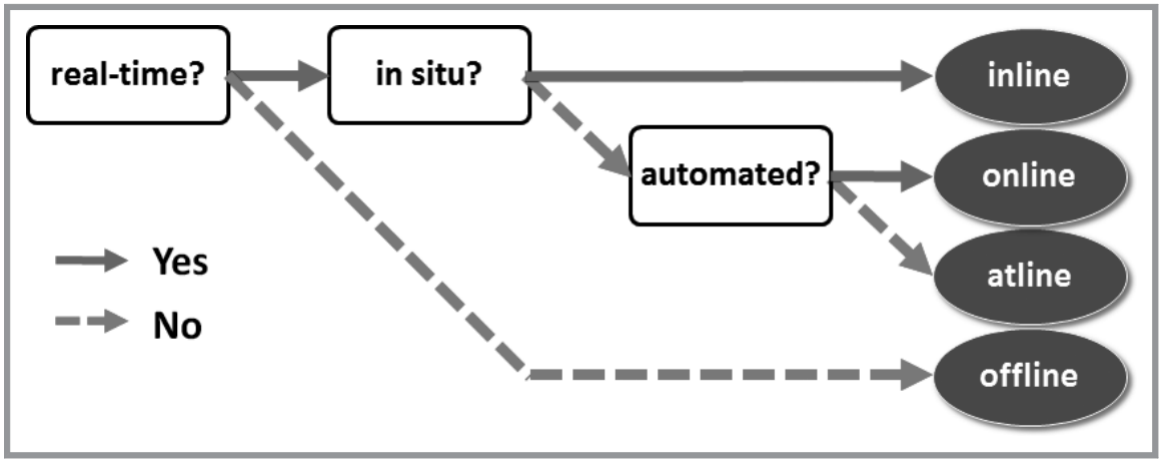


Figure 1.4. Decision tree for the classification of analytical tools in flow (figure reproduced from Minnich *et al.*[16]).

Traditional synthetic research groups have a high availability of *ex situ* analytical techniques (those by which a sample must be taken to the machine and submitted, at-line or off-line). On-line/in-line sampling is preferable as it is more automatable and can often generate more accurate data as samples are more rapidly analysed and thus are more similar to *in situ* analytical tools. An issue with collecting a lot of samples in an automated manner is there is then a large volume of data to analyse. Data analysis is preferably also performed in an automated manner, with minimal human interaction to minimise human error.

Many different analytical tools have been applied in flow and the topic has been reviewed several times, either by highlighting a specific tool,[17–21] or in a more general manner.[22,23] These tools generally fall into two categories, spectroscopic and chromatographic, each with specific benefits and limitations. The different analytical tools can be qualitatively compared by using certain metrics (Table 1.2). However, the choice of a particularly analytical tool will often depend on the chemistry studied and the purpose of the data collection.

Table 1.2. Qualitative assessment of a selection of commonly used PAT tools in flow for organic synthesis.

PAT Tool	General Specificity	Sensitivity	Speed of analysis	In-line capability	Capital cost
Single-wavelength sensors	Low	mM	μs	In-line	£1s
UV/Vis	Low	mM	ms	In-line	£100s
NIR	Low	M	s	In-line	£1000s
IR	Medium	M	s	In-line	£10,000s
NMR	High	M	min	In-line	£100,000s
HPLC	Very high	mM	1 – 10 min	On-line	£10,000s
GC	High	mM	10 – 30 min	On-line	£10,000s
MS	High	μM	ms	On-line	£10,000s
Calorimeter	Low	M	s	In-line	£10,000s

In flow, spectroscopy is normally implemented in-line and affords reaction analysis with good time resolution. Generally, but not exclusively, more expensive spectroscopic tools have benefits over cheaper tools in the amount of information produced, specificity, or generalisability, although they can often be less sensitive. For example, UV/Vis is highly sensitive, but is not very specific as absorbance peaks are broader, more generic, and provide little structural information about the reaction species. In contrast, NMR - a more expensive tool - has greater specificity and can provide more detailed information from the reaction mixture and is more generally applicable as it does not require such specific features of a molecule to be present, such as a chromophore necessary for UV/Vis analysis. There is also a trade-off between the speed of the technique and the sensitivity of the technique due to signal to noise effects, leading to potential conflict between time and material efficiency in transient flow methods. Additionally, spectroscopic techniques do not separate different components in the reaction mixture, so some chemical systems can be challenging to study accurately. Chemometric tools, such as principal component analysis, can help deconvolute data from multicomponent systems, but generally have higher levels of uncertainty associated with the produced data.[24] The use of orthogonal spectroscopic tools can also be used to facilitate the study of more complex mixtures.

Chromatographic analytical tools can increase specificity by physically separating different reaction components before detection by a spectroscopic (UV/vis, fluorescence, ELSD, RI, optical rotation), mass spectrometric, or electrochemical method (FID, ECD).[25] Due to the separation achieved between different components of the reaction mixture, better quantification of multiple reaction species can be achieved than for direct application of spectroscopic methods. In flow, chromatography can not only be performed off-line or at-line, but also on-line.[26–28] The type of chromatography used depends on the molecules that are being studied, typically GC for volatile molecules, LC for small organic molecules, or GPC for polymers. Similarly to spectroscopic tools, different detectors can be used to provide more information from the separated reaction mixture, often in which more expensive detectors provide greater information (mass spectrometric detectors) or more general applicability (ELSD), and detector choice also can depend on the molecules under analysis.[25] More expensive chromatography systems, such as UPLC, can also speed up separation times by facilitating more efficient component separation, thus increasing the possible sample rate of the system.[29] Similarly to the chemometric methods applied to enhance spectroscopic tool data, there has been development of techniques to deconvolute overlapping chromatography. For example, the open-source MOCCA allows faster chromatographic separations to be performed on more challenging mixtures through analysis of multiple wavelengths to estimate areas of overlapping peaks to within 2% error (Fig. 1.5).[30]

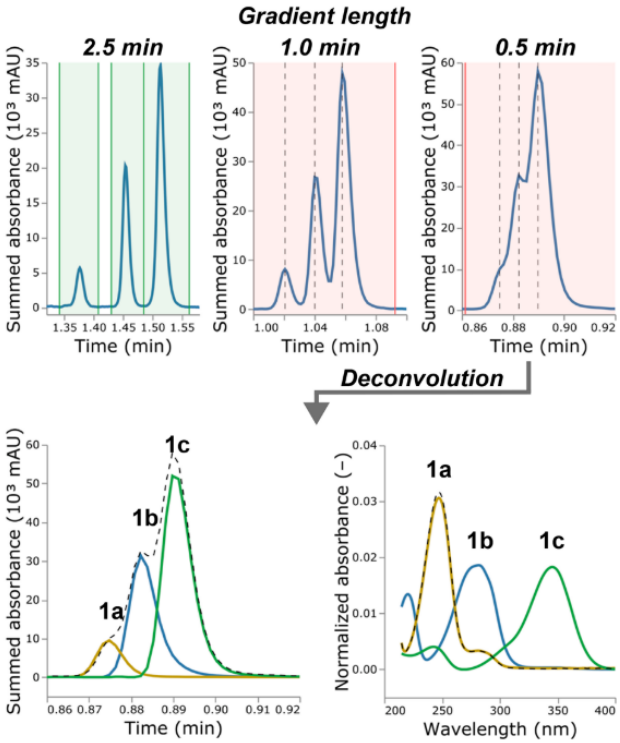


Figure 1.5. An example of an opensource chemometric method for chromatographic analysis (MOCCA) (figure reproduced from Haas *et al.*[30]).

1.4 Types of transient flow parameter

There are two types of reaction parameters in transient flow experimentation: those that affect the entire reactor volume, and those which affect only one part of the reaction stream. The first type of transient flow parameter includes cumulative flow rate and reactor temperature, a change in either of which will affect the entire reactor volume. Under these conditions, each differential volume element of the reaction stream experiences the cumulative, or integral, effect of these parameters changing over the time they are in the reactor, often requiring integration for deconvolution (an "Integral parameter"). In comparison, the second type of transient flow involves setting the reaction parameter(s) at the start of the reactor, which remain unchanged over the length of the reactor ("Proportional parameters"), for example additive concentration or solvent(s).

2 Reaction time transience

For reactions performed in batch reactors, reaction time-series data can be collected simply by monitoring the reaction using *in situ* analytical tools or sampling at multiple times throughout the reaction. This produces time-series reaction data at a spectific time resolution set for the in-line analytical tool (spectroscopy) or frequency of sampling (chromatography) with no need to actively modify any reaction parameter. As time-series data is generally easy to collect in batch, this is generally preferred, particularly for relatively slow homogeneous reactions with no mixing issues.[31] However, flow chemistry can provide more accurate control of reaction conditions and a larger process design window than batch chemistry, providing advantages to collecting reaction time-series data in flow. Additionally, flow chemistry often has better mass and heat transefer, due to the size of the fluidic channels, therefore the reaction time and temperature are generally better defined in a flow system (see section 1.3.2) than in a batch system. Short residence times are also better studied in flow as a precise short residence time can be sustained (high flow rate or small reactor volume) and analysed in a more leisurely manner.

However, steady state flow chemistry is poorly equipped to collect time-series kinetic data. Once a flow rate is set to produce the required steady state, only the reaction output at a certain residence time, corresponding to the reactor volume and flow rate (Eq. 1.3) , is monitored. In order to monitor the reaction output at further time points, another flow rate must be set, or the reactor volume changed. This requires re-equilibration of the system which takes time to reach steady state inherently longer than the residence time.

$$\boldsymbol{\tau = \frac{V_R}{Q_C}} \qquad \text{[Eq. 1.3]}$$

where τ = residence time (min), V_R = active reactor volume (mL), and Q_C = cumulative flow rate (mL min^{-1}).

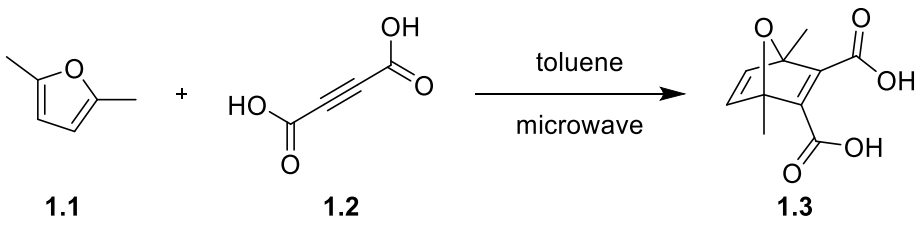
Transient reaction time experiments attempt to retain the benefits of flow chemistry while increasing the rate of collection of time-series data. As the residence time is the quotient of the active reactor volume over the cumualtive flow rate (Eq. 1.3), we have two key variables to use to affect residence time: altering the reactor volume or the cumulative flow rate.

2.1 Varying active reactor volume

Varying the active reactor volume while maintaining the same flow rate allows many of the same claims as steady state data collection to be made. As the flow rate is constant, the fluid dynamics are constant across the flow system both in terms of initial mixing and later flow regimes. The active reactor volume can be varied by changing the reactor volume itself or by changing the energy input instantaneously to "switch on" the reactor.

2.1.1 Energy source switch on methods

By switching on an energy source (heat, light, electric current) to initiate a reaction in a flow system with a fixed flow rate, the active reactor volume experienced by the reaction stream varies linearly. The first such example was provided by Gomez *et al*. using a microwave heated microfluidic reactor coupled with an in-line nanolitre NMR spectrometer (Scheme 1.1).[32] In this case, a microfluidic system was brought to steady state at a fixed flow rate, before microwave irradiation was applied to heat the reaction stream. As the reaction solution nearer the end of the microwave reactor has been exposed less to the microwave irradiation, this corresponds to a shorter reaction time (Fig. 1.6). Conversely, the reaction mixture at the beginning of the microwave reactor will experience the full residence time of the reactor once switched on. This produces a linear ramp of reaction times experienced across the reactor volume. In this particular example, eight NMR spectra were collected at eight time points, collected from a single reaction volume with *circa.* 1 min time resolution between each data point. As the reaction mixture is mixed prior to irradiation, this approach is only suitable for reactions that occur under non-ambient conditions, *i.e.* the reaction is triggered by the application of microwave irradiation.



Scheme 1.1. Diels-Alder reaction performed utilising a microfluidic chip reactor and microwave irradiation by Gomez *et al.*[32]

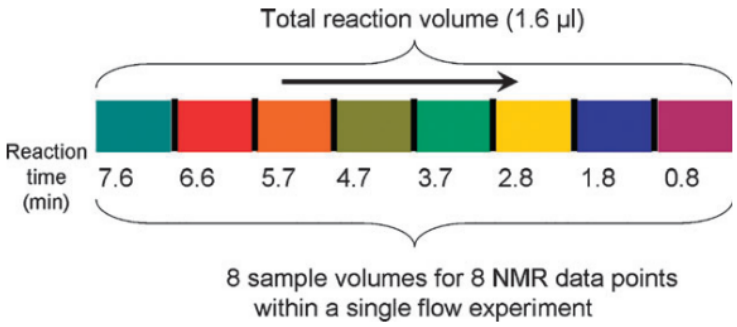


Figure 1.6. Example of how different residence times can be achieved in a single flow experiment by switching on an energy source, such as microwave irradiation, at a fixed flow rate (figure reproduced from Gomez *et al.*[32]).

More recently a similar method was applied to a photochemically initiated reaction, demonstrating the method's use for other energy sources.[33] In this case, the light source was switched off, to avoid discrepancies from the light source warming up. On-line samples were collected from the reaction effluent and analysed using off-line GC, thus decoupling the analysis time from the reaction time resolution. Similar approaches have been used to determine the amount of photon flux into the reactor in a time resolved method (time resolved actinometry in large systems or 'TRAILS').[34] In principle, this can afford actinometry results for short residence times but with good time resolution. In practice, inhomogeneous light sources caused difficulties when combined with time resolved techniques as only cumulative photon flux can be observed. This highlights an important requirement for transient flow techniques: in steady state inhomogeneous energy sources are averaged over the reactor length, but in time resolved transient techniques inhomogeneity can produce unreliable results.

Although methods involving the switch on of an energy source to generate reaction time-series data have proved useful in selected examples, the methods have not seen widespread use, limited to strongly thermally or light initiated reactions. In such cases where the reaction is initiated by reactants mixing other methods must be used to obtain reaction time-series data.

2.1.2 Change in reactor volume methods

A diverse range of methods have been developed to automatically change the working volume of a reactor utilising specially designed systems. Although these approaches may not directly be transient, *i.e.* they do not produce a series of data from changing reaction conditions, they do produce time-series data in an automated manner and thus warrant discussion.

The simplest approach is to sample the reaction at fixed points along the flow path, as shown in a study of the kinetics of a reaction producing a diazo intermediate (Fig. 1.7).[35] In this work, a valve system was set up to redirect the flow stream through either one, two, or three reactor units (R1–R3) to collect three time points, analysed by IR spectroscopy as the in-line PAT tool. This allowed multiple residence times to be analysed in one experimental run, albeit in quite a discrete manner, while minimising the quantity of hazardous material handled.

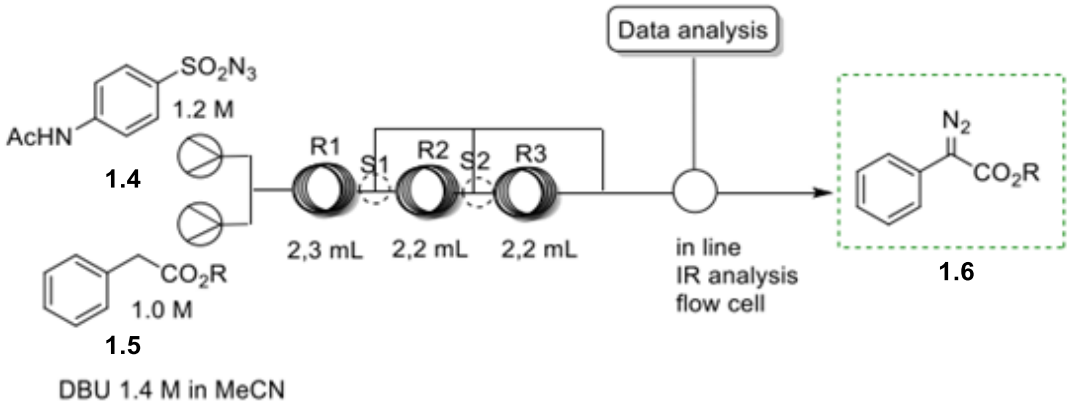


Figure 1.7. Variable reactor volume at fixed flow rate, achieving three time points in one steady state experiment (figure reproduced from Müller *et al.*[35]).

Another approach was to continually recycle the reaction solution around a loop by a recirculating pump through the PAT tool. An in-line conductivity cell was utilised to collect multiple residence time points from an ester hydrolysis reaction.[36] This approach is related to semi batch methods in which analysis is performed in a recirculating flow loop which samples and returns to a batch reactor. However, in this fully flow method the fluid dynamics of the system can be better controlled, and shorter residence times can be analysed.

A third approach combined this recirculating method with segmented flow in a figure-of-eight reactor to automatically sample from 300 μL slugs, at different reaction times, which minimises material wastage (Fig. 1.8).[37] This final approach implemented analysed samples collected automatically on-line with at-line GC. Although this approach proved capable of analysing a broad range of chemical reactions and produced detailed kinetic profiles, such an approach will be challenging to implement in other research laboratories due to the complexity and degree of system control required.

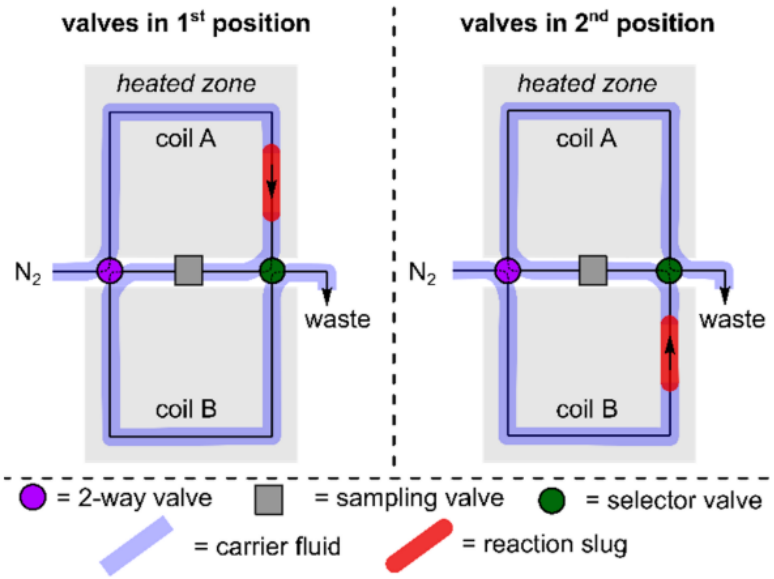


Figure 1.8. Schematic of figure of eight reactor used to recycle single or multiple reaction slugs for multi time point analysis (figure reproduced from Sullivan *et al.*[37]).

An alternative approach is to utilise an analytical tool which analyses the entire reaction course ('mapping'). Infrared thermography is such a technique for kinetic profiling of reactions (Fig. 1.9).[38] Using an infrared camera, the heat output of the reaction can be monitored across the entire reactor length producing spatial separated time-series data. This approach shows promise as an efficient tool for determining reaction rate data but has only been demonstrated thus far on relatively simple reactions such as ester hydrolysis and neutralisation reactions. Techniques which analyse the entire reactor length are limited to simple spectroscopic tools such as single wavelength UV/Vis or IR sensors, limiting the applicability of this approach to more complex reactions. Additionally, the data density collected is limited by the spatial resolution of such sensors which become significantly more expensive with greater resolution.

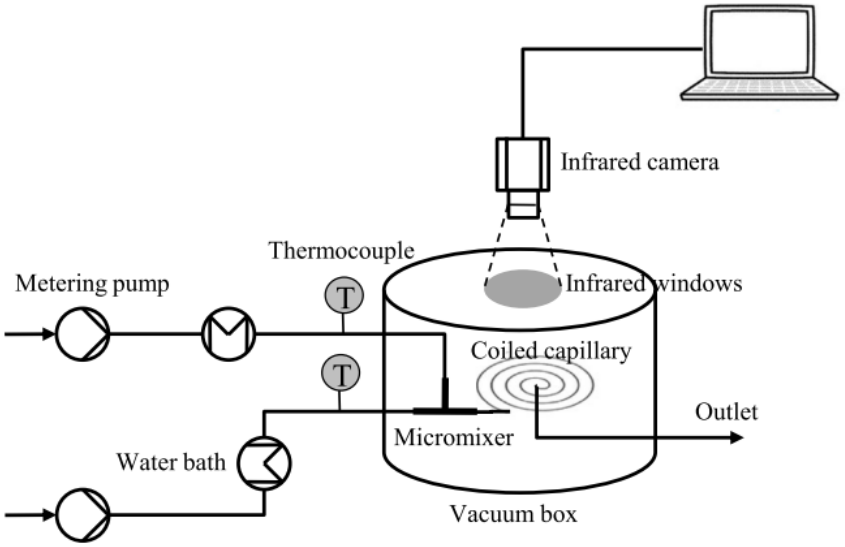


Figure 1.9. The experimental set-up for measuring the temperature profiles of reactions using infrared thermography obtaining time-series data (figure reproduced from Zhang *et al.*[38]).

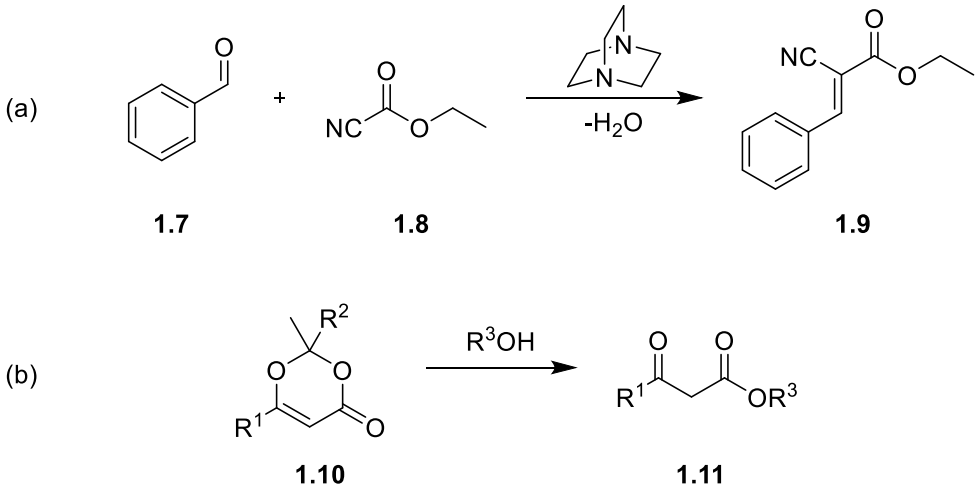
2.2 Changing cumulative flow rate

Maintaining a constant active reactor volume and changing the cumulative flow rate of the system often requires less specialised set ups, compared to varying the active reactor volume as described above. The caveat of this approach is that varying flow rate can also affect the fluid dynamics of the system. However, if performed in an accurate controlled manner, this can yield as accurate results as steady state methods. The simplest way to generate residence time series in flow is by performing a cumulative flow

rate step change although flow rate ramps have seen more significant usage.

2.2.1 Flow rate step change methods

The first publication utilising a change in cumulative flow rate to collect time-series data was by Mozharov *et al.* in 2011.[39] In this work, a Knoevenagel condensation reaction (Scheme 1.2a) is monitored by in-line Raman spectroscopy. After equilibration at an initial steady state, the cumulative flow rate is changed to a higher flow rate as a step function (Fig. 1.10). The reactor volume is displaced, each section of which has experienced a different residence time, until a second steady state is reached. This produces time series data on the reaction at a varying time resolution which was used to construct a kinetic model for the reaction. Further work comparing different in-line and off-line PAT tools, chemometric methods, and step change types allowed kinetic profiling of the thermolysis of 1,3-dioxin-4-ones (Scheme 1.2b).[40] The work focused primarily on step changes from low to high flow rates utilising in-line spectroscopic tools (UV/Vis and FTIR) with fast acquisition times (1.2 and 3.75 s scan rate respectively) to afford good time resolution data over the short transient period (*circa.* 1 min). However, it is mentioned that a step change from high to low flow rates may be advantageous if the analytical device's acquisition time is long. In both of these works, slight deviations from ideal flow rates were observed when performing a step change in flow rate, which is attributed to the time taken for a pump to change to a higher flow rate. These deviations can be, however, corrected to furnish good data for kinetic modelling. It is notable that neither work examined step changes from high to low flow rates in detail, as this would likely yield a more accurate flow rate step change (Chapter 2).



Scheme 1.2. (a) the Knoevenagel condensation monitored by in-line Raman spectroscopy by Mozharov *et al.*[39]; (b) the thermolysis of 1,3-dioxin-4-ones analysed at residence times between 1 – 10 min by Durand *et al.*[40]

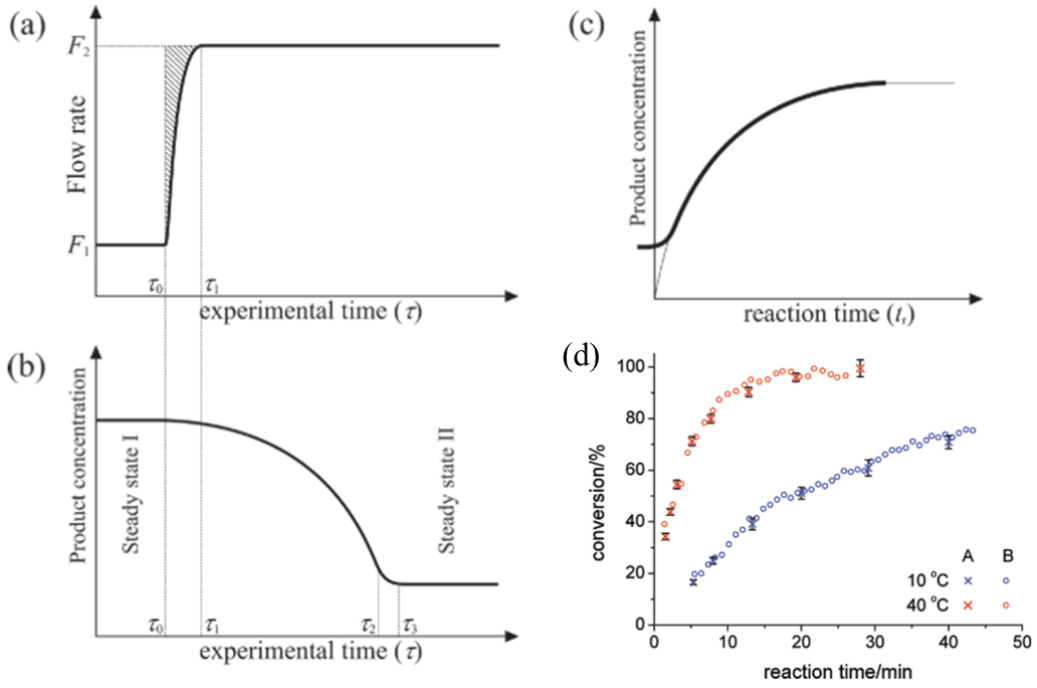
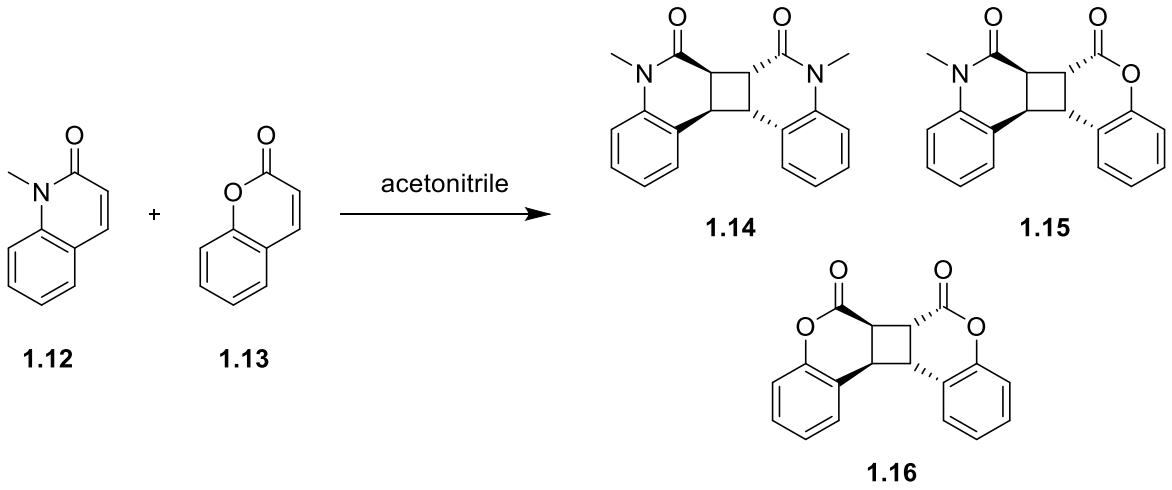


Figure 1.10. Example of the flow rate step change method showing changes in (a) flow rate, (b) the theoretical detected product concentration curve, (c) the theoretical deconvoluted product concentration curve against residence time, and (d) reaction data collected by this method (dots) compared to steady state data points (crosses) (figure reproduced from Mozharov *et al.*[39]).

Cumulative flow rate step change methods benefit from fast in-line analytical tools, however in some cases the reaction system may be more complex and require slower chromatographic analysis. Haas *et al.* utilised technology from 2D HPLC methods to decouple the slow chromatographic analytical time from the fast experimental time of a flow rate step change method studying a photochemical

cycloaddition (Scheme 1.3).[41] This reaction produced a challenging product mixture, thus requiring HPLC analysis, but used relatively expensive materials, thus requiring efficient experimental data collection, hence utilising flow rate step changes. The 2D HPLC technology, multiple heart-cutting, allowed parts of the reaction stream to be removed and stored in sample loops while other samples are being analysed (Fig. 1.11). This allowed a slower analytical tool to be used on-line to collect data from a flow rate step change, although ultimately transient flow data collection was somewhat hindered in this case by inhomogeneities of the light source.



Scheme 1.3. The photochemical [2+2] cycloaddition reaction producing a complex mixture of homo- and hetero-dimerised products analysed by on-line multiple heart-cutting HPLC by Haas *et al.*[41]

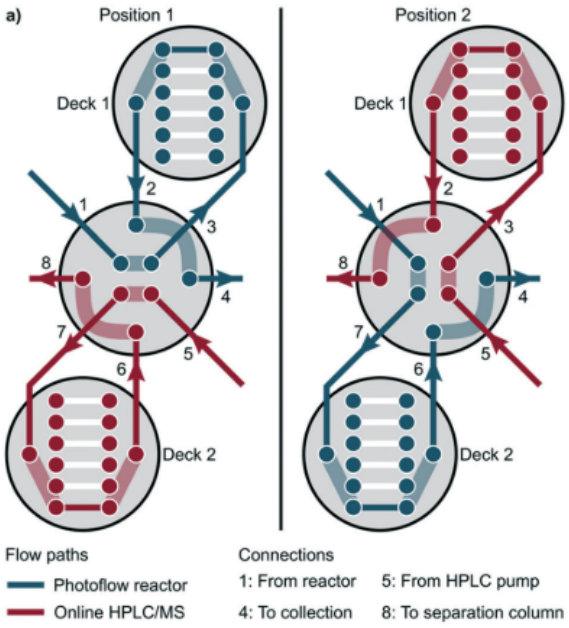
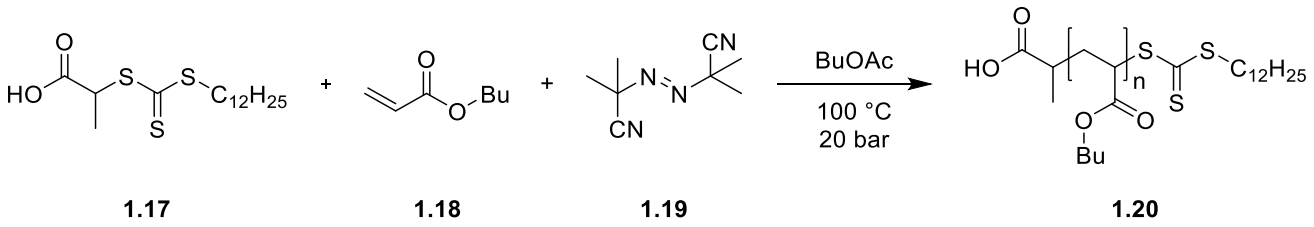


Figure 1.11. Multi-heart cutting technology utilised to increase time resolution of an on-line HPLC system for monitoring a transient flow step change (figure reproduced from Haas *et al.*[41]).

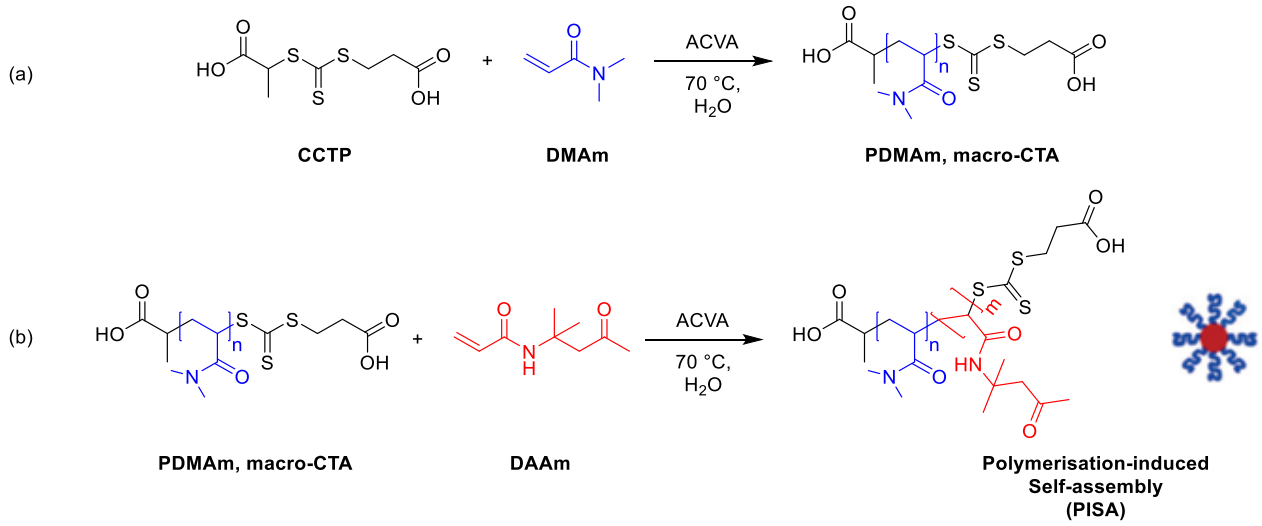
Cumulative flow step changes have been widely applied to study reversible addition−fragmentation chain-transfer, or RAFT, polymerisations. The approach was shown to be advantageous over batch methods due to the sensitivity of the reaction to the ratio of monomer to initiator and relatively short and precise reaction time needs (*circa*. 10 min). In the first example, an on-line MS was used to rapidly sample (every 2.2 s) the reaction mixture, during a flow rate step change from a 1 min residence time steady state to a 5 min steady state.[42] This was used to observe the growth of a butyl acrylate based polymer (Scheme 1.4) in real time and provided information for further steady state screening of reaction parameters (time, temperature, reactant stoichiometry). The same system was also further demonstrated to produce time series data at a range of temperatures (100 – 190 °C) for this polymerisation reaction.[43] 275 data points were collected at each of four selected temperatures using cumulative flow rate step changes to collect time-series data between 1 and 10 min residence time. This was subsequently used to guide steady state experimentation to optimise the conditions for the production of the desired polymer. The on-line MS was used to collect qualitative data series which, although allowing comparison of trends, do not allow concentrations to be determined directly due to differences in ionisation of different species.



1.17 **1.18** **1.19** **1.20**

Scheme 1.4. RAFT polymerisation reaction investigated by Haven *et al.* using a cumulative flow rate step change.[42]

Other work on RAFT polymerisation reactions profiled by flow rate step change methods have further demonstrated advantages of this method over batch and steady state flow methods. An aqueous RAFT polymerisation (Scheme 1.5) was kinetically profiled using a cumulative flow rate step change, demonstrating that higher quality kinetic data could be collected faster than by steady state or batch methods in a cheap continuous flow setup.[44] This kinetic data was then used to scale up the process in flow to produce polymer induced self-assembly products of the desired size monitored by on-line sampling for off-line NMR and GPC, allowing quantification of reaction outcomes. Interestingly, it was found that the reaction proceeded faster in flow than in batch due to the improved heat transfer in the system. This flow system was also modified to incorporate in-line low field NMR for more automated rapid analysis of cumulative flow rate steps on other RAFT and free radical polymerisations.[45] This was advantageous compared to the RAFT polymerisation systems previously discussed, as it allows quantitative conversion data to be collected rapidly in-line. More recently in-line NMR has been used to monitor a RAFT polymerisation reaction using multiple smaller cumulative flow rate step changes targeting different subsets of the reaction time.[46] Combination of in-line NMR with on-line GPC has also proved promising for monitoring RAFT polymerisations to facilitate the collection of more detailed kinetic information.[28] Both techniques are highly orthogonal, with the rapid in-line NMR affording many data points, while the slower on-line GPC provided more detailed information on the product distribution.



Scheme 1.5. Example RAFT polymerisations of (a) $PDMAm_{113}$ macromolecular chain transfer agent; and (b) a PDMAm-PDAAm diblock copolymer.reactions performed in water and kinetically profiled *via* a flow rate step change to vary residence time by Parkinson *et al.*.[44]

2.2.2 Flow rate ramp methods

Flow rate ramps involve varying the cumulative flow rate in a more gradual manner, *c.f.* pseudo-instantaneous flow rate change in the flow rate step methods. This method requires more programmable pumps than that used in flow rate step changes (above), but avoids discrepancies reported in some flow rate step changes (Fig. 1.10) by gradually changing the flow rate. These ramps can be performed as a linear residence time ramp or linear flow rate ramp "magnifying" certain reaction time regions (Fig. 1.12): non-linear flow rate ramps can be used to collect linear residence time ramps, whereas linear flow rate ramps produce a non-linear distribution of residence time data points. For example, linear flow rate ramps produce a higher density of residence time data at shorter residence times, which can be beneficial to elucidate initial rates where there is a rapid change in concentrations of the reacting components. Depending on the equipment used, either type of ramping may be easier to implement and broadly speaking, if the analytical tool is relatively rapid, the ramping methods are practically interchangeable.

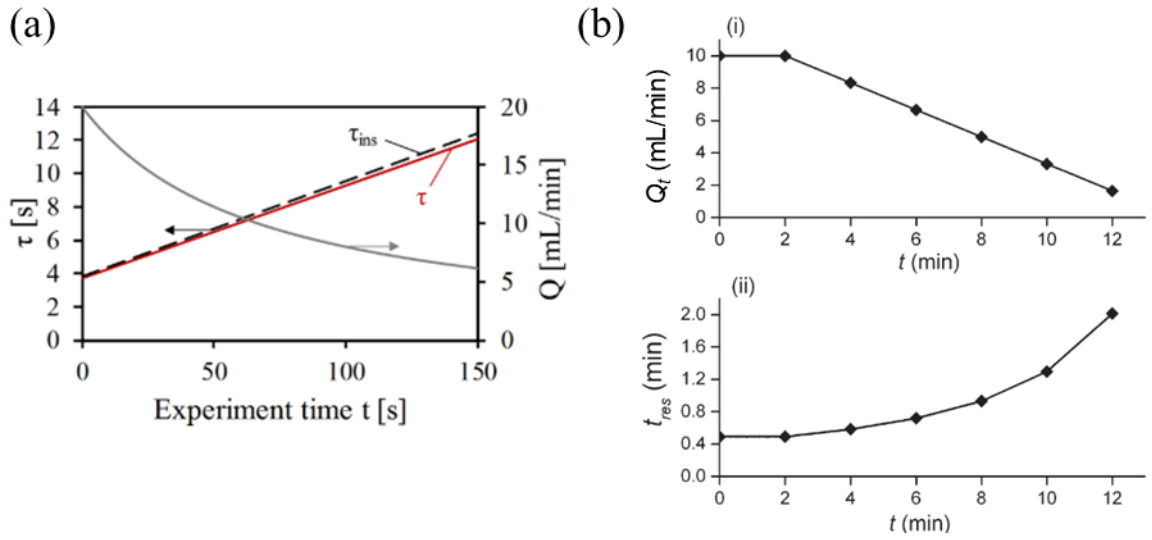
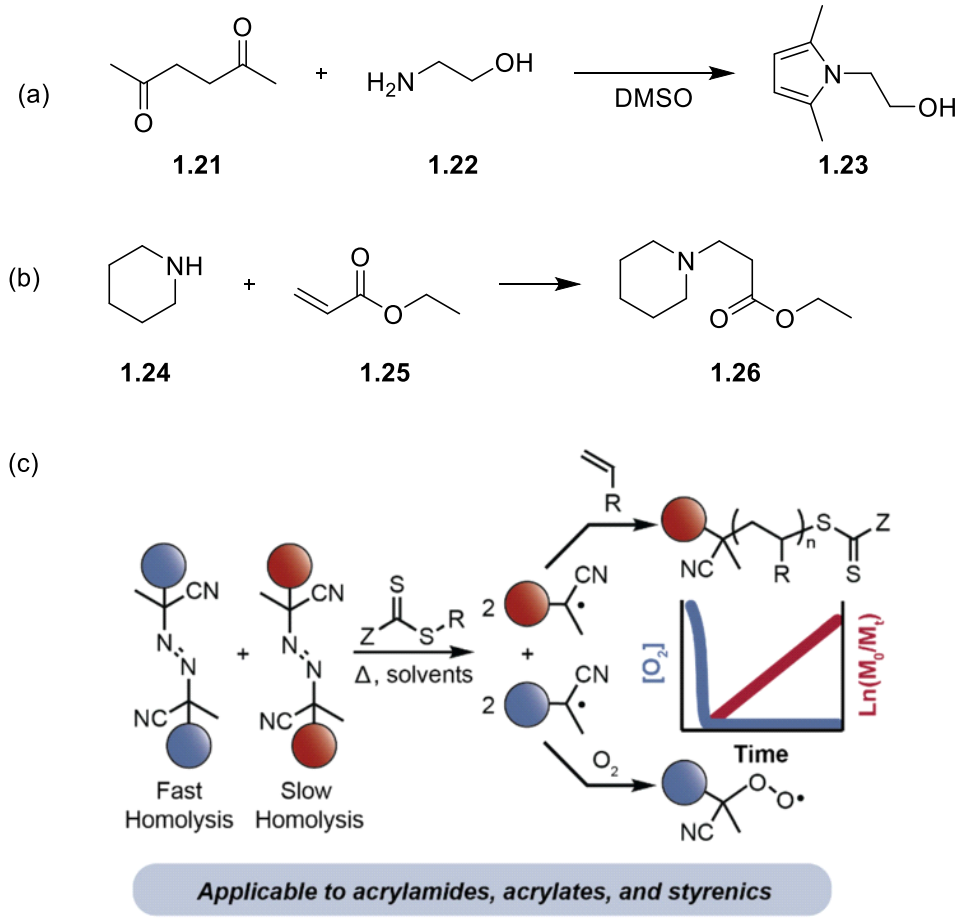


Figure 1.12. The cumulative flow rate and corresponding residence times for (a) a linear residence time ramp (figure reproduced from Schwolow *et al.*[47]) and (b) a linear flow rate ramp (figure reproduced from Hone *et al.*[48]). τ or t_{res} refer to the residence time in the corresponding unit, Q or Q_t refer to the cumulative flow rate of the flow system as a function of experiment time (t).

Linear residence time ramps emulate the collection of batch time-series data, *i.e.* evenly spaced reaction time data, but with generally greater residence time control. The first example of flow rate ramps was reported in 2014, using the Paal-Knorr pyrrole synthesis (Scheme 1.5a) as a case study.[49] By combining linear residence time ramps with in-line FTIR, the same kinetic data was collected eight times faster than by using steady state methods. Flow rate ramps are particularly useful for collecting kinetic date for fast reactions. An example of this was reported in 2015, when Schwolow *et al.* studied an exothermic aza-Michael reaction (Scheme 1.5b) at short residence times between 0.3 – 49 s,[47] which would be very challenging to study accurately using batch methods. Combining linear residence time ramps with calorimetry has also proved useful for the study of exothermic reactions.[10] This approach was applied to the hydrolysis of acetic anhydride to provide kinetic data more efficiently than steady state methods in the same system. RAFT polymerisations have also been studied by linear residence time ramps, albeit only in one example, compared to six examples by cumulative step change method (see section 2.2.1). In this example, a polymerisation-through-oxygen RAFT polymerisation (Scheme 1.5c) was investigated using a linear flow rate ramp between 1 – 30 minutes residence time was performed to provide direct comparison to batch data collected using *in situ*/in-line FTIR .[50] In this case, better

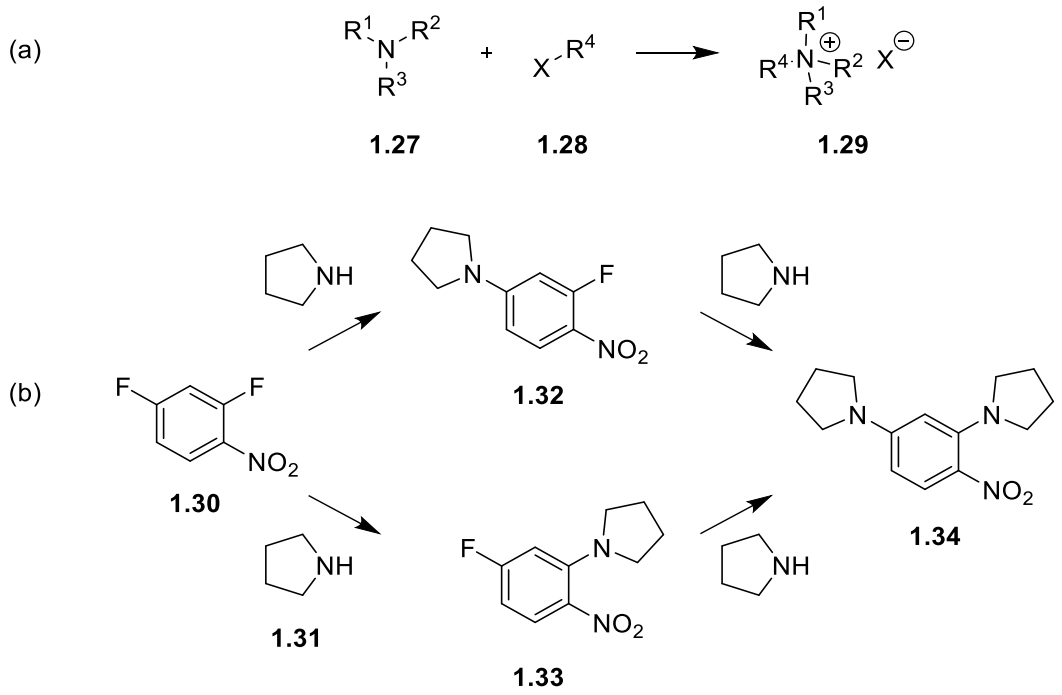
controlled conditions limits oxygen inhibition of the reaction, thus leading to better quality data than that collected from batch experimentation.



Scheme 1.5. Reactions investigated by linear residence time ramping methods: (a) the Paal-Knorr pyrrole synthesis performed by Moore *et al.*[49]; (b) aza-Micheal reaction performed by Schwolow *et al.*[47]; (c) polymerisation-through-oxygen RAFT polymerisation reaction performed by Taylor *et al*. (figure reproduced from Taylor *et al.*).[50]

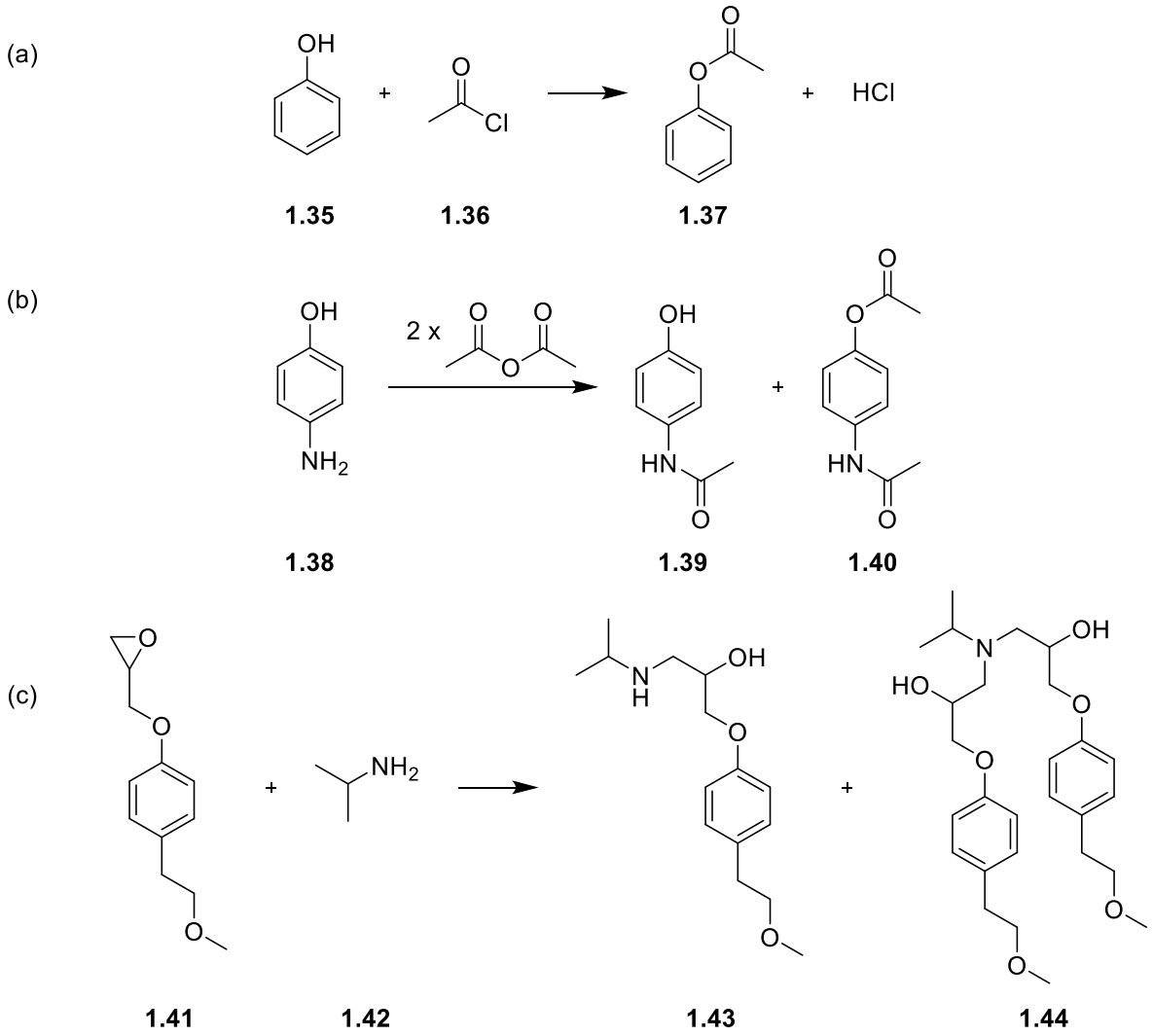
Linear flow rate ramps can be implemented using simpler equipment and provide non-linear residence time data series, over sampling in the low residence time (high flow rate) region. Time-series data produced this way are less similar to *in situ* batch data (evenly time spaced) and more similar to how a chemist might intuitively sample a reaction for kinetic profiling (more data at shorter reaction times when the rate of change is fastest). Although Schaaf and co-workers claimed to be the first to utilise this simpler linear flow rate ramping method (*c.f.* linear residence time ramping) on their study of the kinetics of the Menschutkin reaction (Scheme 1.6a) in 2021,[51] Bourne and co-workers published work using such

an approach as early as 2017,[48] when the method was combined with on-line HPLC to produce kinetic data on a multistep S_NAr reaction (Scheme 1.6b).[48] Previous studies on similar multistep reactions utilising steady state kinetic data collection required the isolated study of individual reaction steps.[52] In comparison, it was shown that all reaction steps could be kinetically fitted simultaneously due to the increased quantity of reaction data using the transient flow method.



Scheme 1.6. Reactions investigated by linear flow rate ramping methods: (a) the Menschutkin reaction investigated by Kleijwegt *et al.* under a range of different solvents[51]; (b) the multistep S_NAr reaction analysed by Hone *et al.*[48]

A similar approach was subsequently applied to multiple industrially relevant reactions (Scheme 1.7a – c) for automated kinetic model discrimination .[53] On-line HPLC-MS was used to monitor and quantify side product formation as well as to better discern between kinetic models (Fig. 1.13). The use of linear flow rate ramps at a slow ramping rate allowed HPLC samples to be collected with ~1 s reaction time resolution, permitting even fast reactions to be studied by this relatively slow analytical tool.



Scheme 1.7. Further reactions investigated by linear flow rate ramping methods: (a) acetylation of phenol with acetyl chloride; (b) acetylation to form paracetamol and side product; (c) epoxide opening reaction to form Metoprolol and undesired *bis*-substituted product.

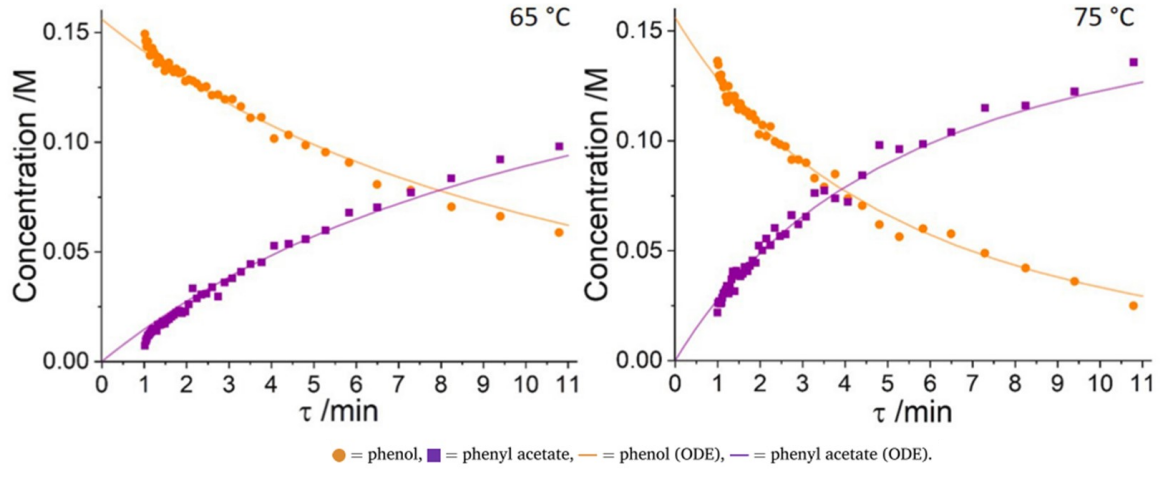
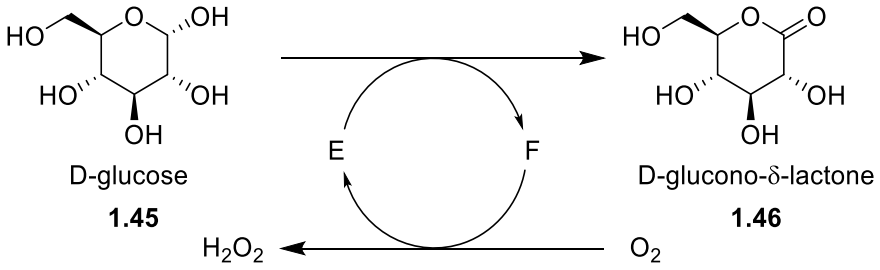


Figure 1.13. Kinetic fitting from flow rate ramps for the formation phenyl acetate from phenol (Scheme 1.7a) demonstrating high time resolution due to slow flow rate ramp (figure reproduced from Taylor *et al.*[53]).

In addition to homogeneous reactions, transient flow rate ramps methods were also used to study gas-liquid reactions utilising tube-in-tube reactors. In one such example the kinetics of an enzyme catalysed oxidation of glucose to glucono-δ-lactone (Scheme 1.8) was monitored using linear residence time ramps (Fig. 1.14).[54] As an over pressure of oxygen was applied to saturate the liquid phase, a constant oxygen concentration can be maintained over the different flow rates. The enzyme kinetics obtained using this system were found to be in good agreement with results obtained by steady state methods despite fears that the large (slow diffusing) enzyme would cause the system to deviate from ideal plug flow. In this regard, it would be interesting to see whether such transient work could be extended to a gas-liquid-solid system with a biocatalyst in a fixed bed.



Scheme 1.8. Gas-liquid enzymatic oxidation system analysed by linear residence time ramping methods by Ringborg *et al.*[54] where E denotes the oxidized free form of the glucose oxidase enzyme and F denotes the reduced form of the free enzyme.

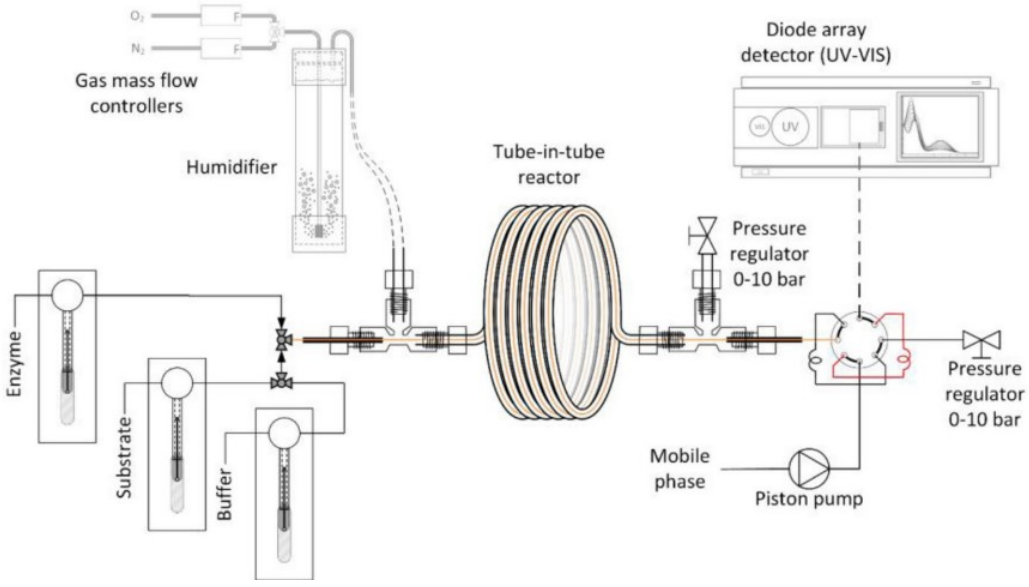
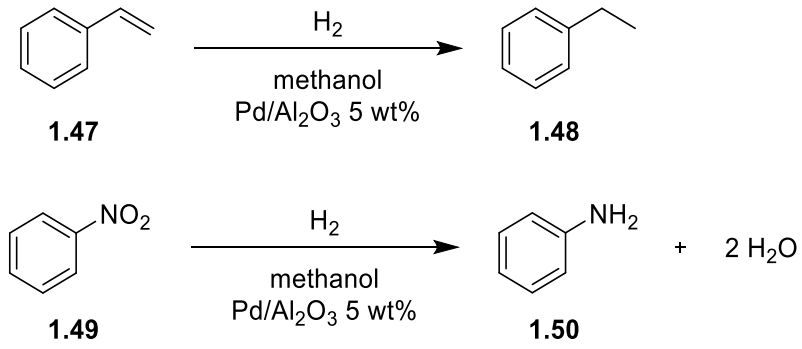


Figure 1.14. Schematic representation of the tube-in-tube reaction system with on-line UV/Vis utilised to perform linear residence time ramping on a gas-liquid enzymatic reaction (figure reproduced from Ringborg *et al.*[54]).

Another tube-in-tube example for a gas-liquid-solid hydrogenation reaction (Scheme 1.9) found that the rate of a linear flow rate ramp could not be increased above a certain point (0.03 mL min^{-1} min^{-1}) without negatively affecting the results, likely dependent on the reactor under study, attributed to a break down of the assumption of pseudo-steady state at these ramping rates.[55] The choice to use a linear flow rate ramp instead of a linear residence time ramp may have been influenced by these findings, avoiding rapid flow rate changes present in parts of a linear residence time ramp. To ensure intrinsic kinetics were collected, every effort was made to eliminate mass transfer limitations either in the tube-in-tube (gas-liquid) or packed bed reactor (liquid-solid). The kinetics of the system were collected through gas uptake and in-line UV/Vis measurements. These studies demonstrate that although multiphasic reaction can be studied by flow rate ramps, more system understanding, such as mixing and diffusion rates, is required to collect reliable reaction kinetics.



Scheme 1.9. Gas-liquid-solid hydrogenation reactions investigated utilising linear flow rate ramping by Jensen and co-workers.[55]

2.3 Best practice

Over the past decade the collection of residence time series data in flow has developed from impractical steady state methods only used as a last resort[31] to transient methods often demonstrating advantages over batch methods. Methods varying the active reactor volume produce high quality data but are limited generally to strongly thermally or light activated reactions. These methods also often require a high degree of specialist skill to implement efficiently. Cumulative flow rate varying methods offer a more

widely applicable approach to the collection of residence time-series data, capable of producing accurate data on reactions activated by any means. Such methods have been further applied beyond homogeneous reactions to catalysed, biocatalysed, and heterogeneous reactions, although examples combining such areas are still limited. Cumulative flow rate ramping methods, both linear residence time and flow rate ramps, are considered best practice among those in the field due to the reliable high quality data produced. However, to instigate wider use of these techniques beyond the flow chemistry community simpler flow rate step changes, requiring less specialised equipment and skills, should be considered if further studies are performed to benchmark the data quality compared to ramping or batch methods.

3 Reaction temperature transience

Reaction temperature often has a profound effect on reaction rates, as dictated by the Arrhenius relationship (Eq. 1.4), but also can affect product selectivity. Traditionally, multiple experiments will be performed at different discrete reaction temperatures to give individual data points required to construct an Arrhenius plot. Collecting such data in a denser and more efficient way can produce significantly more insight into a reaction, especially on selectivity and changes of mechanism, identified by changes of slope of an Arrhenius plot. Quite recently, it has been shown that temperature scanning of a reaction can be performed in batch,[7,8] although this method required multiple temperature ramping experiments to be performed to deconvolute the concurrent effects of changing temperature and progressing reaction time (Fig. 1.15). These experiments are relatively easy to set up, requiring only standard laboratory equipment and an *in situ* probe. However, due to safety issues, these experiments were only conducted at temperatures below or similar to the solvent boiling point. Fast temperature ramps are also hampered by the intrinsic slower heat transfer of a batch reactor. Efficiency of data collection is also hindered by the requirement to perform multiple ramps to deconvolute time and temperature based effects on the reaction.

$$k = Ae^{\frac{E_a}{RT}} \qquad \text{[Eq. 1.4]}$$

where k = reaction rate constant, A = pre-exponential factor, E_a = activation energy of the reaction (J mol^{-1}), R = universal gas constant (J mol^{-1} K^{-1}), and T = absolute temperature (K).

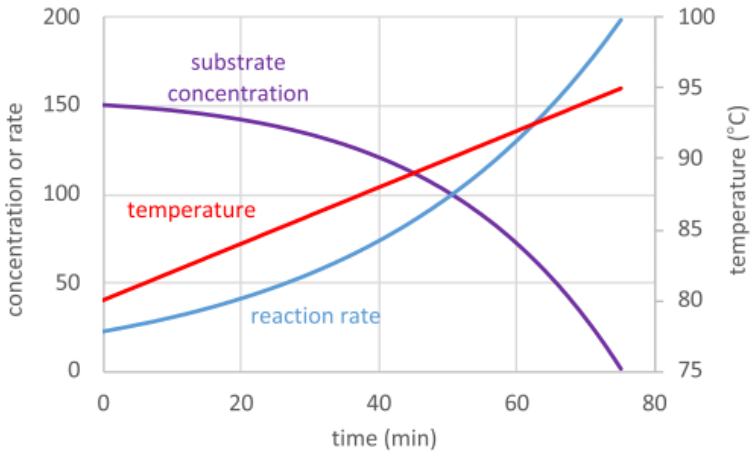
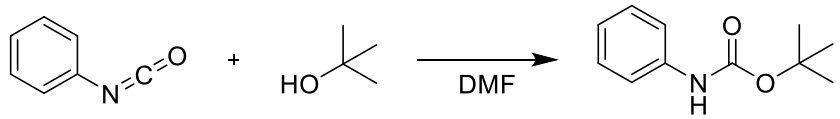


Figure 1.15. Batch methodology for temperature ramping (Temperature Scanning Reaction Protocol) monitoring substrate concentration and reaction rate over a progressing reaction time and changing temperature (figure reproduced from Schmidt *et al.*[8]).

3.1 Transient temperature ramps in flow

Transient temperature experimentation in flow has been well studied over the years, with the Jensen group making many early contributions.[56–58] These approaches utilise in-line FTIR to analyse the reaction of interest after thermal quenching in order to produce a stable calibratable FTIR signal. The first temperature ramp example built on previous work[59] on kinetic model discrimination, adding transient temperature ramps to help fit kinetic models for the reaction of isocyanates with tert-butyl alcohol (Scheme 1.10).[56] Temperature ramps were limited to no more than 3 °C min^{-1} to ensure accurate matching of the temperature set point in the silicon microreactor, a limitation dictated by the equipment used. In another study, temperature ramps were applied to a gas-liquid carbonylation reaction system (Fig. 1.16a) to screen the reaction space, determine activation energies, and construct a process model, again by utilising in-line FTIR (Fig. 1.16).[57] Activation energies were also collected using steady state and off-line GC analysis for comparison, demonstrating substantial efficiency gains in material and time.



1.51 **1.52** **1.53**

Scheme 1.10. The reaction of isocyanates with tert-butyl alcohol performed by Jensen and co-workers.[56]

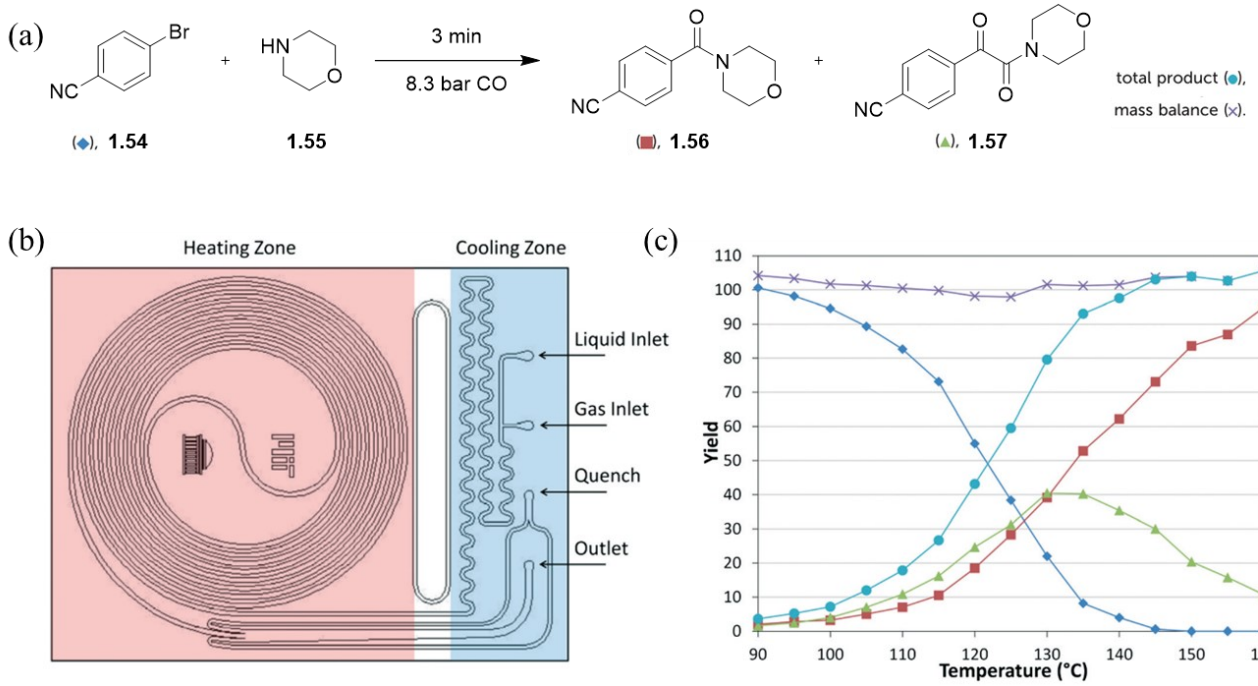


Figure 1.16. The biphasic amide bond forming reaction (a) studied utilising a temperature ramp between 90–160 °C in a custom silicon microreactor (b) for which concentration data (c) could be collected for reaction species **1.54**, **1.56**, and **1.57** *via* in-line FTIR (figure reproduced from Moore *et al.*[57]).

Temperature ramps have also been used to support a Design of Experiments (DoE) model for the nitration of salicylic acid (Fig. 1.17a). In this work, the use of rapid scanning in-line low-field NMR using multivariate analysis was compared to off-line UPLC, to analyse and quantify a product mixture (Fig. 1.17b).[60] In this example two temperature ramps were performed over different time periods over 0 to 35 ºC, the first ramping up over 60 min and the second ramping down over 15 min, although the ramps were not directly compared to each other in the paper. These ramping results were used to confirm the validity of the DoE model for prediction of product distribution.

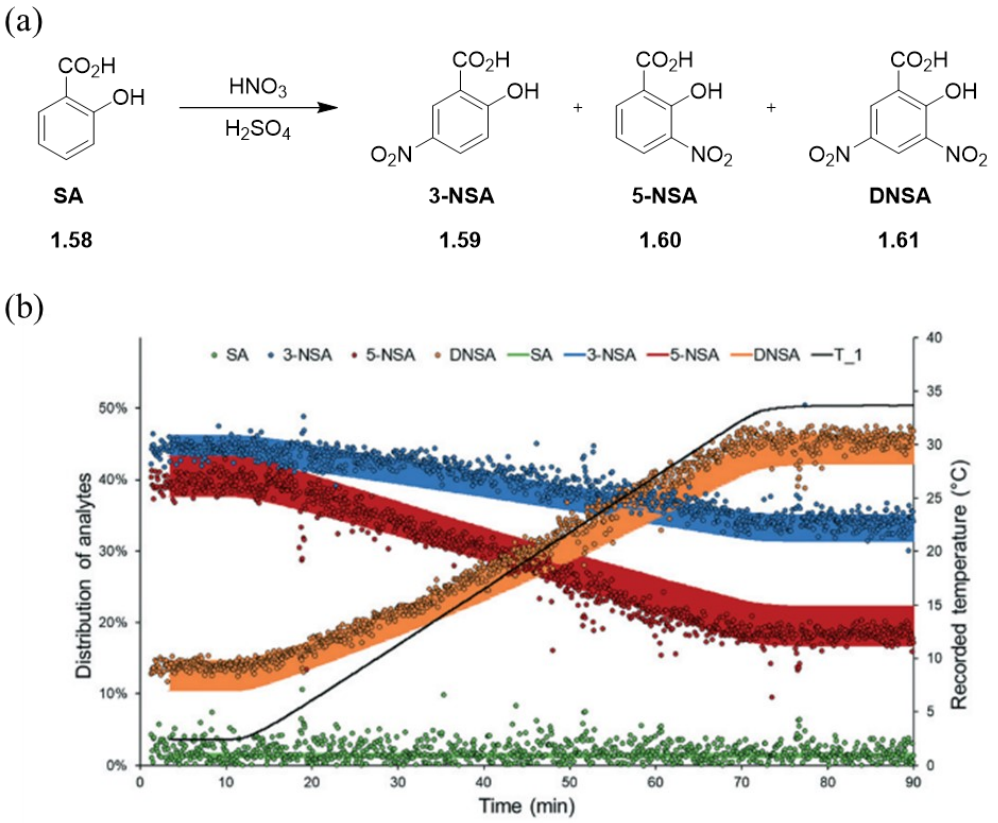


Figure 1.17. (a) the nitration of salicylic acid (**1.58**) producing multiple products (**1.59**, **1.60**, **1.61**); (b) transient temperature ramp experiment performed between 0–35 °C over 60 minutes used to validate a Design of Experiments model (broad lines) for the nitration of salicylic acid (**1.58**) (figure reproduced from Sagmeister *et al.*[60]).

3.2 Bi-variate flow rate-temperature ramps

Revisiting the Paal-Knorr pyrrole synthesis (Scheme 1.5a) previously studied using residence time ramps at fixed temperature,[49] Jensen and co-workers developed a simultaneous temperature and flow rate ramping method.[58] Despite higher error at fast flow rates, due to relatively fast reaction rate compared to the in-line FTIR sampling rate, kinetic profiles of a similar certainty could be fitted in just two orthogonal flow rate-temperature ramps (Fig. 1.18). In this case it was necessary to perform residence time-temperature ramps both in the same (uni-directional) and in opposite (con-directional) directions in order to deconvolute the effect of each parameter.

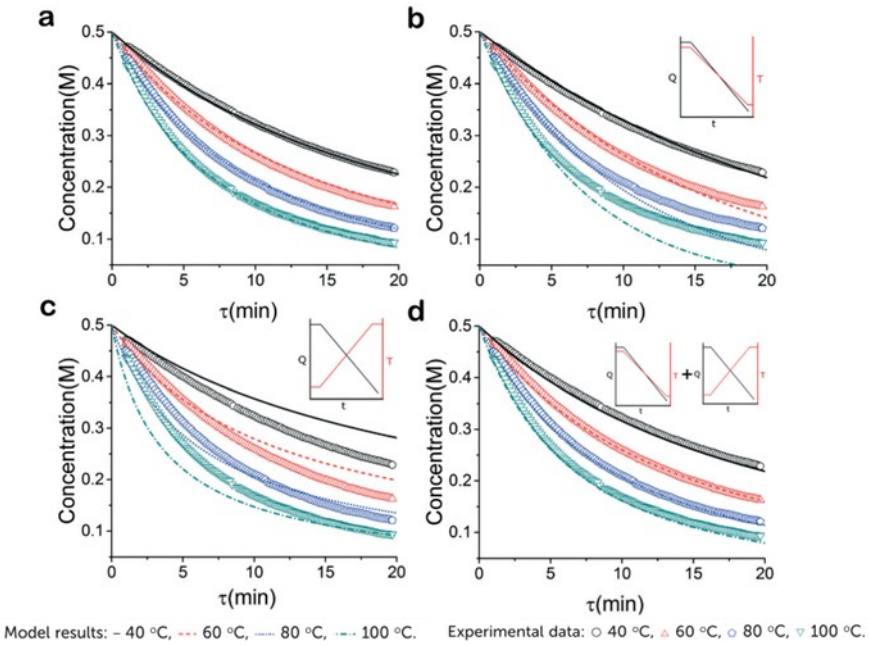
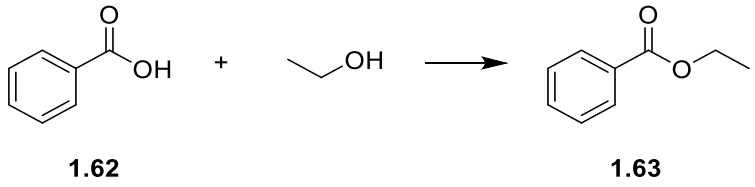


Figure 1.18. Simultaneous ramps of residence time and temperature as compared to data collected at constant temperatures using residence time ramps. (a) residence time ramp data; (b) uni-directional residence time-temperature ramp data; (c) con-directional residence time-temperature ramp data; (d) combination of both residence time and temperature data deconvoluted (figure reproduced from Jensen and co-workers[58]).

Flow rate-temperature ramps have also been demonstrated for minimising uncertainty in fitted kinetic parameters for an esterification reaction (Scheme 1.11) utilising on-line HPLC.[61] This study compared steady state, flow rate ramp, and flow rate-temperature ramp methods and found that the more transient methods had greater levels of uncertainty, but were performed in significantly less time (8, 4, and 2 hours respectively) despite limitations of the sampling rate of the on-line HPLC. Selection of the experiments performed by a Model Based Design of Experiments (MBDoE) approach successfully reduced the uncertainty for the transient methods' kinetic parameter estimates in the same time frame as before.[62] Although this approach was demonstrated on a simple esterification reaction it would be more valuable applied to a more complex chemical reaction.



1.62 **1.63**

Scheme 1.11. The esterification reaction investigated by Gavriilidis and co-workers.[61]

An alternative approach to bi-variate residence time-temperature ramping was demonstrated by modifying an active reactor volume varying method, previously described in section 2.1.1.[32] In this approach, instead of performing an isothermal experiment in a rapidly heating microwave reactor, the microwave reactor takes longer to heat the reactor to temperature (~1.5 minutes).[63] Rapid analysis by in-line nanolitre NMR allows different regimes to be investigated at constant flow rate (Fig. 1.19). When the microwave is first switched on, both the temperature and residence time are increasing as the first reactor volume is pushed out (first cohort). This is followed by a period at the start of the second reactor volume in which the residence time is fixed at its maximum, but the reactor is still heating up (zone c), subsequently followed by a steady state when the reactor has heated up fully and the residence time is stable (zone d). The method was applied to determine the formation kinetics of a variety of 5 membered heterocycles (Scheme 1.12) in an efficient manner. This approach relies on passive temperature ramping at a fixed rate which limits the general applicability of such a technique.

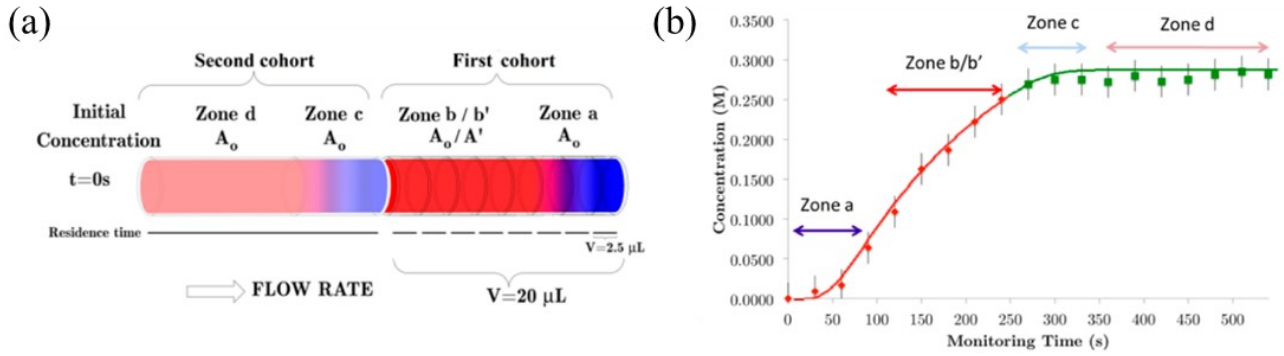
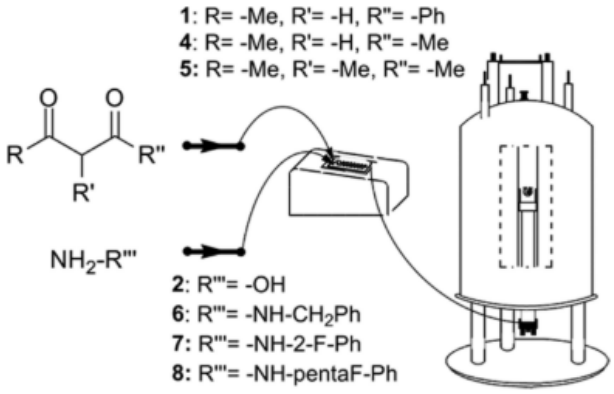


Figure 1.19. Non-isothermal microwave experiments analysed by nanolitre NMR in which a microwave reactor is heated up at a constant flow rate producing different regimes of residence time and temperature ramping (a) producing a deconvolutable concentration profile (b) (figure reproduced from Gomez *et al.*[63]).



Scheme 1.12. Pyrazole and isoxazole forming reactions analysed by non-isothermal energy source switch on methods (figure reproduced from Gomez *et al.*[63]).

3.3 Potential effect of ramp direction

It is worth noting that these earlier examples tend not to perform the same temperature ramp both up and then down, which would be beneficial to demonstrate lack of hysteresis in the system. Without this it is possible that the direction of the temperature ramp could affect the results due to, for example, solvent expansion effecting residence times or temperature dependent solubilities leading to break down of plug flow assumptions. Lack of such control experiments may limit trust in the data produced from such experiments by researchers unsure about flow chemistry.

4 Other transient parameters

Ramping other reaction parameters can produce valuable data for understanding reaction mechanism, fitting kinetics, and exploring a reaction parameter space efficiently, similarly to how a chemist might investigate these parameters by traditional methods. However, often such reaction data series can be harder to use as the equations for kinetics are formulated as dependent on time and temperature series data which chemists are more familiar with handling.

To date, published work on other parameter series has focussed on varying different reaction

concentrations. In batch, such techniques are generally used as qualitative methods to control reactivity, such as slow addition methods, however, recently tentative methods have been suggested to obtain quantitative data from similar experiments in batch, such as the slow addition of catalyst to a batch reactor[64] or base to a CSTR.[65] A disadvantage of performing such methods in batch can be that the effect of a varying reagent concentration over time can be challenging to deconvolute. In flow this can be combatted as an additive concentration range can be investigated efficiently by continuously varying the 'initial concentrations' of the reaction mixture entering the reactor, *i.e.* at reaction initiation.

In an early example in flow, O'Neal *et al.* applied cumulative flow rate ramps and concentration ramps to a ruthenium-catalysed asymmetric hydrogenation reaction (Fig. 1.20a).[66] After first reducing the reaction time to 40 minutes in batch, reaction conditions were screened efficiently in flow utilising a packed bed reactor of stainless steel beads to enhance gas-liquid mass transfer in the biphasic system. Transient ramp data compared favourably to steady state data collected in the system validating these methods in this gas-liquid system, further supported by "approximate plug flow behaviour" observed in the liquid phase of the reactor. In this work cumulative flow rate ramps and concentration ramps are used to efficiently develop system understanding to inform the construction of a larger scale recycle loop system analysed by off-line GC (Fig. 1.20b). Concentration ramps were performed by maintaining the flow rate of all but one reaction component pump and ramping the flow rate of this individual pump. The component (catalyst, substrate, or base) solution in this pump was at high concentration to limit the change in cumulative flow rate of the system when ramping concentrations to 10%, or by using a highly dilute base solution to compensate for the change in flow rate. This work also demonstrates that such flow rate ramps work on more complex gas-liquid systems under pressure (27.66 bar), albeit at room temperature.

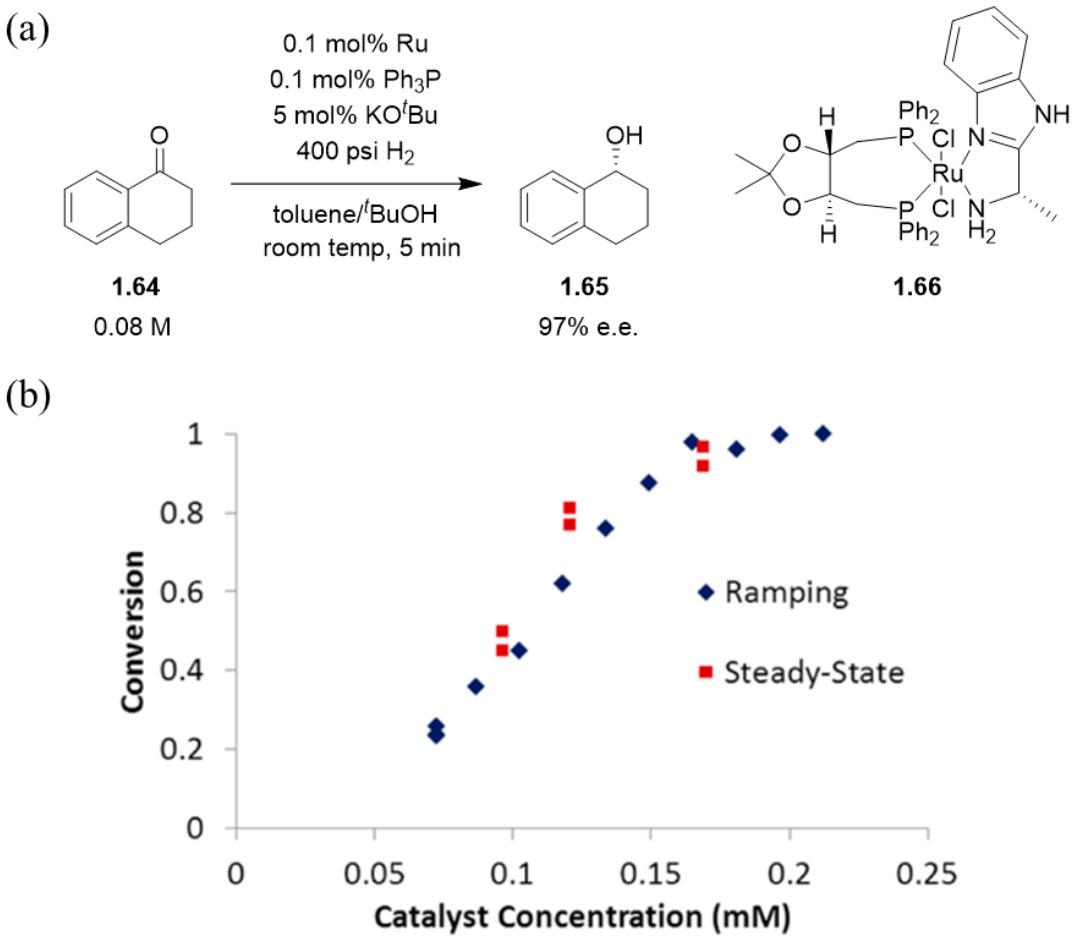
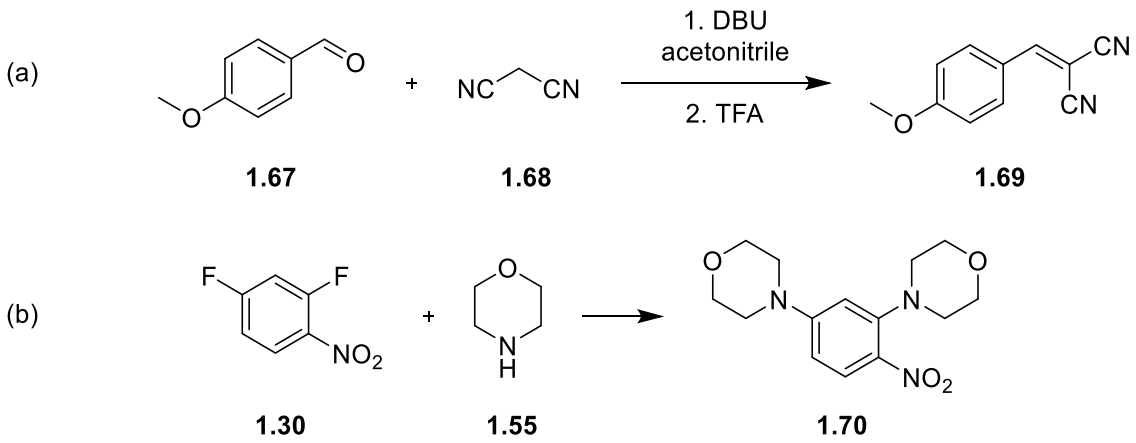


Figure 1.20. (a) asymmetric hydrogenation of ketone **1.64** with a homogeneous ruthenium catalyst **1.66**; (b) off-line GC results for the conversion of the hydrogenation reaction utilising a catalyst concentration ramp performed at a fixed residence time and temperature (figure reproduced from O'Neal *et al.*[66]).

Concentration ramps have also been combined with cumulative flow rate ramps to produce multivariate ramps to gather reaction data for model construction. Wyvratt *et al.* demonstrated linear and non-linear bi-variate residence time-additive equivalent ramps to construct a response model for a Knoevenagel reaction (Scheme 1.13a) utilising in-line FTIR and at-line HPLC analysis orthogonally (Fig. 1.21a).[67] This work demonstrated large time savings compared to steady state methods, but showed the importance of not varying relative flow rates too rapidly to maintain accurate data collection. The same system was also applied for self-optimisation of a reaction using transient flow methods for flow rate and additive concentration ramping for a multistep S_NAr reaction (Scheme 1.13b).[68] Non-linear bi-variate transient flow ramps were used to construct ellipsoids of data around an initial point in the design space (Fig. 1.21b), before the implementation of linear bi-variate ramps in the most promising direction.

This process was repeated until an optimum was found with an ellipsoid of less optimal conditions around it. This allowed efficient self-optimisation while simultaneously gaining more useful process information, although only in a relatively small two parameter design space.



Scheme 1.13. Reactions performed in studies by Wyvratt and McMullen: (a) a Knoevenagel condensation reaction;[67] and (b) a multistep S_NAr reaction.[68]

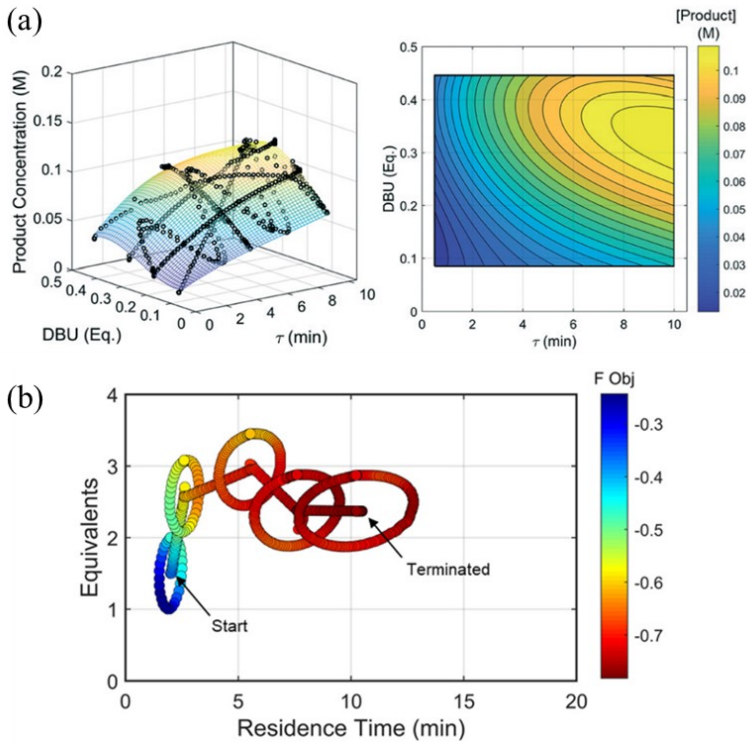
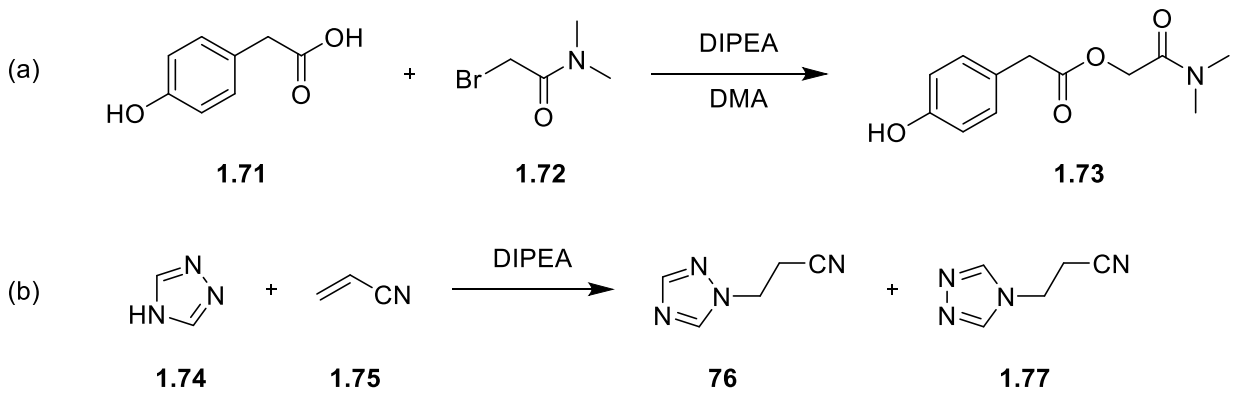


Figure 1.21. (a) response surface plot generated by fitting a polynomial function to bi-variate additive concentration-residence time ramp data (figure reproduced from Wyvratt *et al.*[67]) and (b) an example of a self-optimisation experimental run performing bi-variate additive concentration-residence time ramps utilising a similar flow system (figure reproduced from McMullen and Wyvratt[68]).

Jensen and co-workers performed tri-variate non-linear ramps on time, temperature, and additive equivalents studying an S_N2 ester formation from alkyl bromide **1.72** (Scheme 1.14a).[15] This data was collected by coupling an in-line FTIR with an on-line HPLC-MS to construct a response model for the product yield in this high dimensional design space, also deriving theoretical limits to ramp rate speed (see section 1.3.2). Although this approach was performed on three parameters, there is no theoretical limit to the number of parameters ramped. In fact, recently, Kappe and co-workers applied a five parameter multivariate ramping method to an aza-Micheal reaction which forms regioisomeric products (Scheme 1.14b).[69] The reaction data was used to derive a kinetic model for all the competing reaction pathways, and to build a predictive model for the reaction outcome dependent on residence time, temperature, and three independent species concentrations. Dense and quantitative data collection was facilitated by in-line FTIR and on-line NMR utilising the orthogonal spectroscopic methods to quantify the starting 1,2,4-triazole (**1.74**) and products **1.76** and **1.77** by in-line FTIR, and DIPEA and acrylonitrile concentrations by on-line NMR as IR peaks were challenging to determine.



Scheme 1.14. (a) the S_N2 ester formation reaction performed by Jensen and co-workers;[15] (b) the aza-Micheal reaction studied by Kappe and co-workers.[69]

Beyond residence time, temperature, and reactant concentrations there are many other valuable reaction parameters yet to be explored in an efficient manner. The most obvious example would be ramping the pH of the solution, although this is similar to previously reported additive concentration ramps, a pH method would have great utility.

There are further applications of multivariate transient flow experiments in photo- and electrochemistry that are yet to be explored. Although the effect of residence time has been investigated in photochemical reactions, transient flow could act as a more unique tool for studying the effect of light intensity or wavelength in an efficient manner. Similarly in electrochemistry, no transient flow methods have been performed despite the likely utility in efficient study of different potentials and current densities. There are however challenges in applying transient flow to photo- and electrochemistry due to current equipment not designed for this application. Current light sources can be too inhomogeneous to obtain good transient flow results and both commercial photochemical and electrochemical set ups often lack real time continuous tuneability of parameters. Despite this, once the equipment is available this will be a very promising future area.

5 Conclusions

Transient flow experimentation has grown significantly as a field in the last decade both in the different systems which can be studied, including catalytic and heterogeneous reactions, and also in the manner and diversity of reaction parameters which can be varied (residence time, temperature, concentrations). Despite this growth both in breadth of techniques and usage, there is still some way to go to maximise the impact of this technique. We are still seeing new reaction parameters added to the transient flow arsenal, more complex reaction systems being studied by more complex analytical tools, and more applications of the data produced from these systems. As the reaction space becomes larger we have also seen interest in the development of tools for selection of the optimal transient flow methods.[61,62,70–72] As we seek to tackle bigger and more complex chemical problems, these approaches will become a necessity to ensure efficient implementation of transient flow methods.

Interestingly, much of the work on transient flow methods in the last 10 years had been, in fact, described in a patent published in 2004.[73] Within this patent the claim is made over linear and non-linear transient flow methods changing residence time, flow rate, and additive concentration both individually and

simultaneously to collect reaction data for optimisation of chemical reactions in flow. This broad claim also includes the use of an automated control system for the flow system and the use of in-line and on-line analytical tools and sampling. As often with patents, although the patent claims are broad and question the novelty of much of the last decade of research in transient flow, it is likely that the examples on which the patent are based were a small subset of what is claimed as feasible and thus significant progress has been made in the last decade. This patent also invokes questions about the commercial use of transient flow. To date, transient flow methods are primarily an academic pursuit and have had limited use in industrial settings, as the field gains more examples, methods become more standardised, and equipment becomes more accessible this is likely to change rapidly.

The inclusion of transient flow as a tool in a chemist's toolbox will greatly improve the quality and quantity of reaction data collected and subsequently the chemical solutions we can develop. Technical challenges in methods and equipment are being combatted by a growing community of likeminded scientists increasing the utility of transient flow and lowering the technical barrier to use, although specialised skills are still required to implement transient flow. A greater hurdle may be a cultural barrier among chemists who may value traditional practical synthetic skills and intuition led investigations. Further demonstration of the value gained from transient flow methods in synthetic organic labs and clear communication with the community about synergies with existing workstreams should help bring about positive cultural change.

6 Aim and objectives

In this thesis the primary aim was to develop new methods to efficiently collect and use chemical reaction data in flow for the investigation of organic chemical reactions. The comprehensive assessment of the literature above informed the questions to be investigated to maximise impact of this work, which will be assessed in the conclusions (Chapter 5):

(i) What is the easiest method for collecting time series data in flow, without compromising accuracy?

(ii) Can the continuous reaction parameter space that can be investigated by transient flow methods be extended to provide efficient investigation of a more diverse reaction space? How can this data be best used?

(iii) How can we extend the benefits of transient flow to investigate traditionally discrete reaction parameters?

These questions will be investigated through the implementation, comparison, and development of different transient flow methods and successful answering of these questions will produce multiple novel transient flow methods. In order to ensure the data produced from such methods would be useful, chemical reactions investigated were suggested by industrial collaborators at BASF. It was hoped that the investigation of these example reactions would not just allow method development, but also produce valuable insights into these reactions through kinetic and mechanistic investigation of the effects of different parameters upon these reactions.

The structure of the thesis aims to demonstrate the progress towards the aim. In this introduction, the field of transient flow has been reviewed, grouped by the reaction parameter under investigation. Chapter 2 provides benchmarking of different methods for the most ubiquitous form of transient flow – time series data collection – providing a robust comparison to assess these techniques. The Knorr pyrazole synthesis is then investigated more thoroughly (Chapter 3), allowing the development of a novel reactant

stoichiometry ramp and confirming the use of this and other methods in providing deep insight into the kinetics of this reaction. Discrete reaction parameters are then targeted in the investigation of substituent and solvent effects on the aromatic Claisen rearrangement (Chapter 4). Novel implementation of 'one-pot' methods in flow provide an efficient means of studying the effect of substituent, and solvent ramps demonstrate a novel transformation of solvent from a discrete reaction parameter to a *pseudo*-continuous parameter.

Chapter 2: Comparison of time series data collection in continuous flow

1 Introduction

1.1 Aim and objectives

This Chapter focusses on empirical comparison of simple cumulative flow rate methods for collection of residence time series data. As discussed in Chapter 1 Section 2.2, cumulative flow rate methods have proven effective and general methods for collection of residence time series data, however, no direct comparison has been made between data collected from flow rate step change methods and flow rate ramping methods. For the study described in this Chapter, comparisons are limited to step changes and linear flow rate ramps, not including linear residence time ramps, which require exponential flow rate ramps, to minimise the complexity of automation and control needed for a chemist to implement these methods. The Chapter begins with a discussion of similar work reported previously and the mathematical deconvolution of such approaches, followed by an introduction to the chemical reactions used to compare the methods (Section 2.1) and the flow systems built in which to perform these methods (Sections 2.2 and 2.3). Finally, the results of the method comparisons for each example will be presented, and the implications of the results will be discussed.

The aim for the work in this Chapter is to compare and contrast transient cumulative flow rate methods across a range of chemical reactions, by using two different flow system configurations, with different analytical tools (in-line FTIR and on-line HPLC). This work justifies the methods adopted in later chapters for collecting time series data in flow.

1.2 Background

Prior to the development of transient flow (TF) experiments, it was widely accepted that it is easier to collect kinetic data using batch reactors, compared to using steady state methods in flow.[31] Although steady state methods provide more accurate reaction data, they are too time and material intensive. In the past 15 years, the emergence of a diverse range of transient flow approaches (Chapter 1, Section 2)

began to challenge this perception, by vastly improving data collection efficiency. In order for these new techniques to be adopted, significant benefits over batch experiments must be demonstrated. While the early development of TF methods, involving switching on an energy source or changing the volume of the reactor (see Chapter 1, Section 2.1), improved the time efficiency and data quality of kinetic experimentation, these systems lack general reaction applicability. In comparison, cumulative flow rate changing methods (flow rate step changes and ramps) are easier to implement and more general, as reactions initialised by mixing reagents and/or heating can also be monitored (see Chapter 1, Section 2.2).

Cumulative flow rate step changes were first developed by Mozharov *et al.* in 2011 which were demonstrated to produce kinetic data five times faster than steady state methods.[39] This work focused on "push-out" (PO) step changes in which the initial steady state is at a lower flow rate than the flow rate after the step change. Deviations were reported between the reaction data obtained from this method and steady state methods, purportedly due to the time taken for the flow rate to increase to the higher flow rate. This work compared a range of PO step change flow rates with initial flow rates between 0.2 – 2.4 μL min^{-1} and final flow rates between 4 – 20 μL min^{-1}.

Further comparison between PO step changes, "reverse push out" (RPO) step changes (high to low flow rate) and steady state methods was performed by Durand *et al.*.[40] They noted that a PO step change is likely to have greater error than a RPO step change but uses less material, claiming that the initial higher flow rate for a RPO step change requires a greater volume of solution to reach steady state. However it was noted that RPO step changes are useful when sampling rate is a limitation, although they also suggest smaller PO step changes to combat such a case.

Methods which ramp the cumulative flow rate of the reactor to affect the residence time require greater pump control as the flow rate must be changed gradually. Generally the function of the flow rate ramp

has been either linear[48] or exponential,[49] in order to generate a linear residence time ramp. These ramps have generally been performed in a RPO type manner beginning at a high flow rate and gradually transitioning to a lower flow rate. This direction of ramping seeks to mimic batch experimental data by initially monitoring short reaction times and then gradually longer reaction times. Using the logic of Durand *et al.*[40] it would be expected that this approach would consume more material than the PO ramp for the same quality of data, however, no direct comparison has been performed between PO and RPO flow rate step changes and ramps for investigating a reaction.

In the following studies, comparisons are limited to simple methods that can be easily implemented with standard HPLC pumps. Although some HPLC pumps have the capability to perform exponential flow rate ramps or can be remotely controlled, the methods were limited to linear flow rate ramps, both PO and RPO, as the most generally implementable. This decision was also made as linear flow rate ramps and linear residence time ramps (exponential flow rate ramps) appear to produce similar quality results (see Chapter 1, Section 2.2.2) and thus not all need be compared.

1.3 Mathematical deconvolution

Mathematically, all cumulative flow rate methods have the same underlying mathematical principles. As the cumulative flow rate is an integral parameter (see Chapter 1, Section 1.4), the entire reactor volume is affected by a change in cumulative flow rate. Each differential volume element (or "slice") of the reaction effluent must traverse through the volume of the reactor as propelled by the cumulative flow rate (Q). If this cumulative flow rate is a function of the experimental time ($Q(t)$, *e.g.* in transient flow) then the differential volume (dV) for each differential time element (dt) must be calculated and integrated between the time at which the slice enters the reactor (t_i) and the time it exits the reactor (t_f) which will give the residence time (τ) (Equations 2.1 – 2.3).

$$\frac{dV}{dt} = Q(t) \qquad \text{[Eq. 2.1]}$$

$$\tau = t_f - t_i \qquad \text{[Eq. 2.2]}$$

$$\int_0^{V_R} dV = V_R = \int_{t_i}^{t_f} Q(t)dt \qquad \text{[Eq. 2.3]}$$

In the same manner, any dead volume between the reactor and the analytical tool is also affected by the cumulative flow rate function and can be evaluated similarly by integration of the dead volume (V_D) between the time at which the slice exits the reactor (t_f) and the measurement time (t_m) (Fig. 2.1).

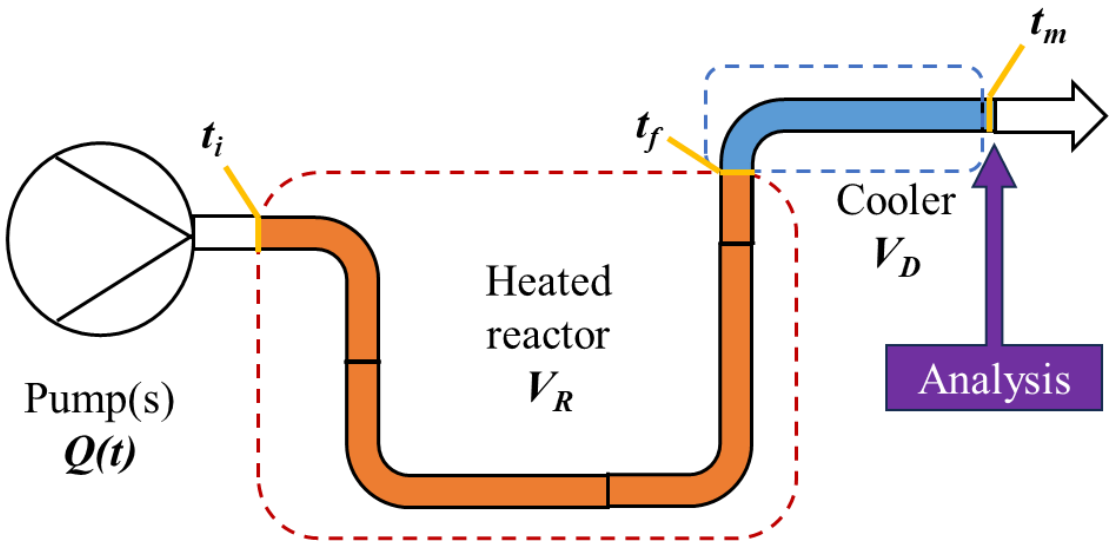


Figure 2.1. Diagrammatic representation of a generic flow reactor system with a dead volume between reactor and analysis device.

The evaluation of the integral is dependent on the cumulative flow rate function(s) utilised, in this case consisting of a step change or a linear ramp (Fig. 2.2). Such flow rate functions have points of discontinuity at which the function changes and thus these integrals must be separated at the points of discontinuity, such as at the step change itself. Figure 2.2 outlines the four method types investigated in the following study as the cumulative flow rate function changing over the experimental time ($Q(t)$): RPO step change, PO step change, RPO ramp, and PO ramp.

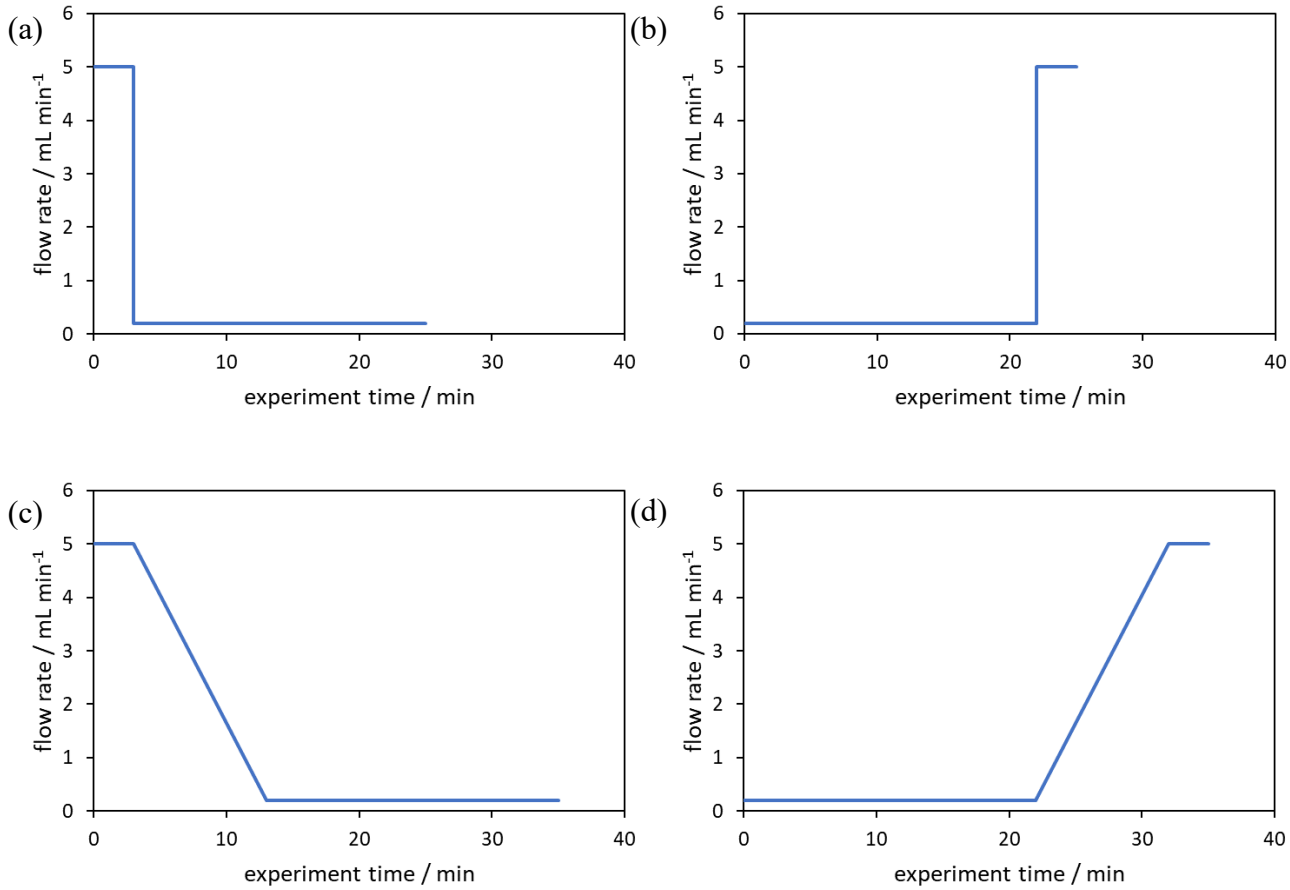


Figure 2.2. Example plots of cumulative flow rate functions with respect to experimental time for: (a) a RPO step change; (b) a PO step change; (c) a RPO ramp; (d) a PO ramp.

1.3.1 Flow rate step changes

For a generic system of reactor volume (V_R) and post reactor dead volume (V_D) before the analytical device, a step change of flow rate from an initial cumulative flow rate (Q_0) to a final cumulative flow rate (Q_{end}) performed instantaneously at t = 0 is evaluated as follows to determine the residence times produced:

$$V_R = \int_{t_i}^{t_f} Q(t)dt = \int_{t_i}^{0} Q_0\, dt + \int_{0}^{t_f} Q_{end}\, dt \qquad \text{[Eq. 2.4]}$$

$$V_R = -Q_0 t_i + Q_{end} t_f \qquad \text{[Eq. 2.5]}$$

There is a flow rate function discontinuity at $t = 0$ when the flow rate is instantaneously changed, leading to two integrals. Substituting for τ and rearranging gives:

$$\tau = \frac{V_R - (Q_{end} - Q_0)t_f}{Q_0} \quad \text{[Eq. 2.6]}$$

However the analytical device is monitoring at a fixed volume after the reactor (V_D), and so this must also be evaluated to give a function for τ in terms of the measurement time (t_m); this time only as one integral as the relevant reaction effluent in this volume will only experience the final flow rate (Q_{end}):

$$V_D = \int_{t_f}^{t_m} Q_{end} dt = Q_{end} t_m - Q_{end} t_f \quad \text{[Eq. 2.7]}$$

$$t_f = t_m - \frac{V_D}{Q_{end}} \quad \text{[Eq. 2.8]}$$

Substituting this into Equation 2.6 gives:

$$\tau = \frac{V_R - (Q_{end} - Q_0)(t_m - \frac{V_D}{Q_{end}})}{Q_0} \quad \text{[Eq. 2.9]}$$

This function for τ holds true for both PO and RPO step changes between $\tau = \frac{V_R}{Q_0}$ and $\tau = \frac{V_R}{Q_{end}}$ which when substituted into Eq 2.9 give limits of t_m outside of which steady state residence times are achieved:

$$\frac{V_D}{Q_{end}} < t_m < \frac{Q_0(V_R + V_D) - Q_{end} V_D}{Q_{end}(Q_0 - Q_{end})} \quad \text{[Eq. 2.10]}$$

1.3.2 Linear flow rate ramps

For a generic system (Fig. 2.1) of reactor volume V_R and post reactor dead volume V_D before the analytical device, a linear flow rate ramp from an initial cumulative flow rate (Q_0) to a final cumulative flow rate (Q_{end}) at a constant ramp rate (ρ) begun at $t = 0$ and finishing at t_{end} must be evaluated in three separate regimes between the initial and final steady states (Fig. 2.3). In previous derivations of residence time from linear flow rate ramps, only the central regime (B) has been evaluated and any dead volume between the end of the reactor and the analytical device (V_D, Figure 2.1) was not accounted for.[48] Some work on linear residence time ramps has accounted for the dead volume, however only a single flow rate function regime was evaluated.[49]

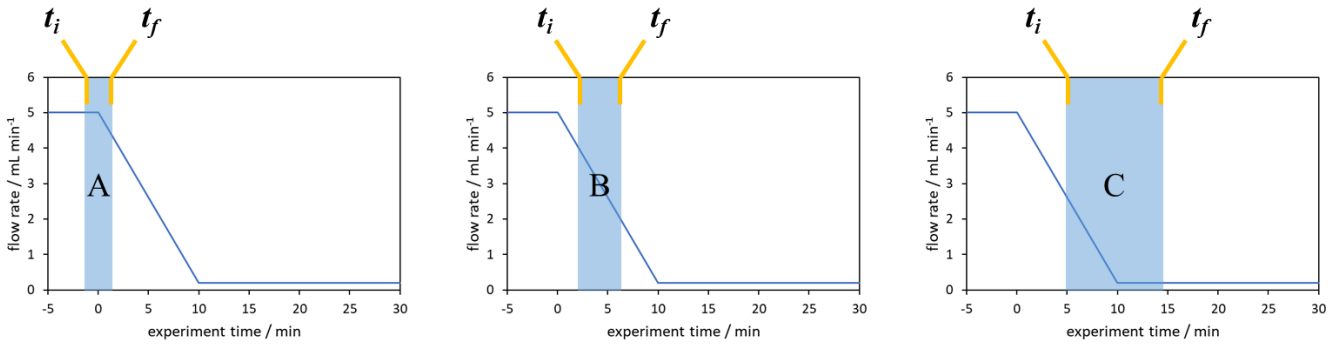


Figure 2.3. The different regimes that must be solved to mathematically deconvolute the residence time from experimental time for a linear flow rate ramp, in this case demonstrated on the RPO ramp from Fig. 2.2c.

Regime A corresponds to when $t_i < 0$ and $t_f > 0$:

This regime requires evaluation of two separate flow rate functions expressed as two limited integrals:

$$V_R = \int_{t_i}^{t_f} Q(t)dt = \int_{t_i}^{0} Q_0\, dt + \int_{0}^{t_f} Q_0 - \rho t\, dt \qquad \text{[Eq. 2.11]}$$

Integrating gives:

$$V_R = Q_0(t_f - t_i) - \frac{1}{2}\rho {t_f}^2 \qquad \text{[Eq. 2.12]}$$

Substituting for τ gives:

$$\tau = \frac{1}{2}\frac{\rho}{Q_0}{t_f}^2 + \frac{V_R}{Q_0} \qquad \text{[Eq. 2.13]}$$

The dead volume can be evaluated as one integral for any data after the initial steady state:

$$V_D = \int_{t_f}^{t_m} Q(t)dt = \int_{t_f}^{t_m} Q_0 - \rho t\, dt \qquad \text{[Eq. 2.14]}$$

Integrating gives:

$$V_D = Q_0(t_m - t_f) - \frac{1}{2}\rho({t_m}^2 - {t_f}^2) \qquad \text{[Eq. 2.15]}$$

Solving this quadratic gives:

$$t_f = \frac{Q_0}{\rho} \pm \sqrt{(\frac{Q_0}{\rho} - t_m)^2 + \frac{2V_D}{\rho}} \qquad \text{[Eq. 2.16]}$$

where the positive or negative root depends on whether a PO or RPO ramp has been performed.

Regime B corresponds to when $t_i > 0$ and $t_f < t_{end}$:

This regime can be expressed as one integral:

$$V_R = \int_{t_i}^{t_f} Q(t)dt = \int_{t_i}^{t_f} Q_0 - \rho t \, dt \qquad \text{[Eq. 2.17]}$$

Integrating gives:

$$V_R = Q_0(t_f - t_i) - \frac{1}{2}\rho({t_f}^2 - {t_i}^2) \qquad \text{[Eq. 2.18]}$$

Substituting for τ gives:

$$0 = \frac{1}{2}\rho\tau^2 + (Q_0 - \rho t_f)\tau - V_R \qquad \text{[Eq. 2.19]}$$

Which solves to produce a solution for τ in terms of t_f:

$$\tau = \frac{-(Q_0 - \rho t_f) + \sqrt{(Q_0 - \rho t_f)^2 + 2\rho V_R}}{\rho} \qquad \text{[Eq. 2.20]}$$

where the positive root has been taken such that when $V_R = 0$, the residence time is 0.

Equation 2.20 is similar to the equation derived by Hone *et al.*,[48] although the sign in the squared term is different, perhaps due to a typographic error. The previous derivation was used to compare between different reaction temperatures and thus replaces the reactor volume (V_R) with the reactor length modified by a temperature dependent solvent expansion term, $\beta(T)$. For the lower temperature isothermal experiments compared in Section 3, temperature dependent solvent expansion effects are negligible and can be excluded. For later studies at significantly elevated temperatures above the solvent boiling point,

however, changes in solvent density have been included (Section 3.3.1). The derivation presented by Hone *et al.* does not correct for a dead volume between the end of the reactor and the analytical device (V_D). In the following derivation this has been corrected for by substituting t_f in terms of t_m as for regime A (Equation 2.16). For regime B, the conversion of t_f in terms of t_m holds until the limit:

$$t_m = t_{end} - \frac{V_D}{2Q_{end}} \qquad \text{[Eq. 2.21]}$$

Above this value of t_m, t_f can be derived as a dead volume time correction when $t_m > t_{end}$:

$$V_D = \int_{t_f}^{t_m} Q(t)dt = \int_{t_f}^{t_m} Q_{end}\, dt = Q_{end}(t_m - t_f) \qquad \text{[Eq. 2.22]}$$

Rearranging gives:

$$t_f = t_m - \frac{V_D}{Q_{end}} \qquad \text{[Eq. 2.23]}$$

Regime C corresponds to when $t_i > 0$ and $t_f > t_{end}$:

Similarly to Regime A, Regime C is set as two limited integral:

$$V_R = \int_{t_i}^{t_f} Q(t)dt = \int_{t_i}^{t_{end}} Q_0 - \rho t\, dt + \int_{t_{end}}^{t_f} Q_{end}\, dt \qquad \text{[Eq. 2.24]}$$

Integrating gives:

$$V_R = Q_0(t_{end} - t_i) - \frac{1}{2}\rho({t_{end}}^2 - {t_i}^2) + Q_{end}(t_f - t_{end}) \qquad \text{[Eq. 2.25]}$$

Substituting τ and rearranging to form a quadratic gives:

$$0 = \frac{1}{2}\rho\tau^2 + \left(Q_0 - \rho t_f\right)\tau - V_R + \left(t_f - t_{end}\right)(Q_0 - Q_{end}) + \rho\left(\frac{{t_{end}}^2 - {t_f}^2}{2}\right) \quad \text{[Eq. 2.26]}$$

which can be evaluated by use of the quadratic formula, again taking the positive root.

Utilising Equation 2.23 substituting for t_f into the residence time equation 2.26 deconvolutes this regime for when $t_f > t_{end}$ for a steady state between t_{end} and t_f.

Determining regime transition points

The transition point (Equation 2.21) between the two equations converting t_f to t_m (Equations 2.16 and 2.23), already derived above, is found by equating these two equations. Similarly the transition points between the regimes for the reactor volume can be derived (Equations 2.27 and 2.28). The transition points are defined in the limits of the integrals as changing when $t_i = 0$ and when $t_f = t_{end}$.

A to B when $t_i = 0$:

$$t_m = \frac{Q_0 - \sqrt{{Q_0}^2 - 2\rho(V_R + V_D)}}{\rho} \quad \text{[Eq. 2.27]}$$

B to C when $t_f = t_{end}$:

$$t_m = t_{end} + \frac{V_D}{Q_{end}} \quad \text{[Eq. 2.28]}$$

The values of t_m at which the deconvolution regimes change are important, in order to correctly deconvolute residence time values from all sections of a linear flow rate ramping experiment. Inclusion of all regimes of a linear flow rate ramp allows increased data to be obtained from an experiment than

previous deconvolution methods. Additionally, inclusion of dead volume terms in this evaluation can be utilised on more systems in which the analytical tool is not directly after the flow reactor and is therefore more generally applicable.

2 Method

Over the course of my PhD research, PO and RPO steps and linear ramps were compared for different chemical reactions, utilising a flow system constructed during the course of the PhD, which was modified for each reaction. The following sections briefly introduces each chemical reaction (Section 2.1), followed by a discussion on the construction and modification of the flow systems (Section 2.2 and 2.3). Deeper discussions on the kinetic data collected for each chemical reaction, and associated analyses, will be covered in more detail in later chapters.

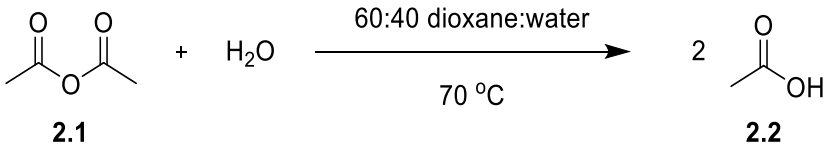
2.1 Example chemical reactions

Three different chemical reactions were studied during the course of this work, to cover a range of the chemical space, with varying levels of complexity. These reactions were also further studied in work on other reaction parameters as described in later Chapters.

2.1.1 Acetic anhydride hydrolysis

The hydrolysis of acetic anhydride to acetic acid (Scheme 2.1) is an exothermic reaction widely used as a benchmark for testing calorimetric systems.[10,74,75] In the presence of excess water, it is a *pseudo*-first order reaction, however its exothermic nature (enthalpy of reaction of -63 kJ mol^{-1} reported in water[10]) can make accurate analysis challenging due to reaction temperature discrepancies. In this work, it was envisaged that this reaction could be studied by in-line FTIR due to the distinct IR absorbances of the anhydride O-C-O bond compared to acetic acid. Previously, kinetic data has been collected on this reaction in flow using a linear residence time ramp with in-line flow calorimetry (see Chapter 1, Section

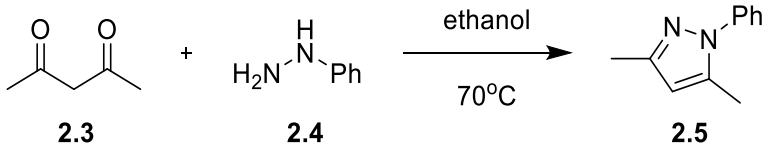
2.2.2).[10] In order to maintain a homogeneous reaction mixture, a mixture of dioxane and water was utilised, as reported in previous studies.[76,77]



Scheme 2.1. The hydrolysis of acetic anhydride utilised in this study, performed in a dioxane-water solvent mixture.

2.1.2 Knorr pyrazole synthesis

The Knorr pyrazole synthesis is a double condensation reaction between a 1,3-diketone and a hydrazine to form the pyrazole heterocycle. The specific reaction chosen for this study was the reaction between acetyl acetone (**2.3**) and phenyl hydrazine (**2.4**) (Scheme 2.2). This bimolecular reaction has a more complex reaction pathway than the hydrolysis of acetic anhydride. The reaction kinetics of this reaction was previously studied in flow, performing an energy source switch on method to collect time series data to fit to a global rate law (Scheme 1.12).[63] A modified version of the reaction was also used to exemplify an approach to accurately maintain reactant stoichiometry in a flow system, supported by in-line FTIR analysis.[78]

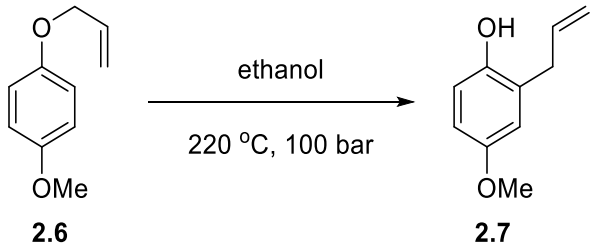


Scheme 2.2. The Knorr pyrazole synthesis reaction performed for this study between acetyl acetone (**2.3**) and phenyl hydrazine (**2.4**).

2.1.3 Aromatic Claisen rearrangement

The aromatic Claisen rearrangement is a [3,3]-sigmatropic pericyclic rearrangement reaction, which is generally thermally activated (Scheme 2.3). This reaction was chosen due to the first order reaction kinetics and extreme conditions (>200 °C) required. The methoxy substituted reactant **2.6** and product **2.7** were analysed quantitatively by on-line HPLC for this study. This reaction has been studied

kinetically in batch reactors in high boiling solvents, asserting the first order kinetics.[79] A previous study reported the investigation of this reaction in ethanol in flow, to facilitate the extreme process window required, utilising only inefficient steady state methods to collect kinetic data.[80]



2.6 **2.7**

Scheme 2.3. The aromatic Claisen rearrangement of *para* methoxyphenyl allyl ether (**2.6**) to phenol product **2.7** under super-ambient conditions.

2.2 Flow system: Configuration 1 (ReactIR)

2.2.1 System development and construction

A flow system (Fig. 2.4) was constructed for the analysis of liquid-phase reactions at elevated temperatures and pressures, prioritising the control of flow rates and temperatures in order to accurately perform transient flow methods.

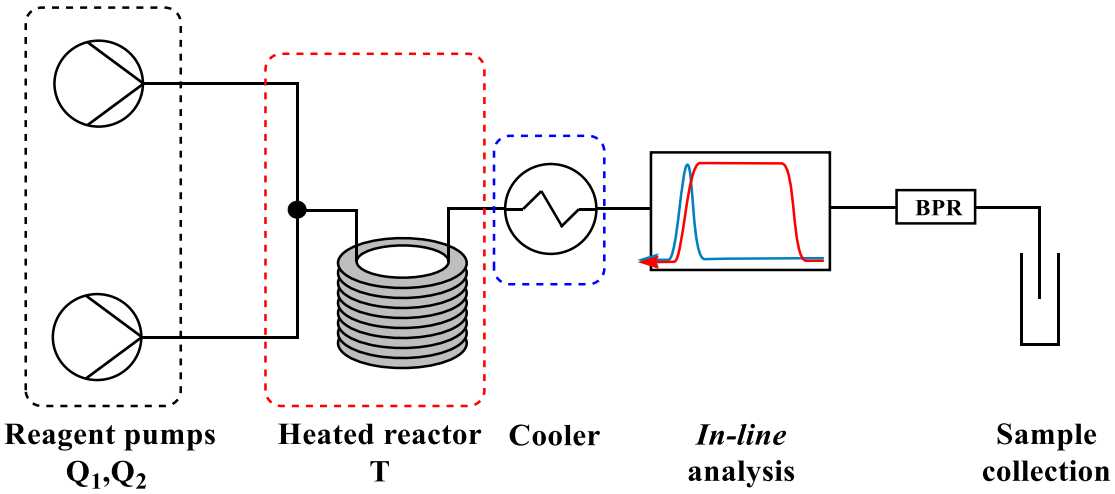


Figure 2.4. Schematic of the flow system for the control of individual flow rate (Q_1 and Q_2) and temperature (T), with in-line analytics.

Fourier transform infrared spectroscopy (FTIR) was selected as an accurate and rapid in-line analytical tool for studying the hydrolysis of acetic anhydride and the Knorr pyrazole synthesis. The flow reactor system consists of two HPLC pumps, which feed the reactants into a T-piece mixer connected to a stainless steel tubular reactor, heated *via* an oil bath. The exit of the tubular reactor is rapidly cooled by a custom Peltier cooling system (Fig. 2.5) for thermal reaction quenching, before flowing directly into the flow cell of the in-line FTIR. The system is kept under an elevated pressure of 8 bar by a back pressure regulator at the end of the flow system, to maintain the reaction mixture in the liquid phase. Further details of the flow system can be found in the experimental (Chapter 6, Section 2.1).

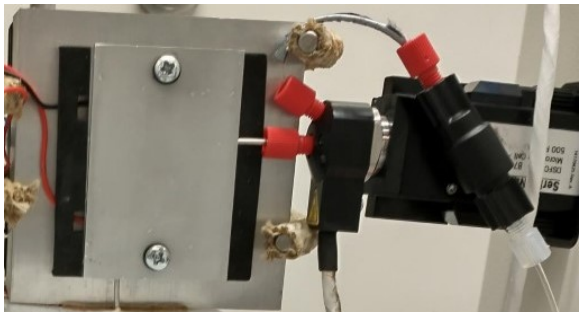


Figure 2.5. The 60 W Peltier assembly connected to a custom aluminium block, covered with insulation when in use, utilised for thermal quenching of reactions in the flow system.

2.2.2 ReactIR methods

In-line FTIR analysis was performed utilising a Mettler Toledo ReactIR 15 instrument, equipped with a 10 μL flow cell with a diamond ATR window. This allowed collection of reaction data at a scan rate of 15 seconds, while still affording good signal to noise.

Diagnostic peaks were identified for the hydrolysis of acetic anhydride from injections of acetic anhydride, acetic acid, and reaction mixtures into the IR flow cell. The optimal peaks were found in the 2nd derivative of the collected IR spectra, as the height to a two point baseline between 1004 – 992 cm^{-1} to a two point baseline at 1015 and 984 cm^{-1} (Fig. 2.6). Calibration of the relevant peak was performed at the start of each experimental run by injection of stock solutions from 0.1 – 0.01 M (prepared in

volumetric flasks by serial dilution) into the IR flow cell, with at least four point calibration for each experimental run. Often samples were also injected at the end of an experimental run to confirm that no drift had occurred in the selected peak. At the end of each experimental run the flow cell was flushed with ethanol and then cleaned with ethanol, water, acetone, and petroleum ethers, drying with compressed air between solvents.

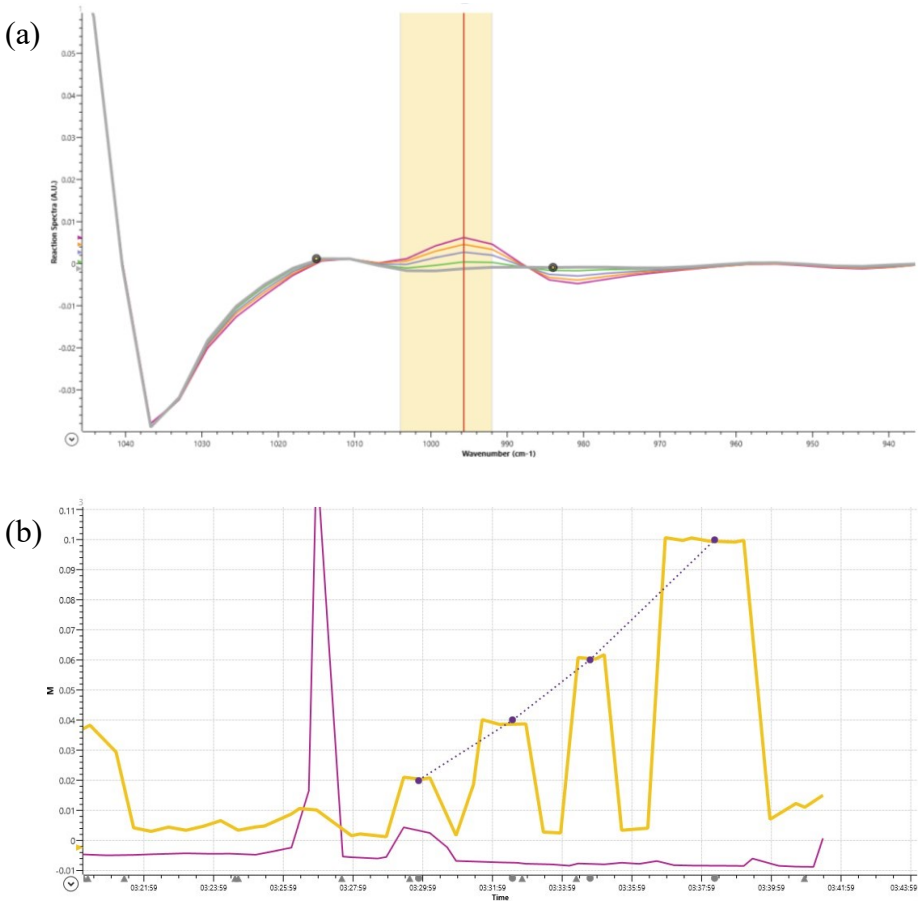


Figure 2.6. (a) example FTIR spectrum peak picking for acetic anhydride on 2nd derivative processed spectra; (b) example injections of acetic anhydride for calibration of the FTIR, calibrated with $R^2 = 0.99$.

Diagnostic peaks were identified for the pyrazole product (**2.5**) based on previous batch work and corroborated by individual injections and mixed injections of the reaction components, further verified by off-line HPLC. The optimal peaks were found in the 2nd derivative of the collected IR spectra as the height to a two point baseline between 1508 – 1496 cm^{-1} to a two point baseline at 1514 and 1495 cm^{-1} (Fig. 2.7). Other FTIR peaks also correlated with the pyrazole product concentration, but this peak had

the best sensitivity, while remaining independent of other reaction components. Identifying unique FTIR peaks for quantification of the reactants (compounds **2.3** and **2.4**) proved challenging, and quantification was similarly challenging using GC, UV/Vis, and off-line HPLC-MS, due respectively to high reactivity of starting materials, lack of distinct chromophores, and poor ionisation. Calibration was performed at the start of each experimental run by injection of known concentration samples from 0.236 – 0.028 M (prepared in volumetric flasks via serial dilution of three independent stock solutions) into the IR flow cell with at least four point calibration for each experimental run. Often samples were also injected at the end of an experimental run to confirm that no drift had occurred in the selected peak. The flow cell was cleaned in the same manner as for the hydrolysis of acetic anhydride example above.

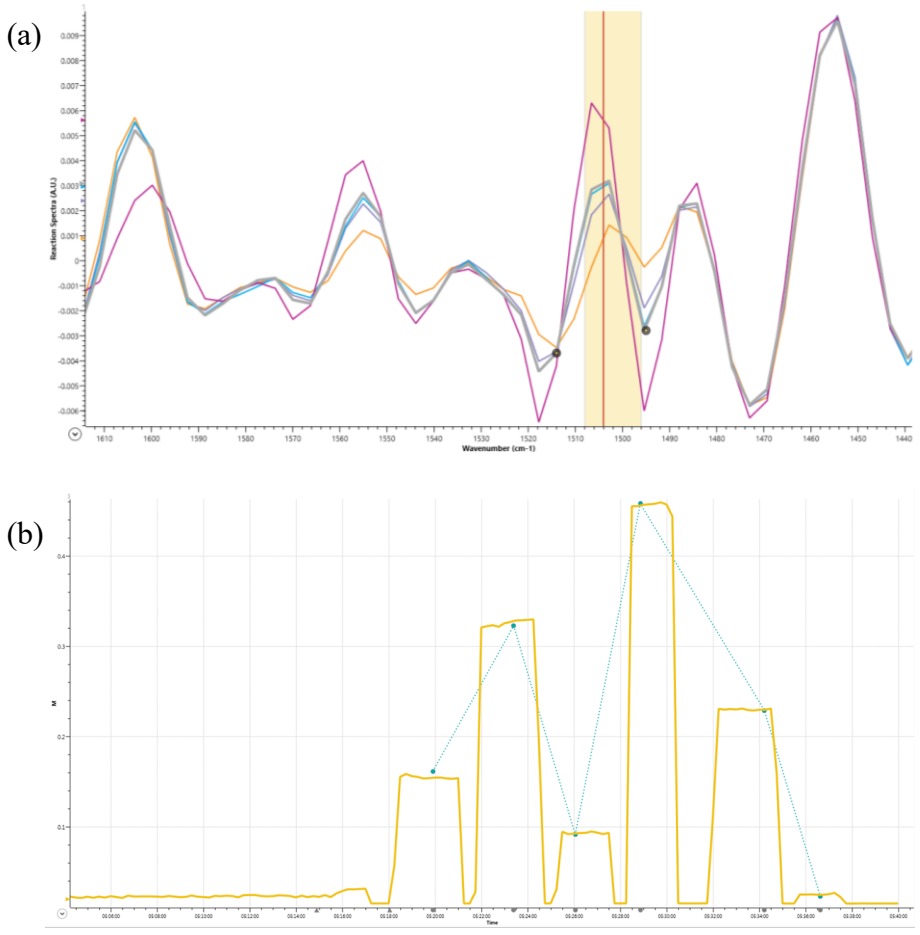


Figure 2.7. (a) example FTIR spectrum peak picking for pyrazole product **2.5** on 2nd derivative processed spectra; (b) example injections of pyrazole product **2.5** for calibration of the FTIR, calibrated with $R^2 = 0.99$.

2.2.3 Residence time distribution study

As discussed earlier (Chapter 1, Section 1.3.1), knowledge of the residence time distribution (RTD) of a flow system can allow better quality data to be produced from transient flow methods. A system with fluid dynamics similar to that of an ideal plug flow reactor (PFR), *i.e.* slow axial dispersion compared to the residence time, is the simplest to obtain reaction data from due to the assumption that each differential volume element is a self-contained reaction.[12]

Utilising the pyrazole product **2.5** as a tracer, the RTD of the flow system was investigated by varying the flow rate ratio of a tracer solution in ethanol and a pure ethanol stream. A step change in tracer concentration was introduced to the system by maintaining a constant tracer solution pump flow rate, while performing a downwards (RPO) step change for the ethanol feed. Utilising in-line FTIR, the corresponding changes in the concentration of the tracer can be collected. Initial experiments performing step changes from ethanol with no tracer feed were hampered in curve fitting as the beginning tracer concentration changes were below the sensitivity limit of the FTIR. It was found that performing the step change in tracer concentration between two non-zero concentrations provided much more valuable data for the RTD studies. A sigmoidal change in tracer concentration was observed and was fitted to the dispersion function (Equation 1.2) in order to calculate the Péclet number (Pe) for this system and hence a description of the extent of the deviation of the system from an ideal PFR (Fig. 2.8).[12]

$$Pe = \frac{L\,u}{D} \qquad \text{[Eq. 1.1]}$$

where Pe = Péclet number (dimensionless), L = characteristic length (m), u = local flow velocity (m s^{-1}), and D = mass diffusion coefficient (m^2 s^{-1}).

$$\frac{dF}{d\theta} = \frac{e^{-\frac{Pe(1-\theta)^2}{4}}}{\sqrt{12.566/Pe}} \qquad \text{[Eq. 1.2]}$$

where F = normalised tracer concentration response to a step change in tracer concentration, θ = normalised residence time, and Pe = Péclet number.

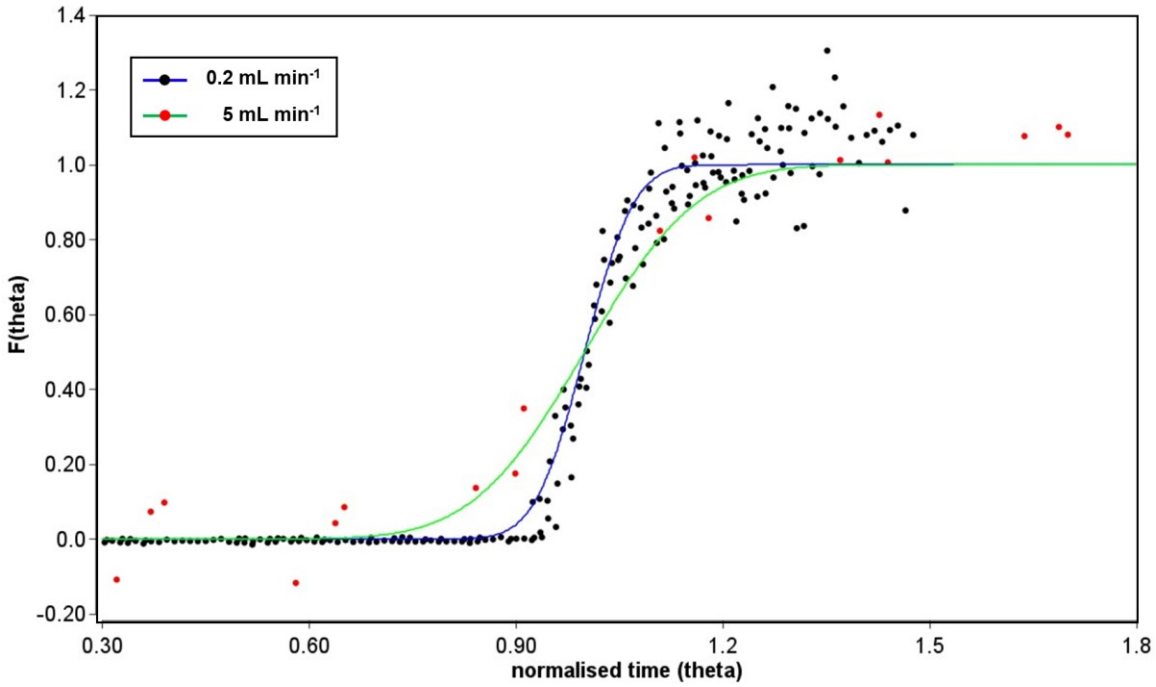


Figure 2.8. Example residence time distribution data fitted in Berkeley Madonna according to equation 1.2 (F(θ) *vs.* θ where θ = normalised residence time) to determine the Péclet number for the system under reaction conditions at the standard initial cumulative flow rate (Q_0, 0.2 mL min^{-1}) and final cumulative flow rate (Q_{end}, 5 mL min^{-1}). Curve fitting had root mean square error (RMSE) equal to 0.066 for 0.2 mL min^{-1} and 0.083 for 5 mL min^{-1}.

The results from the RTD study confirmed that, at the reaction temperature of 70 °C, the mean residence times were as expected. The Péclet numbers for the flow system at minimum and maximum flow rates were calculated (at 0.2 mL min^{-1} *Pe* = 690, at 5 mL min^{-1} *Pe* = 129) and were found to have minimal deviation from an ideal PFR.

The RTD data for intermediary flow rates was then collected which suggested some intermediary flow rates produced RTD curves with a greater deviation from ideal plug flow assumptions (Fig. 2.9). RTD curves were collected for 0.5, 1.5, 2.5, 2.6, and 3.7 mL min^{-1} to assess the Péclet numbers for the system. Between flow rates. 2.5 – 3.7 mL min^{-1} dispersion coefficients (X = 1 / Pe) greater than 0.01 were calculated, which is the generally accepted cut off for assumption of a plug flow fluid dynamic regime. Surprisingly, this data suggests that although low (0.2 – 1.5 mL min^{-1}) and high (5 mL min^{-1}) flow rates fall under the assumption of negligible deviation from an ideal plug flow reactor, the intermediary flow

rates do not. This could be explained by suggesting that high pump rates have increased pulsation which increases radial mixing, but it is also possible that the Péclet number collected at 5 mL min^{-1} is an outlier, although the data point at 3.7 mL min^{-1} could also. Removal of one outlier would lead to either a linear dependency of 1/Pe *vs.* flow rate, or a parabolic dependency. For the majority of the work performed in this thesis, only flow rates of 5 mL min^{-1} or between 0.1 and 2 mL min^{-1} were utilised, which are likely within a small deviation from ideal plug flow. Cumulative flow rate ramps utilise intermediary flow rates within this region of more complex fluid dynamics, however this appears not to affect the results.

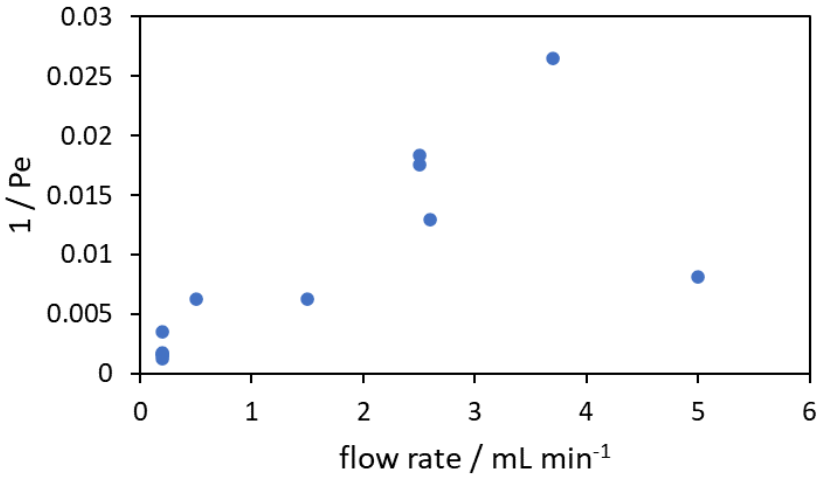


Figure 2.9. The quotient of the Péclet number plotted against flow rate demonstrating the changing flow regime, deviating from plug flow, with increased flow rate.

2.3 Flow system: Configuration 2 (on-line HPLC)

2.3.1 System development

For the study of the aromatic Claisen rearrangement (Scheme 2.3), the original flow reactor system described above in Section 2.2.1 was modified (Fig. 2.10). The fluidic pathway for the reaction was generally kept the same, and therefore RTD analysis was not repeated on this system. The in-line ReactIR was substituted for an on-line HPLC system, further modified to include an in-line dilution pump for use with higher concentration reactions. The oil bath was replaced with a programmable (GC) oven, to provide accurate temperature ramping, and the back pressure regulator was changed to a one

that can maintain the system under a pressure of 100 bar. The mixer was also moved out of the heated zone in order to facilitate pre-mixing of thermally activated reactions before introduction to the heated reactor. Further details on this flow system can be found in the experimental (Chapter 6, Section 2.2).

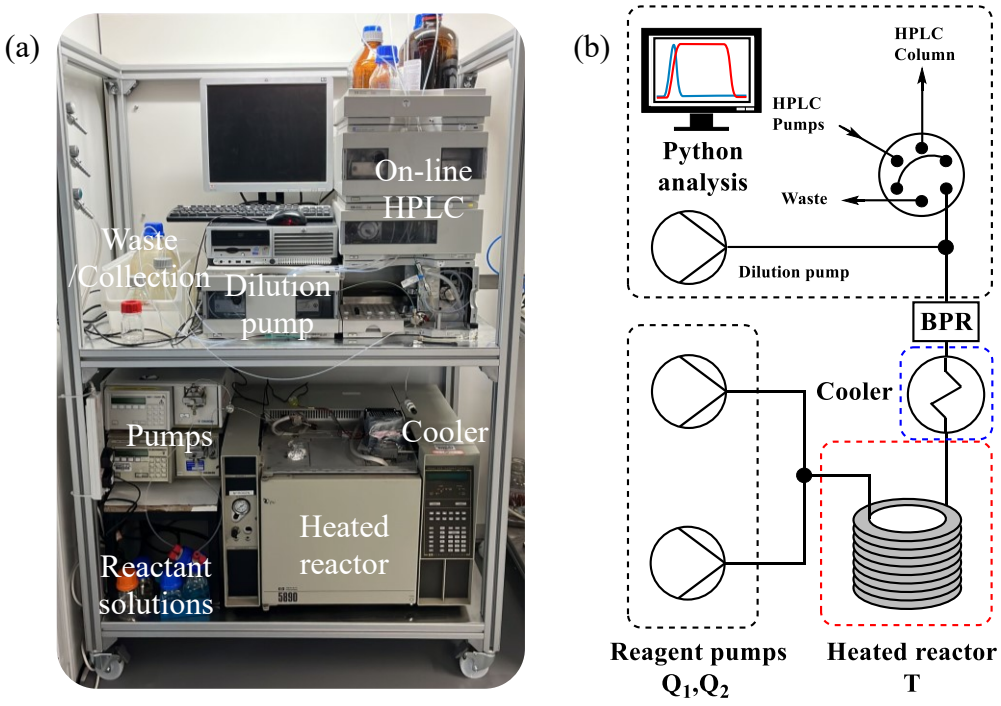


Figure 2.10. (a) the on-line HPLC flow system constructed (configuration 2); (b) a schematic representation of the fluidic path and key components of the on-line HPLC flow system.

2.3.2 On-line HPLC methods

The HPLC instrument was fitted with a diode array detector (DAD) for analysis of reaction component peak areas. The HPLC injector valve was modified to accommodate on-line HPLC analyse of reaction aliquots obtained from the flow path (Fig. 2.11). Dead volumes within the HPLC were minimised to ensure rapid HPLC methods could be developed. The modified valve allows injection of a 0.6 µL sample, which can be a reaction aliquot or a diluted reaction aliquot if needed, using the connected dilution pump, controlled by the HPLC software.

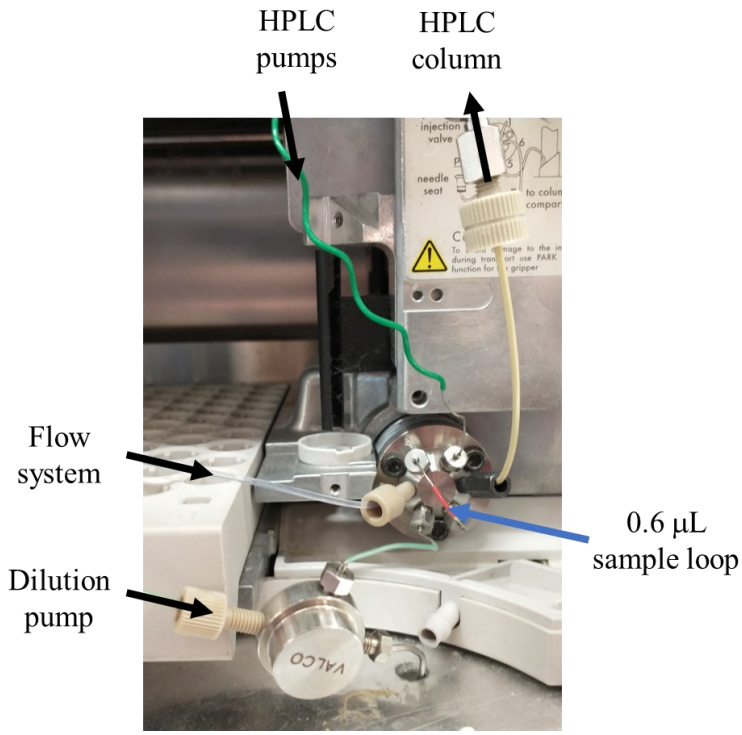


Figure 2.11. The modified HPLC injection valve on the Agilent 1100 series G1313A autosampler for on-line HPLC analysis.

The aromatic Claisen rearrangement reaction was analysed on a C18 HPLC column implementing a isocratic method of 40% acetonitrile in water. This method allowed rapid quantitative analysis of starting material and product concentrations, injecting a new sample from the reaction stream every 4 minutes. The reaction produced quantitative data due to the inclusion of an internal standard (ethyl benzene) in the reaction mixture. Peak areas were calibrated utilising methods outlined in Chapter 4, although non-quantitative direct peak area comparison could also be used for this study. This reaction mixture was injected without dilution of reactant stream. Analysis was performed on a Restek Raptor C18 column (2.7 µm 50 mm x 2.1 mm).

3 Results and discussion

3.1 Acetic anhydride hydrolysis

Performed using the reactor in configuration 1 as outlined in Section 2.2, reaction mixtures were generated by mixing 0.2 M acetic anhydride in dioxane (pump 1) with 1:4 dioxane:water (pump 2).

Kinetic data was recorded between cumulative flow rates of 0.2 and 5 mL min^{-1} at 90 °C. Under these conditions, conversions of up to 99% were observed with a residence time of 20 min.

3.1.1 Steady state and small step changes

Initially, conversions were collected for individual steady state flow rates at 5, 2, 1, 0.4, and 0.2 mL min^{-1} and then repeating 1 and 5 mL min^{-1} (Fig. 2.12a), changing between each steady state as a well-defined step change. This produced comparative data between steady state values and for RPO and PO step changes (Fig. 2.12b). These results showed very good agreement between steady state values (black asterisks) and those obtained from the small RPO step changes (coloured diamonds), however they showed more error in the small PO step changes (coloured squares), potentially simply due to the larger change in flow rate performed in these cases.

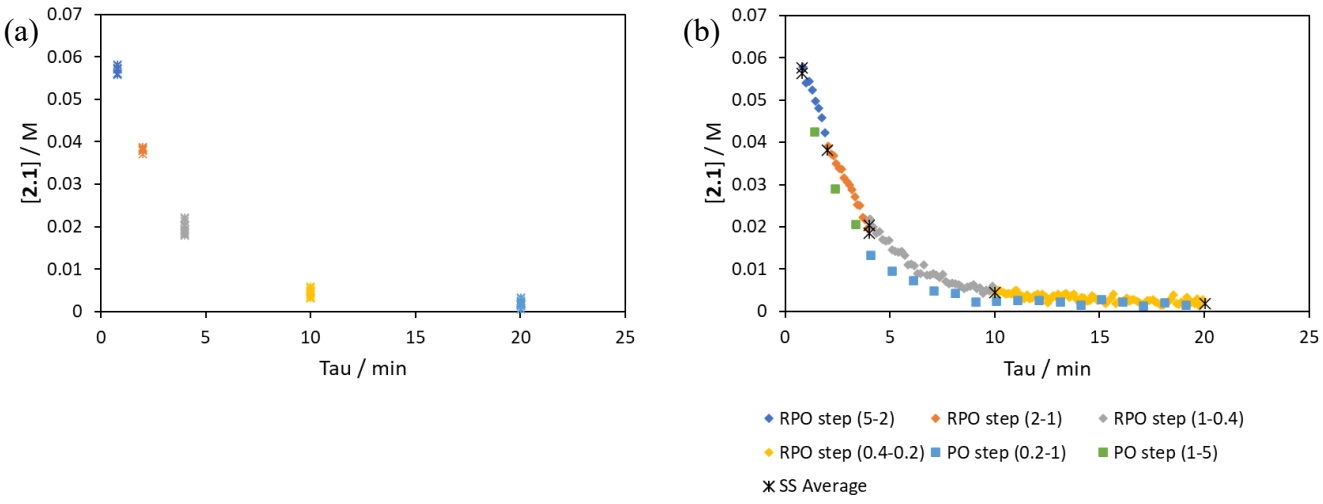


Figure 2.12. Graphs of acetic anhydride (**2.1**) concentration data collected under (a) steady state conditions; (b) small RPO/PO steps, varying cumulative flow rate (mL min^{-1}) between the bracketed values, compared to averaged steady state values.

As this reaction is *pseudo*-first order under these conditions, the plot of the natural logarithm of this data is linear and can visualise the error between methods more meaningfully (Fig. 2.13). This demonstrated, as expected, that below a certain threshold around the calibrated limit of the IR (0.01 M corresponding to -4.6 on a ln([**2.1**] / M) scale), the signal to noise ratio is poor and the results become challenging to

compare, as seen in the 0.4 – 0.2 mL min^{-1} RPO step change data (yellow diamonds, Fig. 2.13b). Above this threshold, the small PO step changes (coloured squares) show deviation from steady state values (black asterisks), and the RPO step changes (coloured diamonds) overlay well with the steady state values.

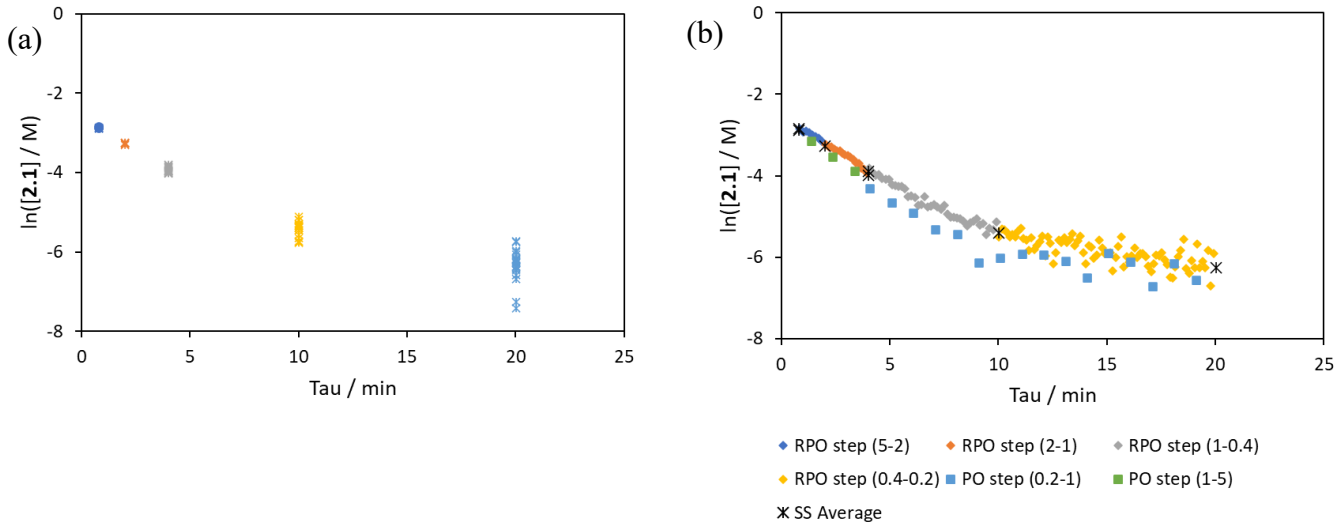


Figure 2.13. Graphs of natural logarithm of acetic anhydride (**2.1**) concentration data collected under (a) steady state conditions; (b) small RPO/PO steps, varying cumulative flow rate (mL min^{-1}) between the bracketed values, compared to averaged steady state values.

3.1.2 Full step change comparison

RPO and PO step changes were also performed across the entire residence time range (red and blue dots, respectively), between 5 – 0.2 mL min^{-1}, thereby maintaining the same step size for RPO and PO. Negligible deviation was observed for the RPO step change whereas the PO step change deviated from the steady state values as visualised in a concentration or natural logarithm of concentration plot (Fig. 2.14). Not only were the results from PO step changes less accurate, but also they produce a significantly lower quantities of data, even with a relatively fast (15 second) analysis sampling time (in-line FTIR).

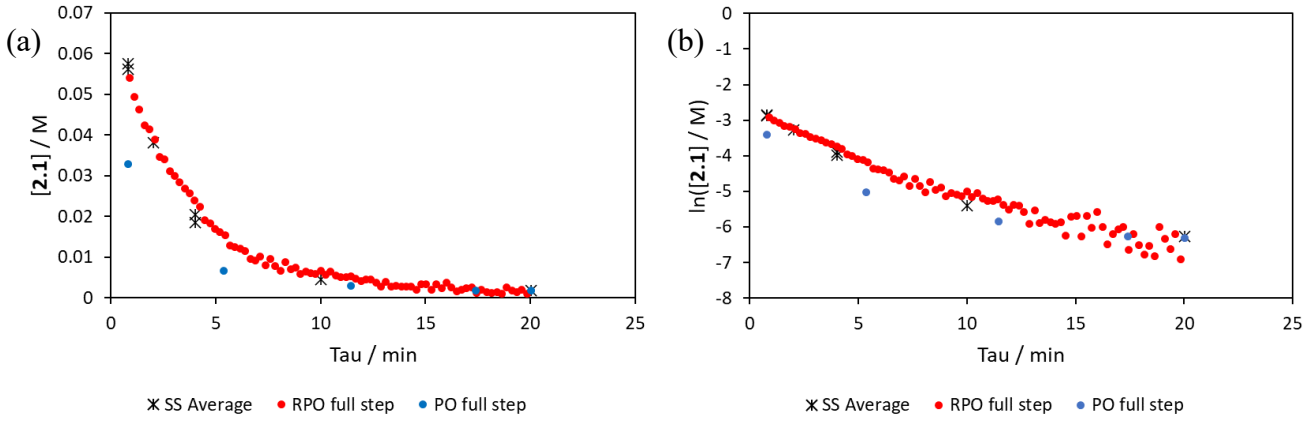


Figure 2.14. Graphs of acetic anhydride (**2.1**) concentration (a) and the natural logarithm of acetic anhydride concentration (b) collected utilising RPO and PO cumulative flow rate step changes between 5 – 0.2 mL min^{-1} compared to averaged steady state values.

3.1.3 Linear flow rate ramp comparisons

Performing 5 minute ramps between 0.2 – 5 mL min^{-1} both upwards in flow rate (PO ramp, blue crosses) and downwards in flow rate (RPO ramp, red crosses) generated comparison data sets for the same residence time range analysed by linear flow rate ramps (Figure 2.15). The data collected by the RPO ramp lined up well with the steady state points (black asterisks), and appears smoother than the RPO full step change (red dots). In this experiment, the PO ramp performed better than the full PO step change (blue dots) at short residence times, but still remained inaccurate in the rest of the flow rate range, albeit with more data points collected.

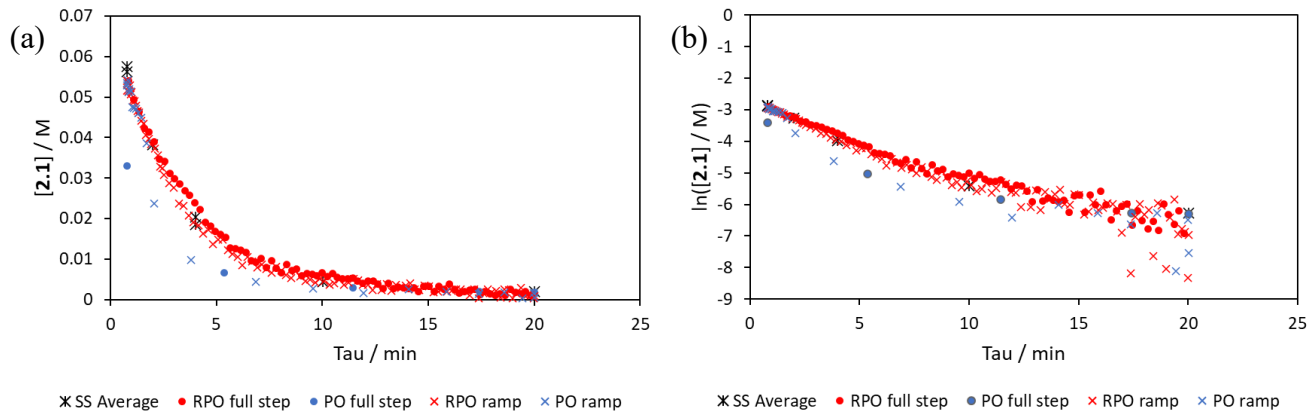


Figure 2.15. Graphs of acetic anhydride (**2.1**) concentration (a) and the natural logarithm of acetic anhydride concentration (b) collected utilising 5 minute RPO and PO linear flow rate ramps between 5 – 0.2 mL min^{-1} compared to averaged steady state values and data collected by RPO and PO step changes (Fig. 2.14).

It is worth noting that these flow rate ramps (5 – 0.2 mL min^{-1} over a 5 min ramp) were relatively fast compared to other linear flow rate ramps. For example, Hone *et al.* performed RPO flow rate ramps between 10 and 1 mL min^{-1} over a 10 min ramp also in a *circa.* 4 mL reactor.[48] These flow rate ramps (Fig. 2.15b) were performed because a fast analytical tool (15 s scan rate, in-line FTIR) was used and the efficiency of the method is greater at faster ramp rates.

For this acetic anhydride hydrolysis example, PO step and ramp methods exhibited greater consumption of acetic anhydride compared to equivalent steady state time points, *i.e.* greater reaction progress (Fig. 2.15). For PO step experiments, this is presumably due to the delayed time in reaching a flow rate set point when increasing the flow rate, therefore producing residence times consistently greater than those expected. The persistent error in the PO ramp is more surprising, arising primarily at intermediary residence times. This might be explained by the cumulative effect of increasing flow rate. These intermediary data have experienced the flow rate changing for their entire residence time and thus any small errors in changing flow rate to a faster flow rate (slight delays) will be most pronounced in these data. The data collected before and after the intermediary region will have experienced a fixed flow rate for some of their residence time and thus will have less error.

3.1.4 Error analysis

For a quantitative comparison of the results obtained from the different methods, a linear fit was performed for the natural logarithm of the steady state method data (black asterisks) only in the concentration region which had been calibrated for (above *circa.* 0.01 M) (Fig. 2.16a). Data from the other methods were then compared with the predicted values from this linear fit to better understand discrepancies in the data collected. As described above in sections 3.1.1 – 3.1.3, the largest discrepancies from the fitted steady state first order plot were found for the PO step (coloured squares in Fig. 2.16b, blue dots in Fig. 2.16c–d) and ramp methods (blue crosses). The error from PO methods was to greater conversions whereas that from RPO methods (coloured diamonds, red dots and red crosses) was more

normally distributed. Despite the observed parabolic trend in Péclet numbers *vs.* cumulative flow rate, demonstrating deviation from plug flow behaviour at intermediary flow rates, no trend was observed to this effect in the collected concentration data. For example although the small RPO steps, small PO steps, RPO linear ramp, and PO linear ramp all utilise intermediary flow rates, the error observed varies significantly between these methods.

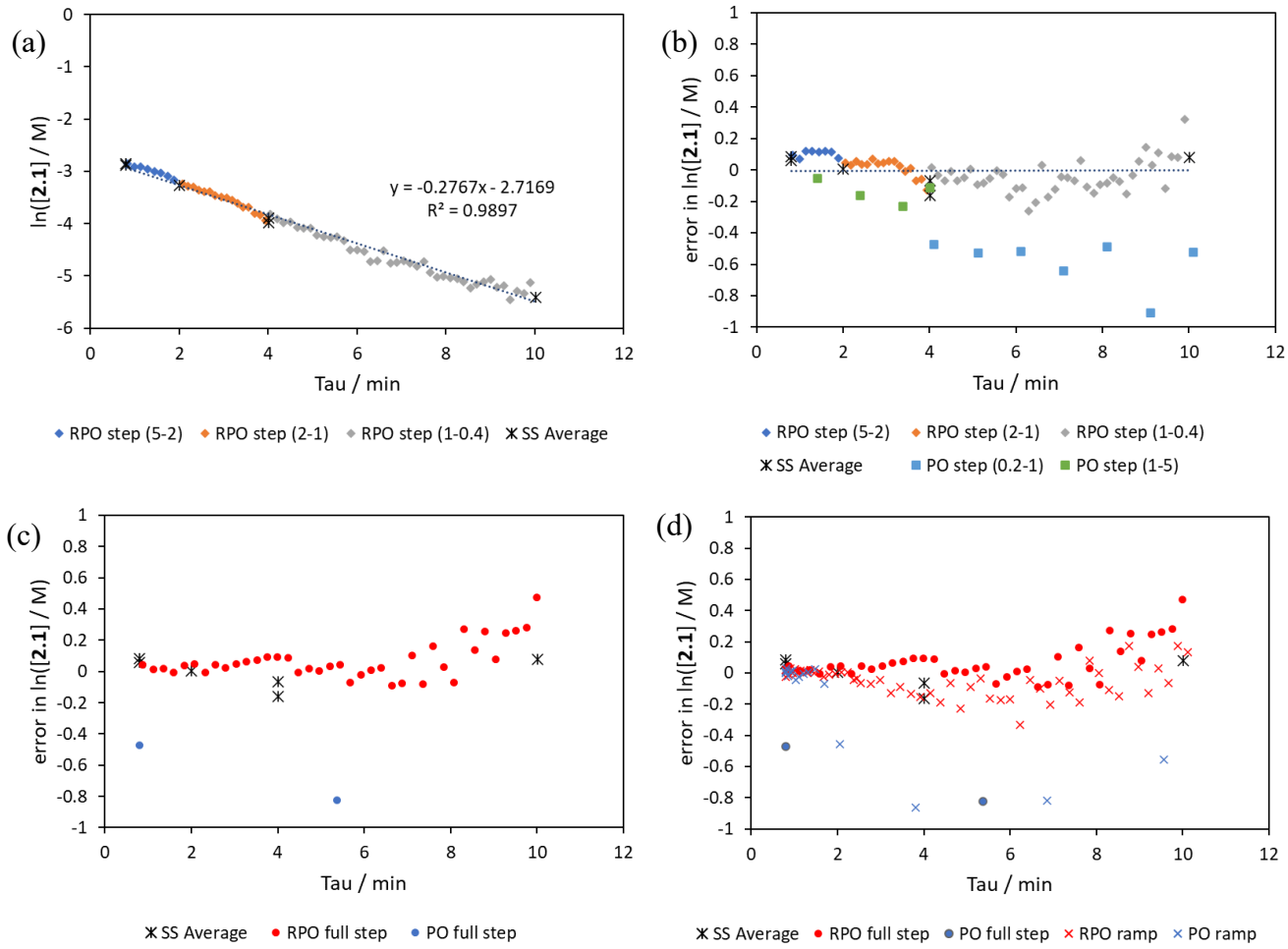


Figure 2.16. (a) linear fitting for the natural logarithm of acetic acid concentration average steady state values including fitted function and goodness of fit. Error analysis for the natural logarithm of acetic anhydride concentration for: (b) small RPO and PO step change methods; (c) full RPO and PO step change methods; and (d) RPO and PO linear flow rate ramp methods. The values in brackets refer to the cumulative flow rates (mL min^{-1}) for the start and end of smaller step change methods.

3.2 Knorr pyrazole synthesis

The heterocyclic synthesis was performed with the flow reactor in configuration 1 by mixing a 0.4 M solution of phenyl hydrazine in ethanol with 0.4 M acetyl acetone in ethanol. The reaction was performed at 70 °C at 8 bar, between flow rates of 0.2 – 5 mL min^{-1}, which afforded yields up to 75% at a residence time of 20 minutes.

The comparison of residence time series collection methods in this section was performed primarily in one continuous automated experiment (Fig. 2.17), in order to avoid any human error in multiple solution preparation and system set up. This allows direct comparison between the different residence time collection methods. This experiment consisted of, in order: a full RPO step, a full PO step, a RPO ramp, a PO ramp, two smaller RPO steps, and two smaller PO steps. At the end of this automated method, further steady state points were collected and a slower PO ramp (over 15 min) to provide independent verification of the TF results. The following subsections analyse and discuss the results of these experiments.

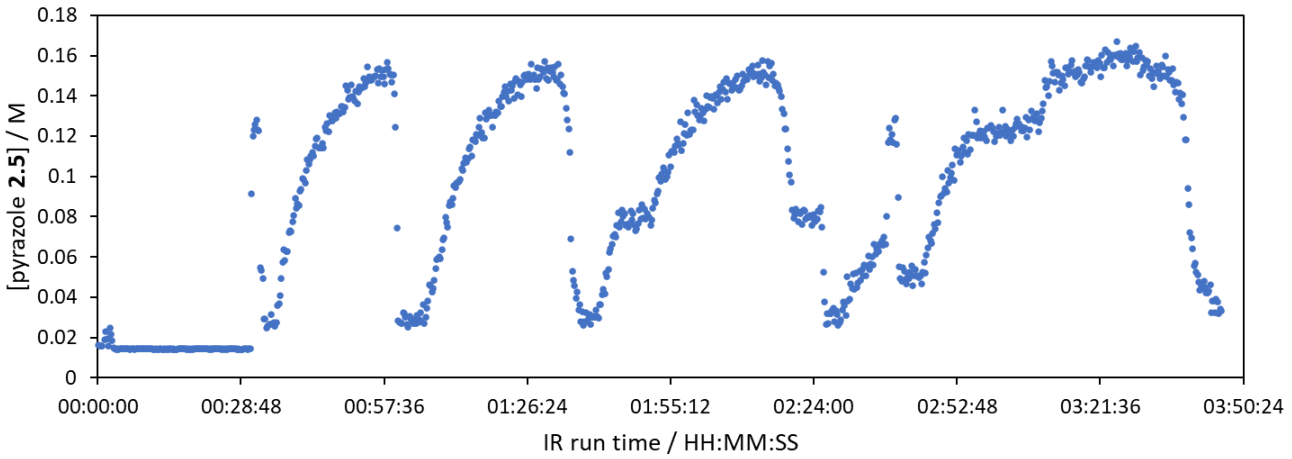


Figure 2.17. The concentration of pyrazole **2.5** for the Knorr pyrazole reaction described as monitored in one continuous experiment by an in-line FTIR instrument while performing various residence time series data collection methods.

3.2.1 Steady state and step change comparison

Similarly to the above acetic anhydride example (Section 3.1), steady state data points were collected

after small controlled PO and RPO steps at 5, 2, 1, 0.4, and 0.2 mL min^{-1}. However unlike the above example in which the concentration data could be linearised due to the first order rate equation, the Knorr pyrazole reaction has a more complicated rate equation (see Chapter 3) and so data was compared directly as concentrations (Fig. 2.18). Comparison of small and full RPO step changes (Fig. 2.18a, coloured diamonds and red dots respectively) with steady state average conversions (black asterisks) again revealed good agreement between the data obtained from different methods.

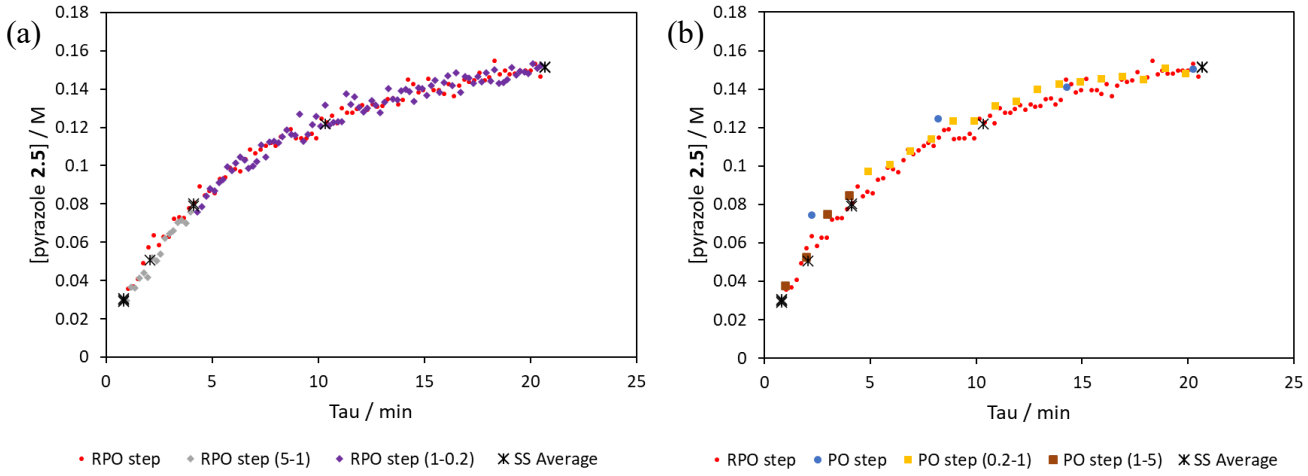


Figure 2.18. Graphs of pyrazole product (**2.5**) concentration data collected utilising (a) RPO step changes; (b) PO step changes. Cumulative flow rates (mL min^{-1}) were varied between the bracketed values (those steps without are the standard step between 0.2 – 5 mL min^{-1}) and compared to averaged steady state values.

Small PO step changes (0.2 – 1 mL min^{-1} and 1 – 5 mL min^{-1}) show relatively good agreement with steady state data (Fig. 2.18b, comparing coloured squares with black asterisks), although they deviate slightly more than the RPO step change data (red dots). However, once again the full PO step change (blue dots) shows significant deviation from steady state data points, representing longer residence times than expected in all cases (an increase in product concentration).

3.2.2 Flow rate ramp comparison with previous methods

Flow rate ramps, performed between 0.2 – 5 mL min-1 over 5 min, align with previous results (Fig. 2.19a): RPO ramps (red crosses) agree with steady state data (black asterisks), PO ramps (blue crosses)

deviate in the middle third of residence times. In this example, a longer 15 minute PO ramp (purple crosses) was compared, which appears to have less deviation from steady state data although this data is relatively noisy (Fig. 2.19b). This slower ramp rate may mitigate deviations from the steady state data by increasing flow rate at a rate at which the pumps can accurately change. If the pump rate of change is the key factor in the observed deviations of PO experiments, this could potentially be mitigated with syringe pumps as these have a smoother transition in flow rate, although syringe pumps have other limitations such as lower maximum working pressures and limited volumes.

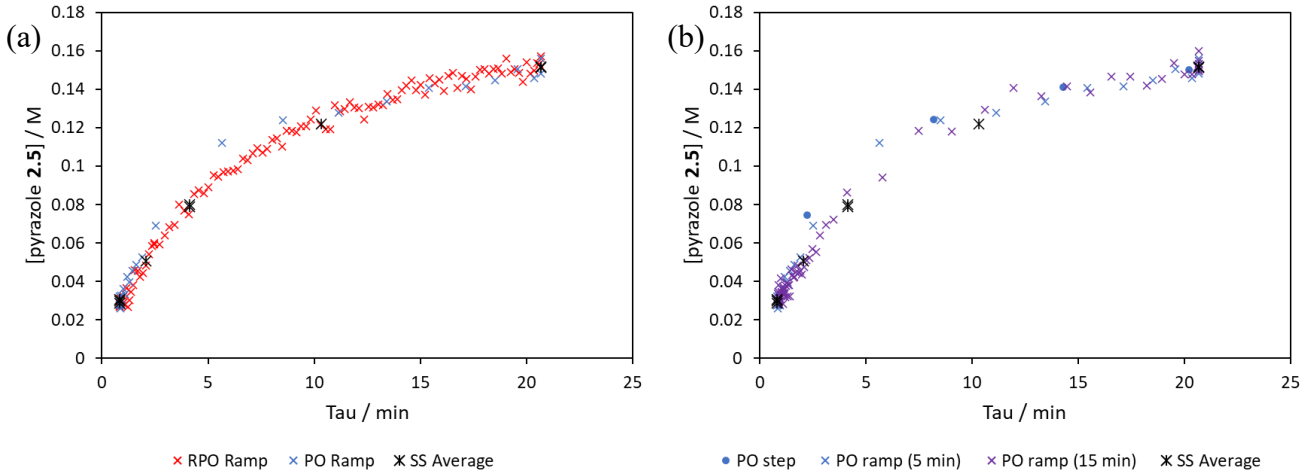


Figure 2.19. Graphs of pyrazole product (**2.5**) concentration data collected utilising (a) 5 minute RPO and PO linear flow rate ramps; (b) a PO step change, a 5 min PO linear flow rate ramp, and a 15 min PO linear flow rate ramp. Cumulative flow rates (mL min^{-1}) were varied between 0.2 – 5 mL min^{-1} and the pyrazole product (**2.5**) concentration data are compared to averaged steady state values.

3.2.3 Error analysis

In order to compare more quantitatively between methods in this example, a curve was fitted to the steady state data (black asterisks) to determine the absolute and proportional error in each method for this example (Fig. 2.20). Initially, the steady state data curve fit was poor when compared to the denser RPO full step data (blue dots), over fitting the steady state data (Fig. 2.20a). This was due to a lack of steady state data between 10 and 20 min residence time. To correct for this, a representative data point from the RPO full step data at 15 min residence time was added to the steady state points (Fig. 2.20b). Fitting a 4^{th} order polynomial to this data gave a curve from which other data could be compared to

assess residuals from the other methods. It is worth noting that this curve does not pass through the origin and is a simplification of the actual kinetic system, simply required as a comparison for the data in the fitted range.

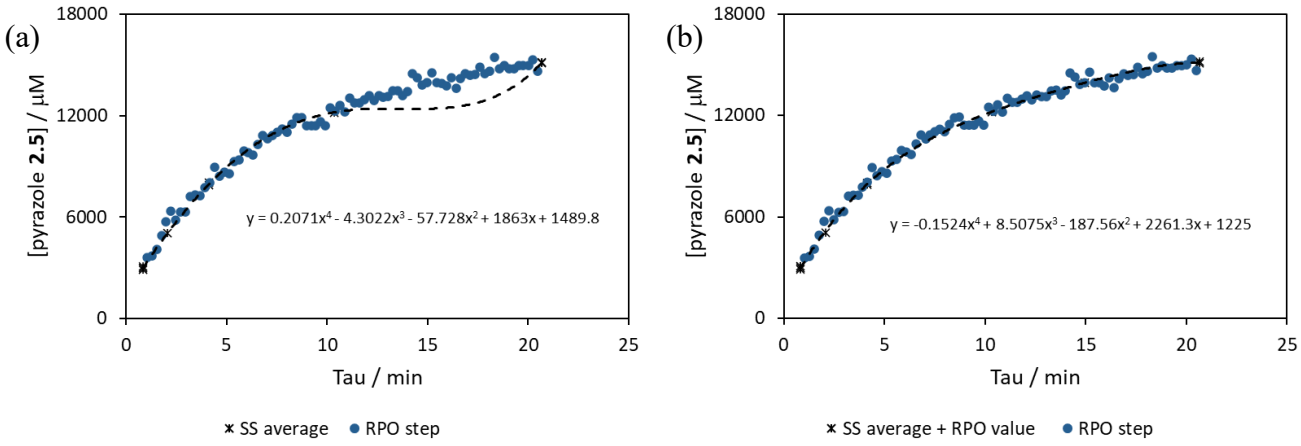


Figure 2.20. Comparison between fitted 4th order polynomial curves to steady state average (a) or steady state average and 15 min RPO step point data (b) compared to RPO step change data. These curves were fitted to pyrazole product (**2.5**) concentration data in µM for simple curve fitting.

This analysis provides quantitative results supporting the previous observations. RPO methods have very little error compared to steady state data (Fig. 2.21a, b, and d), although the error at the beginning of the RPO ramp is greater than expected. Interestingly, the error is negative suggesting a lower residence time early on in the experiment than expected (Fig. 2.21d). The PO full step method (Fig. 2.21c) has significant error with both % error (blue dots) and absolute error (orange triangles) decreasing as the residence time increases. This suggests lower error at the beginning of the experiment and gradually more error as the experiment progresses, presumably as the later data has experienced a greater time in the reactor at a flow rate which was below the expected value. PO ramp data for both the 5 minute and 15 minute ramp (Fig. 2.21e and f, respectively) show good agreement with steady state data at the beginning of the experiment (high residence times) and then increase in error during intermediary residence times before decreasing again towards the final steady state. The longer 15-minute PO ramp method (Fig. 2.21f) had more significant error towards the shortest residence times, this is potentially

due to solution reservoirs running low towards the end of this experiment, potentially leading to some cavitation in the solvent stream affecting the flowrate.

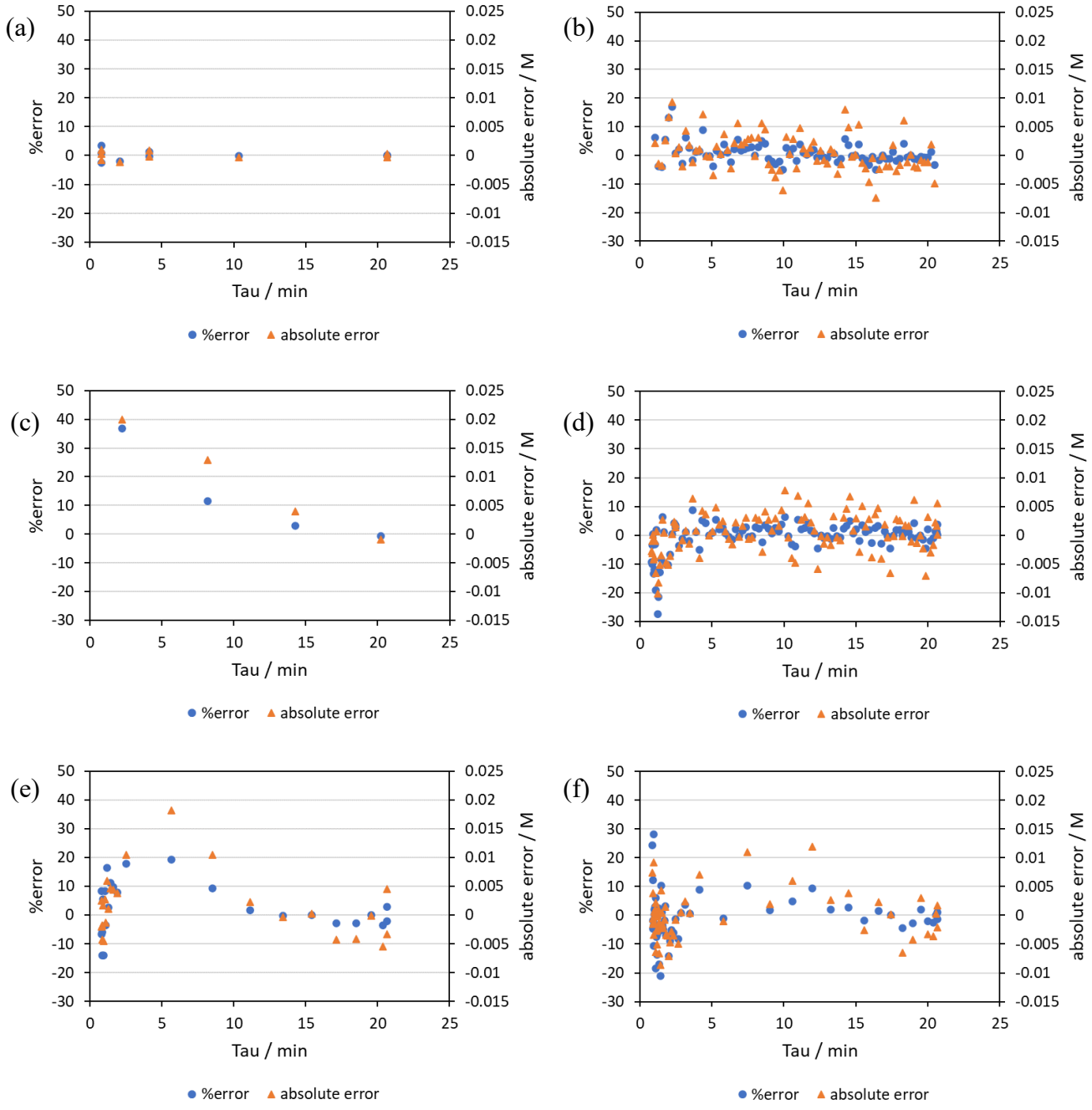


Figure 2.21. Error analysis of the concentration of pyrazole **2.5** utilising different residence time collection methods on the Knorr pyrazole reaction: (a) steady state data; (b) RPO full step; (c) PO full step; (d) RPO 5 min ramp; (e) PO 5 min ramp; (f) PO 15 min ramp.

3.3 Aromatic Claisen rearrangement

Performed with the flow reactor in configuration 2 (Section 2.3), without in-line dilution using 2 mM *para*-methoxyphenyl allyl ether solution in ethanol with ethyl benzene added as an internal standard. The reaction was run at 220 °C at 100 bar between flow rates of 0.1 – 1 mL min^{-1} producing yields up to 88% after 40 min of residence time. Data was collected across two experiments, the first (Fig. 2.22a) performing all PO and RPO step changes, both large and small, and the second (Fig. 2.22b) performing a PO and RPO ramp. In both experiments on-line HPLC analysis allowed quantification of the starting phenyl ether **2.6** concentration (blue dots) and the product phenol **2.7** concentration (red dots), and subsequently yield (grey dots), through comparison of peak areas for **2.6** and **2.7** compared to the area of the internal standard peak.

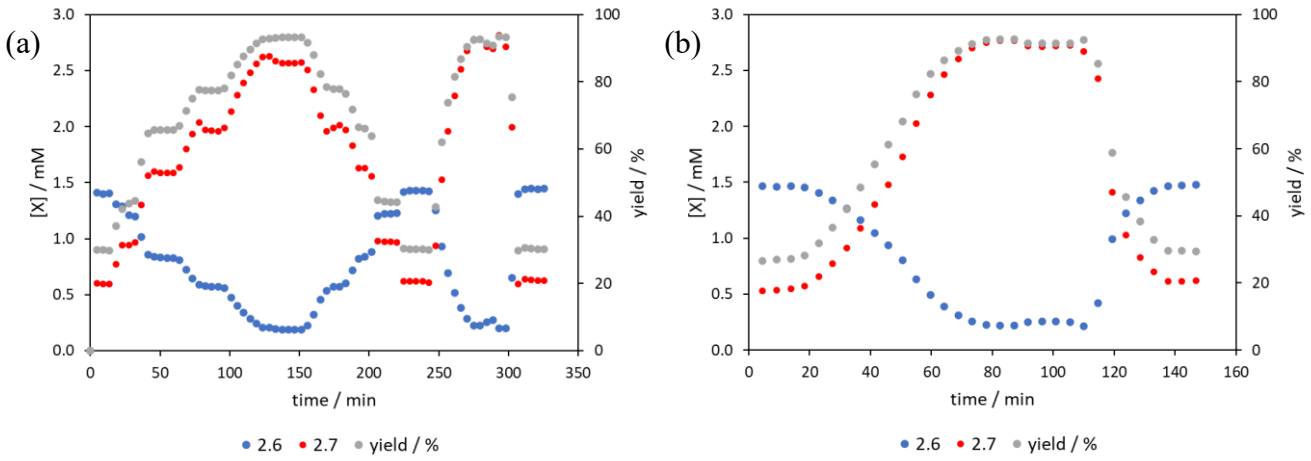


Figure 2.22. Transient flow experiment runs for the aromatic Claisen rearrangement. (a) multiple PO and RPO step changes; and (b) PO and RPO ramps. All show quantified starting material (**2.6**) and product (**2.7**) concentration and yield against experimental time.

3.3.1 Solvent expansion

Liquids are known to change density with changing temperature and pressure, often described simply by the Tait equations (Equation 2.29 and 2.30 respectively).[81] Often this effect is negligible at near-ambient conditions, but under temperatures and pressures accessible in a flow reactor the effects become more significant, leading to a variation in solvent volume and thus residence time. The Claisen aromatic rearrangement was studied at very high temperature (220 °C) and pressure (100 bar),

whereupon solvent expansion becomes non-negligible. As mentioned in Section 1.3.1 in discussion of Equation 2.20, Hone *et al.* included solvent expansion in their calculation of residence time from a transient flow rate ramp by replacing the reactor volume constant with a temperature dependent term. In this work, a different method was used to account for the solvent expansion by calculating the expected residence time if the solvent did not change density (constant reactor volume) and then modifying this term utilising the Tait equations to determine the ratio of densities under relevant conditions.[81] This allowed true residence times to be accurately tracked allowing concentration plots to be linearised (due to first order kinetic behaviour) for error analysis of methods, as well as visual comparison of yield plots.

$$\rho_1 = \frac{\rho_0}{1 - \frac{P_1 - P_0}{E}} \qquad \text{[Eq. 2.29]}$$

$$\rho_1 = \frac{\rho_0}{1 + \beta(T_1 - T_2)} \qquad \text{[Eq. 2.30]}$$

where ρ = density of ethanol (kg m^{-3}), P = applied pressure (bar), T = temperature (K), E = bulk modulus of elasticity (10600 bar for ethanol), and β = volumetric expansion coefficient (0.0011 K^{-1} for ethanol).

3.3.2 Method comparison

In the initial experiment small RPO and PO steps (Fig. 2.23a, coloured diamonds and squares, respectively) were performed, followed by full RPO and PO steps between 0.1 – 1 mL min^{-1} (Fig. 2.23b, red and blue dots, respectively) to capture the reactive time course of the reaction. These yield data show good consistency between different experimental methods, although a comparison between PO and RPO methods shows that PO methods always under predict yield, whereas RPO methods slightly over predicting yield. This contrasts with the previous examples in which the reaction data was found to be over predicted for PO experiments (see sections 3.1 and 3.2). The inverse occurring in this case could be caused by the more extreme conditions as the higher temperature (220 °C) will take a greater reactor length to accurately heat to the reaction temperature at faster flow rates. This would cause PO methods

- in which the reaction data is primarily collected at faster flow rates - to have a shorter reactor length at the reaction temperature.

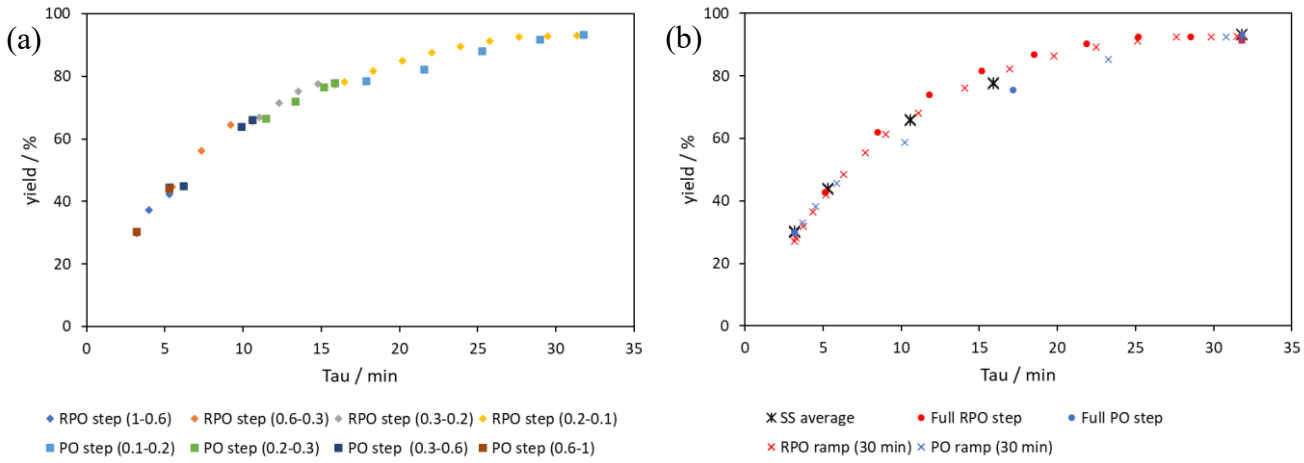


Figure 2.23. Graphs of yield of the aromatic Claisen reaction to produce phenol **2.7** utilising (a) small RPO and PO cumulative flow rate step changes between the bracketed cumulative flow rates (mL min^{-1}) and (b) full RPO and PO cumulative flow rate step changes between cumulative flow rates of 1 – 0.1 mL min^{-1} and 30 min RPO and PO linear flow rate ramps between the same values, compared to averaged steady state values.

Due to the *pseudo*-first order behaviour of this reaction, the data can be linearised *via* a natural logarithm of the starting material (**2.6**) concentration to better compare error between methods (Fig. 2.24a). On performing this linearisation, it becomes apparent from the denser RPO methods (red dots and crosses) that there is an asymptote in the data after a residence time of 28 minutes at *circa.* 92% yield. This deviation from *pseudo*-first order kinetics could potentially be attributed to product auto inhibition or unseen side reactions. It is noteworthy that this asymptotic behaviour is not readily observable from the less data dense methods such as the full PO step change (blue dots), PO ramp (blue crosses), or steady state data points (black asterisks). This discrepancy from *pseudo*-first order behaviour unfortunately makes method comparison by fitting a straight line to linearised steady state data points invalid. Further options for method comparison were curve fitting an arbitrary polynomial to the (low density) steady state data points (as in Section 3.2.3 for an unknown kinetic rate law) or moving any data points at longer residence time than the asymptote time (28 min) to the asymptote time. The second option (Fig. 2.24b) was selected in this case to avoid inclusion of any potentially erroneous RPO data in the fitting.

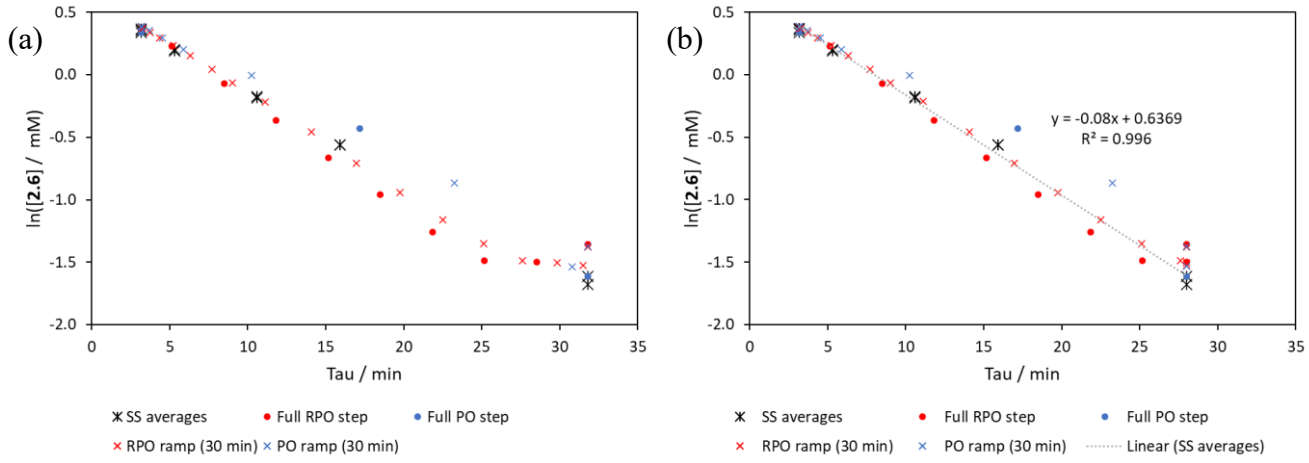


Figure 2.24. (a) a graph of the natural logarithm of the concentration of the staring phenyl ether **2.6** for the full residence time range collected, noting the kink at 28 minutes; (b) linear fitting for the natural logarithm of the concentration of the staring phenyl ether **2.6** average steady state values over a shortened residence time range, including fitted function and goodness of fit.

Utilising the linearisation of this modified data, the error in the different methods can now be compared (Fig. 2.25), revealing as in previous examples greater discrepancy from PO methods (blue dots and crosses, and coloured squares). These data demonstrate that data collected *via* RPO methods are more accurate in all cases than those from PO methods, and that the best quality data can be obtained from shorter RPO step changes (Fig. 2.25b, coloured diamonds) or RPO ramps (Fig. 2.25a, red crosses), although the full RPO step (Fig. 2.25a, red dots) still produces relatively accurate data.

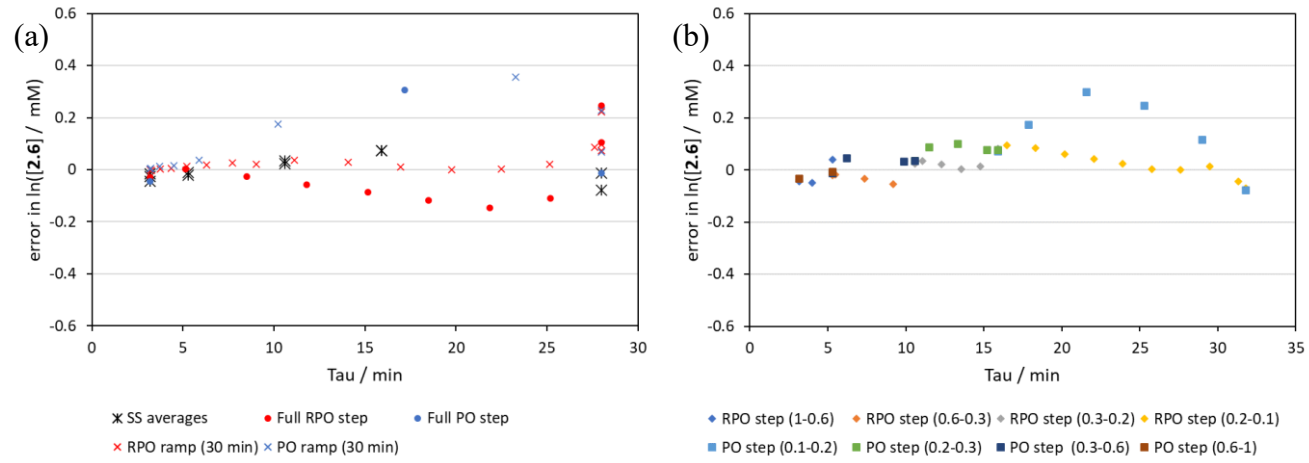


Figure 2.25. Error analysis of the concentration of starting phenyl ether **2.6** utilising different residence time collection methods on the aromatic Claisen rearrangement reaction: (a) averaged steady state values, full RPO and PO cumulative flow rate steps between 1 – 0.1 mL min^{-1}, and 30 min RPO and PO linear flow rate ramps over the same flow rate range; and (b) RPO and PO small cumulative flow rate step changes between the bracketed values of cumulative flow rates (mL min^{-1}).

4 Conclusions

In this chapter, the construction of two flow systems (Configurations 1 and 2) was described, utilising different heating elements and analytical tools. These systems are deployed in the work contained in the later Chapters of this thesis.

Mathematical derivation of deconvolutional for PO and RPO step changes and linear flow rate ramps was developed. The deconvolution discussed herein built on previous work from Mozharov *et al.*,[39] Moore *et al,*[49] and Hone *et al.*[48] by including correction for dead volume between the reactor volume and the analytical tool. Further to this, the deconvolution for PO and RPO ramps also allows more data to be obtained from ramping methods by analysing three regimes within a ramping experiment.

PO and RPO step and ramping methods were compared for three example reactions of varying complexity: the hydrolysis of acetic anhydride, the Knorr pyrazole synthesis, and the aromatic Claisen rearrangement reaction. Through direct comparison of data obtained from the different methods, and through quantitative error analysis, all examples demonstrated that RPO methods produce more accurate data than PO methods, counter to the *status quo* for step change methods used by Mozharov *et al.*[39] and Durand *et al.*.[40] These results are still consistent with the previously reported results, demonstrating that discrepancies observed in their work were an issue of specifically PO step changes, not step changes in general. Utilising linear flow rate ramps it was demonstrated that RPO ramps were also more accurate than their equivalent PO ramps, although by ramping at a slow enough ramp discrepancies could be mitigated. This demonstrates that the standard use of RPO type linear flow rate ramps (as discussed in Chapter 1, Section 2.2), and adjacent linear residence time ramps, is justified in comparison to PO ramps.

Residence time distribution studies under reaction conditions for the Knorr pyrazole reaction demonstrated deviation from ideal plug flow fluid dynamics at intermediary flow rates. These deviations were found not to have an observable effect on the results collected, demonstrated by significantly

different error in results obtained from methods utilising these intermediary flow rates.

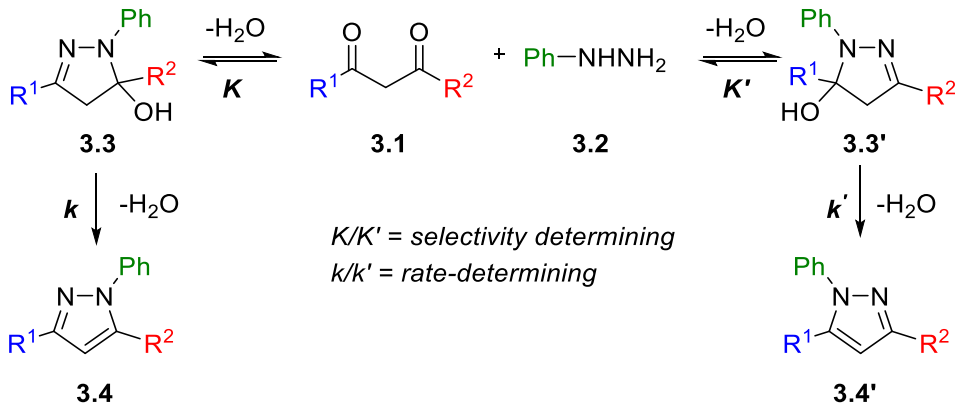
Comparing RPO step changes to RPO ramps show similar data accuracy and data density in the discussed examples. In light of this work RPO step changes should become the preferred method for reaction time series data collection in flow; except in exceptional cases in which residence times are so small in comparison to analytical speed that more data density must be obtained from a slow ramp. Other than these cases the RPO step method offers the same data accuracy while requiring simpler deconvolutional methods, cheaper less sophisticated equipment, less experimental time, and less material than a RPO ramp method (either linear flow rate or linear residence time).

Chapter 3: Discovery of an unexpectedly complex mechanism for the Knorr pyrazole synthesis

1 Introduction

1.1 Aim and objectives

The (original) aim of this work was to construct a predictive model for a regioselective Knorr pyrazole synthesis from challenging unsymmetrical diketones. The initial hypothesis was that, if the widely touted two step kinetic model (Scheme 3.1) - consisting of an equilibrium to intermediate **3.3** followed by a dehydration step, the equilibrium and rate constants (*K* and *k* respectively) - could be determined for symmetric diketones (where $R^1 = R^2$), then these could be combined to predict the regioselectivity of a reaction with an unsymmetrical diketone (where $R^1 \neq R^2$), which would be more expensive to monitor. This hypothesis assumes that: (i) the reaction follows a simple bimolecular kinetic model; and (ii) each kinetic step is only affected by the alkyl group directly attached to it, thus allowing symmetric diketone rate constants to be used for the unsymmetric diketone. For this study, the condensation of phenyl hydrazine (**3.2**) with acetyl acetone ($R^1 = R^2 =$ Me, **3.1a**) and heptane-3,5-dione ($R^1 = R^2 =$ Et, **3.1b**) were chosen to predict the regioselectivity between the unsymmetric diketone ($R^1 =$ Me, $R^2 =$ Et, **3.1c)** with phenyl hydrazine. It was hoped that by comparison of rate constants in the fitted microkinetic model for the reactions of phenyl hydrazine (**3.2**) with acetyl acetone ($R^1 = R^2$=Me, **3.1a**) and heptane-3,5-dione ($R^1 = R^2$=Et, **3.1b**), qualitative knowledge of regioselective control could be obtained.



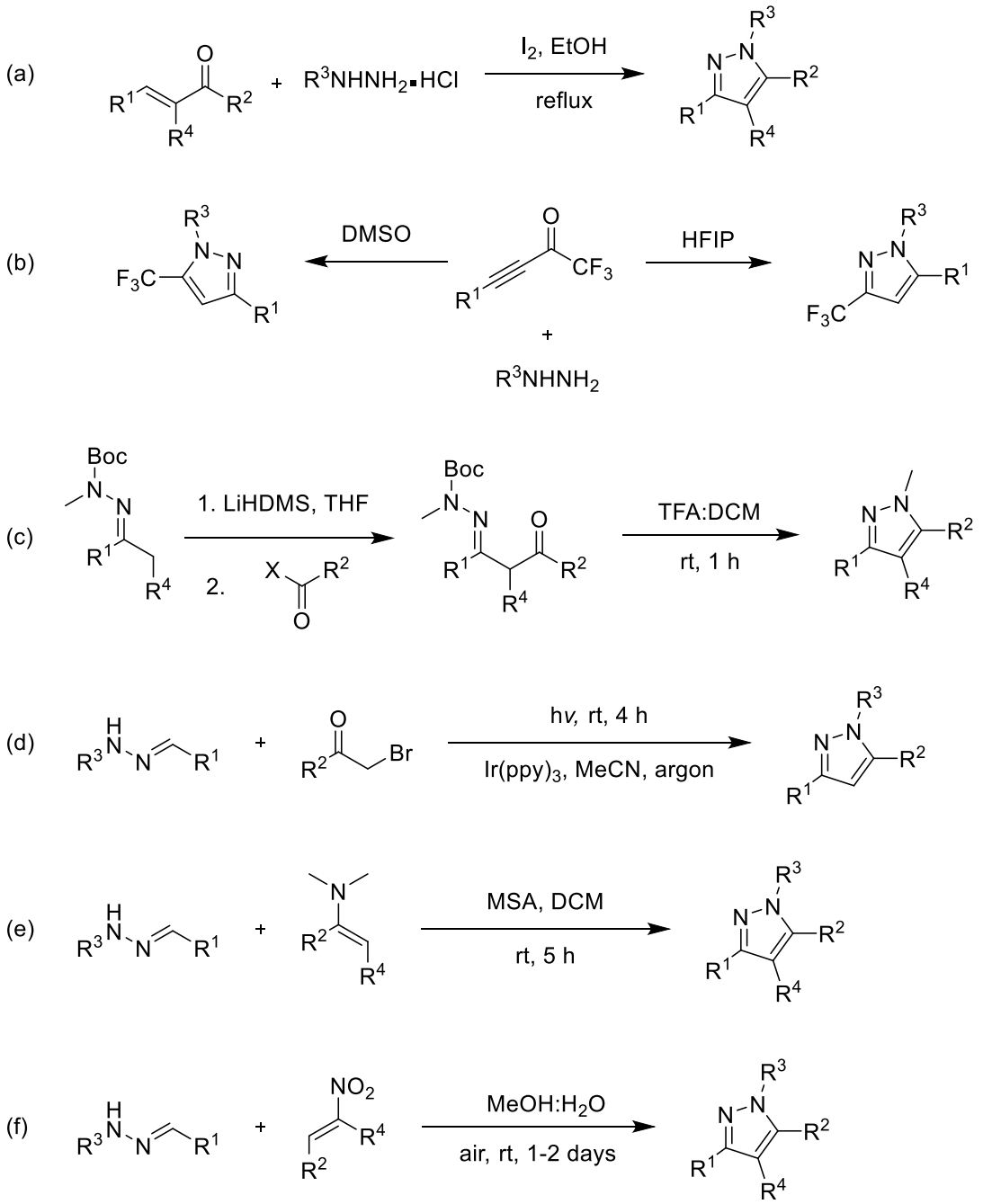
Scheme 3.1. The Knorr pyrazole synthesis of an unsymmetric 1,3-diketone **3.1** and phenyl hydrazine **3.2** *via* the widely accepted mechanism to form pyrazoles **3.4** and **3.4'**.

The research presented in this chapter focuses on utilising transient flow methods to investigate the mechanism of the Knorr pyrazole synthesis. Kinetic data was collected on this reaction from transient residence time experiments (RPO step changes), additive ramps, novel reaction stoichiometry ramps and multivariate ramps. These data, supplemented by other methods, were used to probe the mechanistic pathways of this reaction through microkinetic modelling. This provided new insights, including identification of new autocatalytic pathways and an unexpected reaction intermediate. The complexity of the final microkinetic model was prohibitive in constructing a microkinetic model for the unsymmetric diketone reaction. Finally, insights into the regioisomeric outcomes were obtained and tested.

1.2 The Knorr pyrazole reaction

The pyrazole ring is a common motif present in many active pharmaceutical and agrochemical ingredients. The Knorr pyrazole synthesis (Scheme 3.1) is a ubiquitous simple reaction used to prepare the 5-membered heterocycle from 1,3-diketone and hydrazine precursors, a large variety of which are commercially available.[82,83] The reaction has been utilised in flow for synthesis of a range of biologically interesting pyrazole containing molecules[78,84] and the kinetics of the reaction was studied briefly in flow, assuming a second order rate equation.[63] The reaction has also proven a good case study for developing new techniques in flow such as a control loop to correctly dose in a second reagent[78] and the development of non-isothermal variable active reactor volume methods[63] (Chapter 1, Section 2.1.2).

The Knorr pyrazole synthesis forms a mixture of regioisomeric pyrazoles from unsymmetrical 1,3-diketone substrates (Scheme 3.1). Although other synthetic methodologies can provide unsymmetrically substituted pyrazoles regioselectively (Scheme 3.2),[85–90] these methods are significantly less atom efficient and require less commercially available and viable starting materials.



Scheme 3.2. A selection of other routes for regioselective synthesis of pyrazoles. (a) Iodine catalysed example by Zhang *et al.*[85]; (b) solvent controlled regioselectivity from alkyne example by Muzalevskiy *et al.*[87]; (c) boc protected hydrazone example by Tinarelli *et al.*[88]; (d) Iridium catalysed light mediated example by Fan *et al.*[89]; (e) methanesulfonic acid mediated example by Duan *et al.*[90]; (f) air mediated example by Deng *et al.*[86]. A list of acronyms can be found at the start of this thesis.

The regioselectivity of the Knorr pyrazole synthesis has been shown to be affected by solvent, pH, and the stereoelectronic characteristics of the substituents (R^1 and R^2) .[91,92,93] Correlations proposed in these studies are largely based on a small number of empirical observations of product distributions obtained from different reaction conditions. These studies support the progression of the reaction *via* a

hydroxylpyrazolidine intermediate **3.3**, which can be isolated in certain cases,[93–95] and observed by Selivanov *et al.* and Norris *et al.* in others.[92,96] Consequently, the dehydration of **3.3** to form the product is accepted as the rate-determining step under neutral conditions.

In the most detailed kinetic study,[95] performed by Sloop *et al*, reaction kinetics were determined by a series of ^{19}F NMR experiments for the reactions between arylhydrazines (R^3 = Ar) with trifluoromethyl-substituted diketones (R^1 = CF_3). NMR spectra were collected at 180-seconds intervals, and the initial rate was "obtained as a slope of a best-fit line to the earliest linear portion of the data (t < 600 s)", *i.e.* based on fewer than 3 data points. The reaction was found to be first order in both reactants (Equation 3.1) at pH > 1.6, based on initial rates data, and a variety of reaction intermediates were invoked including the isolation of intermediate **3.3** in some cases. A cautious assessment of this study reveals obtained rates may be inaccurate due to room temperature premixing of reactions and limited mass transfer in NMR tube experiments. Furthermore, as initial rates methods were used to obtain rate constants, this kinetic model may not hold true after greater reaction progress. It is also worth noting that as the study was performed solely on fluorinated compounds, to allow ^{19}F NMR analysis, the unique stereo-electronics of the substrates may influence the intermediates formed.

$$rate = k[diketone][hydrazine] \qquad \text{[Eq. 3.1]}$$

where k = rate constant (M^{-1} min^{-1}), *rate* has units of M min^{-1} and concentrations have units of M.

1.3 Transient flow methods

Reaction kinetics have been studied in flow using various techniques, a subject that had been reviewed by Taylor *et al.*.[6] Among the different methods of collecting kinetic data, transient time series collection methods have proved popular, due to the efficiency and quality of the data collected. As discussed in Chapter 1, Section 3, performing other transient flow experiments on reaction temperature and multivariate residence time-temperature ramps have provided valuable data for kinetic modelling,

especially when combined with different Bayesian methods to minimise uncertainty in fitted kinetic parameters or even to choose between a selection of rate equations.

Prior to the work described in this chapter, there were limited literature precedence on utilising transient concentration ramps to build process understanding.[66,67] As discussed earlier (Chapter 1, Section 4), Jensen and co-workers utilised transient concentration ramps to investigate an asymmetric hydrogenation reaction (Fig. 1.20), to inform subsequent system design for scale-up.[66] Notably, the concentration ramps were only performed in one direction, thus not sufficient to confirm that the results are unaffected by ramp direction (*e.g.* solubility of product may change over the gradient). Nevertheless, these ramps provided sensitivity analysis for substrates concentration, suggesting a zero reaction order for substrate and additives. A concentration ramp screened over a range of catalyst concentrations, to establish the optimal catalyst concentration for scale-up, without detailed kinetic evaluation or mechanistic explanation. In a later paper Wyvratt *et al.* expanded on this method to study linear and non-linear additive concentration ramps, utilising the data to generate a response surface for the Knoevenagel condensation reaction (Scheme 1.13).[67] In this work, collection of reaction data points were repeated and verified by implementing bi-directional ramps in different experiments. The response surface constructed could be used to predict reaction yields across a range of residence time and additive concentration, but did not seek to fit any explicit kinetic model or calculate rate constants.

A survey of the literature conducted at this time uncovered a need for a reactant stoichiometry ramping method, which could inform reaction kinetic models and proposed mechanisms. The Knorr pyrazole synthesis appeared to be a perfect candidate to develop this method: as a bimolecular reaction in which both reactants are likely to have a non-zero order. Such a method would be a versatile approach to confirm any kinetic model fitted as an orthogonal source of reaction data independent of initial concentration deviation, that may be caused by human error in weighing.

Since then, literature examples utilising concentration ramps have emerged,[15,68] including our own publication.[97] Following their initial work described above, Jensen and co-workers produced more detailed work on tri-variate ramps (residence time, temperature, and additive concentration varied simultaneously) with more mathematical rigour.[15] This work included theoretical calculation of maximum ramping rates (as discussed in Chapter 1, Section 1.3.2) verified by bi-directional ramps. This method was used as an approach for data-rich exploration of a design space; while it was stated that the data could be used to aid kinetic elucidation also, this was not implemented. Wyvratt *et al.* also further utilised the method they developed for self-optimisation of a reaction, as discussed in Chapter 1, Section 4,[68] where the concentration of one reactant was varied while keeping the other reactant concentration constant and a kinetic model for the reaction was obtained from the response surface fitted to the data collected for self-optimisation.

2 Different excess residence time transience

2.1 Batch experimentation

Preliminary research was performed during my MRes year in which the Knorr pyrazole reaction between acetyl acetone (**3.1a**) and phenyl hydrazine was performed in a semiautomated batch reactor (Mettler Toledo EasyMax 102), monitored by *in situ* FTIR and extracted aliquots, utilising the Mettler Toledo EasySampler, for HPLC analysis (Fig. 3.1).[98] This reaction was performed in ethanol at 50 °C utilising different equivalents of acetyl acetone **3.1a** and phenyl hydrazine **3.2** where the concentration of one reactant was kept constant at 0.2 M, while the other was varied. The original intention was to perform visual kinetic analysis, including variable time normalisation analysis (VTNA) as championed by Burés.[99] However, it became quickly apparent that the reaction kinetics may not be as simple as that proposed in literature due to the partial order in acetyl acetone (Fig. 3.1b) and the poor optimal overlap for varying phenyl hydrazine reactions (Fig. 3.1d). The data obtained from the varying phenyl hydrazine experiments (Fig. 3.1d) were particularly strange, demonstrating good overlap at shorter reaction times

and poor overlap at longer reaction times, suggesting that the reaction kinetics cannot be explained by a simple global rate equation obtained by VTNA methods. It was also found that even under these mild conditions, solvent evaporation was affecting the reaction concentrations, complicating interpretation of the results.

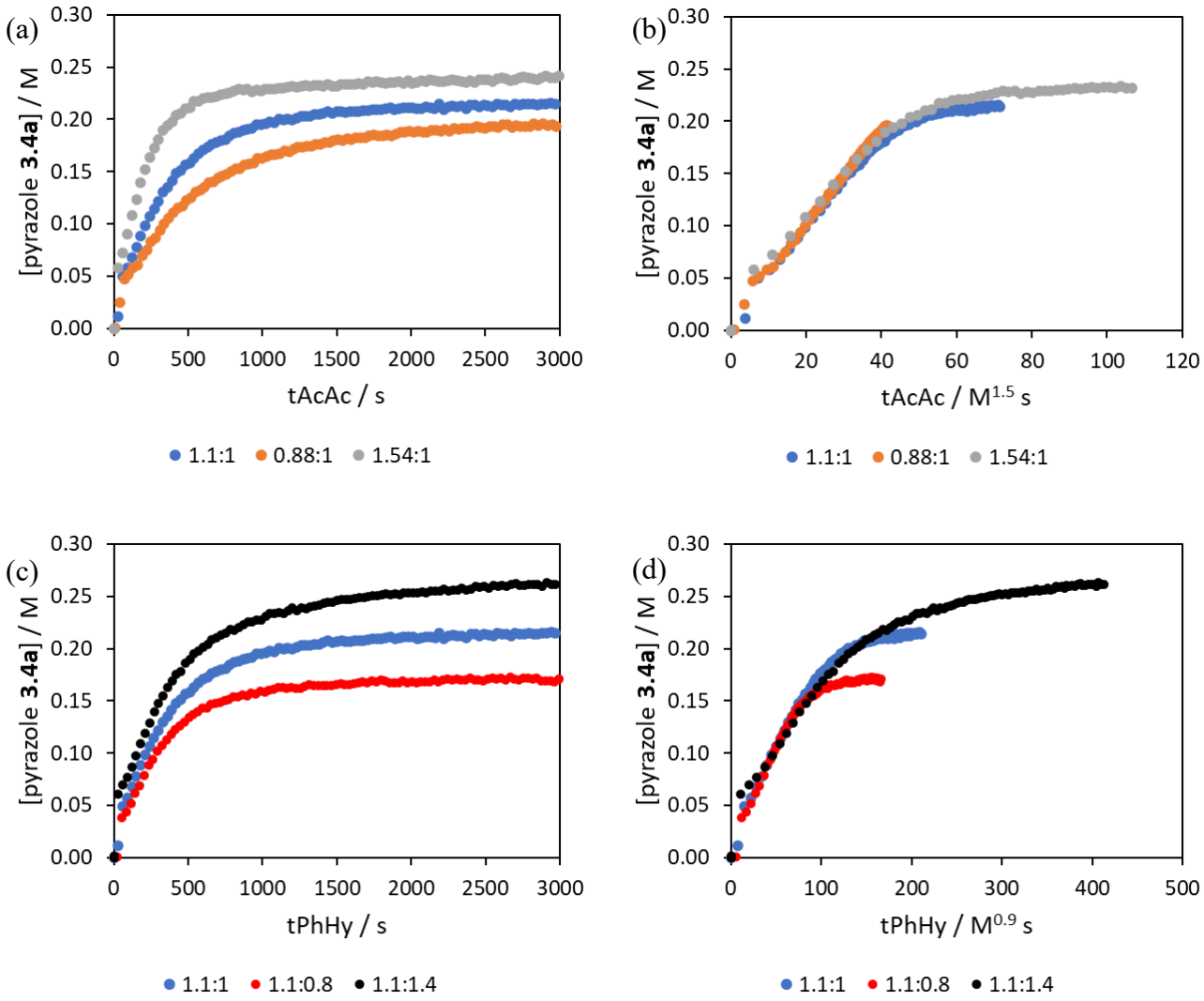
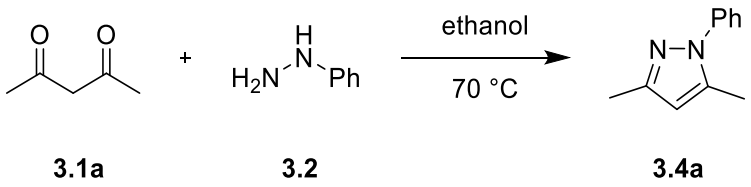


Figure 3.1. Graphs showing variable time normalisation analysis (VTNA) methods performed in previous work in batch: comparing different excess experiments with ratios of **3.1a**:**3.2** equivalents, where tAcAc and tPhHy refer to the normalised time axis normalised by the concentration term for **3.1a** or **3.2** respectively. VTNA performed utilising: (a) reaction order in **3.1a** = 0; (b) reaction order in **3.1a** = 1.5; (c) reaction order in **3.2** = 0; (d) reaction order in **3.2** = 0.9. This figure is reproduced from MRes dissertation by Linden Schrecker, 2020.[98]

2.2 Initial transient flow experiments

Following the preliminary experiments with a batch reactor, all further studies, unless otherwise stated, where performed in flow system configuration 1 as described in Chapter 2, Section 2.2. For this study the choice of ethanol (boiling point 78 °C) as a solvent was maintained, as it is environmentally benign, readily available, and commonly used for this reaction. The flow system was thus maintained at 8 bar *via* a back pressure regulator to avoid evaporation of solvent at the elevated temperature. Initial exploration of residence times, during the transient method comparison studies (Chapter 2, Section 3.2) establish a suitable reaction window to study the condensation of phenyl hydrazine and acetyl acetone (Scheme 3.3) at 70 °C at a concentration of 0.2 M, achieving *circa.* 80% yield of pyrazole product **3.4a** after 20 minutes residence time.



Scheme 3.3. The intermolecular cyclization between acetyl acetone (**3.1a**) and phenyl hydrazine (**3.2**) to produce pyrazole **3.4a**.

Reverse push out (RPO) step changes were performed using flow rates between 5 – 0.2 mL min^{-1} to cover a 0.8 – 21 min residence time range. The ReactIR was calibrated to monitor the concentration of pyrazole **3.4a** in the reaction mixture, confirmed against off-line HPLC data collected from extracted reaction aliquots (see Chapter 2, Section 2.2.2). Initial RPO step changes at an equimolar ratio of acetyl acetone and phenyl hydrazine showed good repeatability across experiments performed using different stock solutions and on different days (Fig. 3.2). Attempts were made to monitor and quantify changes in the concentrations of other reaction species, but these were ultimately unsuccessful due to the high reactivity of the starting materials hindering *ex situ* analysis by chromatographic methods and challenging similarities between unstable intermediates and the starting materials complicating *in situ* spectroscopic analysis.

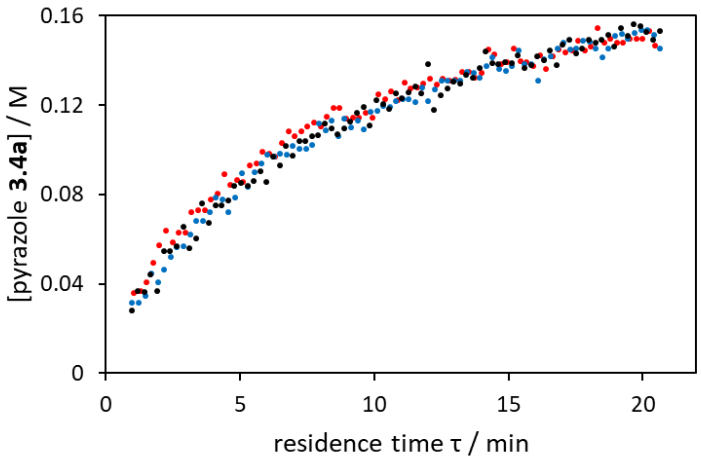


Figure 3.2. Repeatability of RPO method on the Knorr pyrazole synthesis of pyrazole **3.4a** from acetyl acetone and phenyl hydrazine at 70 °C, 0.2 M in ethanol across three repeated experiments.

2.3 'Different excess' experiments

In 'different excess' experiments, the same reaction is performed under the same conditions, except the stoichiometry of the reactants is varied. Reaction data collected from these experiments can be used to probe the effect on the reaction kinetics of the different reactants, such as the reaction order of these reactants. Multiple different reactant stoichiometry RPO experiments were conducted in order to investigate the effect of each reactant concentration on product formation (Fig. 3.3, Table 3.1, A – C). These were implemented by utilising equimolar stock solutions of the two reactants and varying the relative pump flow rate (%B) thus effecting the reaction stoichiometry. Residual 0.01 M water is present in the HPLC grade ethanol used in these experiments, and has been included in the initial concentrations to allow later quantification of the potential effect of water on the reaction (Table 3.1).

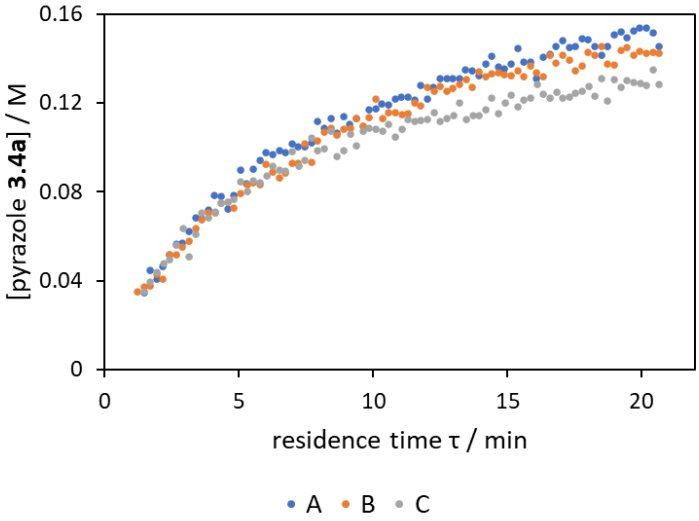


Figure 3.3. Time series data collected for the reaction of diketone **3.1a** and phenyl hydrazine **3.2** using residence time ramps over a range of different excess experiments, described in Table 3.1.

Table 3.1. Initial concentrations for the set of time series kinetic experiments.

Experiment	[3.1a] / M	[3.2] / M	[3.4a] / M	[H_2O] / M
A	0.2	0.2	0	0.01
B	0.16	0.24	0	0.01
C	0.24	0.16	0	0.01

Before more quantitative kinetic analysis was applied (see Section 4), qualitative assessment of these data reveal interesting observations. Comparison of the different excess experiments (A – C) suggests the kinetic model is more complex than previously thought. In the proposed simple bimolecular reaction model (Scheme 3.1), changing the initial concentration of diketone **3.1a** would be expected to have the same effect as changing that of phenyl hydrazine **3.2** by the same amount (Table 3.1, experiments B and C), because in this model these species are mathematically interchangeable. This would be manifested in a visualisation of the reaction data by overlap of the data series produced for experiments B and C. However, experiments B and C are not superimposable; hence, the proposed simple bimolecular reaction model must be incorrect and a more complex model is required.

2.4 'Same excess' and 'doping' experiments

'Same excess' experiments are experiments in which the same reaction is performed under the same conditions maintaining the reactant stoichiometry, but utilising a different overall reaction concentration. Reaction data collected from these experiments can be used to investigate product autocatalysis or inhibition of the reaction, by shifting these data in time and product concentration observing (lack of) overlap with other 'same excess' experiments. 'Doping' experiments modify 'same excess' experiments by adding the concentration of product or byproduct that would be expected in the standard reaction progress for the given reactant concentrations. If the doped compound is responsible for the catalysis or inhibitory effect observed in the 'same excess' experiments, then the corresponding change in product formation will be observed compared to the standard reaction.

For this reaction, in order to investigate the effects of the products, pyrazole **3.4a** and water, a 'same excess' experiment was performed at half the concentration of experiment A (Table 3.2, experiment D Fig. 3.4a, orange dots). Doping experiments were also performed in which pyrazole **3.4a** (product), and both pyrazole **3.4a** and water (product and by-product, respectively) were added in the quantities that would be expected in the standard reaction at this half reactant concentration (Table 3.2, experiments E and F respectively and Fig. 3.4a, light blue and green dots respectively). Comparison with a repeat of experiment A, shifting data from experiments D – F in both residence time and pyrazole **4a** concentration (Fig. 3.4b), revealed overlap for doped experiments (light blue and green dots) but a lack of overlap for the undoped experiment D (orange dots) thus implying product autocatalysis as an important kinetic pathway. In order to confirm the effect was not due to pre-activation of phenyl hydrazine or acetyl acetone by pyrazole product **3.4a**, experiment E was repeated, in which pyrazole **3.4a** was added into the acetyl acetone pump solution (experiment E') instead of the phenyl hydrazine solution (experiment E). The overlap of experiments E, E', and F (light blue, dark blue, and green, respectively) confirmed no pre-activated complex is formed, the *in operando* concentration of water does not affect the reaction, and pyrazole product **3.4a** acts in an autocatalytic manner on the reaction.

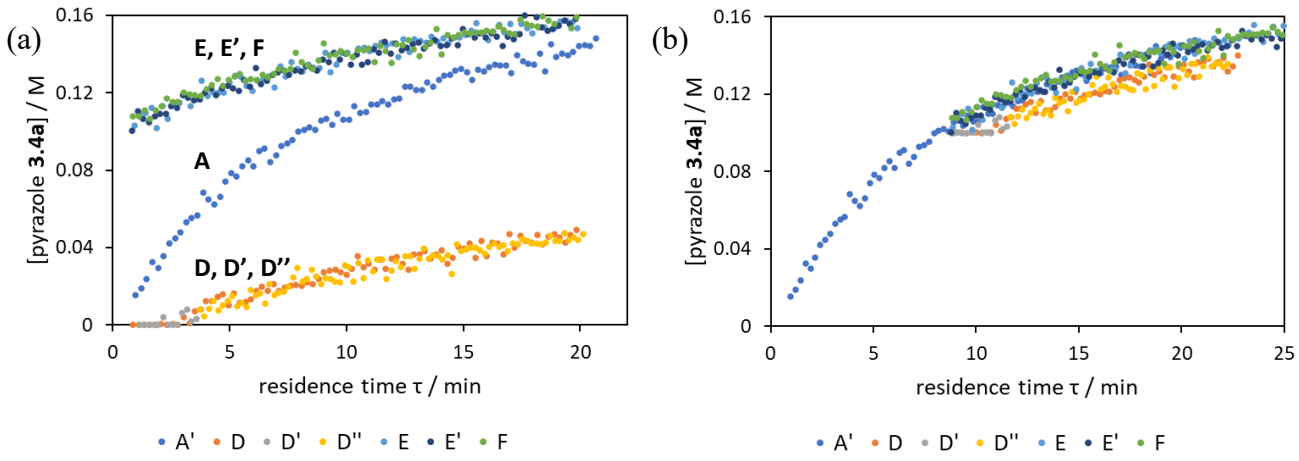


Figure 3.4. Time series data collected for the reaction of diketone **3.1a** and phenyl hydrazine **3.2** using residence time ramps over a range of same excess and doping experiments, described in Table 3.2, visualised as the collected experimental data (a) and as time and concentration shifted data series to visualise overlap (b).

Table 3.2. Initial concentrations for the set of time series kinetic experiments for same excess and doping experiments.

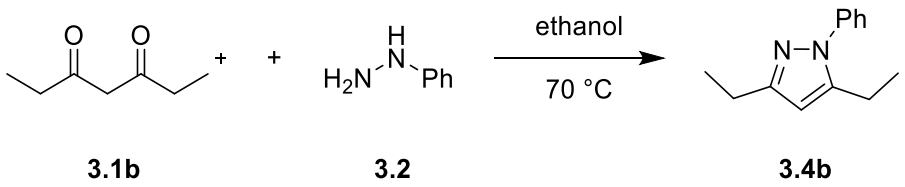
Experiment	[3.1a] / M	[3.2] / M	[3.4a] / M	[H_2O] / M
D	0.1	0.1	0	0.01
E	0.1	0.1	0.1	0.01
F	0.1	0.1	0.1	0.21

Experiment D exhibits a peculiar plateau period at low residence times, thought to potentially pertain to an induction period that could be further investigated *via* smaller RPO step changes (5 to 1 to 0.2 mL min^{-1}, D' and D'', Fig. 3.4). These smaller RPO step change experiments (grey and yellow dots) appeared relatively similar to the full RPO step change experiment (orange dots). As this concentration range was below the calibrated range of the ReactIR, it was determined the flat period was likely an artifact of the analytical method and thus could be ignored. For future experiments, data was truncated at the lower calibration limit of the ReactIR calibration (0.02 M) to guarantee valid data.

2.5 Diethyl pyrazole 3.4b kinetic data

Next, kinetic data was collected for the reaction of phenyl hydrazine (**3.2**) and heptane-3,5-dione (**3.1b**) to form pyrazole **3.4b** (Scheme 3.4). This data was collected as a comparison to the kinetic data collected

for the formation of pyrazole **3.4a**, such that the effect of a small change in substituent (methyl to ethyl) could be investigated and insight could be gained on the regioisomeric outcome of the corresponding unsymmetric diketone reaction.



3.1b **3.2** **3.4b**

Scheme 3.4. The reaction between heptane-3,5-dione (**3.1b**) and phenyl hydrazine (**3.2**) to produce pyrazole **3.4b**.

Different excess transient residence time experiments (Table 3.1, A, B, and C) were replicated in a semi-automated manner for the reaction of diketone **3.1b** and phenyl hydrazine **3.2** (Fig. 3.5). The in-line FTIR instrument was calibrated for the concentration of pyrazole **3.4b** allowing quantified product concentrations to be determined.

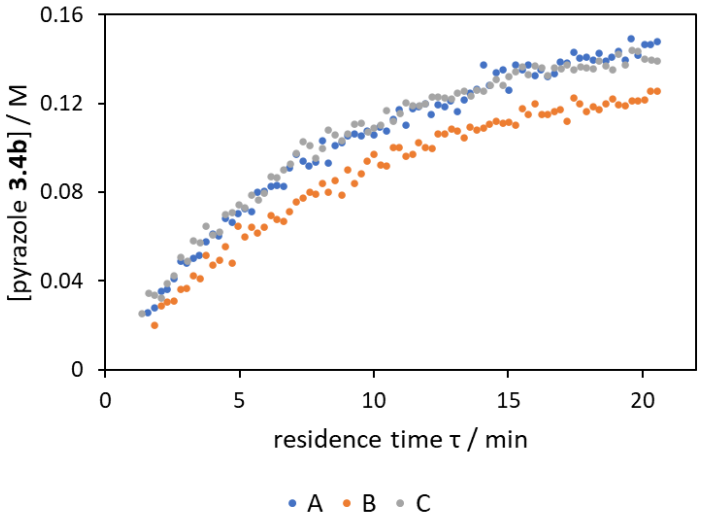


Figure 3.5. Time series data collected for the reaction of diketone **3.1b** and phenyl hydrazine **3.2** using residence time ramps for different excess experiments A, B, and C, described in Table 3.1.

An initial visual comparison of the different excess kinetic data for diketone **3.1a** and **3.1b** reveals a marked difference between the two reactions (blue, orange, and grey data in Fig. 3.3 and Fig. 3.5,

respectively). Whereas for diketone **3.1a** experiments A and B produce comparable product concentrations, for diketone **3.1b** experiments A and C are more similar, where experiment A is an equimolar reaction and experiments B and C are different excess experiments of **3.2** or **3.1a**/**b** respectively. This suggests that even though the two reactions should fit the same kinetic model, as the reactive centres are the same, the slight change in alkyl chain from methyl to ethyl causes a non-negligible change in relative rates of different kinetic pathways within the potential kinetic model.

3 Reactant stoichiometry and additive transience

3.1 Reactant stoichiometry method

To further investigate the effects of reactant stoichiometry on this reaction, and to probe the complexity of the reaction kinetics, a new transient flow method was developed by varying the reactant stoichiometry. By maintaining a constant cumulative flow rate (a fixed residence time) and varying the relative flow rate of the two reactant pumps, a series of different reactant stoichiometry data could be obtained efficiently (Fig. 3.6a). Applying this method to the Knorr pyrazole reaction at 70 °C with a 20 min residence time, and utilising 0.4 M stock solutions of the reactants produced pyrazole product (**3.4**) concentration data efficiently between a reactant stoichiometry of [**3.1a**]:[**3.2**] of 1.5:1 to 1:1.5 (Fig. 3.6b). Plotting this pyrazole **3.4a** concentration data against the reactant stoichiometry ratio, both as [**3.1a**]/[**3.2**] (red dots) and [**3.2**]/[**3.1a**] (blue dots), efficiently provides information on the kinetic model. If the reaction kinetics were the simple bimolecular kinetic model, as described in the literature (Scheme 3.1, where R_1=R_2=Me and R_3=Ph), in which reactants **3.1a** and **3.2** are interchangeable in the kinetic equations we would expect these data (red and blue dots) to overlap. In a single reactant stoichiometry ramp experiment, strong evidence is collected disproving this simple bimolecular model, and that suggests a more complex kinetic model in which the concentrations of reactants **3.1** and **3.2** are not mathematically interchangeable. This further verified observations from different excess, same excess, doping experiments, and VTNA of batch experimental data suggesting a more complex kinetic model.

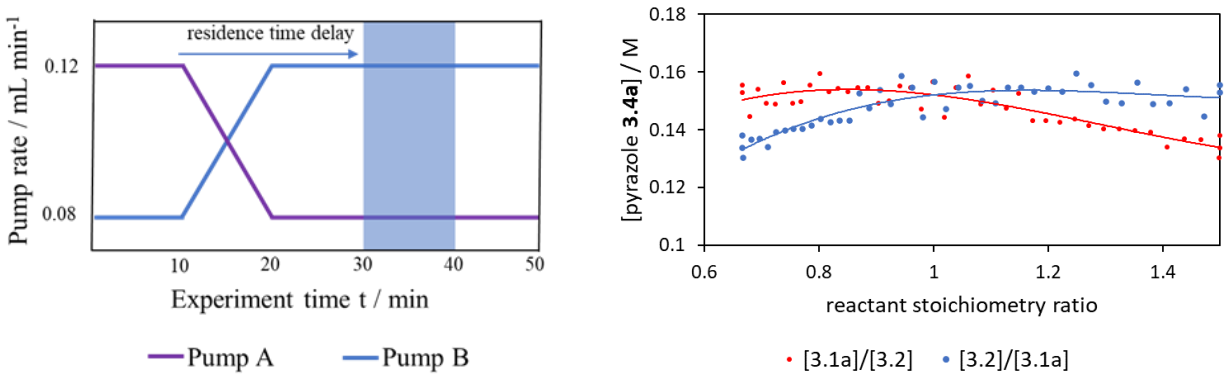


Figure 3.6. Reactant stoichiometry ramp method (a) and results (b) at a 20 minute residence time, 70 °C and using 0.4 M stock solutions of **3.1a** and **3.2** between ratios of [**3.1a**]/[**3.2**] of 0.16 M:0.24 M to 0.24 M:0.16 M plotted against [**3.1a**]/[**3.2**] and [**3.2**]/[**3.1a**] demonstrating clear conflict with the simple rate law (Equation 3.1). The fitted 3º lines are as a visual aid.

Performing this method utilising different cumulative flow rates (0.3 and 0.4 mL min^{-1}, corresponding to residence times of 14 and 10 min, respectively) produced further valuable reaction data (Fig. 3.7a). Product concentration data collected by this method can appear somewhat misleading, as the maximum product concentration obtainable varies, limited by the reactant stoichiometry. At uneven reactant concentrations (reactant stoichiometry ≠ 1), one of the reactants becomes the limiting reagent, therefore the reaction data may be better visually assessed if plotted against yield of product, based on the limiting reactant (Fig. 3.7b). This visualisation of the reaction data reveals more keenly that although an excess of phenyl hydrazine (**3.2**) increases the rate of reaction most markedly, an excess of acetyl acetone (**3.1a**) also increases the rate relative to that of an equimolar stoichiometry.

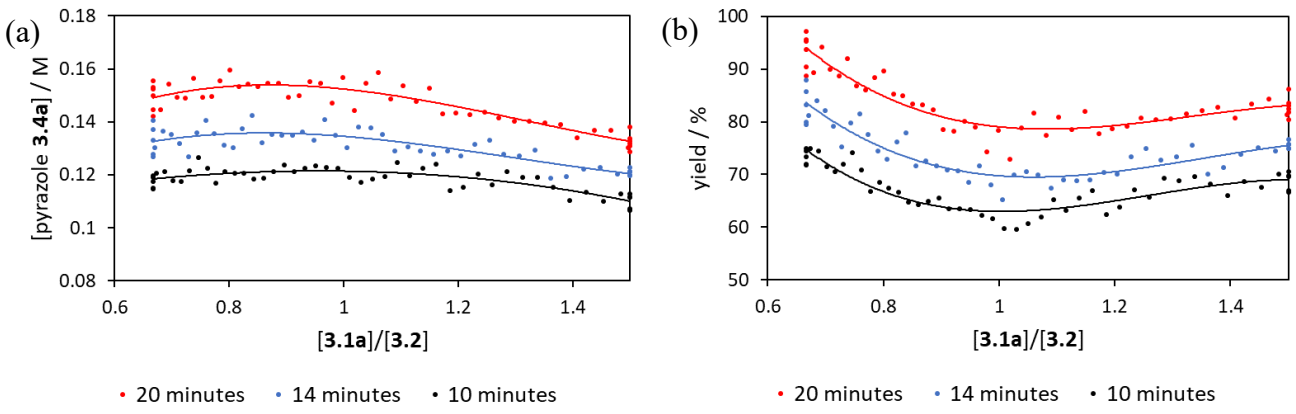


Figure 3.7. Reactant stoichiometry ramp method results at stated residence times, 70 °C and using 0.4 M stock solutions of **3.1a** and **3.2** between ratios of [**3.1a**]/[**3.2**] of 0.16 M:0.24 M to 0.24 M:0.16 M plotted against [**3.1a**]/[**3.2**] and [**3.2**]/[**3.1a**] plotted as pyrazole **3.4a** concentration / M (a) and yield based on limiting reactant / % (b). The fitted 3º lines are as a visual aid.

Reaction stoichiometry ramps were also utilised to study the reaction of diketone **3.1b** and phenyl hydrazine **3.2** at 10 min (grey data) and 20 min residence times (blue data) (Fig. 3.8). These experiments also included a second reactant stoichiometry ramp at 20 min, performed at the same ramp rate between relative flowrates but beginning with an excess of **3.1b** and ending with an excess of **3.2** (orange data). These data were compared with the previous ramp (blue data) in which there is initially an excess of **3.2** and the experiment ends with an excess of **3.1b**. Good agreement was found between the experiments, suggesting data collected by this method is independent of ramping direction.

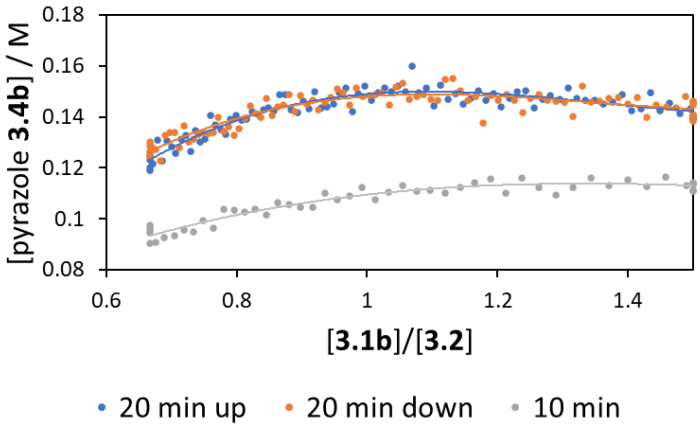


Figure 3.8. Reactant stoichiometry ramp method results at stated residence times, 70 °C and using 0.4 M stock solutions of **3.1b** and **3.2** between ratios of [**3.1b**]/[**3.2**] of 0.16 M:0.24 M to 0.24 M:0.16 M (or the inverse for the "down ramp") plotted against pyrazole **3.4b** concentration / M. The fitted 3° lines are as a visual aid.

Comparison was then made between the reactant stoichiometry ramp data obtained for the formation of pyrazole **3.4a** and **3.4b** both as a plot of pyrazole product concentration (Fig. 3.9a) and as product yield from the limiting reactant (Fig. 3.9b). These data suggest a substantial difference in the dominant kinetic pathway for the different diketone reactants, revealed most strongly by the intersection of the data collected at 20 minutes residence time for diketone **3.1a** (red data) and **3.1b** (dark blue data). As one would expect the same kinetic pathways to be available to both reactions as the reactive sites are the same, this observation suggests that there are multiple kinetic pathways available for this reaction, which have relative rates strongly dependent upon the reactants.

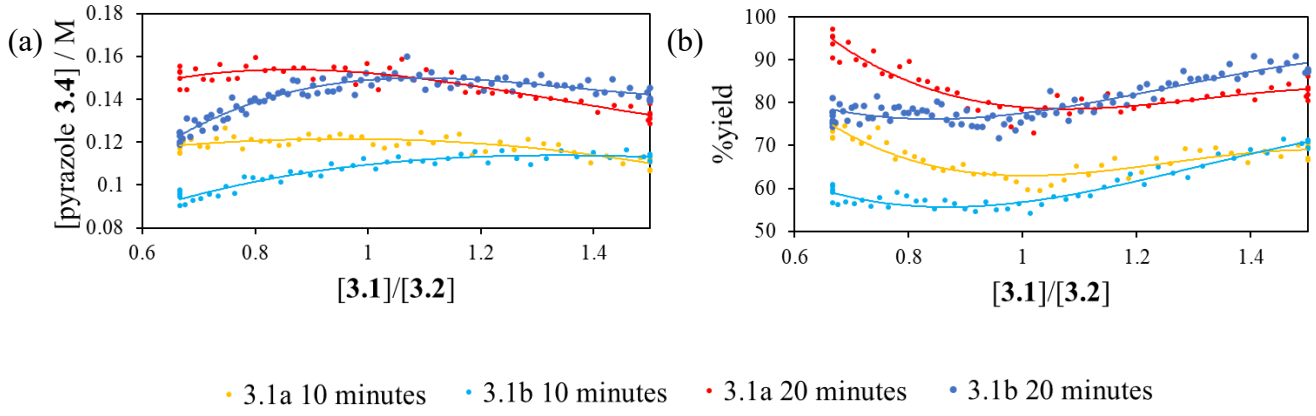


Figure 3.9. Comparison of reactant stoichiometry ramps between at a fixed residence time (20.67 min): (a) pyrazole product concentration or (b) conversion of the limiting substrate *vs.* reactant stoichiometry ratio [**3.1**]/[**3.2**].

3.2 Multivariate residence time-reactant stoichiometry ramps

To further facilitate efficient collection of reaction data across a reaction time-reactant stoichiometry space to robustly develop kinetic understanding, the development of a multivariate ramp was envisaged, based on earlier reports of residence time-reaction temperature ramps[58] and residence time-additive concentration ramps.[67] For this reaction time-reactant stoichiometry ramp, the developed method consists of priming the flow reactor volume (4.13 mL) with a reactant stoichiometry ramp at an initial flow rate and then performing an RPO cumulative flow rate step change (Fig. 3.10). By performing the initial reactant stoichiometry ramp in the reverse direction before the RPO cumulative flow rate step change, the orthogonal reaction data series can be produced.

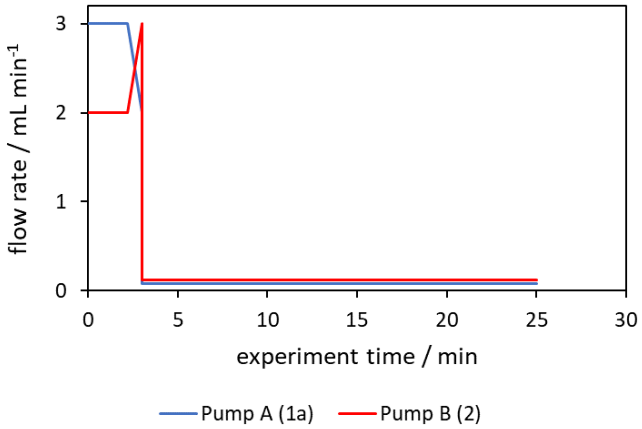


Figure 3.10. Cumulative volumetric flow rate method for a standard transient residence time-reactant stoichiometry ramp experiment performed over a residence time range between 0.8 – 20 minutes and a reactant stoichiometry ratio ([**3.1a**]/[**3.2**]) range between 1.5 – 0.8.

Performing such ramps on the Knorr pyrazole reaction under study efficiently produced reaction data across the reaction parameter space investigated by the previous residence time and reaction stoichiometry ramps (Fig. 3.11a). Each data series on its own is less interpretable than a single variable (residence time or reactant stoichiometry) ramp, however together they provide such data more efficiently while also providing repeat data to confirm data collected by the previous methods. Such data is best presented on a 3D plot, and can as such be compared to reaction data collected by single variable ramping methods (Fig. 3.11b).

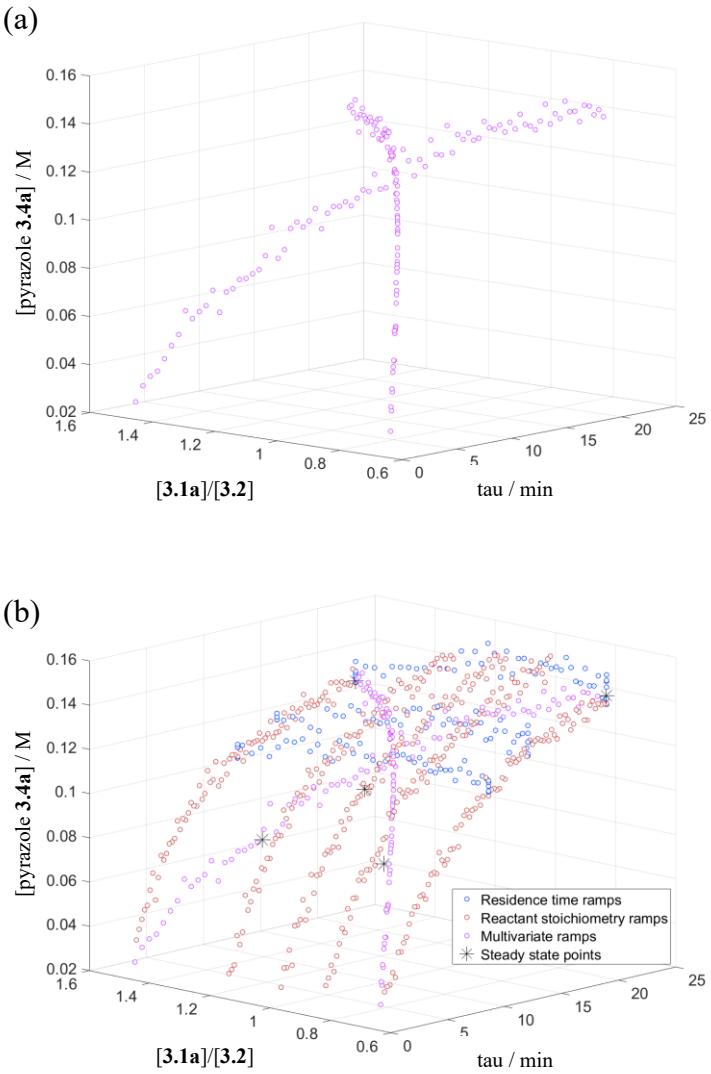
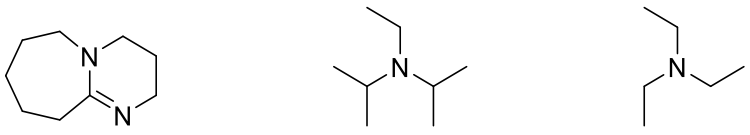


Figure 3.11. Reaction data collected for the formation of pyrazole **3.4a**: (a) two combined residence time-reactant stoichiometry ramps; and (b) residence time, reactant stoichiometry, and residence time-reactant stoichiometry ("multivariate") ramps compared to steady state experimental data.

3.3 Additive concentration ramps

The autocatalytic role of the pyrazole product was thought to be the facilitation of the dehydration steps (acid-base catalysis) to form intermediate **3.3** or pyrazole **3.4** from intermediate **3.3**. In order to confirm the mode of catalysis, acid (acetic acid) and base additives (sodium ethoxide, DBU, DIPEA, and TEA, Scheme 3.5) ramps were performed *via* a three-pump system (Fig. 3.12). 0.4 M solutions of phenyl hydrazine and acetyl acetone were delivered by two of the pumps, with the third delivering one of the reactants at 0.4 M with the additive. By ramping the third pump's flow rate against the corresponding reactant pump, the concentration of additive could be changed while maintaining the same reactant stoichiometry and residence time - in this case an equal reaction stoichiometry and 4.13 min residence time (Fig. 3.13). These additive ramps were performed both with increasing and decreasing additive concentration, to identify any discrepancies in product concentration potentially caused by formation of solids on additive ramping. Such issues would be identified by differing product concentrations observed on the up and down ramps. A slight discrepancy was observed for the acetic acid additive ramp (light blue dots, Fig. 3.13) although this effect disappears at higher acetic acid concentrations. This was likely due to the failure to pre-cool the Peltier for a sufficient time in this case.



DBU **DIPEA** **TEA**

Scheme 3.5. Organic bases utilised in additive ramping experiments. DBU: 1,8-diazabicyclo[5.4.0]undec-7-ene; DIPEA: N,N-diisopropylethylamine; TEA: triethylamine.

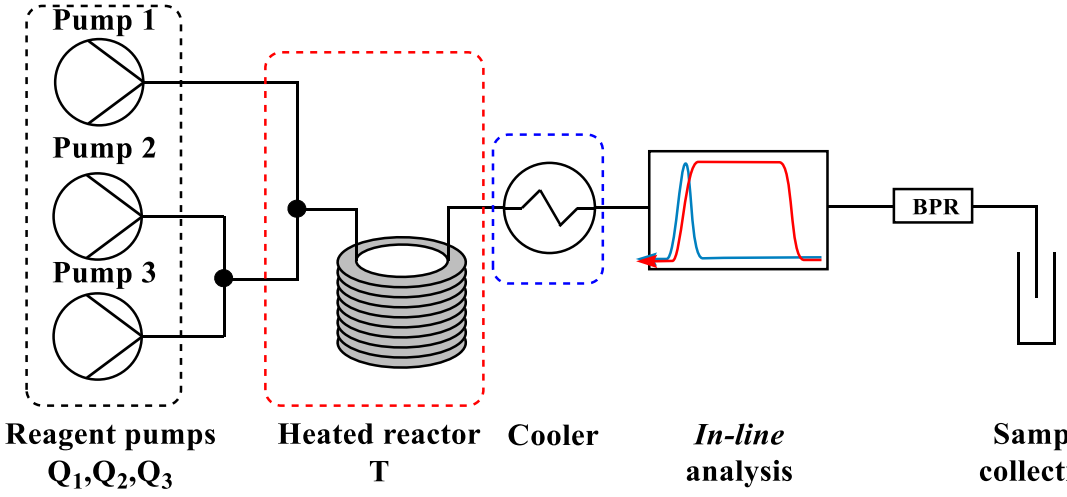


Figure 3.12. Schematic of the three-pump flow system for the control of individual flow rate (Q_1, Q_2, and Q_3) and temperature (T), with in-line analytics. Pump 2 and pump 3 always contained the same reactant as each other (1 or 2).

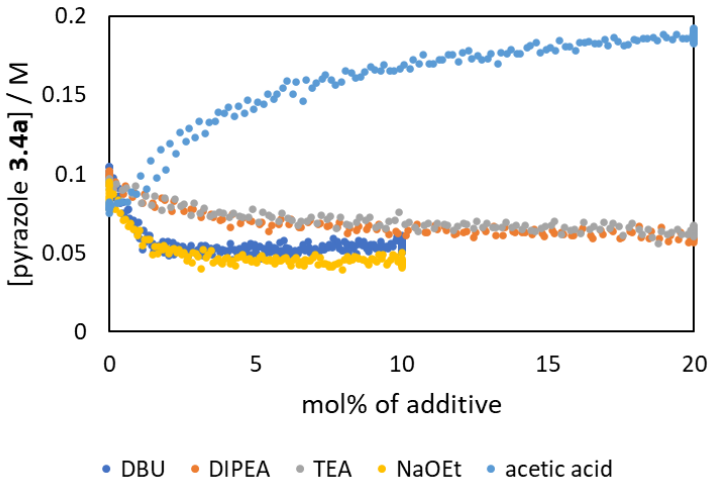


Figure 3.13. Acid - base ramping experimental pyrazole product (**3.4a**) concentration data collected for the reaction of diketone **3.1a** and phenyl hydrazine at 70 °C, 0.2 M reactant concentrations of **3.1a** and **3.2**, and 4.13 minutes residence time.

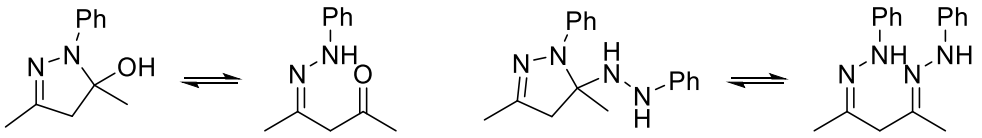
It was found that base additives (TEA, DIPEA, DBU, NaOEt) of varying strengths and nucleophilicities inhibited the reaction to an extent, even at < 5 mol%, whereas the addition of acetic acid catalysed the reaction (light blue dots). The stronger bases (DBU and NaOEt, dark blue and yellow dots) had a bigger effect on slowing the reaction; however, beyond a certain concentration of base additive (between 2–5 mol%), adding more base does not further slow the reaction, implying that base is preventing a protonation event, rather than deprotonating an intermediate. This supports the hypothesis that the pyrazole product **3.4** is acting as an acid catalyst in its protonated form, and its catalytic activity is

quenched with addition of base; at which point the uncatalysed pathway could still occur at a slower rate. Therefore, the pyrazole is likely acting as a catalytic proton source to eliminate water from intermediate **3.3**.

4 Intermediate analysis

4.1 Off-line HPLC-MS analysis

Off-line HPLC-MS analysis of reaction aliquots revealed a peak with a m/z of 191.2, which corresponds to the previously reported intermediate **3.3a** (or **3.6a**, Scheme 3.6). Surprisingly, the presence of an additional peak at m/z 281.2 was also observed, which appears to correspond to a di-addition intermediate (**3.5a** or **3.7a**, Scheme 3.6), that was present in the reaction mixtures of 'different excess' experiments. This peak disappeared over time if the sample was left to stand in ambient conditions, confirming its transient nature as a reaction intermediate, rather than an artifact of the analysis method. Attempts to isolate either intermediate (**3.3a**/**3.6a** or **3.5a**/**3.7a**) proved unsuccessful due to the instability of the intermediate, converting to pyrazole **3.4a** even under ambient conditions.

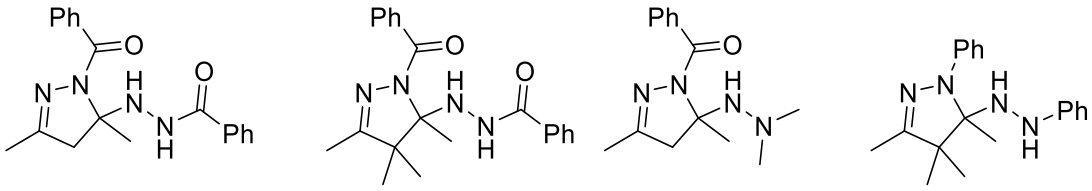


3.3a **3.6a** **3.5a** **3.7a**

Scheme 3.6. The possible forms of the mono-addition intermediate (**3.3a**/**3.6a**) and di-addition intermediate (**3.5a**/**3.7a**).

By HPLC-MS analysis alone it was impossible to distinguish between the closed (**3.3a** and **3.5a**) and open (**3.6a** and **3.7a**) forms of these intermediates, due to the identical molecular masses. While there is previous precedent for the observation of mono-addition intermediates[92,96] such as **3.3a**, the identification of di-addition intermediates such as **3.5a** have not previously been reported. However, similar molecules can be isolated and characterised, in cases when the molecule is unable to eliminate a

hydrazine to rearomatize, characterised by NMR spectroscopy (Scheme 3.7).[100,101]



Scheme 3.7. Previously reported di-addition type pyrazolines reported by Yakimovich and co-workers.[100,101]

4.2 *In-situ* ^{1}H and ^{13}C NMR analysis

To further probe the structure of the intermediates, *in situ* NMR experiments were performed. The reaction was initiated in an NMR tube by mixing 0.2 M phenyl hydrazine and acetyl acetone at room temperature in CD_3OD, and analysed by ^{1}H and ^{13}C NMR spectroscopy within 5 minutes of reaction initialisation. ^{1}H NMR spectra recorded of the reaction mixture (purple spectra, Figure 3.14a) revealed new peaks not present in starting materials (phenyl hydrazine, blue spectra, or diketone **3.1a**, red spectra), or pyrazole product **3.4a** (green spectra) (Fig. 3.14a). These additional peaks are observed in the alkyl shift region in both ^{1}H and ^{13}C NMR spectra (Fig. 3.14b and c, 0.8 – 2.6 ppm and 0 – 45 ppm, respectively) marked by asterisks. The number of alkyl peaks suggests multiple intermediates are present, however identification of intermediate structures is challenging due to the low concentrations present.

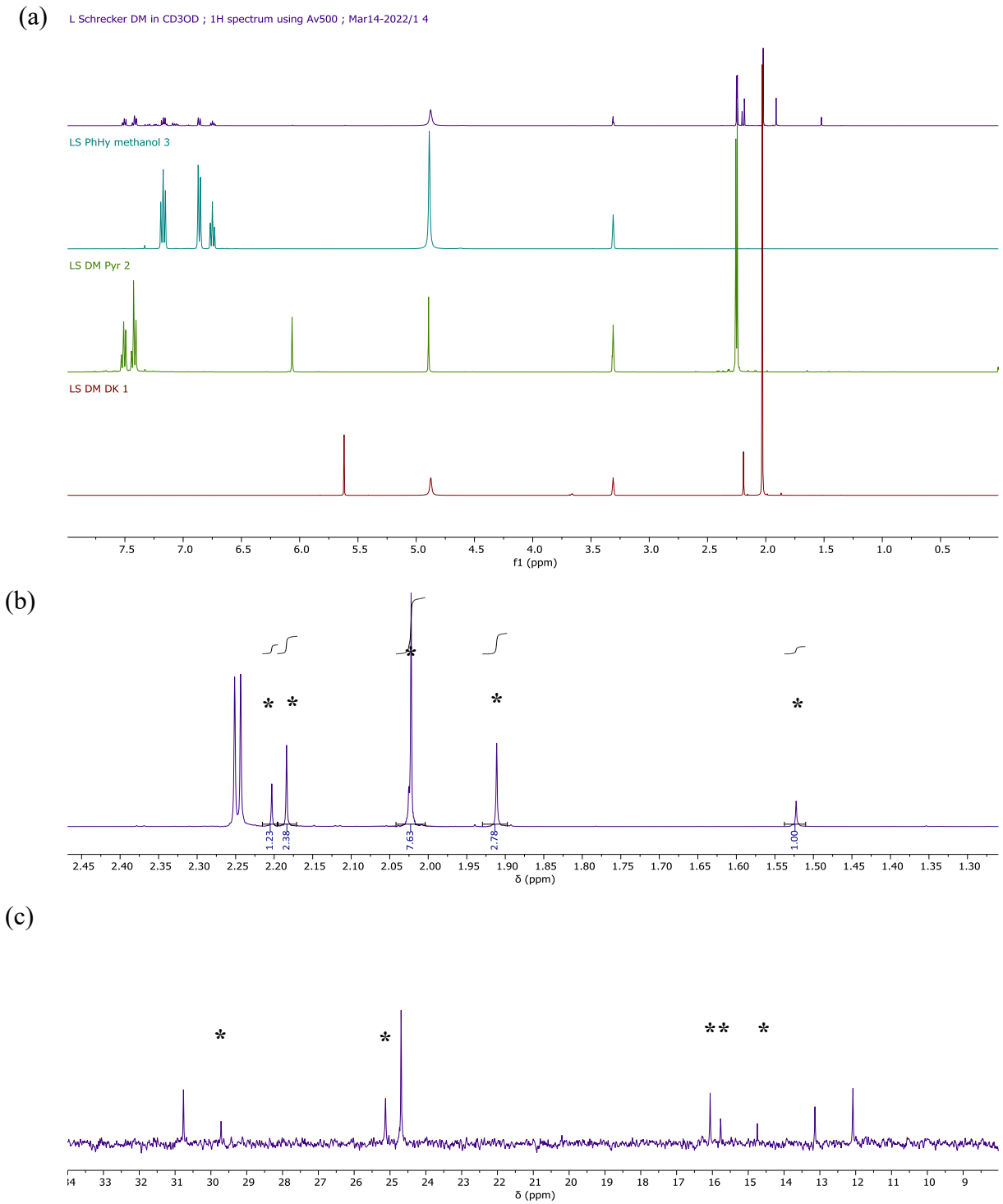


Figure 3.14. (a) ^{1}H NMR spectra, (b) the alkyl region of the ^{1}H NMR spectra, and (c) the alkyl region of the ^{13}C NMR spectra taken under 5 minutes from the initiation of the reaction of diketone **3.1a** and phenyl hydrazine in CD_3OD with comparative spectra for phenyl hydrazine, pyrazole **3.4a** and diketone **3.1a**. New peaks in the reaction mixture are marked in (b) and (c) by black asterisks.

4.3 Other symmetric substrates

To further investigate the formation of this previously unseen intermediate (**5**), further symmetric alkyl substituted diketones (**3.1b-e**, where R= Et, *i*-Pr, *i*-Bu and *t*-Bu, respectively) were reacted with phenyl hydrazine in ethanol at room temperature. Aliquots of the reaction mixtures were analysed by HPLC-MS to identify the presence of reaction intermediates, analysed by taking an extracted ion chromatogram (EIC) for the mass to charge ratio corresponding to pyrazole product **3.4**, mono-addition intermediate (**3.3** or **3.6**), and di-addition intermediate (**3.5** or **3.7**) (Fig. 3.15). Mono-addition intermediates (**3.3** or **3.6**) were identified in all cases in reaction aliquot extracted at 10 minute or 1 hour, except for diketone **3.1e,** which did not react, even when heated to 70 °C for 1 hour. A peak corresponding to the mass of a di-addition intermediate (**3.5** or **3.7**) was only detected for diketone **3.5b** (R = Et) and **3.5d** (R = ^{i}Bu); presumably the formation of **3.5c** (R = ^{i}Pr) is prevented by steric hinderance.

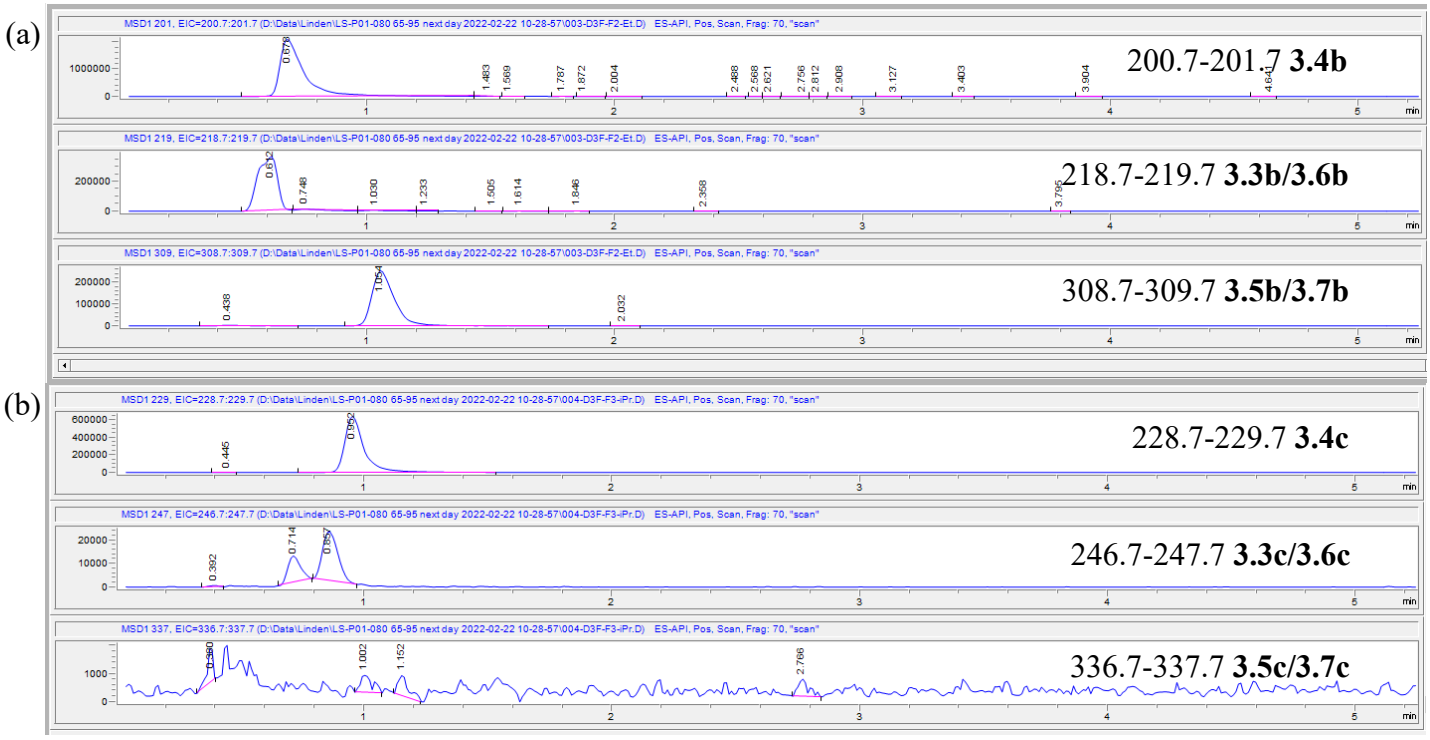


Figure 3.15. Extracted Ion Chromatograms (EICs) of pyrazole product **3.4**, mono-addition intermediates **3.3**/**3.6**, and di-addition intermediates **3.5**/**3.7** of the stated m/z values, extracted from total ion chromatograms (TICs) utilising a positive electron spray ionisation. Example EICs for the reaction of phenyl hydrazine with diketone **3.1b** (a) and **3.1c** (b).

In situ ^{13}C NMR analysis was also performed on the reaction of diketone **3.1b** and phenyl hydrazine in CD_3OD (0.2 M) at room temperature. DEPT-135 edited ^{13}C NMR was chosen as a fast NMR experiment, which would reveal the number of new CH_2 carbon environments to identify whether any intermediates were symmetrical (odd number of CH_2 carbon environments) (Fig. 3.16). Five minutes after reaction initialisation, at least 4 new CH_2 environments (black asterisks) were identified in the reaction mixture (purple spectra) when compared to phenyl hydrazine (blue spectra), pyrazole product **3.4b** (green spectra), and diketone **3.1b** (red spectra), suggesting most plausibly two unsymmetrical intermediates.

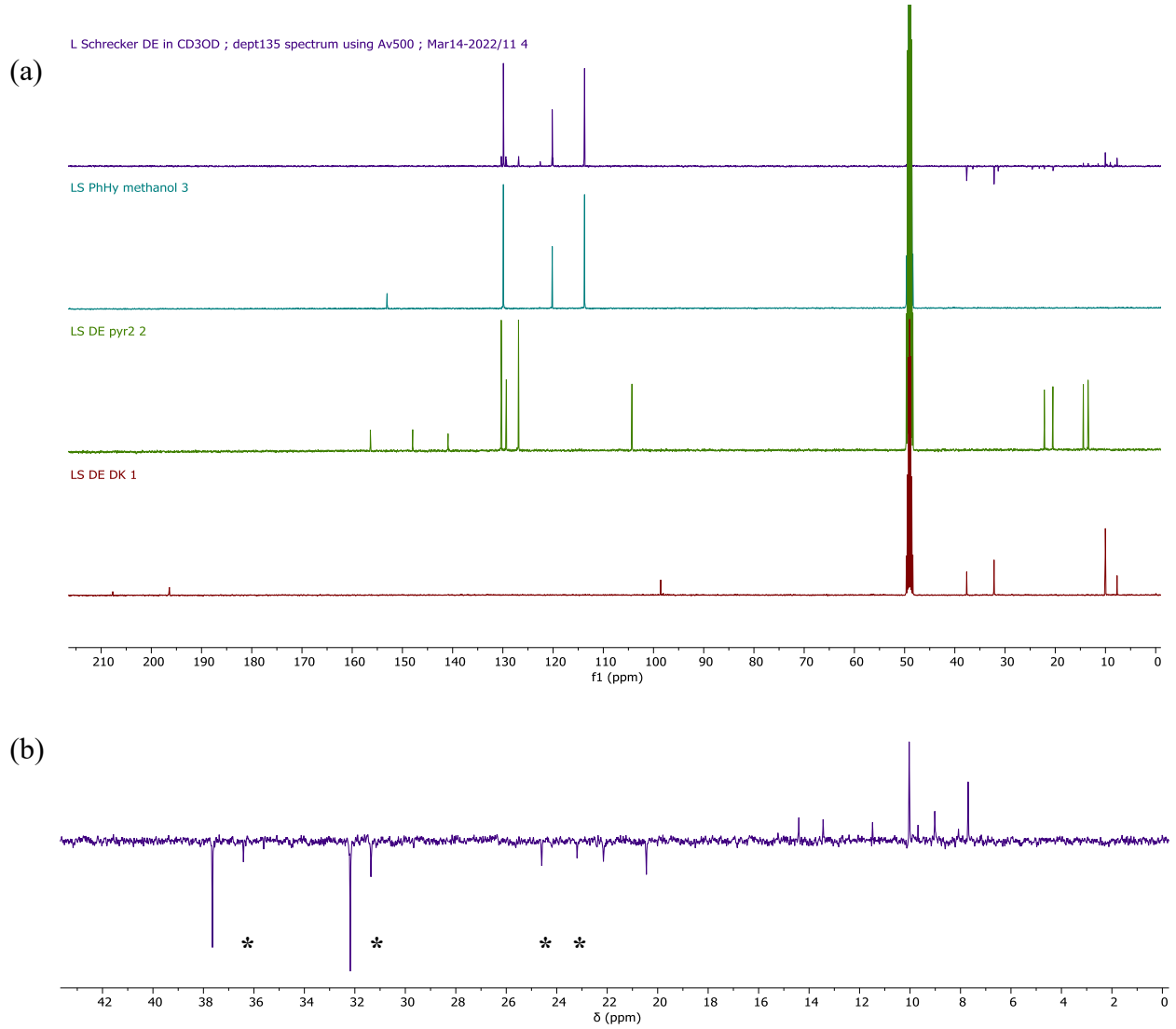


Figure 3.16. (a) DEPT-135 NMR spectra taken under 5 minutes from the initiation of the reaction of diketone **3.1b** and phenyl hydrazine in CD_3OD with comparative ^{13}C NMR spectra for phenyl hydrazine, pyrazole **3.4a** and diketone **3.1a**. (b) the alkyl region of the spectra shown in part (a). Additional CH_2 carbon environments within the reaction mixture are marked with asterisks.

5 Microkinetic modelling

5.1 Reaction data used for model fitting

Before commencing construction and fitting of microkinetic models, two further 'same excess' experiments (Fig. 3.17, Table 3.3, experiments G and H) were performed with diketones **3.1a** and **3.1b**. These experiments were performed at higher concentrations (0.14 and 0.11 M) than the previous 'same excess' experiments, in order to gather more useful reaction data above the calibration limit of the ReactIR. The reaction data obtained from these experiments was combined with the 'different excess' experimental data, and 'doping' experimental data for diketone **3.1a** (Fig. 3.17a for diketone **3.1a** and Fig. 3.17b for diketone **3.1b**). The initial 'same excess' experiment (experiment D) was not utilised for microkinetic model training due to much of this experimental data falling below the concentration calibration limit for the ReactIR. 'Doping' experiments were not performed for diketone **3.1b** because 'same excess' experiments G and H provide equivalent information as would be obtained from these experiments.

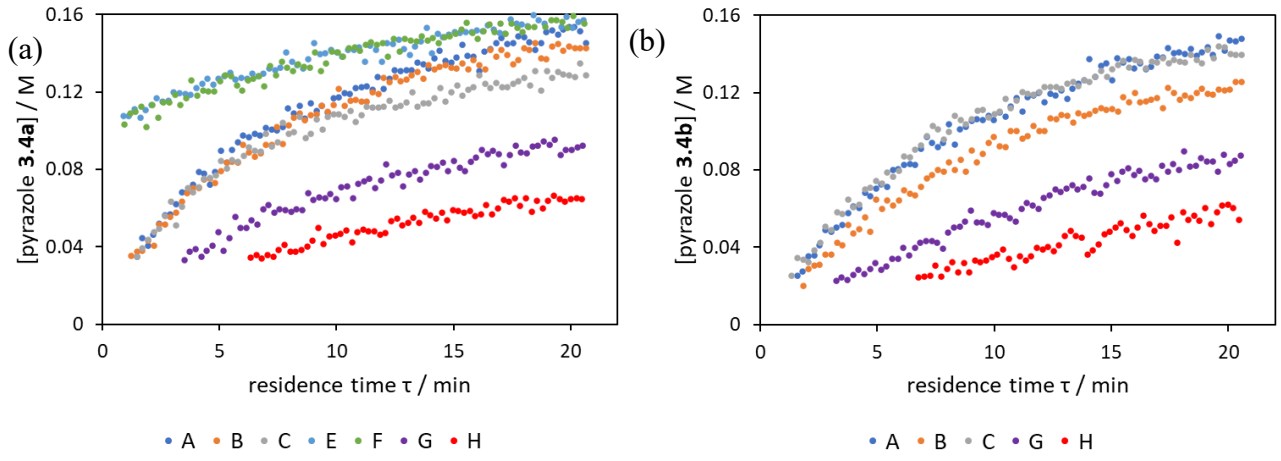


Figure 3.17. Time series data collected for the reaction of diketone **3.1a** (a) or diketone **3.1b** (b) and phenyl hydrazine **3.2** using residence time ramps over a range of different excess, same excess and doping experiments, described in Table 3.3.

Table 3.3. Initial concentrations for the set of time series kinetic experiments utilised for microkinetic model fitting. All were used for the diketone **3.1a** and experiments A – C, G, and H were used for diketone **3.1b**.

Experiment	[3.1] / M	[3.2] / M	[3.4] / M	[H_2O] / M
A	0.2	0.2	0	0.01
B	0.16	0.24	0	0.01
C	0.24	0.16	0	0.01
E	0.1	0.1	0.1	0.01
F	0.1	0.1	0.1	0.21
G	0.14	0.14	0	0.01
H	0.11	0.11	0	0.01

5.2 Microkinetic modelling setup

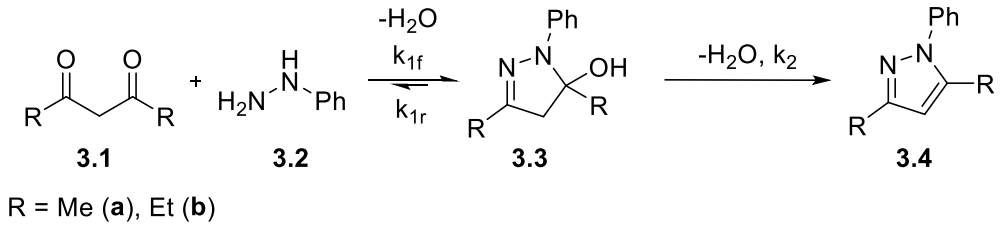
Based on the experimental observations from off-line analysis and transient flow methods, a series of progressively more complex microkinetic models were constructed. As the same reactive sites are available independent of the diketone reacting (**3.1a** or **3.1b**), models constructed must obtain good fits to both the reactions of diketone **3.1a** or **3.1b** and phenyl hydrazine, utilising the same kinetic pathways but different fitted rate constants. The models were constructed and fitted to reaction data using the ordinary differential equation (ODE) solver Berkeley Madonna (BM) to fit and optimise all rate constants simultaneously.[102] The models were initially fitted to data collected utilising residence time ramping experiments A – C and E – H for diketone **3.1a** (Fig. 3.17a). Reaction data from experiments A – C, G, and H performed with diketone **3.1b** and phenyl hydrazine were then used to refit the models to test the models' applicability to this reaction also (Fig. 3.17b). The multicurve fitting function in BM was used implementing the solver Runge-Kutta 4 initially, but then transferring to Rosenbrock (stiff) as a solver once the model complexity increased. The Rosenbrock (stiff) solver is designed to better handle highly coupled series of ODEs as was the case in these microkinetic models and thus ran more efficiently.

Reaction data obtained from the other transient flow methods (Section 3), reactant stoichiometry and residence time-reactant stoichiometry ramps, proved challenging to use in model fitting. This is because

ODE series solvers rely on time series data and become significantly more computationally expensive with a large number (10+) of time series at different initial concentrations to fit. The complexity of the ODE series for the microkinetic models also precluded the algebraic evaluation of the differential equations to generate a surface function, which then could be fitted to the data. In order to best utilise this reaction data, it was decided that an arbitrary surface function could be generated from the fitted form of the microkinetic model ODEs, which could then be visually compared to the reaction stoichiometry and residence time-reaction stoichiometry ramps.

5.3 Iterative development of microkinetic model

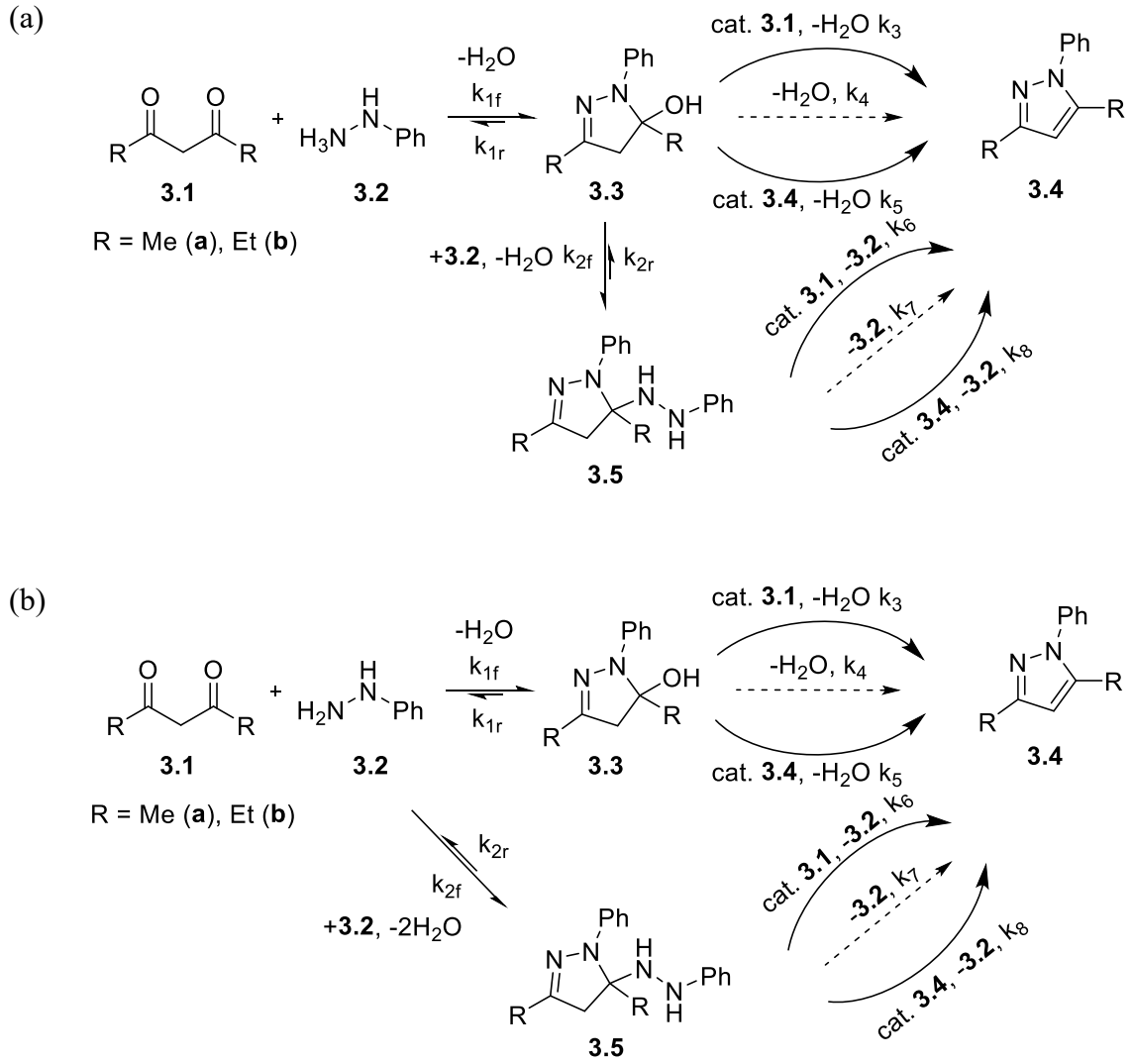
In order to benchmark further microkinetic model development, the initial model fitted was the simple linear model *via* intermediate **3.3** proposed in previous work (Model A, Scheme 3.8). As expected, fitting this model to the reaction data for either diketone **3.1a** or **3.1b** produced a quantitatively and qualitatively poor fit, with a root mean squared error (RMSE) of greater than 0.3 and clear visual misalignment.



Scheme 3.8. Scheme of the initial simple linear model (Model A) involving 5 species and 3 fitting parameters.

More complex models (Model B1 and B2, Scheme 3.9) were constructed to incorporate insights gained from other experiments by individually introducing new pathways (extra ODEs) that would improve the accuracy of the model. The lack of overlay for reactant stoichiometry ramps (Fig. 3.7b) suggested reactants **3.1** and **3.2** must be algebraically non-equivalent in the model. This could be incorporated in combination with evidence from the NMR and HPLC-MS experiments through the inclusion of a di-addition intermediate **3.5**. Product-doping experiments led to the inclusion of product catalysed pathways and reaction stoichiometry ramps for diketone **3.1b,** suggesting that the diketone itself could

be taking part in some cases as an acidic catalyst, as supported by acid-base ramping experiments.

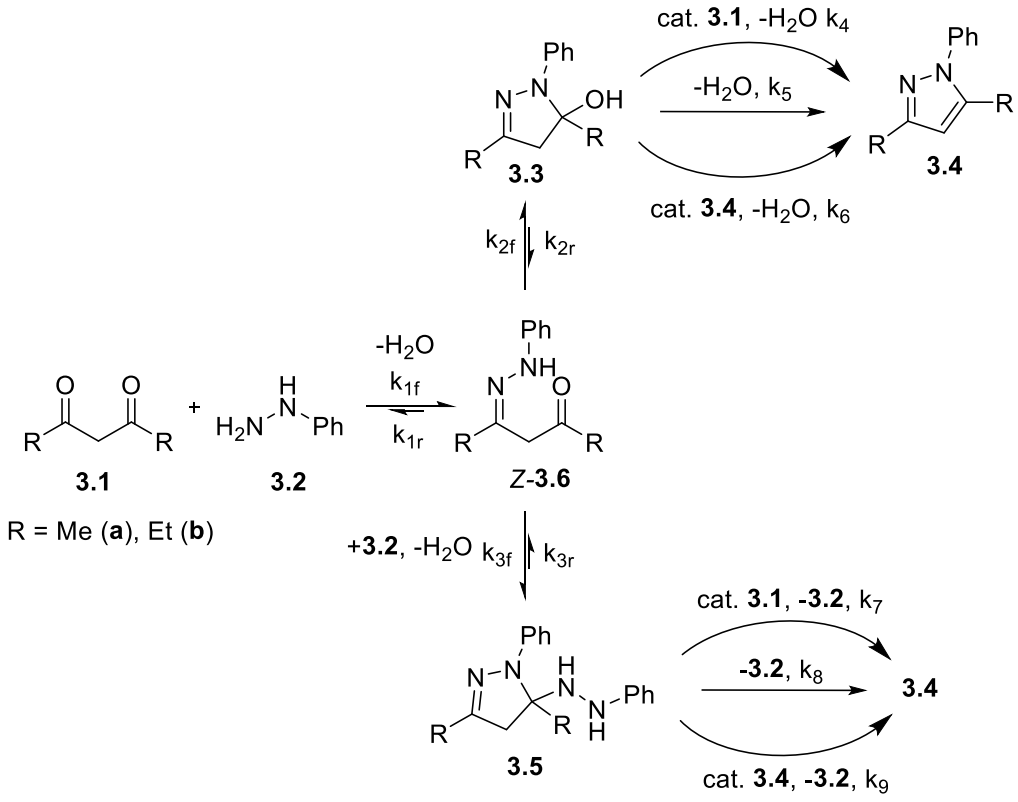


Scheme 3.9. Scheme of the more complex models involving 6 species and 10 fitting parameters developed from insight into the reaction from other experiments either constructed as: (a) a competitive model (Model B1) or; (b) a divergent model (Model B2).

The inclusion of these extra pathways improved the quantitative accuracy of the model (RMSE < 0.05 for both Model B1 and B2) however the models performed poorly qualitatively when visually compared to reaction data. Both models B1 and B2 have a strong dependency on water concentration which was not observed in the water doping experiments E and F (Fig. 3.5b), notably in opposite directions. Model B1 predicts slower product **3.4** formation with additional water, whereas Model B2 predicts faster product **3.4** formation. Additionally Model B1 poorly predicts reactions with an excess of diketone **3.1a** and Model B2 poorly predicts reactions with equimolar reactant stoichiometries. The good quantitative

fit but poor qualitative fit suggests the models are overfitting the experimental data on which they are trained, and thus adding further kinetic parameters to the model would not necessarily improve the qualitative fit although the RMSE may continue to decrease. Thus a different form of microkinetic model was deemed necessary to best fit the reaction.

Model B1 and B2 do not include intermediate **3.6**, from which both intermediate **3.3** and di-addition intermediate **3.5** must mechanistically be formed. It was envisaged that by including the hydrazone **3.6** as a common intermediate in the microkinetic model, more faithful to the likely underlying reaction mechanism, a better model may be obtained. This change of microkinetic model pathways led to a quantitatively similarly fitting model (RMSE < 0.05) but qualitatively better fitting model more closely aligned with likely mechanism (Model C, Scheme 3.10). However as this modification involved addition of fitted rate constants to an already overfitting model, it was determined this model should be modified to simplify the model.



Scheme 3.10. Scheme of the competitive divergent model (Model C) involving 7 species and 12 fitting parameters.

Reducing the number of fitted rate constants allows the subset of rate constants to be fitted with more accuracy as the computational power needed for optimisation of the fitting becomes less. If the model still quantitatively fits well and is simpler, this also helps prevent over fitting and produces a more interpretable model, highlighting the interplay between the most dominant kinetic pathways. In order to reduce the number of fitted rate constants, an iterative method was developed by which (i) the model was first fitted with all rate constants, (ii) rate constants < 1 x 10^{-5} were deemed kinetically negligible, are set to zero and removed from the list of fitted parameters, (iii) the model is than refitted with the shortened kinetic parameter list with remaining kinetic parameters initially set to those optimised in the previous iteration. This method was repeated until all rate constants are above 1 x 10^{-5} and the RMSE is no longer decreasing on further iteration.

Using this iterative method for Model C for the reaction of diketone **3.1a** and phenyl hydrazine (Fig. 3.18 where red indicates kinetically irrelevant pathways in each iteration), it was found that this method worked well as a first pass but could be improved further by resetting k_4 – k_6 and k_7 – k_9 to the mean value of each set before a further reoptimisation, which improved the qualitative fit and RMSE further. These parameters were more challenging presumably as dictate groups of kinetic pathways which can directly compensate for each other, as they have the same starting materials and product, and thus are more likely to settle on a local optimum.

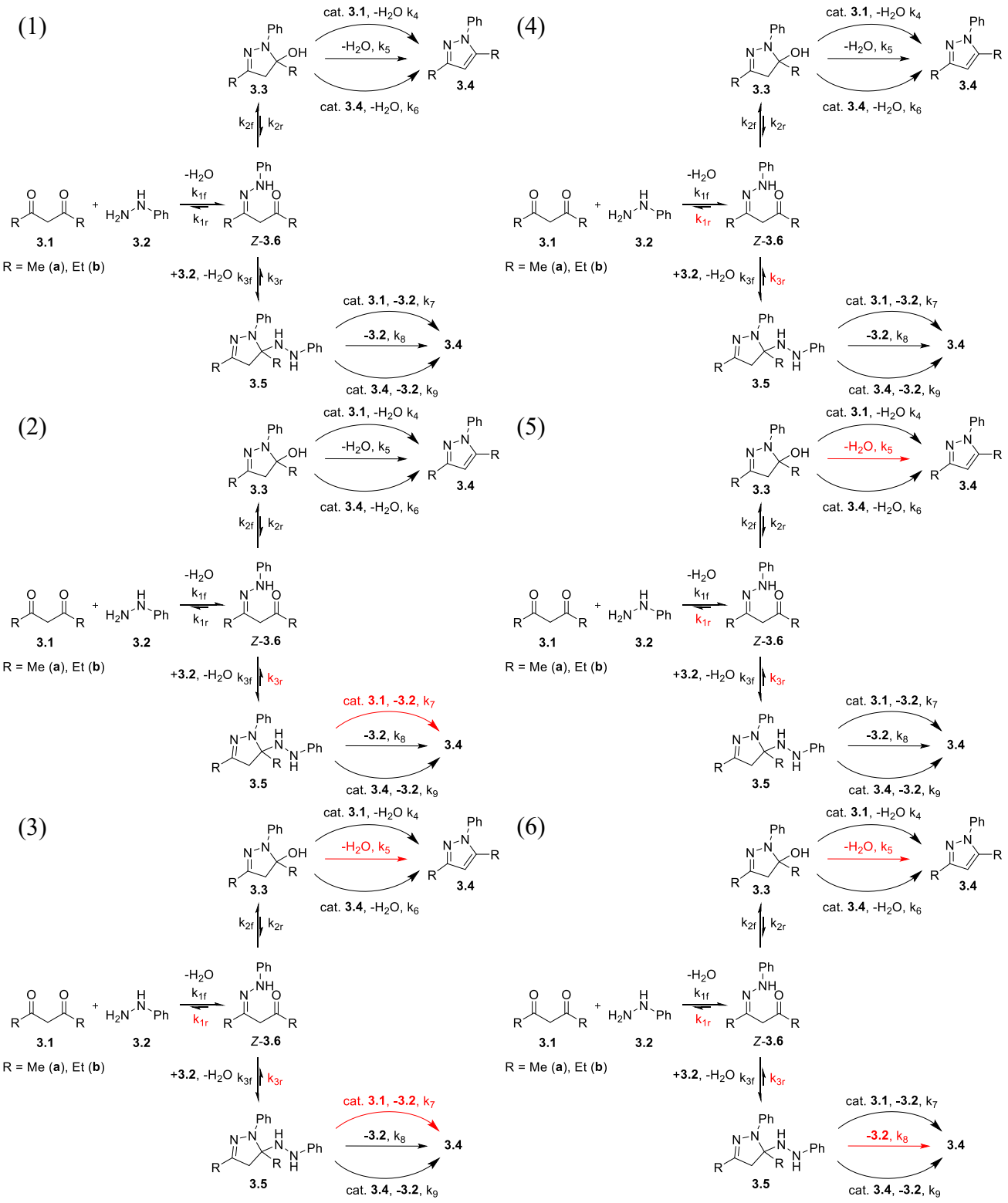
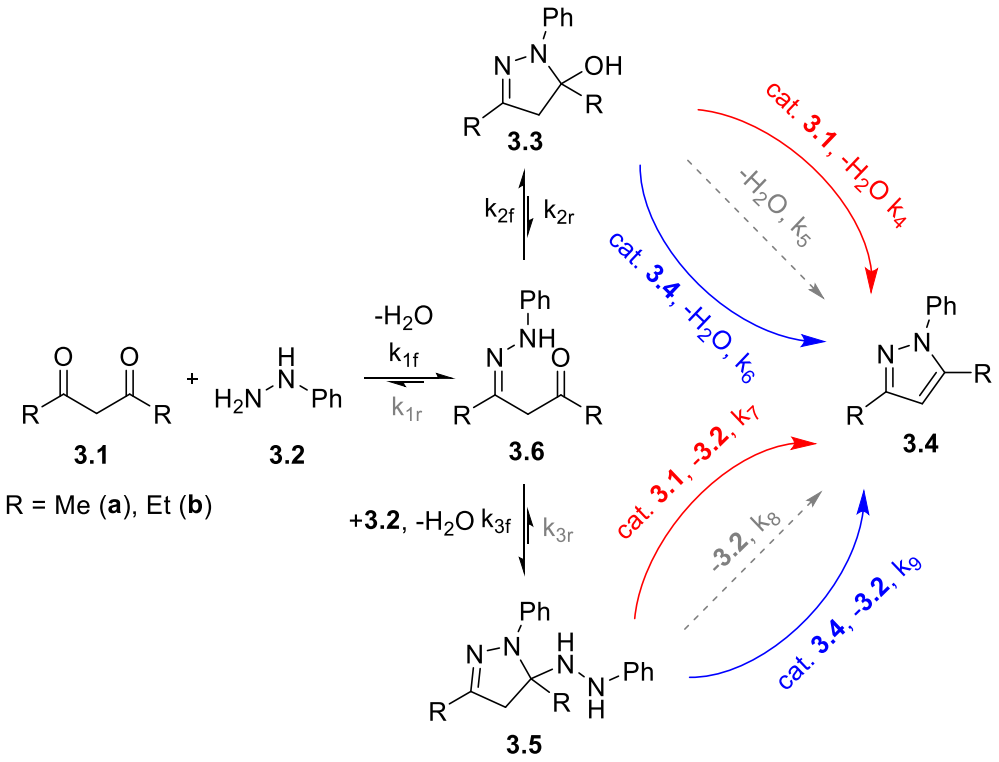


Figure 3.18. An example of the progression of model C (1) when fitted to data for the reaction of diketone **3.1a** using experiments A – C and E – H (Table 3.3) through our IFDO (iterative fitting drop-out) method. This leads to the dropping and refitting of the equilibrium steps (K_1-K_3) to produce two irreversible steps k_{1f} and k_{3f} and one equilibrium K_2. The later irreversible steps (k_4-k_9) are then given the mean value of their respective group (k_4-k_6 and k_7-k_9) (4) before performing IFDO again to reach a stable simple functional model (6).

5.4 Final microkinetic model

The iterative method produced model fittings for diketone **3.1a** and **3.1b** which contained the same active kinetic pathways but with different relative rate constants. Once final models were determined for both cases, the model was then solved with the optimal fitted values produced by the Rosenbruck (stiff) solver utilising two different ODE solving methods (Runge-Kutta 2 and Runge-Kutta 4) which are more computationally expensive for coupled ODEs. These methods produced similar optimal fitting parameters confirming the fitted rate constants are solver independent and stable optima. The final microkinetic model (Scheme 3.11) quantitatively well fitted the reaction data utilised for fitting (RMSE < 0.02) and also compared well qualitatively in a visual inspection. The microkinetic model is in a simple interpretable form from which comparison can be made between the fitted values for the reaction of diketone **3.1a** and diketone **3.1b** (Table 3.4).



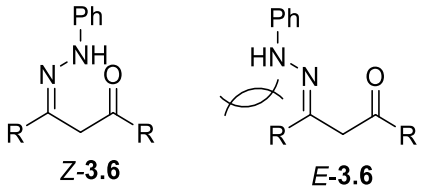
Scheme 3.11. The revised mechanism of the addition of phenyl hydrazine to **3.1a** and **3.1b** *via* catalysed pathways from intermediates **3.3** and **3.5**. Reaction pathways in grey were found to be kinetically non-competitive ($k < 1x10^{-5}$).

R	Me	Et
k_{1f}	2.23589	6.22879
k_{1r}	0	0
k_{2f}	1753.989	81.44262
k_{2r}	0.25614	0.01174
k_{3f}	13860.73	551.6668
k_{3r}	0	0
k_4	0.63061	0.74228
k_5	0	0
k_6	0.0399	0.44781
k_7	11.87965	3.26931
k_8	0	0
k_9	3.69715	4.97573
RMSE	0.01755	0.01801

Table 3.4. Fitted rate constants for the microkinetic model for the reaction of phenyl hydrazine and diketone **3.1a** (R = Me) and **3.1b** (R = Et) fitted to experiments A – C and E – H (R = Me), and experiments A – C, G and H (R = Et) (Table 3.3), and the root mean squared error (RMSE) of the corresponding models.

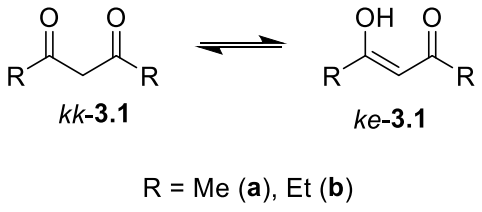
Some interesting features of the final models include:

1. The initial condensation of phenyl hydrazine with diketone **3.1b** (R = Et, k_{1f} = 6.2) is faster than that with diketone **3.1a** (R = Me, k_{1f} = 2.2) for forming the corresponding intermediate **3.6**. The hydrazone intermediate **3.6** can be formed as two isomers (*E* and *Z*, Scheme 3.12) and only *Z*-**3.6** can productively form intermediate **3.3** or **3.5** whereas *E*-**3.6** must dissociate back to **3.1** and **3.2**. Presumably the rate of nucleophilic attack to form *E*-**3.6** and *Z*-**3.6** is faster for diketone **3.1a** as there is less steric hinderance, however for diketone **3.1b** the formation of *E*-**3.6b** is hindered by 1,3-(aza)allylic strain and thus the relative concentration of **3.1b** and **3.2** is higher for faster formation of the productive *Z*-**3.6b** intermediate.[103]



Scheme 3.12. The two isomeric forms of intermediate **3.6**, demonstrating the 1,3-(aza)allylic strain present in intermediate *E*-**3.6b**.

2. As expected from the intermediate's ubiquitous role in previous mechanisms for the Knorr pyrazole synthesis, intermediate **3.3** is kinetically favoured over intermediate **3.6** to a similar amount in both the methyl (**3.3a**) and ethyl (**3.3b**) substituted cases ($K_2 = k_{2f}/k_{2r} \sim 7{,}000$). Rate of formation of intermediate **3.5** however was found to be better described by an irreversible reaction (k_{3f}) and was found to be ~25 times faster for the formation of intermediate **3.5a** (R = Me) than for intermediate **3.5b** (R = Et). Such an effect was attributed to the increased steric strain at the highly substituted quaternary carbon.
3. Uncatalysed pathways from intermediates **3.3** or **3.5** to the pyrazole product (**3.4**) are not appreciable in this microkinetic model (k_5 and $k_8 \approx 0$). Both product **3.4** (k_6 and k_9) and diketone **3.1** (k_4 and k_7) pathways proceed to product, presumably both as primarily acid catalysed type pathways as suggested by the acid and base ramping experiments. It is presumed that the diketone **3.1** (pKa ≈ 9) acts as an acid catalyst in its keto-enol form (Scheme 3.13) and the pyrazole product **3.4** acts as a catalyst in its protonated form. Interestingly NMR studies show no significant ion pair interaction between product and diketone.



Scheme 3.13. The two isomeric forms of diketone **3.1** in equilibrium.

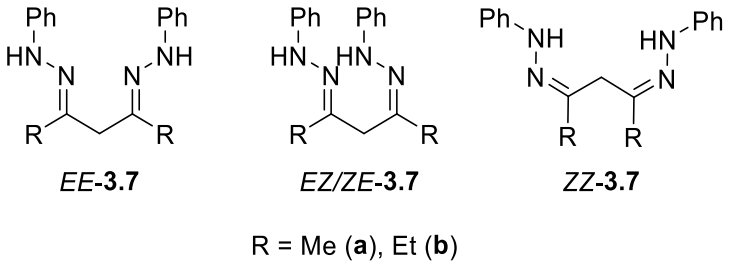
4. The di-addition intermediate **3.5** much more rapidly aromatises (k_7 and k_9) than intermediate **3.3** (k_4 and k_6) to form pyrazole product **3.4** than intermediate **3.3**, faster by orders of magnitude. This is due to the increased steric strain around the quaternary carbon in intermediate **3.5** relative to that in intermediate **3.3**.

5.5 Components not included in microkinetic model

As mentioned in the above section, reactions and species not present in the final microkinetic model are important in interpreting the determined rate constants. The aim of fitting the microkinetic model was to develop the simplest well fitting interpretable model for this reaction to understand the difference between the reactivity of diketone **3.1a** and **3.1b**, thus some reaction steps and species were not included explicitly. However, for future kinetic investigation of like reactions these reactions and species should be considered for inclusion. Noteworthy excluded reaction pathways and species:

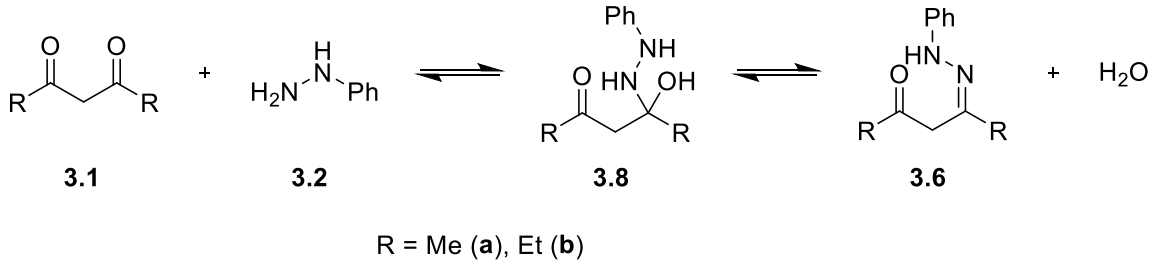
1. Diketones **3.1a** and **3.1b** are known to be in equilibrium with their keto-enol isomeric form, in fact in the case of diketone **3.1a** the major form of the diketone is the keto-enol form (*ke*-**3.1**) in solution. As previously postulated, it may also be possible for the keto-enol form to react with phenyl hydrazine forming an enol isomer of intermediate **3.6** which then must isomerise to form the active form.[95]
2. Intermediate **3.6** in the ketone form exists as two stereoisomers, *Z*-**3.6** and *E*-**3.6**, of which only one, *Z*-**3.6** can directly proceed to form intermediate **3.3**. The equilibrium of starting materials **3.1** and **3.2** with *E*-**3.6** is likely to affect the actual concentrations of these species, interpreted in this microkinetic model through k_{1f} and k_{1r}.
3. The proposed intermediate **3.7** is missing from this microkinetic model as it did not prove kinetically necessary to include. Similarly to intermediate **3.6**, this intermediate would exist as multiple stereoisomers (Scheme 3.14, *ZZ, EE,* and *EZ/ZE* form) along productive and unproductive routes to intermediate **3.5**. The complexity of these competing pathways is

simplified in this microkinetic model in the interpretation of k_{3f}.



Scheme 3.14. The stereoisomeric forms of intermediate **3.7**.

4. Each condensation step is described in this microkinetic model as one step with forward and reverse rate constants associated with it. These steps mechanistically consist of first a nucleophilic attack followed by a dehydration step, the complexity of which has been simplified for this approach (Scheme 3.15).



Scheme 3.15. An example of the first kinetic reaction step separated into its constituent mechanistic reaction steps.

5.6 Comparison of microkinetic model surface to other transient reaction data

The final microkinetic models with fitted rate constant values was used to generate response surfaces in MATLAB. These surfaces could be compared with experimental data gathered by different excess experiments, reactant stoichiometry ramps, and residence time-reactant stoichiometry ramps (Fig. 3.19a). Good agreement was found between the model surface and the additional experimental data, confirming the robustness and accuracy of the final model (Model C), as well as verifying the reproducibility of experimental data collected by different methods through overlapping data. By

plotting the response surfaces for both diketone **3.1a** (red surface) and **3.1b** (blue surface) reactions on the same axis, clear differences can be observed visually as well as through the previously discussed rate constants (Fig. 3.19b). The intersecting of these two surfaces demonstrates that in some residence time reactant stoichiometry combinations the reaction of diketone **3.1a** (R= Me) is faster and in some combinations the reaction of diketone **3.1b** (R = Et) is faster.

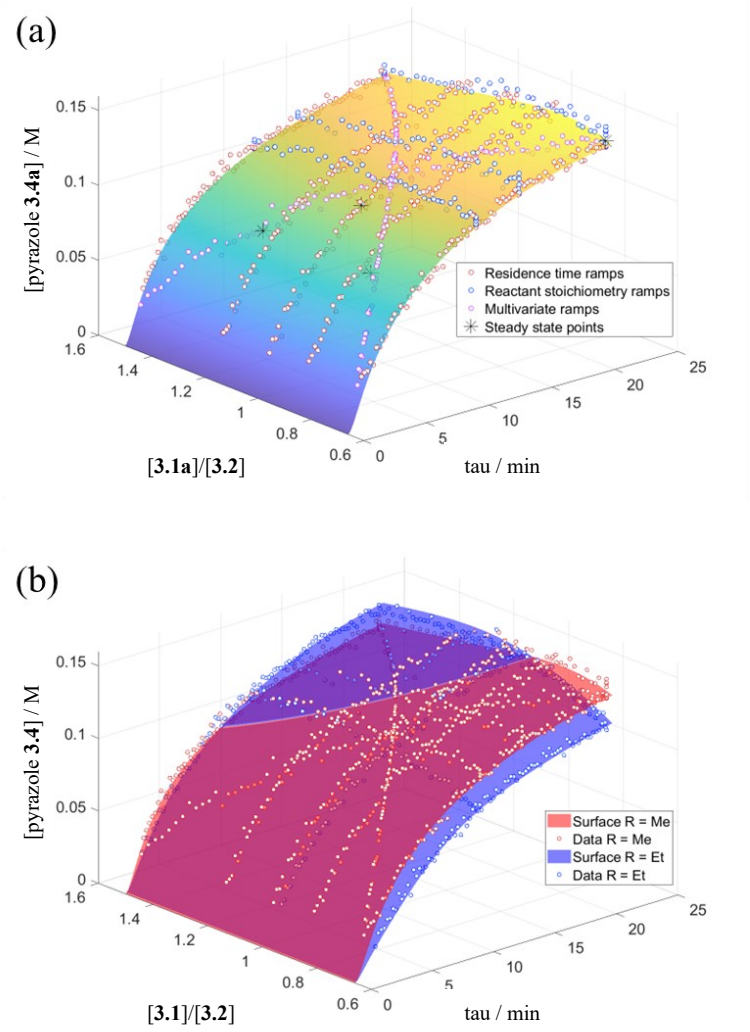
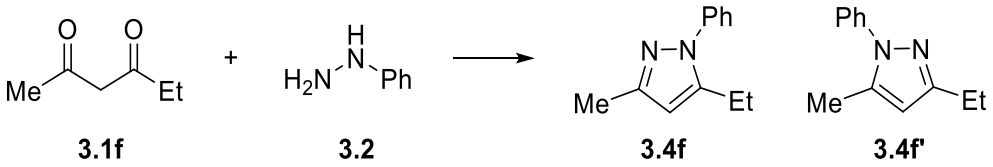


Figure 3.19. The response surface based on our kinetic model for: (a) the reaction of diketone **3.1a** with phenyl hydrazine overlayed with data from multiple different excess experiments, reactant stoichiometry ramp experiments and multi-variate experiments; (b) an interaction plot between the response surfaces of diketones **3.1a** and **3.1b** to form pyrazoles **3.4a** and **3.4b** respectively.

6 Unsymmetric methyl-ethyl diketone

Reactant stoichiometry ramps (Fig. 3.10) and microkinetic model response surfaces (Fig. 3.19b) both show that methyl substituted diketone **3.1a** and ethyl substituted diketone **3.1b** respond differently to the reactant stoichiometry. In the presence of an excess of phenyl hydrazine, the reaction of the acetylacetone (**3.1a**) is faster that its ethyl congener (**3.1b**). However, in the presence of an excess of the respective diketone at longer residence times, the reaction of **3.1b** forms more product **3.4** than the reaction of **3.1a** does, under the same conditions. This suggests that for the reaction of phenyl hydrazine and the corresponding unsymmetric diketone (hexane-2,4-dione, **3.1f**), the product regioisomeric distribution (pyrazoles **3.4f** and **3.4f'**) may be affected by the reactant stoichiometry (Scheme 3.16). This was envisaged as a novel method to control regioselectivity without relying on invasive changes of conditions.[104]

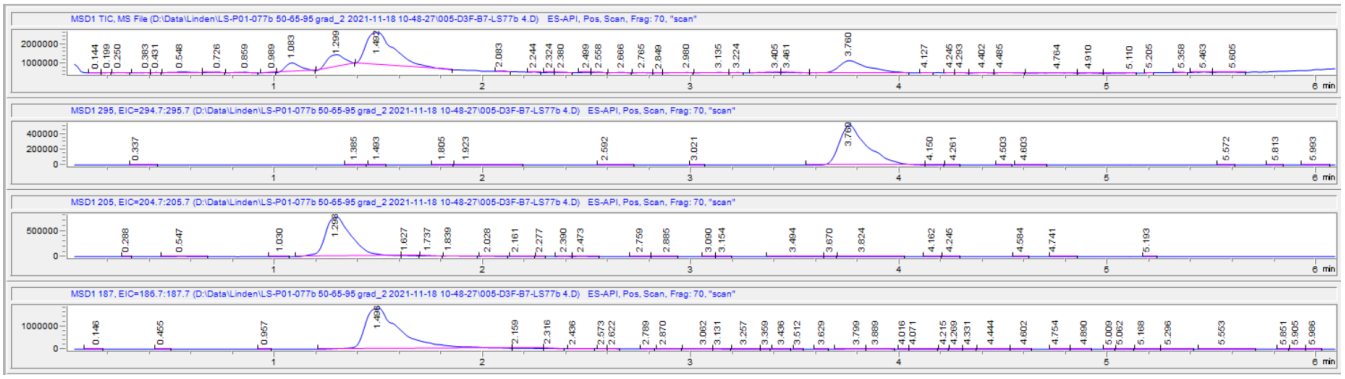


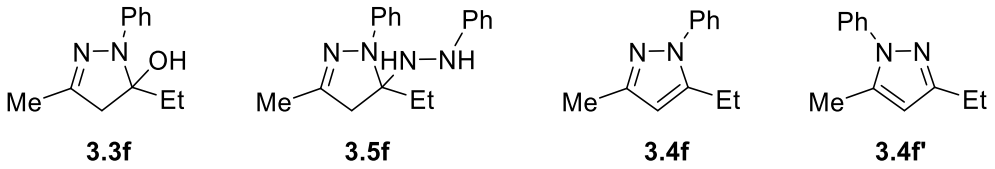
3.1f **3.2** **3.4f** **3.4f'**

Scheme 3.16. The reaction of unsymmetrical diketone **3.1f** and phenyl hydrazine to form regioisomeric pyrazole products **3.4f** and **3.4f'**.

To prove this hypothesis, the reaction of phenyl hydrazine and hexane-2,4-dione (**3.1f**) to form regioisomeric pyrazole products **3.4f** and **3.4f'** was performed in the flow system (configuration 1). Using 0.4 M stock solutions of each compound in ethanol, the reaction was performed at 70 °C at a cumulative flow rate of 0.2 mL min^{-1}, corresponding to a ~20 minutes residence time - the same conditions as that utilised for the reactant stoichiometry ramps performed on diketone **3.1a** and **3.1b**. The flow system was run at relative flow rates which produced reaction stoichiometries ([**3.1f**]/[**3.2**]) of 1.5 and 0.66 (corresponding to 40%B and 60%B where %B is the percentage of the cumulative flow rate generated by the phenyl hydrazine solution pump). Reaction aliquots were collected from both experiments once the system had reached steady state and analysed by HPLC-MS and NMR spectroscopy.

HPLC-MS analyse did not separate regioisomeric pyrazole products **3.4f** and **3.4f'** but did reveal peaks corresponding to the mass of intermediates **3.3f** and **3.5f**, although the regioisomeric nature of these intermediates is not known (Fig. 3.20). The pyrazoles were found to be the major products, compared to intermediate peak areas; and on evaporation of ethanol, only the pyrazole products were obtained. This resultant mixture was analysed by ^{1}H NMR spectroscopy (Fig.3.21a), where the regioisomeric pyrazole products can be distinguished using a selective nuclear Overhauser effect (nOe) NMR method (Fig. 3.21b). The regioisomers can be differentiated by the through-space proximity of the ethyl and methyl groups to the ortho phenyl proton (inset scheme in Fig. 3.21b).





3.3f **3.5f** **3.4f** **3.4f'**

Figure 3.20. Separation and identification of mono-addition intermediate **3.3f** and di-addition intermediate **3.5f** using HPLC-MS while attempting to separate regioisomeric pyrazoles **3.4f** and **3.4f'** for the reaction of diketone **3.1f** and phenyl hydrazine. The figure consists of the TIC from the mass spectrometer, followed by the EIC for the di-addition intermediate **3.5f** (m/z = 295.2), mono-addition intermediate **3.3f** (m/z = 205.2) and pyrazole products **3.4f**/**3.4f'** (m/z = 187.2).

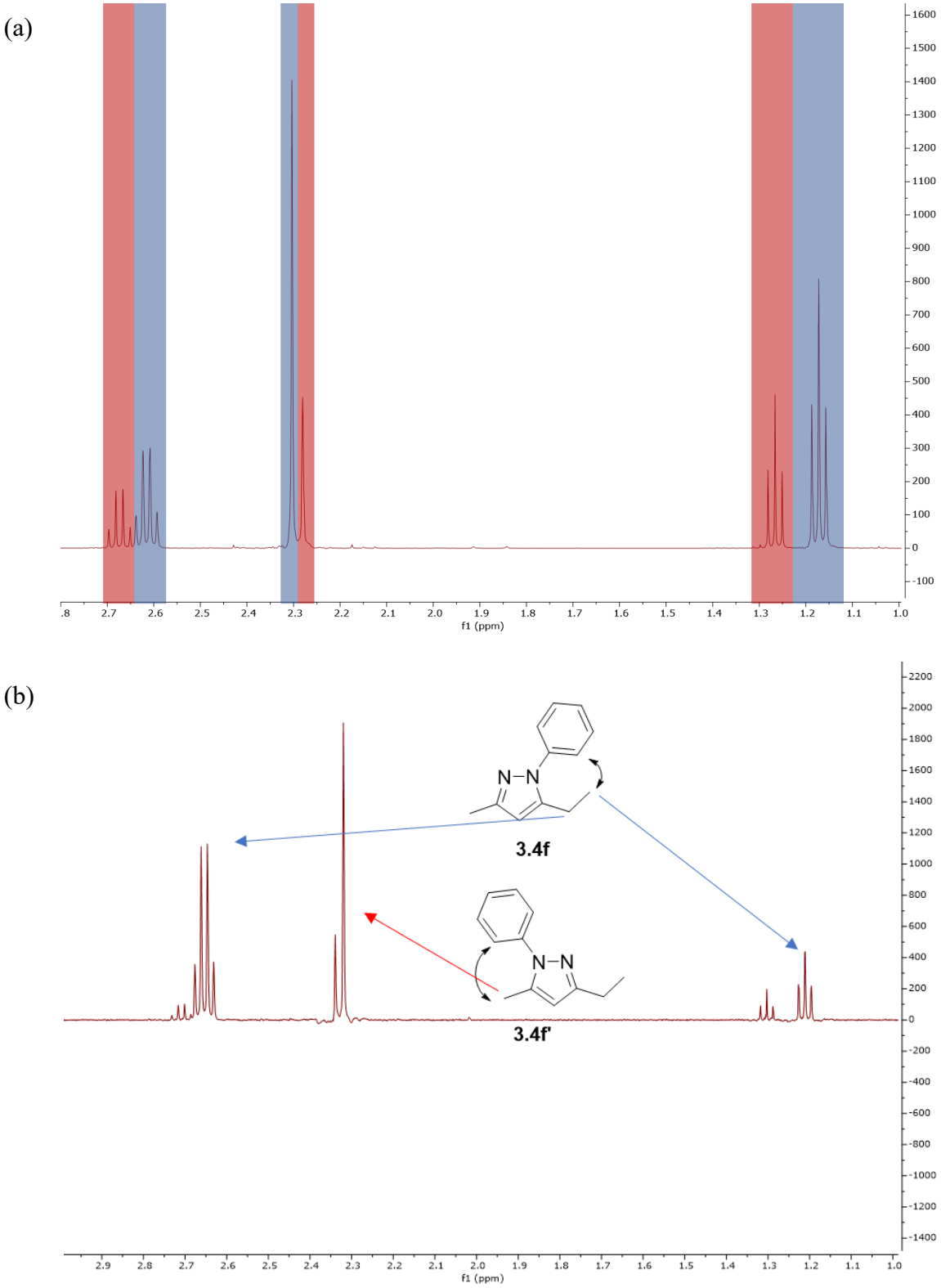


Figure 3.21. The alkyl regions of the ^{1}H NMR, where blue highlighting indicates peaks for **3.4f** and red for **3.4f'** (a) and the selective excitation nOe spectra (excited at 7.44 ppm) (b) in $CDCl_3$ of the isolated product mixture of the reaction of 1 equivalent of diketone **3.1f** and 1.5 equivalents of phenyl hydrazine.

The different reactant stoichiometry experiments demonstrated that, although neither experiment was regiospecific, the regioisomeric ratio of products (**3.4f**:**3.4f'**) can indeed be affected by which reactant was in excess. Both experiments produced pyrazole **3.4f** as the major product with the excess phenyl hydrazine experiment producing a product ratio of 1.7:1 and the excess diketone experiment producing a product ratio of 2.5:1. The increased selectivity for the diketone excess experiment is somewhat surprising, as the symmetric diketone tests on **3.1a** and **3.1b** demonstrated a greater difference in product yield under these conditions than phenyl hydrazine excess conditions (Fig. 3.10b). This result also demonstrates that the original hypothesis to combine rate constants from the symmetric diketone **3.1a** and **3.1b** experiments on relevant kinetic steps to predict the regioisomeric outcomes would not work, presumably due to a more complex interplay between the two alkyl groups in the reaction steps.

7 Conclusions

The Knorr pyrazole synthesis was investigated with the aim of predicting the regioisomeric outcomes of unsymmetric 1,3-diketone substrates. Through the use of transient flow experiments and off-line analysis, it became apparent that the widely assumed simple kinetic model for this reaction was inadequate to explain even the reaction of simple symmetric diketones and thus a more detailed microkinetic model was devised.

More detailed kinetic investigation revealed the presence of autocatalysis and the presence of a di-addition intermediate **3.5** was identified for the first time to be involved as part of an important kinetic pathway to form the pyrazole product **3.4**. Comparison between the methyl substituted diketone **3.1a** and the ethyl substituted diketone **3.1b** revealed that this small change in alkyl chain length had a significant effect on the relative rates of different kinetic pathways within the microkinetic model. These differences can be explained by various arguments, but a more detailed DFT study of these different reactants could provide more detailed understanding of the distinction between the two diketones.

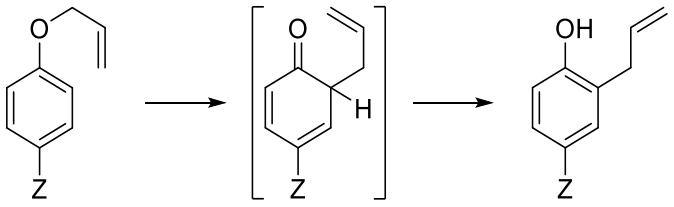
This work also led to the development of novel reactant stoichiometry ramps, which proved efficient tools for providing valuable insights into the reaction kinetics. These methods were not only instrumental in determining the non-linear nature of the reaction kinetics but also provided insight into the possibility that varying reactant stoichiometry could affect the regioisomeric ratio of the unsymmetric diketone **3.1f**. These data and data collected by residence time-reactant stoichiometry ramps rapidly collected reaction data in a more efficient and accurate manner than experimentation in batch vessels. This reaction data proved useful to confirm the robustness of the constructed microkinetic model and is now being utilised by multiple computational teams to further study this reaction and better train their algorithms on challenging to collect real-world data.

Chapter 4: Investigation of traditionally discrete reaction parameters

1 Introduction

1.1 Aim and objectives

The aim of the work, described in this Chapter, was to develop efficient methods for investigating the effects of traditionally discrete reaction parameters. As chemical sciences are becoming more data driven, there is a drive to utilise modern machine learning (ML) methods to build understanding.[1,105] ML methods require large amounts of data on which to build accurate models, however, collection of reaction data is still laborious, especially when investigating combined continuous-discrete reaction parameter spaces. High throughput experimentation utilising multi-well plates facilitates screening across diverse discrete variables, including different substrates and catalysts, but cannot efficiently vary continuous reaction parameters.[106] Transient flow methods, in combination with other experimental techniques, may help facilitate the more efficient collection of reaction data, but generally is less efficient in collecting data to investigate the effect of discrete reaction parameters. In this Chapter, substrate and solvent were targeted as two key discrete reaction parameters, which could be investigated by developing new transient flow methods. These two factors both can have significant effects on reaction rates and are amenable to parameterisation, allowing trends to be produced and numerical models to be constructed. The aromatic Claisen rearrangement was chosen as a simple test reaction on which to develop these methods (Scheme 4.1).



4.1 **4.2**

Scheme 4.1. The aromatic Claisen rearrangement reaction.

To investigate the effect of substrate on reaction rate, a 'one-pot' transient flow method was envisaged (Fig. 4.1). This method would utilise automated on-line HPLC analysis,[15,26,48,52,61,107–109] implemented

in flow system configuration 2, to analyse multiple reactions simultaneously over a transient temperature ramp, thus collecting reaction data on the effects of substrate and temperature simultaneously. Fulfilling the objective of this efficient data generation leads to a further objective of how best to use this data. Fundamental thermodynamic parameters could be afforded from this data, shedding light on the effects of substituent and temperature on the reaction rate. Also, a predictive model could be trained on this data to predict the reaction rate constants of a substrate at a given temperature, which could facilitate feasibility prediction of a reaction in a synthetic route and to benchmark computational simulations.

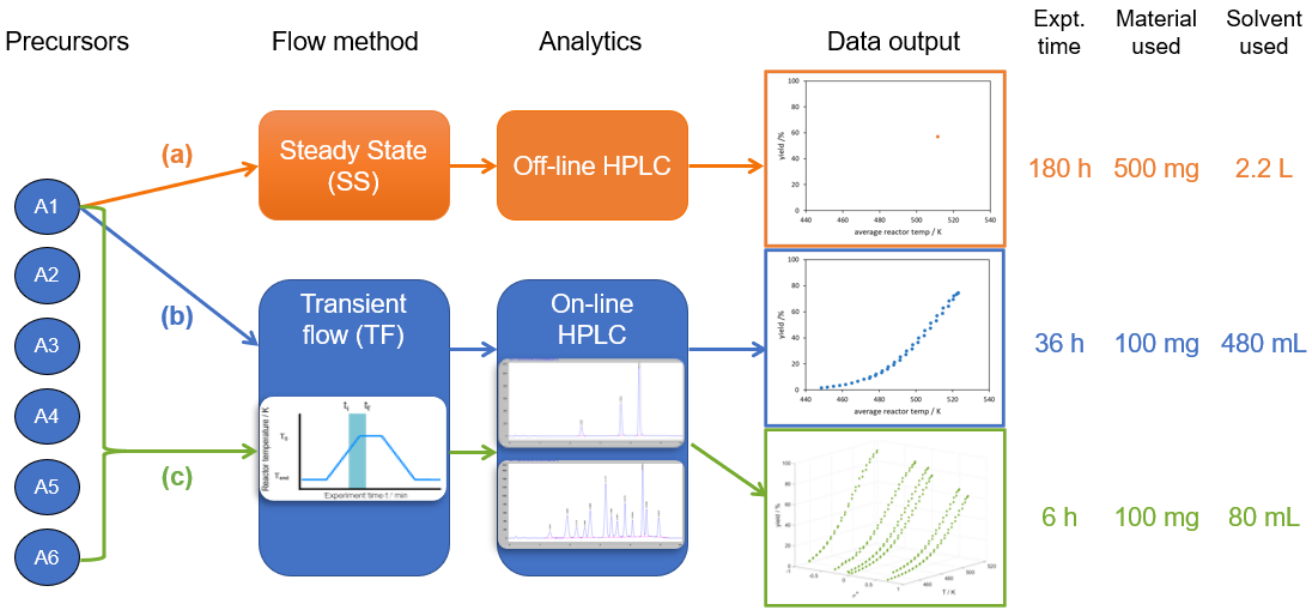


Figure 4.1. Comparison of different flow methods for collecting kinetic data: (a) individual substrate steady state flow (IS-SS); (b) individual substrate transient flow (IS-TF); and (c) one-pot transient flow (OP-TF). Estimated amount of experimental time, material, and reaction solvent required for each method to collect the same number of datapoints as the one-pot transient flow method.

Solvent choice is a crucial decision in chemical synthesis which can vary the reaction rate by several orders of magnitude and even change the reaction outcome.[104,110–112] There is also increasing regulatory (REACH, EPA, *etc.*) and societal pressure to find replacements for unsustainable solvents, exacerbating the challenge of choosing the optimal reaction solvent.[113,114] Solvent choice in a reaction is generally considered a discrete reaction parameter, but utilising transient flow it was determined this parameter could be transformed into a *pseudo*-continuous parameter. A ramping method was envisaged in which

solvent mixtures could be screened efficiently, thus investigating the effect of different solvent properties on the rate of the reaction. The data collected for the aromatic Claisen rearrangement would provide evidence to comprehensively understand the solvent effect on this reaction, a much debated topic in the computational chemistry community.[115–119] Such a method could then be combined with the previous 'one-pot' method to further increase data generation efficiency.

1.2 The aromatic Claisen rearrangement

The aromatic Claisen rearrangement (Scheme 4.1) is a [3,3]-sigmatropic rearrangement first reported by Ludwig Claisen in 1912,[120] and since has been deployed in the synthesis of numerous biologically active molecules.[121] Despite being part of the mainstream synthetic chemistry toolbox for over a century, the reaction has rarely been studied kinetically. Most of the kinetic studies of this reaction were performed between 1958 – 1962,[79,122–126] with only two of these studies focusing specifically on the reaction of *para*-substituted phenyl allyl ethers.[79,122] Much of this work focussed on the effect of the substituent on the rate of reaction, in order to establish the Hammett relationship for this reaction, *i.e.* a linear free energy relationship between relative rates of reaction and substituent (Eq. 4.1). These studies suggested the reaction proceeded with first order kinetics *via* a polar transition state, although this has been much discussed in computational work. The activation energies (E_a) for the thermal rearrangement were determined for five *para*-substituted phenyl allyl ethers (125-142 kJ mol^{-1}) by White *et al.* with three temperature points in carbitol.[79] Goering *et al.* calculated activation energies for 14 *para*-substituted phenyl allyl ethers (124-146 kJ mol^{-1}) using two temperature points in diphenyl ether.[122] Even in these detailed kinetic studies, the activation energies were derived from Arrhenius plots constructed from only two or three temperatures, which may have high error associated with these values.

$$\log\left(\frac{k_X}{k_H}\right) = \rho\sigma^+ \qquad \text{[Eq. 4.1]}$$

where k_X/k_H = relative reaction rate constants of a substituted substrate and unsubstituted substrate; ρ = slope of Hammett plot; and σ^+ = a Hammett parameter.

More recently, the aromatic Claisen rearrangement of phenyl allyl ether **4.1** to **4.2** (Z = H) has been studied in flow by Noël and Hessel, to explore the reaction in alcoholic solvents at high temperatures and pressures (300 °C, 100 bar), exploiting the wider process window provided by flow reactors compared to batch reactors.[80] Kinetic data was collected at a range of residence times, temperatures, alcoholic solvents, and pressures using steady state methods. All of these parameters affected the yield of the reaction to varying amounts, although some of these effects may be linked to changes in residence time due to solvent expansion. For example, increasing pressure or changing to a higher boiling point alcohol increased the reaction yield. Notably, no other aryl allyl ethers were investigated, thus this study only provided kinetic data for an isolated example (Z = H), not allowing for the prediction of the kinetics of other substrates.

1.3 One-pot methods

As discussed in previous Chapters, transient flow has been utilised to accurately and efficiently collect temporal kinetic data,[15,39,49,53,67] as well as reaction data on other continuous reaction parameters such as temperature,[15,57,58,60,63] initial reactant stoichiometry,[97] and additive concentration.[15,67] However, investigation of the effects of discrete reaction parameters, such as substituent, solvent or catalyst, is challenging using transient flow methods, generally studied individually in flow[108,127] or more efficiently in parallel by high throughput batch methods utilising multiwell plates.[106] In contrast, these high throughput batch methods are inefficient at investigating the effect of continuous reaction parameters on the reaction. Reactant and additive concentrations must be investigated as discrete experiments and each multiwell plate is generally limited to investigating a single reaction temperature

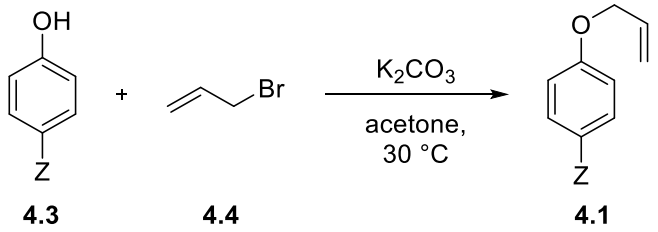
at a time. Even collecting reaction time series data can be challenging; *in situ* analysis of parallel batch reactions is expensive, and collection and analysis of multiple reaction aliquots is time consuming and laborious, even if the process is automated.

'One-pot' or 'competition' experiments, previously used in batch to investigate Hammett relationships,[128–133] represent a different approach to parallelising reactions with different discrete reaction parameters. This method consists of performing and monitoring multiple similar reaction in the same reaction solution simultaneously; either as non-interacting reactions ('one-pot') or reaction competing for the same reactant or catalyst ('competition').[134–136] This method requires a good analytical tool, which can accurately analyse all the reaction species of the multiple reactions in a rapid and reliable manner. Although previously performed in batch reactors and monitored either with end-point analysis or as the reaction progresses over time, this method if combined with transient flow would allow investigation of discrete and continuous parameter series simultaneously (Fig. 4.1).

2 Substrate synthesis and HPLC method development

2.1 Parallel synthesis of reactants

This study started with the preparation of a range of substituted phenyl allyl ethers **4.1a-h** with a range of electron withdrawing and donating substituents, from allyl bromide and the corresponding substituted phenols (Williamson synthesis, Scheme 4.2).[137] In order to produce substituted phenyl allyl ethers in an efficient manner, a parallel reactor (ReactArray) was utilised to synthesis up to 10 compounds simultaneously. The allyl ether products (**4.1**) were isolated from the reaction mixture by simple filtration of the reaction mixture through celite, removing the deprotonated phenol starting material as a salt. When an excess of the starting phenol and potassium carbonate were used, this resulted in pure product on concentration of the solution.



	Z	isolated yield / %
a	OMe	55
b	Me	73
c	F	79
d	H	-
e	$C(O)CH_3$	91
f	CN	70
g	NHAc	80
h	Br	87

Scheme 4.2. The reaction to synthesise phenyl allyl ethers and the phenyl allyl ethers produced.

It was envisaged that the rearrangement of six *para*-substituted phenyl allyl ethers would be studied simultaneously in 'one-pot'. In principle, the efficiency of data collection could be increased six-fold by performing six reactions in a quantifiable manner simultaneously in a single flow stream, while ramping reaction temperature or residence time. For this study a wide range of electron donating and withdrawing substituents was included: **4.1a-f** (Z = OMe (**a**), Me (**b**), F (**c**), H (**d**), $C(O)CH_3$ (**e**), CN (**f**)). The substituents could be characterised by their σ^+ parameters,[138,139] a parameter shown previously to produce a good linear Hammett correlation for this reaction.[79,122]

2.2 HPLC method development

As described in Chapter 2, section 2.3, a transient flow reactor was constructed, equipped with on-line HPLC capabilities (configuration 2). In order to obtain efficient collection of kinetic data, a quick HPLC method was required, which could offer baseline separation of 13 compounds (6 starting compounds, 6 products, and an internal standard). The inclusion of an internal standard allows concentrations of the reaction components to be calibrated and quantified, also producing mass balance knowledge, so that degradation, side reactions, or peak overlap can be readily identified.

Subsequently, an appropriate HPLC method was developed through the following steps: (i) developing quick isocratic methods for each compound to determine a suitable HPLC column and solvent system range, (ii) combining six starting compounds (**4.1a-f**) together and developing a gradient method to

separate these compounds, (iii) adding the six reaction products (**4.2a-f**) to this mixture and developing a gradient method to separate these compounds while maintaining the separation of the later eluting starting compounds, (iv) screening a range of potential internal standard compounds (~20) to identify a suitable compound, which could be separated from the starting and product compound mixture without method modification.

This method development produced a 6-minute HPLC method capable of resolving the mixture of 13 compounds (Table 4.1, Fig. 4.2). The method used a C18 column (2.7µm particle size, 50 mm x 2.1 mm) and a solvent gradient of water and acetonitrile as described in Table 4.1. Ethyl benzene was selected as the internal standard as a non-interacting, UV absorbing, ethanol soluble compound, which would not decompose under the reaction conditions. The method involved two different gradients within it, as well as a step change back to the initial solvent ratio before the end of the method, in order to facilitate re-equilibration of the HPLC column. This method allowed injections of reaction aliquots every 6.5 minutes.

Table 4.1. Key parameters set for the HPLC method used in this work for on-line HPLC analysis.

Flow rate / mL min^{-1}	0.7
Stoptime / min	5.75
Posttime / min	0.29
Solvent A	H_2O
Solvent B	MeCN
DAD wavelength / nm	210

Time / min	**%B**
0	25
1.2	30
3.5	50
3.51	60
3.85	60
3.86	25

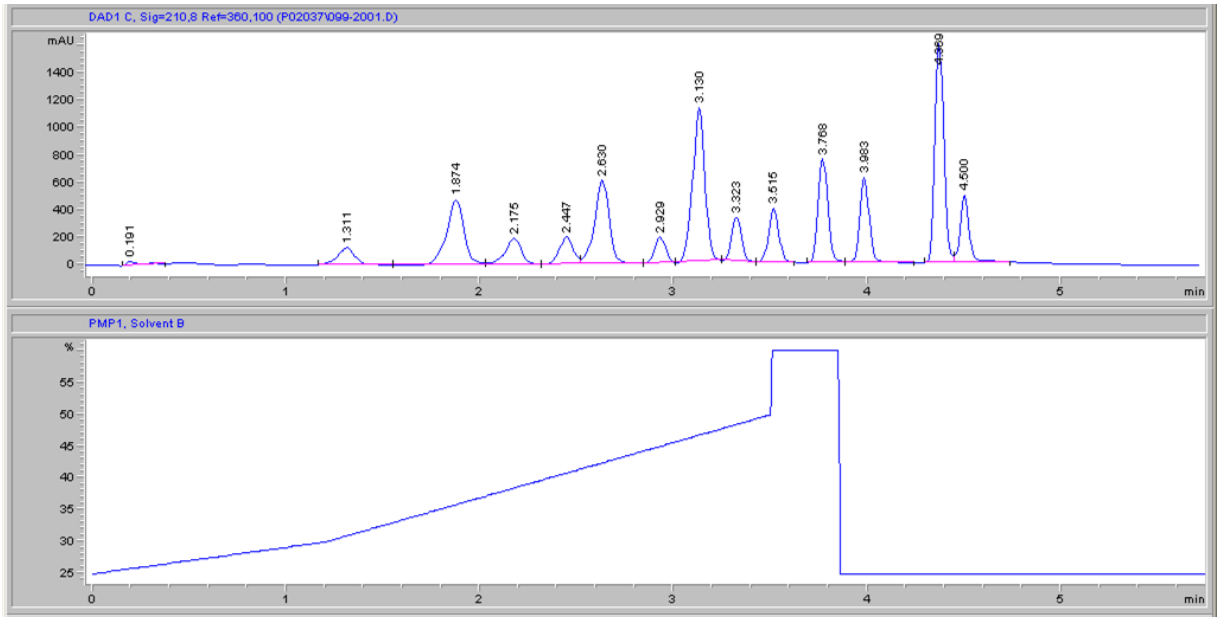


Figure 4.2. An example chromatogram of a "one-pot" method using the HPLC method discussed above. The lower diagram shows a diagrammatic representation of the HPLC method.

Table 4.2. HPLC retention times for aryl allyl ether (**4.1**) and their corresponding Claisen rearrangement products (**4.2**) (Figure 4.2).

4.1/**4.2**	Z	Retention time of **4.1** / min	Retention time of **4.2** / min
a	*p*-MeO	3.52	1.87
b	*p*-Me	4.50	3.32
c	*p*-F	3.98	2.93
d	H	3.77	2.45
e	*p*-C(O)CH_3	2.63	1.31
f	*p*-CN	3.13	2.18
-	ethyl benzene	4.39	

The HPLC method produced 13 integrated peak areas every 6.5 minutes and thus, to assist data management and analysis, an extraction script was necessary to produce this data in an accessible format. A Python script was written to efficiently extract the chromatographic data into a tabulated form. This script, developed in collaboration with MSci students Marvin Alberts and Daniel Dalland, combined the injection time of the reaction aliquot, the compound names, and extracted (pre-integrated) peak areas corresponding to a time range around the compounds' retention times. If multiple peaks were present within a time range, the largest would be selected and a warning would be provided to highlight potential issues with the chromatogram.

2.3 HPLC calibration methods

Utilising the above HPLC method, peak areas of the allyl ether precursors (**4.1**) and rearrangement products (**4.2**) were measured with reference to the internal standard peak area (ethyl benzene). To transform these relative peak areas into concentrations of reaction species calibration curves were constructed for each reactant species. Initially calibration was performed *via* a standard method by preparing multiple stock solutions containing different concentrations of a substituted phenyl allyl ether **4.1** and the same concentration of ethyl benzene, using pipettes and volumetric flasks. These solutions were diluted and injected manually into the on-line HPLC by disconnecting the flow reactor from the sample valve to produce a 5-point calibration curve (Fig. 4.3).

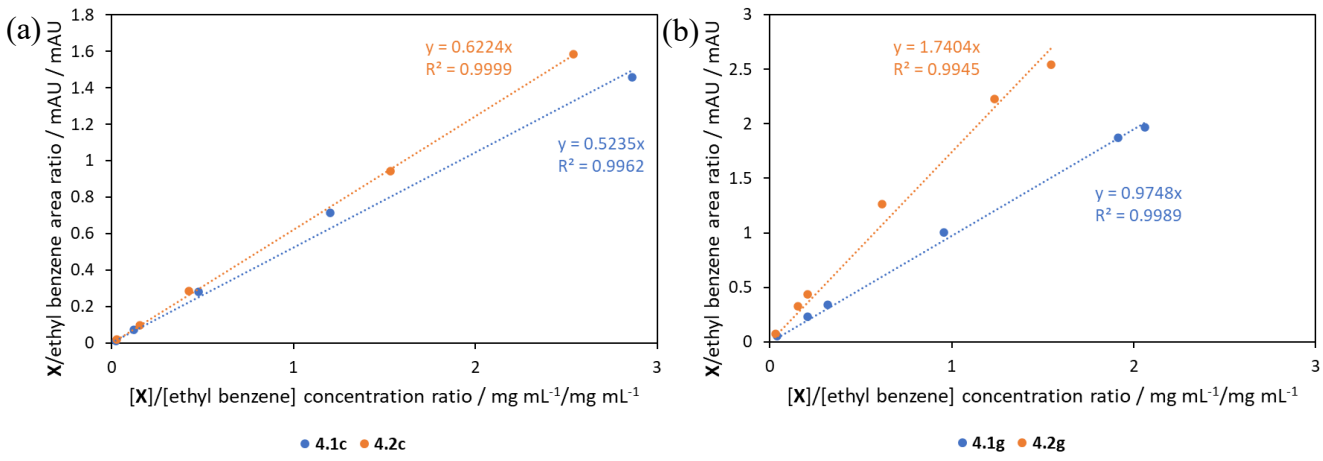


Figure 4.3. An example manually generated HPLC calibration curve collected for (a) allyl ether **4.1c** and phenol **4.2c** (R = F); and (b) allyl ether **4.1g** and phenol **4.2g** (R = NHAc).

A new calibration method was developed utilising transient flow, by which calibration curves could be generated in a more automated manner. In this new method, two independent stock solutions containing the same reaction species were prepared (Solution A), in order to avoid systematic error produced from any inaccuracies in weighing materials. Separately, ethyl benzene stock solutions were also prepared (Solution B). Utilising the flow system in configuration 2, Solutions A and B were fed through separate pumps. By implementing a reaction stoichiometry ramp, a continuous varying ratio of ethyl benzene and the reactant species to can be produced. The process can be repeated with stock solutions containing all

six reaction species (**4.1a-g**) to generate six calibration curves simultaneously, thus efficiently allowing quantified concentration data to be obtained for all 12 reaction species. (Fig. 4.4). This method produced calibration curves efficiently, which have > 10 data points per calibration curve, although this method does rely on accurately and precisely controlled pump flow rates. It is also important to note that unlike normal calibration methods, where the internal standard concentration is kept constant, concentrations of both internal standard and reaction species are changing in this method, thus the method is only applicable when both internal standard and reaction species are within the Beer-Lambert linear absorption region.

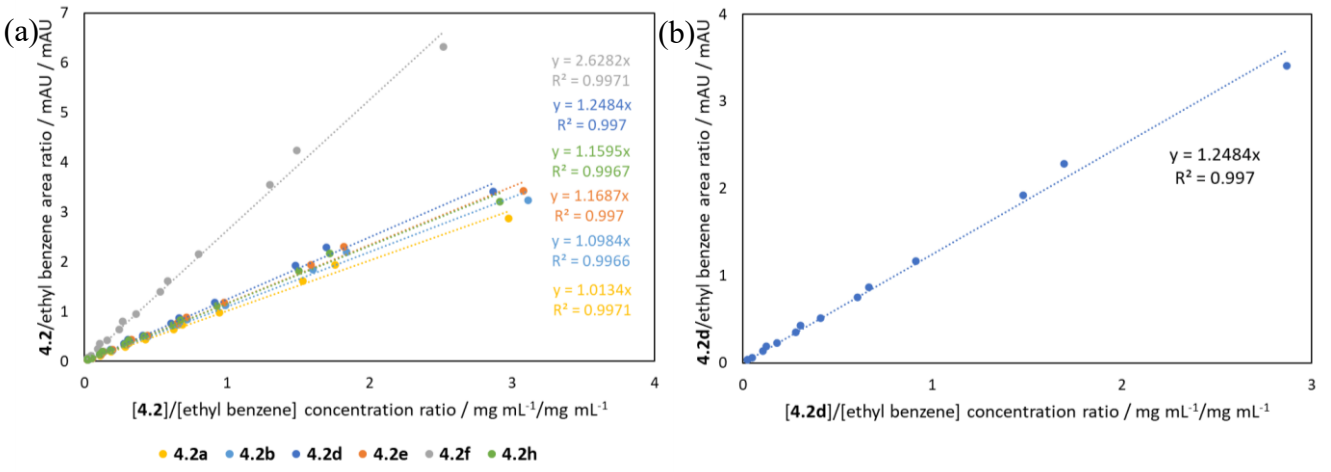


Figure 4.4. An example HPLC calibration curve collected *via* a flow rate ramp between a solution containing (a) six product phenols **4.2** and a solution containing ethyl benzene as an internal standard, and (b) an extracted plot of the calibration curve for product phenol **4.2d** collected by a multispecies calibration ramp, extracted for clearer visualisation.

3 Individual substrate transient flow

3.1 Solvent expansion effects

Under ambient conditions, the residence time of the flow reactor can be calculated as 19.6 minutes at a flow rate of 0.2 mL min^{-1}. However, as previously reported by Noël and co-workers, it was found that even at high pressures (100 bar), solvent expansion is significant for the reaction temperature range under investigation (170 – 250 °C).[80] As discussed in Chapter 2, the Tait equations (Eq. 2.29 and 2.30) can be utilised to predict the density change of a solvent from a change in pressure and temperature based on the solvent's bulk modulus of elasticity (E) and volumetric expansion coefficient (β). These equations allow the residence time of the system under reaction conditions to be calculated under non-ambient conditions.

$$\rho_1 = \frac{\rho_0}{1 - \frac{P_1 - P_0}{E}} \qquad \text{[Eq. 2.29]}$$

$$\rho_1 = \frac{\rho_0}{1 + \beta(T_1 - T_2)} \qquad \text{[Eq. 2.30]}$$

where ρ = density of ethanol (kg m^{-3}), P = applied pressure (bar), T = temperature (K), E = bulk modulus of elasticity (10600 bar for ethanol), and β = volumetric expansion coefficient (0.0011 K^{-1} for ethanol).[140,141]

In the flow system utilised in this work, the corrected residence time was calculated to be 16.4 min at 170 °C and 100 bar and 15.1 min at 250 °C and 100 bar, demonstrating a notable difference in residence time across the temperature range. Thus, this corrected residence time was used in the calculation of first order rate constants (k) from reaction species concentrations and residence times (Eq 4.2). It is worth noting that this correction of residence time, despite its size, still may have a negligible effect on values of ln(k) compared to the effect of temperature.

Based on equation 4.2, a change of residence time from 16 to 15 minutes will only generate a difference

in ln(k) of ln(16/15) = 0.06, which is likely insignificant compared to the effect of temperature on this value for the expected magnitude of ln(k) (~ -2 – -8), based off previously reported activation energies.

$$k = \frac{\ln([\mathbf{4.1}]_0) - \ln([\mathbf{4.1}])}{\tau} \qquad \text{[Eq. 4.2]}$$

where k = rate constant (min^{-1}), $[\mathbf{4.1}]_0$ = initial concentration of **4.1** (M or mg mL^{-1}), $[\mathbf{4.1}]$ = concentration of **4.1** at residence time τ (M or mg mL^{-1}), and τ = residence time (min).

3.2 Residence time ramps

The reaction of unsubstituted allylphenyl ether **4.1d** to phenol **4.2d** was chosen as a model reaction to validate the flow system and transient methods for the aromatic Claisen rearrangement. Residence time ramps were implemented on this reaction via a RPO cumulative flow rate step change between 1 – 0.2 mL min^{-1} (3 – 16 min residence time) at 200, 220, and 240 °C while maintaining a back pressure of 95 – 105 bar (Fig. 4.5a). Maintaining a high and constant back pressure is important, not only to avoid variable pressure dependent solvent expansion, but also to avoid potential pressure dependent fluctuations in the solvent properties of ethanol in the near critical region.[142] This reaction was observed to produce solely ortho-allyl substituted phenol (**4.2d**) under these conditions, *i.e.* no formation of the potential Claisen-Cope rearrangement product **4.5d** was observed in HPLC chromatograms or by isolated NMR spectra (Scheme 4.3).

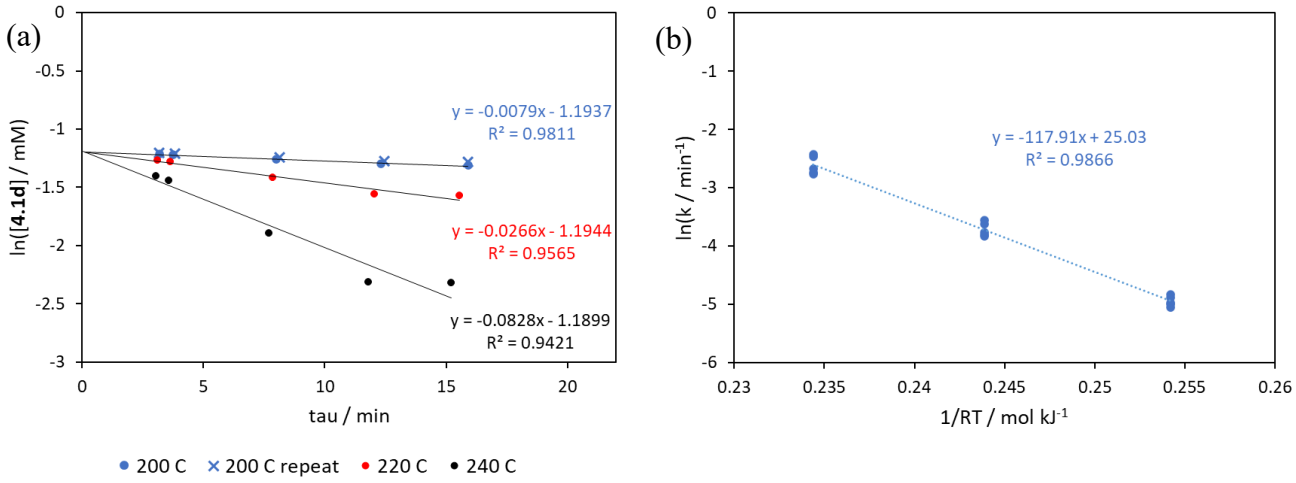
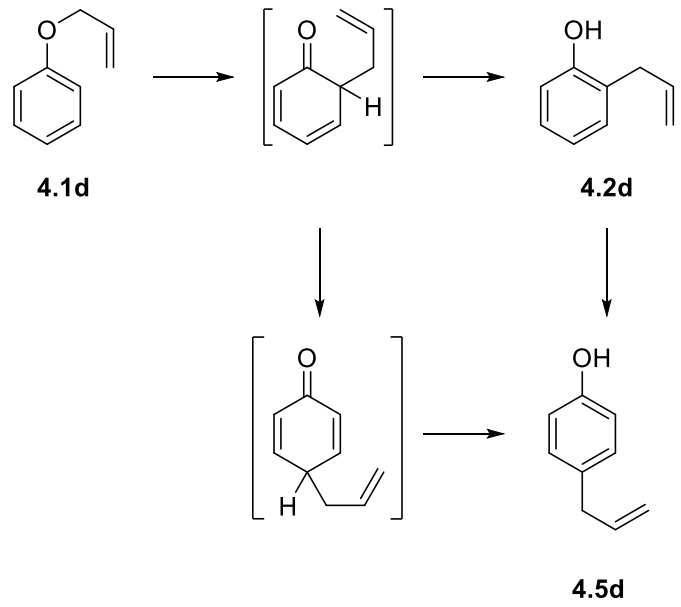


Figure 4.5. Data collected on the aromatic Claisen rearrangement of phenyl allyl ether (**4.1d**) *via* transient residence time step change methodology at three temperatures expressed as: (a) a first order kinetic plot; (b) an Arrhenius plot.



Scheme 4.3. The potential competitive formation of Cope product **4.5d** during the Claisen rearrangement reaction of **4.1d** to **4.2d**.

As can be seen from the natural logarithm plots of starting allyl ether **4.1d** concentration, this reaction proceeds with the expected first order kinetics, under these conditions. This kinetic regime allows a rate constant to be calculated from the starting compound concentration at a single residence time point and the initial concentration due to the linearizability of the reaction data. By calculating the rate for each residence time point and over the three temperatures investigated, an Arrhenius plot (Eq. 1.4, Fig. 4.5b) can be generated. The Arrhenius plot yields an activation energy comparable to the previous literature

value collected in ethanol (118 kJ mol^{-1}, *cf.* 116 kJ mol^{-1}).[80]

$$k = Ae^{\frac{E_a}{RT}} \qquad \text{[Eq. 1.4]}$$

where k = reaction rate constant, A = pre-exponential factor, E_a = activation energy of the reaction (J mol^{-1}), R = universal gas constant (J mol^{-1} K^{-1}), and T = absolute temperature (K).

The consistency of the reaction rate constants calculated from different single residence times for a given reaction temperature demonstrates the validity of calculating the rate of the reaction from a single residence time point. This can be interpreted as an insensitivity of the calculated rate constant to the residence time of the conversion data utilised to calculate the constant. This result demonstrates that an Arrhenius plot could be produced from a single transient temperature experiment at a fixed flow rate without a loss in accuracy of the kinetic parameters collected.

3.3 Temperature ramps

Transient temperature ramps[15,57,58,60,63] (Chapter 1, Section 3) are an efficient method to investigate the effects of temperature on a reaction *via* a continuous range of pseudo-steady state reactions across a temperature range. Due to the first order nature of the aromatic Claisen reaction, Arrhenius (Eq. 1.4) or Eyring plots (Eq. 4.3) can be generated in one transient temperature experiment.

$$k = \frac{\kappa k_B T}{h} e^{\frac{\Delta S^{\ddagger}}{R}} e^{-\frac{\Delta H^{\ddagger}}{RT}} \qquad \text{[Eq. 4.3]}$$

where k = reaction rate constant; κ = transmission coefficient; k_B = Boltzmann constant (J K^{-1}); T = absolute temperature (K); h = Planck's constant (J s); $\Delta S^{\ddagger}$ = entropy of activation (J mol^{-1} K^{-1}); $\Delta H^{\ddagger}$ = enthalpy of activation (J mol^{-1}); R = molar gas constant (J mol^{-1} K^{-1}).

A standard transient temperature ramp (Fig. 4.6) was performed fixing the flow rate at 0.2 mL min^{-1}

(*circa.* 16 min residence time) at the initial reactor temperature under steady state conditions. The temperature was then increased from 170 °C, at a rate of 0.5 °C min^{-1} over 160 min, to reach a second steady state at 250 °C. Generally, once the second steady state has been achieved, a second ramp is performed; this time in the reverse direction, by reducing the temperature at the same rate down to 170 °C, in order to confirm a lack of hysteresis in the system. This relatively slow temperature ramping rate (0.5 °C min^{-1}) allows the average reactor temperature to be assigned to each differential volume element of the reaction mixture, retaining accuracy as each differential volume element will experience a temperature range of <10 °C over its traversing of the reactor. Notably, an increase in ramping rate to 1 °C min^{-1} produces clear discrepancy between the up and down temperature ramps, potentially due to the effect of averaging temperature over a larger temperature range or due to theoretical limits on heat transfer as suggested by Florit *et al.*.[15] Reactions with lower activation energies will likely require slower temperature ramping as a temperature range of 10 °C will have a larger effect on such a reaction.

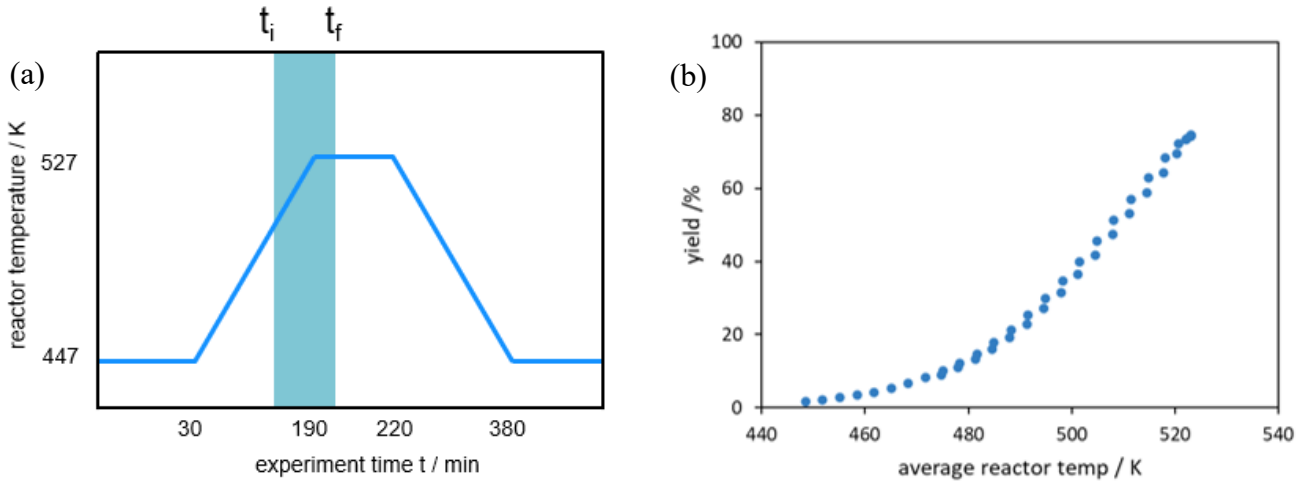


Figure 4.6. (a) A standard transient bi-directional temperature ramp experiments (170 – 250 – 170 °C) performed at a ramp rate of 0.5 °C min^{-1}; (b) the data collected utilising this ramp on the aromatic Claisen rearrangement of phenyl allyl ether (**4.1d**) collected for a 16 min residence time, plotted as yield (%).

The reaction data obtained from these temperature ramps was used to produce almost ideal Arrhenius and Eyring plots for the reaction of **4.1d** to **4.2d** (Fig. 4.7). Repeat experiments and ramps over different temperature ranges were performed to confirm the robustness of the result demonstrating excellent

reproducibility, furnishing an activation energy (E_a) of 118 ± 0.48 kJ mol^{-1} and enthalpy of activation ($\Delta H^{\ddagger}$) of 114 ± 0.47 kJ mol^{-1} ($R^2 > 0.99$). Noting the supercritical point of ethanol at 241 °C, 63 bar,[143] at which it has been reported ethanol becomes much more apolar, it was somewhat surprising that the Arrhenius and Eyring plot remain linear above this point. It was expected that the high data density of this temperature ramping method, any changes of the gradient of these plots would be observed and thus changes in activation energy or enthalpy of activation corresponding to these could be calculated. The lack of such change in gradient suggests that this rearrangement is insensitive to the change in solvent polarity due to this phase change, contradicting computational studies suggesting a strong polar/apolar solvent effect on this reaction.[142]

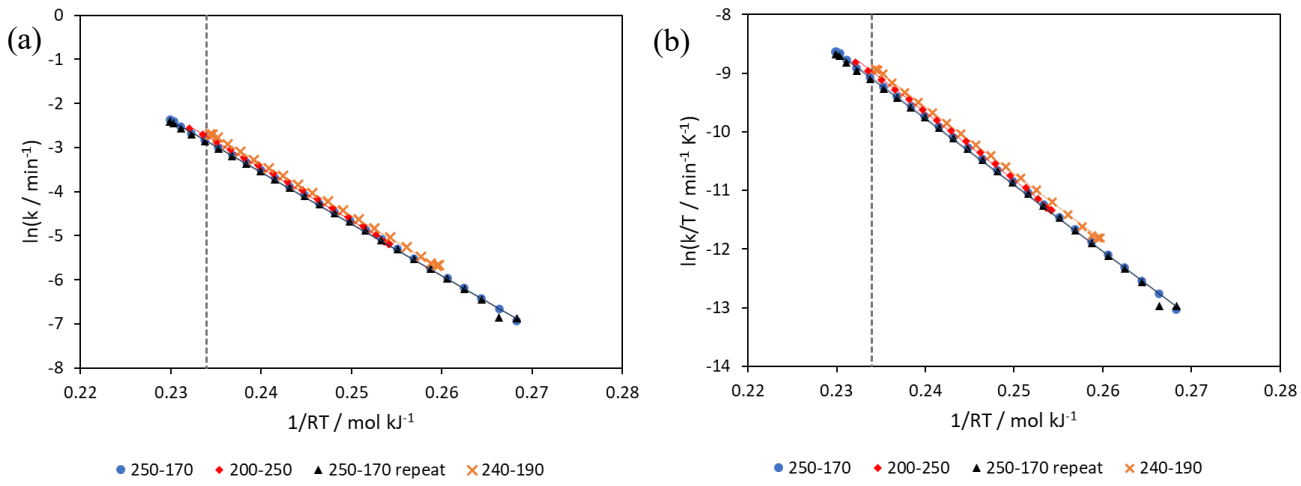


Figure 4.7 Arrhenius (a) and Eyring (b) plots generated from transient temperature ramp experiments on allylphenylether (**4.1d**) over different temperature ranges (°C), including those over the supercritical point of ethanol (dashed grey line), where *k* is the rate constant of the reaction, R is the molar gas constant, and T is the absolute temperature.

4 ‘One-pot’ transient flow

4.1 Residence time ramps

Equimolar mixtures of starting allyl ethers **4.1a-f** containing ethyl benzene as an internal standard were prepared. As previously mentioned, the on-line HPLC method was developed to allow quantitative monitoring of staring allyl ether **4.1** and product phenol **4.2** concentrations of all 12 compounds simultaneously. Individual reaction of the starting allyl ether with the strongest electron donating group (**4.1a**, Z = OMe) over a temperature range demonstrated that the previous temperatures for the residence time ramps on allyl ether **4.1d** produced full conversion in this case. Therefore, for the ‘one-pot’ residence time ramps, lower reaction temperatures were utilised: 190, 210, and 230 °C. These experiments demonstrated first order kinetics for all the reactions performed simultaneously, which can be seen from an Arrhenius plot constructed from these data, observing high precision between rate constants generated from different residence time data (Fig. 4.8).

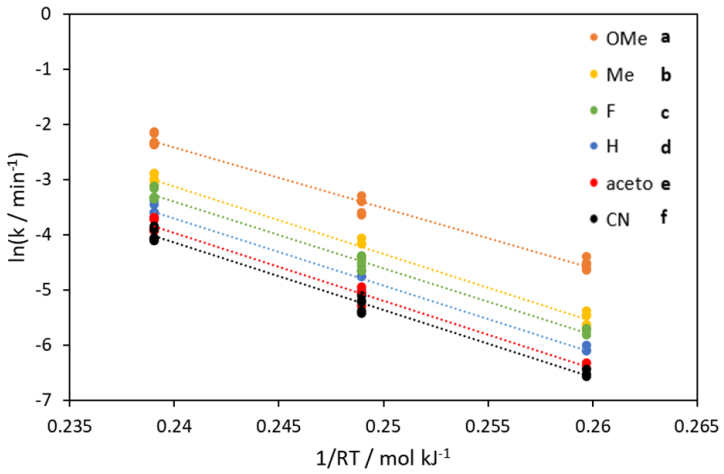


Figure 4.8. Data collected on the aromatic Claisen rearrangement of phenyl allyl ether (**4.1d**) *via* transient residence time step change methodology at three temperatures expressed as an Arrhenius plot.

4.2 Temperature ramps

Application of the same bi-directional temperature ramp (170 – 250 – 170 °C, 0.5 °C min^{-1} ramp rate) to the reaction mixture containing **4.1a-f** afforded six data rich Arrhenius plots from one experiment (Fig. 4.9, dots). The activation energies of the six reactions could be obtained from the Arrhenius plot data affording values between 112.9 – 122.4 kJ mol^{-1}. This experiment was performed again (Fig. 4.9, crosses) in order to confirm the repeatability of these results and to afford estimated error on the fitted values for the activation energy (E_a) and the pre-exponential factor (A).

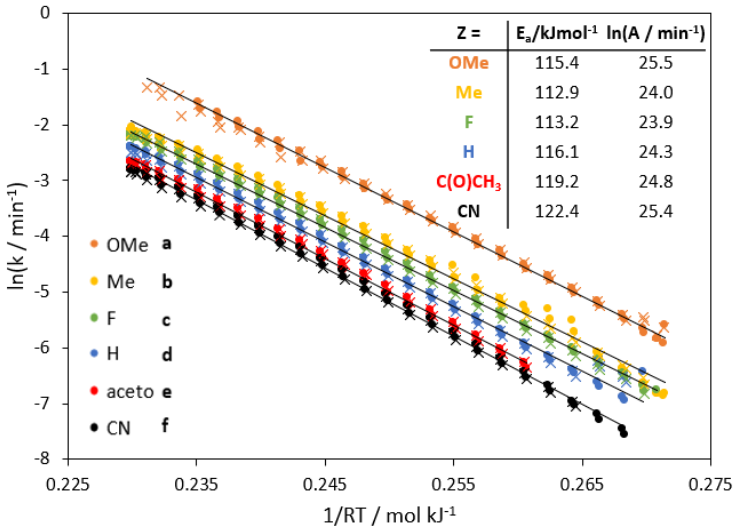


Figure 4.9. Arrhenius plots generated from transient temperature ramp experiments on a mixture of six substrates **4.1a-f** over two repeated (dots and crosses) bi-directional temperature ramp experiments (170 – 250 – 170 °C) (OP-TF). E_a is the activation energy and A is the pre-exponential factor of the Hammett plot.

The activation energy afforded for the reaction of **4.1d** from the 'one-pot' method data was is in close agreement with the previously reported literature value (116 *cf.* 116 kJ mol^{-1}).[80] In order to confirm the utility of the 'one-pot' method to produce similar data to that collected on an individual substrate, all individual substrate (IS-TF, full lines) and 'one-pot' (OP-TF, dotted lines) transient temperature experiments on the reaction of **4.1d** were compared (Fig. 4.10). The similar data and fitted kinetic values obtained from these two methods suggests any interaction between different substrates has a negligible effect on the kinetic data gathered via the 'one-pot' method.

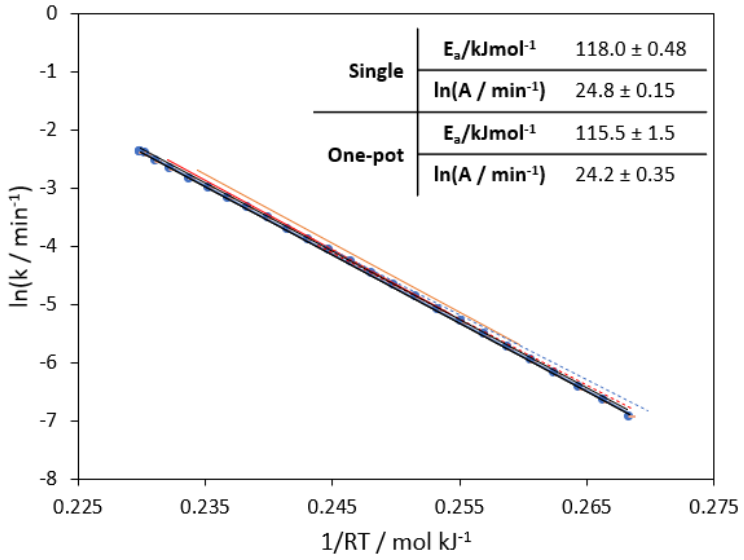


Figure 4.10. Arrhenius plots generated from transient temperature ramp experiments for allylphenylether (**4.1d**) over different temperature ranges collected from a single substrate (IS-TF, full lines) and in the presence of 5 other substrates (OP-TF, dotted lines). E_a is the activation energy and A is the pre-exponential factor of the Hammett plot.

4.3 Mass balance

The calibration curves provide the absolute concentration of **4.1** and **4.2,** thus allowing mass balances to be monitored. It is important to monitor mass balance, especially in more complex reaction mixtures, to identify if any side reactions are occurring, which could affect the validity of the results. The reaction mass balance was calculated by equation 4.4 and was plotted against varying reaction temperature for the transient temperature ramps (Fig. 4.11). Mass balances were found to be between 95 – 110% for these temperature ramps. Mass balance was calculated for all experiments and was generally within this range, although in some cases slight trending could be observed with increasing temperature potentially caused by slight miscalibration of product or starting material.

$$mass\ balance\ /\% = \frac{[\mathbf{4.1}] + [\mathbf{4.2}]}{[\mathbf{4.1}]_0} \qquad \text{[Eq. 4.4]}$$

where $[\mathbf{4.1}]_0$ = initial concentration of **4.1** (M or mg mL^{-1}), [**4.1**] and [**4.2**] = reaction concentration of **4.1** or **4.2** respectively (M or mg mL^{-1}).

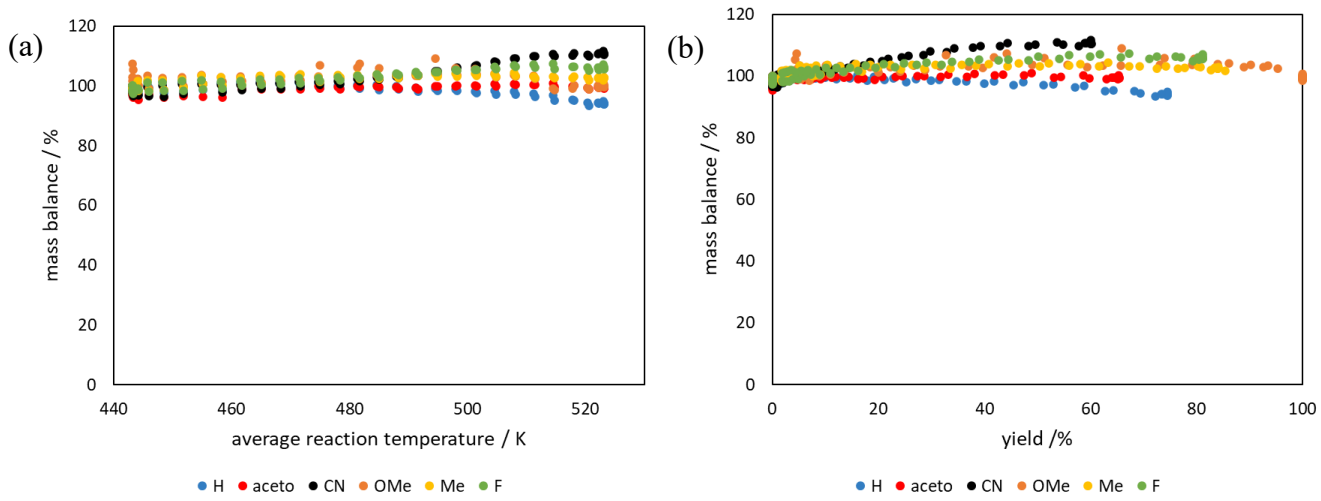


Figure 4.11. Example mass balance calculations for one of the 170 – 250 – 170 °C 'one-pot' transient temperature ramp experiments described in figure 4.9 plotted against: (a) average reaction temperature; and (b) reaction yield.

4.4 Hammett plots

In order to interpret the effect of substituent on the rate of the reaction, the linear free energy relationship known as a Hammett plot is often utilised (Eq. 4.1).[144,145] By plotting the logarithm of the relative reaction rate constant for a substituted compound compared to the unsubstituted compound against an empirically derived Hammett constant (σ) related to the substituent, a linear dependency can be obtained. There are multiple empirically derived Hammett constants (σ_p, σ_m, σ^+, σ^-) derived from different standard reactions (Table 4.3).[139,145,146] Previously, σ^+ derived from the dissociation of cumyl chloride (Scheme 4.4), has been reported to best represent the substituent effect on the thermal aromatic Claisen rearrangement of para-allyl phenyl ethers.[79,122]

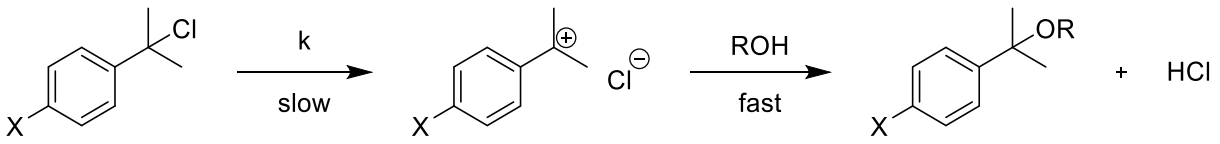
$$\log\left(\frac{k_X}{k_H}\right) = \rho\sigma^+ \qquad \text{[Eq. 4.1]}$$

where k_X/k_H = relative reaction rate constants of a substituted substrate and unsubstituted substrate; ρ = slope of Hammett plot; and σ^+ = a Hammett parameter.

Table 4.3. *Para*-substituents (Z) for phenyl allyl ether substrates and their corresponding Hammett parameters. σ^+ values were obtained from work by McDaniel and Brown.[139] All other σ were obtained from a review by Taft *et al.*, which also contains the aforementioned σ^+.[146]

4.1/4.2	Z	σ^+	σ_p	σ_m	σ^-
a	MeO	-0.78	-0.27	0.12	-0.26
b	Me	-0.31	-0.16	-0.07	-0.17
c	F	-0.07	0.06	0.34	-0.03
d	H	0	0	0	0
e	$C(O)CH_3$	0.50 [a]	0.50	0.38	0.84
f	CN	0.66	0.66	0.56	1.0
g	NHAc	-0.60	0	0.21	-0.46
h	Br	0.15	0.23	0.39	0.25

[a] no σ^+ value was available for Z = $C(O)CH_3$ so the σ_p value was used.



4.6 **4.7**

Scheme 4.4. The dissociation reaction of cumyl chloride (**4.6**) from whose relative rate constants (k_X/k_H) the Hammett parameter σ^+ is derived.[138,139]

Utilising the reaction rate data at 190 °C at 0.2 mL min^{-1} collected *via* a 170 – 250 °C temperature ramp, $\ln(k_X/k_H)$ - a measure of relative reaction rate constants utilised for Hammett plots - was plotted against σ_p, σ_m, σ^+, and σ^- (Fig. 4.12). These plots demonstrate that σ^+ (blue data) is the best Hammett parameter to use to represent the reactivity trend of different substituents for the aromatic Claisen rearrangement reaction; affording an R^2 fitting value of 0.96 compared to 0.79, 0.35, and 0.72 for σ_p, σ_m, and σ^-, respectively. The negative gradient of these plots (ρ) is commensurate with the involvement of a polar transition state in this reaction, which would be destabilized by electron withdrawing substituents (greater σ^+ values).

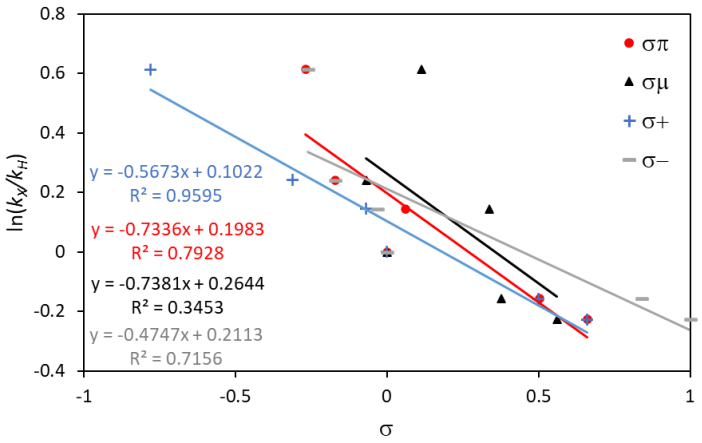


Figure 4.12. Data collected at 190 °C at 0.2 mL min^{-1} on the aromatic Claisen rearrangement of phenyl allyl ether (**4.1d**), plotted against a range of Hammett parameters as described in Table 4.3.

Individual Hammett plots obtained over a range of temperatures could be generated from the kinetic data gathered from the OP-TF experiments (Fig. 4.13a). These plots facilitate comparison of the effect of the substituent at different temperatures, previously postulated to vary with temperature.[145] The reaction data collected was plotted as Hammett plots for 190, 210, and 230 °C, demonstrating a decrease in the magnitude of the gradient (ρ) from -0.57 to -0.50 over this temperature range, *i.e.* the effect of the substituent is less prominent at higher temperatures. This data can also be visualised as a 3D surface across the entire temperature ramp range, which allows a more rigorous evaluation of the assumed Hammett dependency (Fig. 4.13b). This plot clearly shows the temperature dependence of the Hammett plots for this reaction, showing that the greatest changes in relative rate occur for the most electron donating substituents (lower σ^+ values).

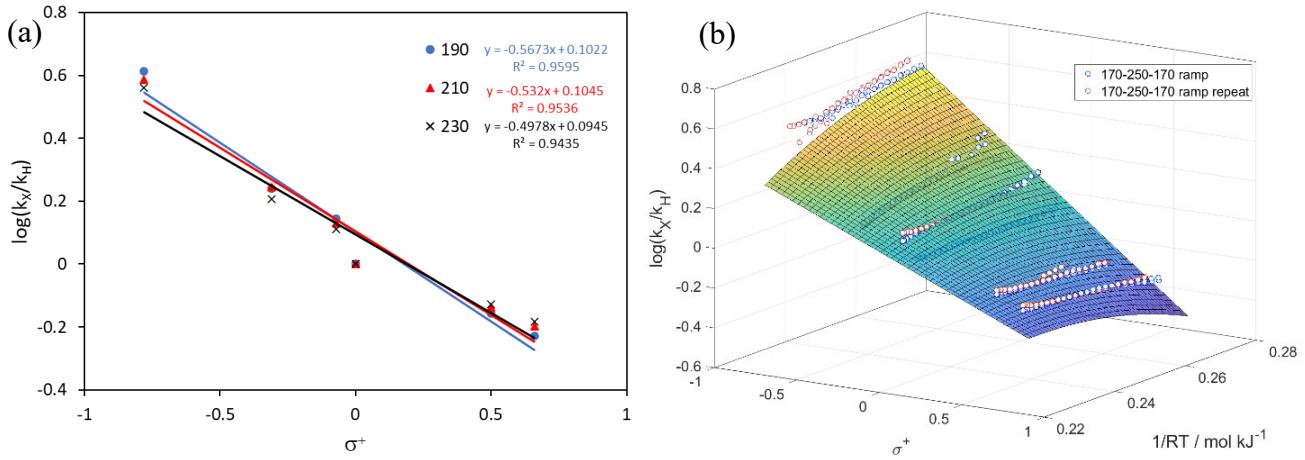


Figure 4.13. (a) Hammett plots at 190, 210 and 230 °C generated from OP-TF experiments; (b) temperature dependent Hammett plot visualizations of two 170 – 250 – 170 °C temperature ramping experiment on a mixture of six substrates **4.1a-f**. The surface fitting is first order in σ^+ and second order in 1/RT with average absolute residual = 0.03 and root mean square error RMSE = 0.0564.

5 Applications: thermodynamics and predictive model

The reaction data collected *via* the 'one-pot' transient flow method was collected with the intention of deriving fundamental thermodynamic dependencies for this reaction, made possible by the diverse and rich data collected by this method. This data could also be used for constructing a predictive model for reaction rate constants for different substituents and temperatures, tested against other substrates to confirm predictive capabilities.

5.1 Thermodynamics

The reaction data collected by the 'one-pot' transient temperature ramping method allows the thermodynamic effect of both temperature and substituent to be investigated. Previously, it has been hypothesised that the gradient of a Hammett plot (Eq. 4.1) should change proportionally with 1/RT.[145] From the reaction data collected, a good fit (Fig. 4.13b, $R^2 = 0.9489$) could be obtained from a surface function of a first order dependence in σ^+ and a second order dependence in 1/RT. This at first glance agrees with the previously hypothesised dependency, as this would afford a changing gradient in the Hammett dimensions [$\ln(k_X/k_H)$ *vs.* σ^+] of $\rho = m(1/RT)$; where m is a constant. However, differentiation

of the fitted polynomial surface with respect to σ^+ affords the relationship: $\rho = 1.035 - 6.31(1/RT)$, including a non-zero intercept not accounted for in the previously hypothesised form. In previous work, the gradient m was hypothesised to be dependent on the dielectric constant of the solvent and the distance of the substituent from the reaction site.[145] It was determined that from the reaction data collected, the dependency of the fundamental thermodynamic terms – entropy and enthalpy of reaction – on substituent could better be investigated.

Mathematically, this dependency can be derived by combining the Hammett equation (Eq. 4.1) with the Eyring equation (Eq. 4.3).

$$\log\left(\frac{k_X}{k_H}\right) = \rho\sigma^+ \qquad \text{[Eq. 4.1]}$$

$$k = \frac{\kappa k_B T}{h} e^{\frac{\Delta S^\ddagger}{R}} e^{-\frac{\Delta H^\ddagger}{RT}} \qquad \text{[Eq. 4.3]}$$

Beginning by converting $\log_{10}$ to the natural logarithm for Eq. 4.1:

$$\log\left(\frac{k_X}{k_H}\right) = \rho\sigma^+ = \frac{1}{\ln(10)} \ln\left(\frac{k_X}{k_H}\right) \qquad \text{[Eq. 4.5]}$$

Differentiating gives:

$$\rho = \frac{1}{\ln(10)} \frac{d(\ln\left(\frac{k_X}{k_H}\right))}{d\sigma^+} \qquad \text{[Eq. 4.6]}$$

Utilising the Eyring equation (Eq. 4.3) for both substituted (k_X) and unsubstituted (k_H) cases, relative rates can be found and simplified to give:

$$\ln\left(\frac{k_X}{k_H}\right) = \ln\left(\frac{\kappa_X}{\kappa_H}\right) + \frac{\Delta S_X^{\ddagger}}{R} - \frac{\Delta S_H^{\ddagger}}{R} - \frac{\Delta H_X^{\ddagger}}{RT} + \frac{\Delta H_H^{\ddagger}}{RT} \qquad \text{[Eq. 4.7]}$$

Generally, κ (the transmission coefficient) is assumed to be 1. For these purposes of this derivation, the less presumptuous assumption $\kappa_X \approx \kappa_H$ can be used, thus removing this relative logarithmic term. Combining the two above equations by differentiating $\ln\left(\frac{k_X}{k_H}\right)$ by σ^+ gives:

$$\rho = \frac{d}{d\sigma^+}\left(\log\left(\frac{k_X}{k_H}\right)\right) = \frac{1}{R\ln(10)}\frac{d}{d\sigma^+}\left(\Delta S_X^{\ddagger}\right) - \frac{1}{\ln(10)}\frac{d}{d\sigma^+}\left(\Delta H_X^{\ddagger}\right)\frac{1}{RT} \qquad \text{[Eq. 4.8]}$$

Separately, the OP-TF data was used to fit an equation with a first order dependence in σ^+ and a second order dependence in 1/RT of the form:

$$\log\left(\frac{k_X}{k_H}\right) = A + B\sigma^+ + C\left(\frac{1}{RT} * 10^3\right) + D\sigma^+\left(\frac{1}{RT} * 10^3\right) + E\left(\frac{1}{RT} * 10^3\right)^2 \qquad \text{[Eq. 4.9]}$$

This gives fitting constants with $R^2 = 0.93$ (0.95 for repeated experiment). Differentiation of this fitted equation leads to an equation in the form of equation 4.8, which allows comparison of fitting constants to the theoretical equation:

$$\frac{1}{R\ln(10)}\frac{d\Delta S^{\ddagger}}{d\sigma^+} = 1.138\ (1.044) \qquad \text{[Eq. 4.10]}$$

$$\frac{1}{\ln(10)}\frac{d\Delta H^{\ddagger}}{d\sigma^+} = 6.648 * 10^3 (6.332 * 10^3) \qquad \text{[Eq. 4.11]}$$

where bracketed values are calculated from repeated experiment.

These can be rearranged, and averaged, to produce values for how the reaction entropy and enthalpy change with varying substituent.

$$\frac{d\Delta S^{\ddagger}}{d\sigma^{+}} = 20.9 \text{ J mol}^{-1}\text{K}^{-1} \qquad \text{[Eq. 4.12]}$$

$$\frac{d\Delta H^{\ddagger}}{d\sigma^{+}} = 14.9 \text{ kJ mol}^{-1} \qquad \text{[Eq. 4.13]}$$

Again utilising equation 4.8, the isokinetic temperature[147] (β) can be derived when $\rho = 0$:

$$T = \beta = \frac{6.490 * 10^{3}}{1.091\ R} = 715 \text{ K} \qquad \text{[Eq. 4.14]}$$

The derived values for changes in reaction entropy ($d\Delta S^{\ddagger}/d\sigma^{+}$) and enthalpy ($d\Delta H^{\ddagger}/d\sigma^{+}$) with changing substituent represent an interplay between the entropic and enthalpic contributions to the aromatic Claisen rearrangement reaction. This interplay implies a temperature at which all phenyl allyl ether **4.1** compounds react at the same rate independent of the substituents on the aromatic ring (isokinetic temperature, Eq. 4.14).[147]

5.2 Predictive model

The reaction data was also used to build a model to predict reaction rate constants for a given reaction temperature and substrate (Fig. 4.14, σ^{+} *vs.* 1/RT *vs.* ln(k)). It was determined that although log(k_X/k_H) could be predicted from the thermodynamic understanding developed previously, ln(k) was a more useful quantity to predict, without overly relying on data collected for the unsubstituted compound **4.1d**. It was envisaged that this model could be used by synthetic chemists to predict whether the aromatic Claisen rearrangement reaction would be viable in a synthetic route without degrading the rest of the molecule of interest. This model would predict the rate constant from which reaction time and

temperature could be selected to give a certain yield for a reaction based on its substituent(s), thus derisking the synthetic route.

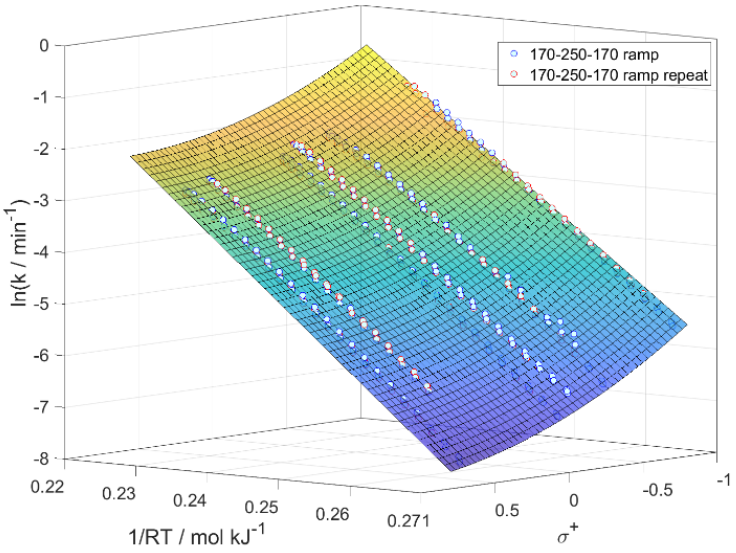


Figure 4.14. "Arrhenius-Hammett model" surface with two bi-directional temperature ramping experiments (170–250–170 °C) generated from the six training substrates **4.1a-f**.

The reaction data used to fit the model was collected in two bi-directional temperature ramps (170 – 250 – 170 °C, 0.5 °C min^{-1}) at 0.2 mL min^{-1} on all six substrates simultaneously (OP-TF). The model was fitted as a polynomial multivariate regression - 1st order in 1/RT and 2nd order in σ^+ - for an accurate empirical fit to be obtained for ln(*k*) (Fig. 4.14). To validate the model fitting, the ln(*k*) values for the training substrates **4.1a-f** were simulated by the model, over the temperature range used for training the model (Fig. 4.15). From the predicted ln(*k*) values, activation energies (E_a) and pre-exponential factors (A) were calculated. The prediction of ln(*k*) values afforded good results with low mean absolute error (MAE) between 0.060 – 0.114 on absolute values of between -2 – -8, compared with experimental data over the temperature range (Table 4.4). As a 1st order fit in 1/RT is used for the model, the Arrhenius dependency is built into the model and as such activation energies and pre-exponential factors were generally accurately predicted, within *circa* 1 kJ mol^{-1} of observed values. The notable exception to this was allyl ether **4.1a** (Z = OMe), which had a poorly predicted activation energy: under-estimated by 8 kJ mol^{-1}. This effect may be attributed to this compound lying on the upper extreme of the model, the

highest σ^+ value, or could also be affected by hydrogen bonding effects due to the presence of the oxygen lone pair in this compound.

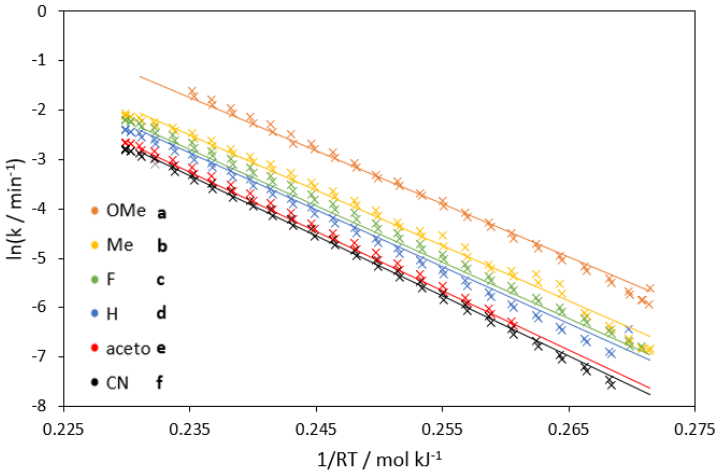


Figure 4.15. Comparison of experimental data (crosses) and model simulations (lines) of Arrhenius plots on the 'training' substrates **4.1a-f**.

Table 4.4. Comparison of the predicted results of the "Arrhenius-Hammett model" and the experimental results obtained for the training set (**4.1a-f**) and test set (**4.1g-h**).

4.1x/4.2x	Z	MAE* of ln(k / min^{-1}) predictions	E_a / kJ mol^{-1}		ln(A / min^{-1})	
			Exp.	Pred.	Exp.	Pred.
a	MeO	0.086	115.4	107.5	25.5	23.5
b	Me	0.114	112.9	112.0	24.0	23.8
c	F	0.110	113.2	114.3	23.9	24.1
d	H	0.101	116.1	115.0	24.3	24.2
e	$C(O)CH_3$	0.064	119.2	119.8	24.8	24.9
f	CN	0.060	122.4	121.3	25.4	25.2

*Mean absolute error (MAE) is a measure of prediction accuracy.

5.3 Test substrates

In order to confirm the capability of the model for predicting rate constants for compounds which the model had not been trained on, two further *para*-substituted phenyl allyl ethers **4.1g** (Z = NHAc, σ^+= -0.60) and **4.1h** (Z = Br, σ^+ = 0.15) were introduced to this study. These substrates were chosen to be within the trained σ^+ range, in parts not close to the model training substrates values. These substrates were previously synthesised by parallel synthesis and calibration curves were produced for starting allyl

ethers **4.1** and product phenols **4.2**. Based on the σ^+ values, the rate constants for these reactions were predicted across the wide temperature range of the model (170 – 250 °C); subsequently reaction data were collected for both compounds individually, utilising a bi-directional temperature ramp between 170 – 250 °C (Fig. 4.16). Pleasingly, the predicted and experimental values appeared similar, although **4.1h** (Z = NHAc, orange data) produced the worst MAE, which can be visually seen to be simply from a systematic error shifting the data (Table 4.5, Fig. 4.16). Activation energies and pre-exponential factors were also adequately predicted (Table 4.5). These further test reactions confirmed the validity of the model for interpolating the rate constants of other substrates over the trained temperature range.

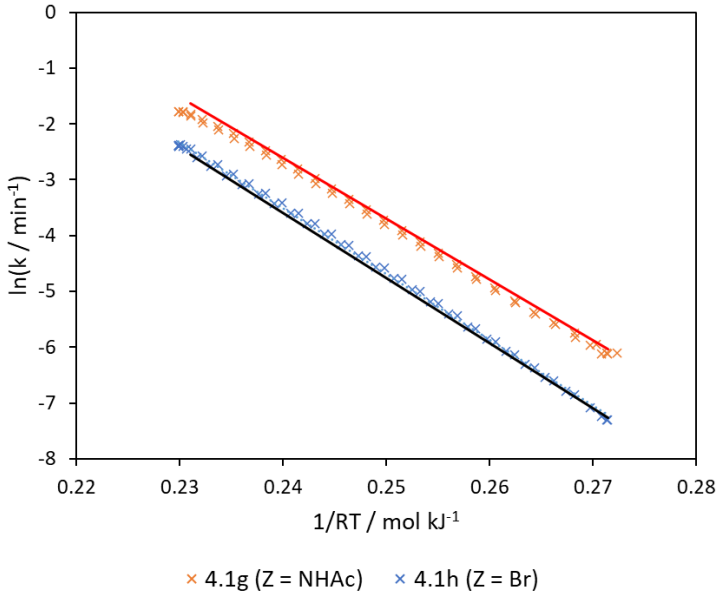


Figure 4.16. Arrhenius plots generated from bi-directional temperature ramp experiments (170–250–170 °C) (crosses) compared to Arrhenius-Hammett model predictions (lines) for phenyl allyl ether **4.1g** (Z = NHAc) and **4.1h** (Z = Br).

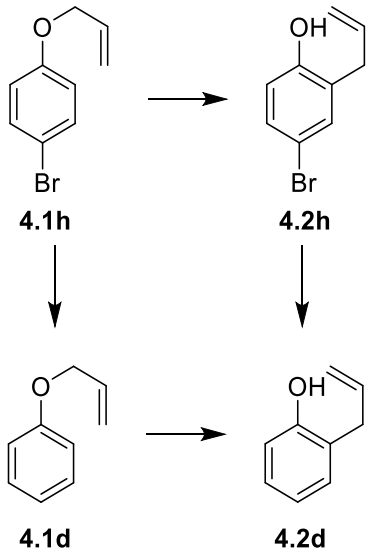
Table 4.5. Comparison of the predicted results of the "Arrhenius-Hammett model" and the experimental results obtained for the training set (**4.1a-f**) and test set (**4.1g-h**).

4.1x/4.2x	Z	MAE* of ln(k / min^{-1}) predictions	E_a / kJ mol^{-1}		ln(A / min^{-1})	
			Exp.	Pred.	Exp.	Pred.
g	NHAc	0.205	106.9	109.3	22.9	23.6
h	Br	0.086	117.9	116.4	24.8	24.3

*Mean absolute error (MAE) is a measure of prediction accuracy.

5.4 *para*-Bromine side reaction

During the study of the para-bromo-substituted compound **4.1h** (Z = Br), the formation of an unexpected side product was observed by on-line HPLC (Scheme 4.5). Above 240 °C (513 K), non-negligible concentrations of **4.2d**, the unsubstituted aromatic Claisen phenol product, were observed (Fig. 4. 17, grey dots). This side product was identified due to the formation of a peak at the corresponding retention time in the 'one-pot' HPLC method, and was also confirmed by off-line HPLC-MS, however, was found to be in too low concentrations to isolate.



Scheme 4.5. Aromatic Claisen rearrangement for *para*-bromophenyl allyl ether (**4.1h**) and the protodebromination side products.

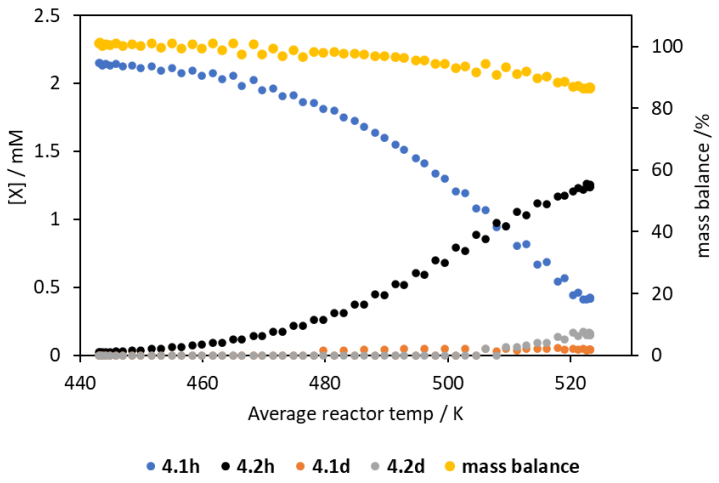


Figure 4.17. Concentration *vs.* temperature data collected *via* a 170 – 250 – 170 °C transient temperature ramp on **4.1h** (Z = Br) for the test set data for model prediction. This data shows some debromination leading to the formation of **4.1d** and **4.2d**, as well as a drop in mass balance potentially caused by further product degradation.

The debrominated product **4.2d** was produced in up to 5% yield from the brominated allyl ether starting compound (**4.1h**, blue dots), although concentrations of the debrominated starting allyl ether **4.1d** (orange dots) remained negligible throughout the temperature ramping experiment. The mass balance data (yellow dots, Fig. 4.17) reveal a further 10% of the substrate is unaccounted for, potentially due to further degradation products under the extreme conditions. Comparing experimental activation energies for the aromatic Claisen rearrangement of **4.1d** and **4.1h** demonstrates that **4.1d** will more easily rearrange than **4.1h** (Tables 4.4 and 4.5). Thus it is plausible that **1d** is formed from **4.1h**, however rearrangement of **4.1d** to **4.2d** is at such a fast rate that none of **4.1d** is observed (steady state kinetics). As this debromination product **4.2d** only begins to emerge in observable concentrations above the supercritical point of ethanol (241 °C, 63 bar[143]), it is tempting to infer that this reaction requires the change in solvent properties this brings. However, it is likely this is coincidental and simply a result of the increased temperature of the reaction. The mechanism of this dehalogenation process is currently unknown, it could potentially occur through the loss of bromine thermally either *via* a radical or a cationic bromine species, or it is also likely the bromine atom is lost through a nickel catalysed insertion process, catalysed by the stainless steel tubing of the reactor.[148] Attempts to extract the rate constant of the unknown debromination reaction proved challenging due to the low concentration of debrominated product **4.2d** and the lack of identification of the further missing material in the mass balance calculations.

6 Solvent ramping

6.1 Premise

Solvents are a crucial component of a reaction, the properties of which can alter the reaction rate by orders of magnitude or even change the reaction outcome.[104,111] Traditionally, solvent selection is often based on past precedent for a reaction and 'chemical intuition', although more numerical approaches have emerged in recent years.[112] Even in more data driven approaches to solvent selection, solvent systems are treated as discrete variables with a pre-defined group of numerical properties (polarity, dielectric constant, *etc.*). Solvent mixtures allow continuous modification of these properties between discrete pure solvent points, accessing a greater range of the possible solvent parameter space, thus providing more data to probe solvent effects and more potential optimal solvent systems for a reaction.

Solvents are inherently wasteful in synthesis as they are not part of the reaction product but generally make up over 90% of the reaction mass (process mass intensity), however, they are often vital for reaction progress by facilitating mixing of reactants. The use of certain solvents, especially those containing chlorine (dichloromethane, carbon tetrachloride), as well as dioxane, dimethylformamide (DMF) and N-methyl-2-pyrrolidone (NMP) are either already or becoming banned or more tightly regulated by EPA and REACH regulations, for their toxicity and detrimental effect on the environment and human health.[113] Finding more sustainable and benign replacements for these solvents is therefore a top priority for many chemical companies in the coming years.[114]

A transient flow method (Fig. 4.18) for collecting reaction data for many solvent mixture environments at a fixed residence time and temperature was viewed as a valuable and efficient solution for investigating solvent effects and finding replacements for harmful solvents. The aromatic Claisen rearrangement again appeared a good example reaction on which to test this new method. The reaction is often performed in harmful solvents such as NMP or DMF,[149] and has often been reported to experience strong solvent effects, linked to increasing solvent polarity.[119]

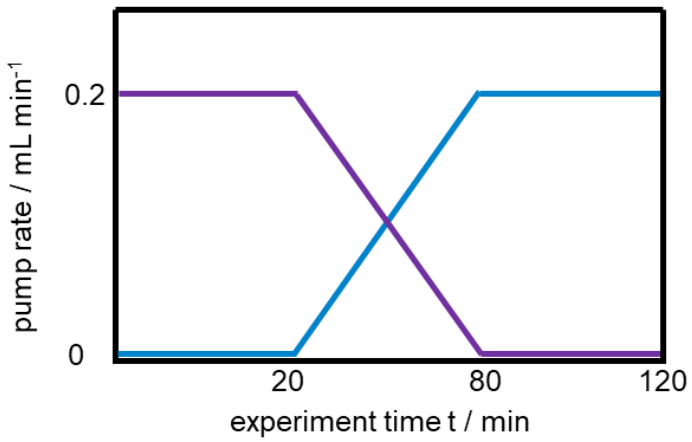


Figure 4.18. Solvent ramping method for a binary solvent mixture, maintaining the same cumulative flow rate while varying the flow rate ratio of the two solvent reaction solution pumps.

For these solvent ramps, it was noted that mixing solvents together within the flow system would affect the residence time in two ways:

- Firstly, following the Tait equations (Eq. 2.29 and 2.30) different solvents will change density by different amounts on heating and pressurising when entering the reactor. This will vary the volumetric flow rate by different amounts between the set cumulative flow rate and that present within the reactor dependent on the solvent mixture. However, this effect will be relatively small (<10% change in residence time) and will not affect the relative solvent amounts.
- Secondly, mixing two solvents together is known to often produce a change in cumulative volume. For example, on mixing ethanol and water overall volume in known to reduce by up to 20%. The differences in volume that may occur on mixing different binary solvents together under high temperatures and pressures was considered a problem best tested empirically.

Fortunately, these effects are likely to act in opposite directions with the first increasing nominative solvent volume and the second reducing it. Although, the effect of these terms when compared across solvents is not known, the reaction data afforded by solvent ramping method will, at the very least, allow trends in solvent effects and ‘black box’ models of changing solvent in this specific flow system to be generated.

6.2 Reaction in DMF

To provide a benchmark, a bi-directional temperature ramp was performed for the reaction of allyl ether **4.1d** in DMF at a flow rate of 0.2 mL min^{-1}, a residence time of *circa* 20 min (Fig. 4.19a). At a reaction temperature of 220 °C, 37% yield was achieved, which was considered a suitable middling yield to which the reaction in other solvent systems at this temperature could be compared. From the collected data, an activation energy of 150 kJ mol^{-1} was calculated for the reaction in DMF (Fig. 4.19b), which is significantly higher than the same reaction conducted in ethanol (117 kJ mol^{-1}). Despite this significant difference in activation energies, there is also a substantial difference in pre-exponential factor (Fig. 4.19b: in DMF, ln(A) = 32.8 compared to 24.6 in ethanol), at 220 °C, the reaction yield in DMF (37%) is not too dissimilar to that in ethanol (28%). This is better investigated by use of the Eyring equation (Eq. 4.3) to calculate the entropy of activation ($\Delta S^{\ddagger}$ in J mol^{-1} K^{-1}) and enthalpy of activation ($\Delta H^{\ddagger}$). $\Delta H^{\ddagger}$ as expected is more favourable in ethanol than DMF (112 compared to 146 kJ mol^{-1}). However, $\Delta S^{\ddagger}$ is positive in DMF (+15.4 J mol^{-1}) and negative in ethanol (-54.6 J mol^{-1}), producing a similar rate constant for the reaction in either solvent at 220 °C. The negative entropy of activation suggests that the reaction transition state is more ordered, potentially due to more hydrogen bonding interactions, than that of the ground state reactant system.

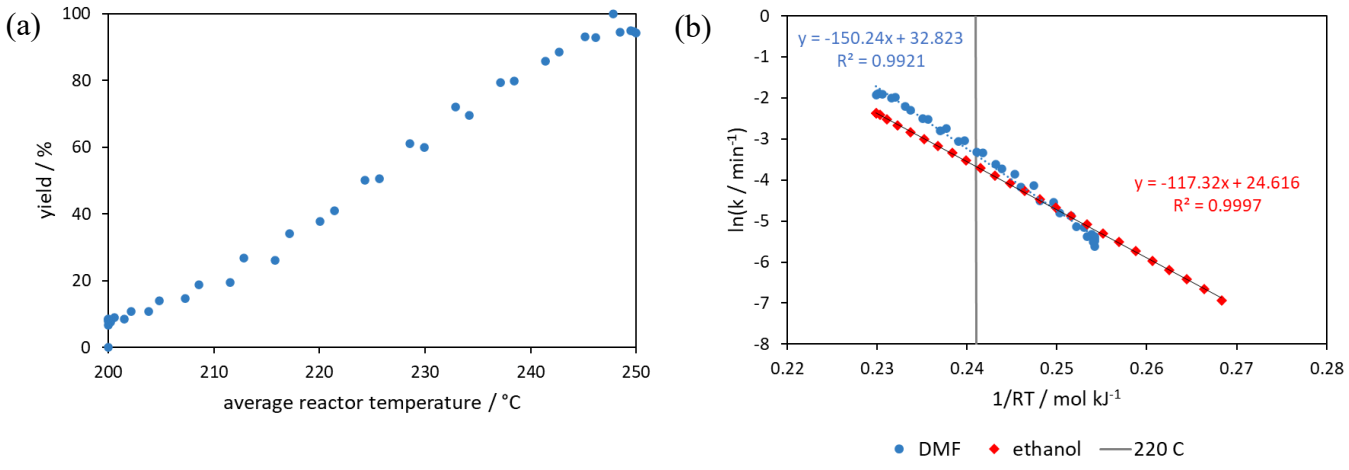


Figure 4.19. (a) the yield of the reaction of **4.1d** to form **4.2d** in DMF at a flow rate of 0.2 mL min^{-1} collected utilising a bi-directional temperature ramp between 200 – 250 – 200 °C at 0.5 °C min^{-1}; (b) an Arrhenius plot of the same reaction data compared to that for the same reaction in ethanol with gradient equal to the activation energy in kJ mol^{-1}.

6.3 Solvent ramps

Next, a number of solvents were selected intuitively, to cover a range of solvent properties, while remaining relatively benign and solubilising to the starting allyl ether **4.1d**. The final list consisted of 11 solvents, ranging in polarity from cyclohexane to water (Table 4.6). From the earlier work described above, ethanol was already known to reduce the activation energy compared to that for the reaction in DMF, therefore a wider range of polar and protic solvents were included, in order to interrogate this effect more closely.

Table 4.6. Solvents selected for solvent ramping experiments for the reaction of **4.1d**. Some solvent properties are also listed when available, if the reference of the data source is not by the value, then the reference is that of the column header.

Solvent	dielectric constant[150]	Reichardt's polarity scale ($E_T(30)$)[151]
cyclohexane	2.02	30.9
ethyl acetate	6.02	38.1
acetic acid	6.15	51.7
2-Me THF	6.97[152]	36.5
HFIP	16.7[153]	62.1
IPA	17.9	50.7
ethanol	24.5	51.9
methanol	32.7	55.4
ethylene glycol	37	56.3
acetonitrile	37.5	45.6
water	80.1	63.1

For this study, it is important to use miscible solvent systems for the generation of solvent ramps, to avoid more complex biphasic mixtures. Additionally, ramps were only performed within the solubility limit of the starting allyl ether **4.1d** and product phenol **4.2d**, which places an upper limit for certain solvents, such as water, to be use in in the solvent ramps. The solvent ramps performed in this experiment are listed in Table 4.7 and summarised as a series of data points collected in Figure 4.20. Each solvent ramp was performed bi-directionally, in order to avoid any effects on the data caused by ramp direction.

Table 4.7. Solvents ramps performed on the reaction of **4.1d** to **4.2d**. Graph reference refers to the figure in which the reaction data collected by the given solvent ramp is shown.

Solvent A	Solvent B	Graph reference
ethyl acetate	methanol	21a
50%w/v water in methanol	methanol	21b
50%w/v water in ethanol	ethanol	22
cyclohexane	ethanol	23
ethylene glycol	2-methyl THF	24a
ethylene glycol	methanol	24b
ethylene glycol	60%w/v water in ethylene glycol	25
IPA	HFIP	26
acetonitrile	acetic acid	27

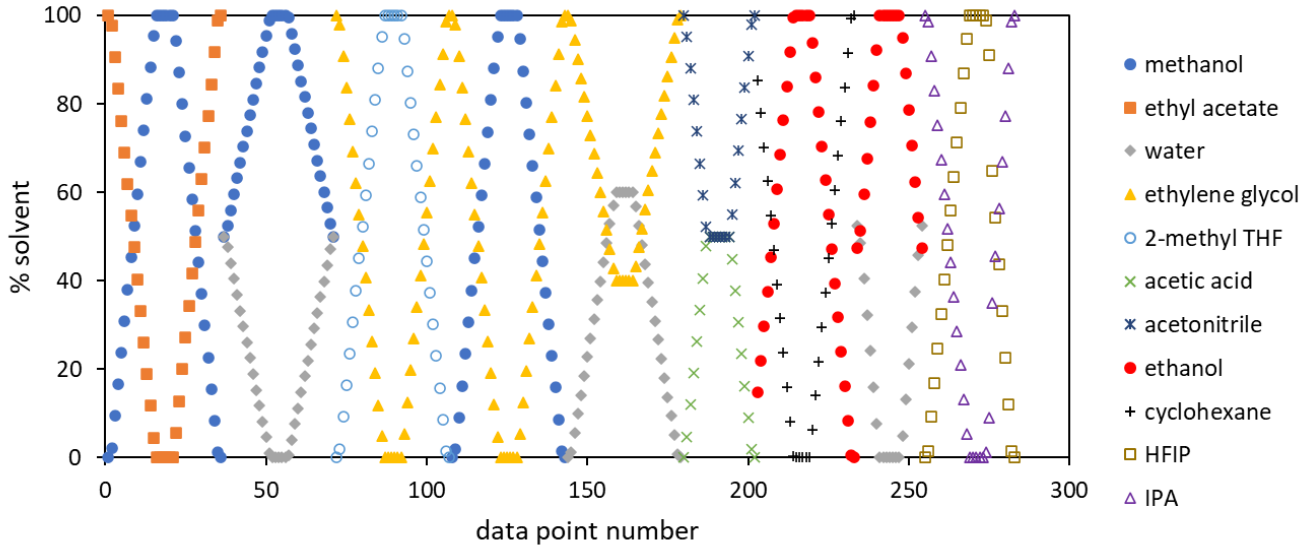


Figure 4.20. A figure representing all the solvent combination tested in a series of solvent ramping experiments described in Table 4.7. Some ramps are limited to certain solvent percentages due to pre-screened solubility limits of **4.1d** and **4.2d**.

Each of the solvent ramps described produced a series of reaction species concentrations, which could be converted into yields. The steady state reaction data collected at the beginning and end of each ramp were found to be consistent between experiments, acting as a repeated point to validate cross comparison between different experiments (Fig. 4.21, for example).

In the first set of experiments, a solvent ramp between ethyl acetate and methanol, and a ramp between methanol and 50% weight by volume (%w/v) water in methanol (Fig. 4.21) were performed. The data obtained from these ramps demonstrate the reactivity in ethyl acetate is about half that in methanol,

which is, in turn, approximately half that of the reaction in 50%w/v water in methanol. There appears to be a period between 0–30%v/v methanol in ethyl acetate, where the yield remains broadly the same, whereafter the yield of the reaction increases linearly with increasing methanol concentration (Fig. 4.21a). Increasing the amount of water in a methanolic solution appears to produce a linear increase in the yield of the reaction (Fig. 4.21b). Assuming proportional combinations of different solvent description parameters from Table 4.6, correlation could plausibly be obtained with dielectric constant or Reichardt empirical polarity metric $E_T(30)$.

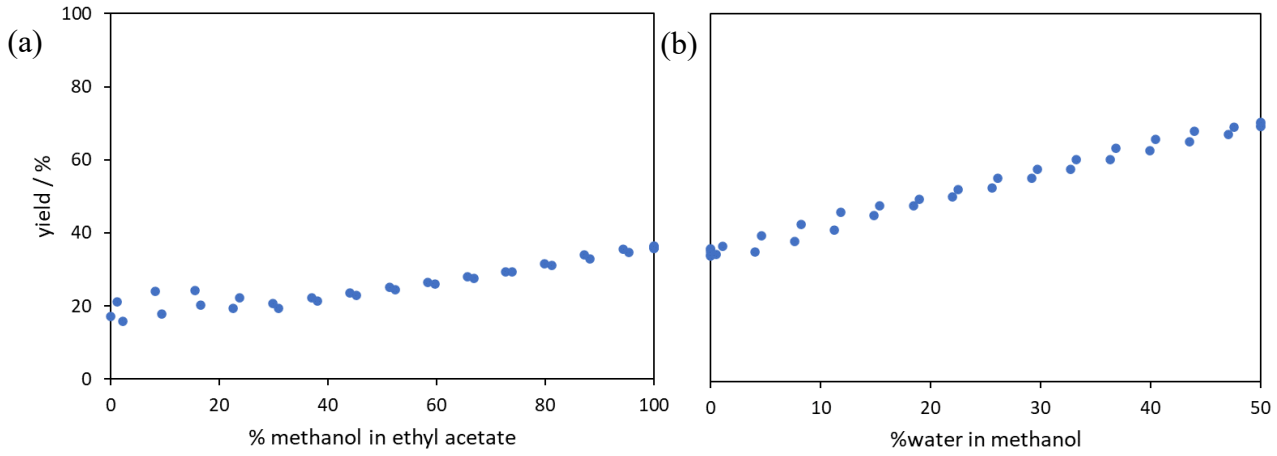


Figure 4.21. Bi-directional solvent ramping experiment results between (a) ethyl acetate and methanol; and (b) methanol and 50%w/v water in methanol, performed at 220 °C and a cumulative flow rate of 0.2 mL min^{-1} for the reaction of **4.1d** to **4.2d**.

Next, a solvent ramp experiment between ethanol and 50%w/v water in ethanol was performed (Fig. 4.22), which also demonstrated consistency between the ethanol steady state yield and those data obtained by previous temperature ramps (Fig. 4.6). Notably, comparison between a methanol-water ramp (blue dots) and ethanol-water ramp (orange dots) reveals relatively similar results when more than 25%w/v water is included, despite the relatively substantial differences between the collected polarity measures for methanol and ethanol (Table 4.6). The difference in yield between ethanol and methanol at the beginning of the ramps is closer to what might be assumed from the polarity metrics, methanol yielding 36% and ethanol yielding 28%. This suggests there are solvent properties that are not captured by these initially selected parameters, which are important to the yield of the reaction.

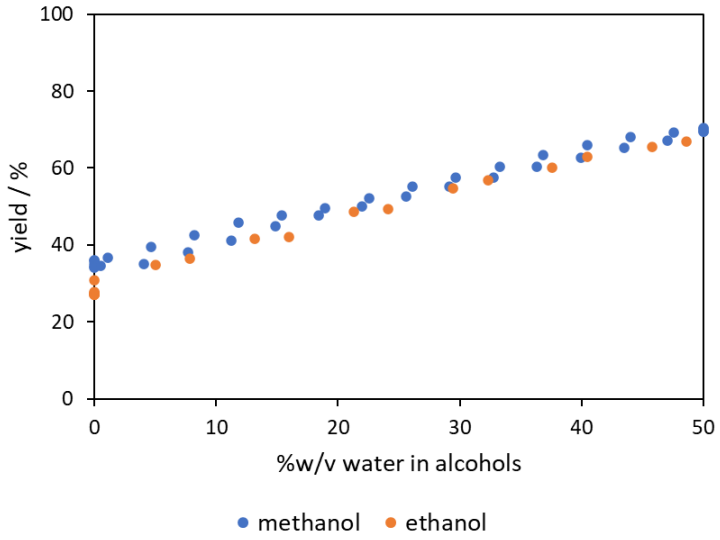


Figure 4.22. Bi-directional solvent ramping experiment results between an alcohol and 50%w/v water in alcohol performed at 220 °C and a cumulative flow rate of 0.2 mL min^{-1} for the reaction of **4.1d** to **4.2d**.

Solvent ramps between cyclohexane and ethanol (Fig. 4.23) produce a similar response to the ethyl acetate and methanol ramp (Fig. 4.21a): beginning with a range of low yield up to *circa* 30% ethanol in cyclohexane, followed by a linear response region after this point. This experiment was repeated due to relatively high noise in the low ethanol percentage region (outlier, orange square). Examining the chromatograms for this range further, the noise was attributed to poor peak shapes, potentially caused by the immiscibility of cyclohexane with the HPLC mobile phase (water and acetonitrile).

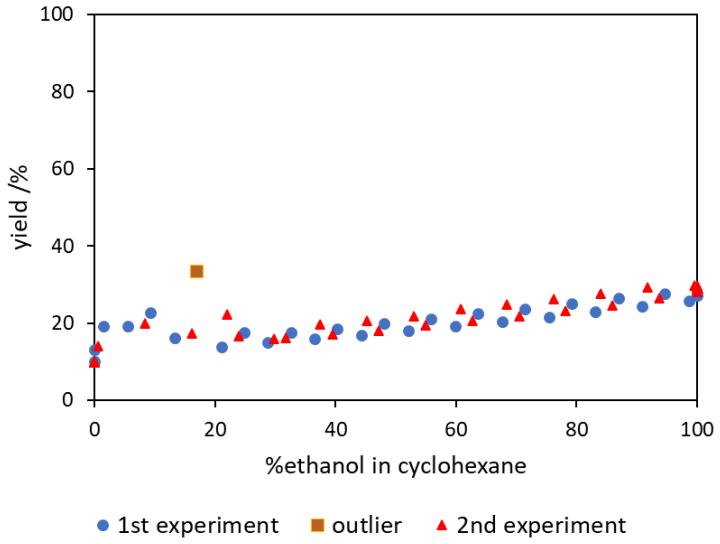


Figure 4.23. Bi-directional solvent ramping experiment results between cyclohexane and ethanol performed at 220 °C and a cumulative flow rate of 0.2 mL min^{-1} for the reaction of **4.1d** to **4.2d**. This experiment was repeated twice, and an outlier was observed in the first experiment.

Solvent ramps involving ethylene glycol in 2-Me-THF or methanol both afforded high yields at high percentages of ethylene glycol (Fig. 4.24). 2-Methyl THF, an aprotic low polarity solvent, afforded low yields, which increased linearly as the percentage of ethylene glycol in the solvent solution was increased (Fig. 4.24a). A solvent ramp of ethylene glycol and methanol, predicted to be similar yielding solvents from solvent polarity metrics collected in Table 4.6, produced a slightly parabolic response, affording approximately twice the reaction yield in ethylene glycol compared with in methanol. This suggests that the protic nature of the solvent is an important feature on the rate of the aromatic Claisen rearrangement.

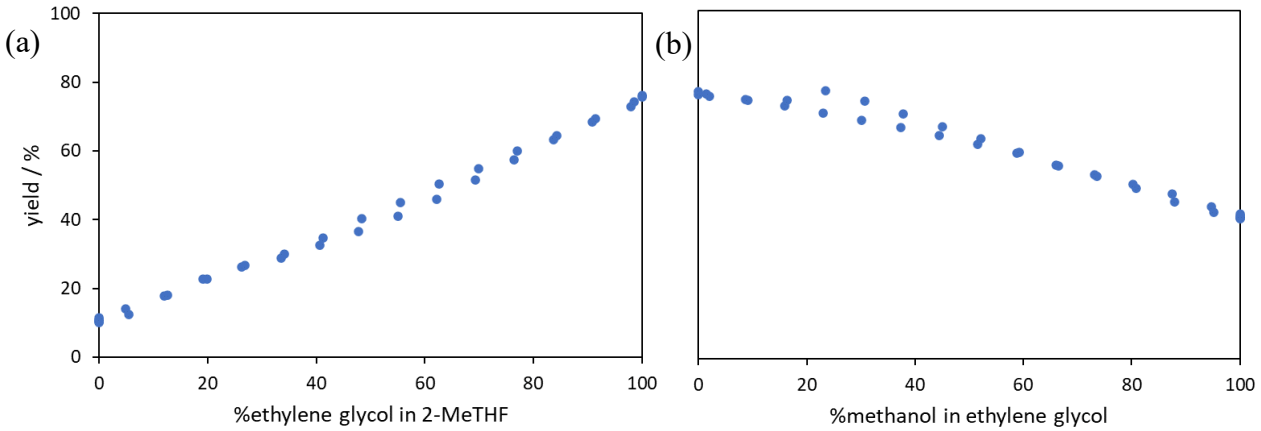


Figure 4.24. Bi-directional solvent ramping experiment results between: (a) 2-methyl THF and ethylene glycol; and (b) ethylene glycol and methanol, performed at 220 °C and a cumulative flow rate of 0.2 mL min^{-1} for the reaction of **4.1d** to **4.2d**.

A ramp between the two best performing solvents from these previous ramps – ethylene glycol and water – demonstrated that the reaction yield in ethylene glycol could be improved by the addition of water to the solvent mixture (blue dots, Fig. 4.25). However, it is worth noting that this ramp was restricted to 60%w/v water in ethylene glycol, due to solubility concerns of the starting allyl ether in higher water percentage mixtures. This solvent ramp also produced different yield data dependent on ramp direction: the ramp to greater water percentages produced lower yielding data than the ramp reducing water percentage. Although these results are not vastly disparate, this is the most prominent difference observed in this collection of solvent ramps. This could potentially be attributed to the high viscosity of ethylene glycol and water mixtures leading to worse initial mixing or differences in fluid dynamics,

which could be solved by utilising a static mixer with better mixing properties, such as an arrowhead mixer.

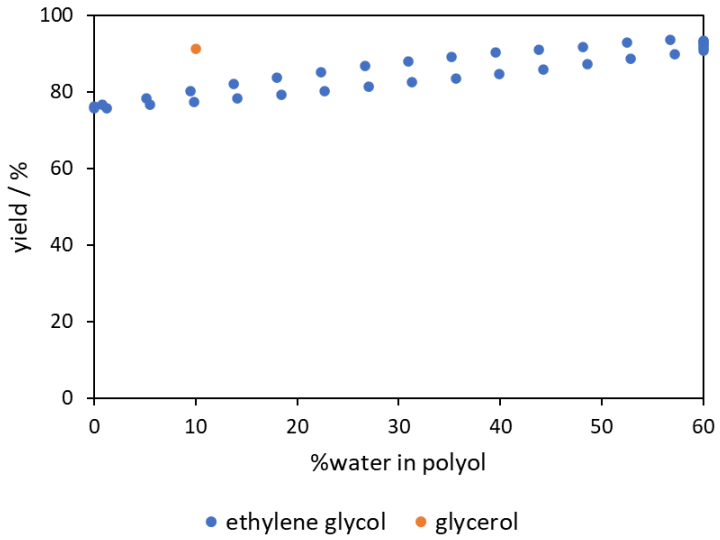


Figure 4.25. Bi-directional solvent ramping experiment results between a polyol and 60%w/v water in polyol performed at 220 °C and a cumulative flow rate of 0.2 mL min^{-1} for the reaction of **4.1d** to **4.2d**.

Glycerol was considered another likely high yielding polyol. However, the solubility of the starting allyl ether **4.1d** was poor in pure glycerol and the solution had high viscosity. An attempted solvent ramp between 10%w/v water in glycerol and 60%w/v water in glycerol proved challenging due to the biphasic separation of the higher water percentage solution. As such, only a steady state yield was recorded for 10%w/v water in glycerol (91%, orange data point, Fig. 4.25).

The effects of hydrogen bonding interactions were further probed utilising a solvent ramp between *iso*-propyl alcohol (IPA) and its polyfluorinated analogue, hexafluoro *iso*-propyl alcohol (HFIP) (Fig. 4.26). HFIP is known to be a strong hydrogen bond acceptor, due to its high fluorine count, and also to contain a more acidic hydroxy proton than IPA, due to both the electron withdrawing and hydrogen bonding effects of the fluorine atoms. It is worth noting HFIP is not a sustainable solvent, but has been widely used in academia to provide 'privileged' reactivity.[153,154] These data demonstrate a marked increase in yield with increasing HFIP percentage in what appears to be a sigmoidal manner (Fig. 4.26), potentially due to HFIP forming hydrogen bonding macrostructures with IPA in different ratios depending on the

solvent percentage. The reaction in IPA was found to have a slightly lower yield than that in ethanol or methanol (HFIP>methanol>ethanol>IPA), commensurate with results in previous work by Kobayashi *et al.*, which found that the reaction rate in ethanol was greater than that in IPA.[80]

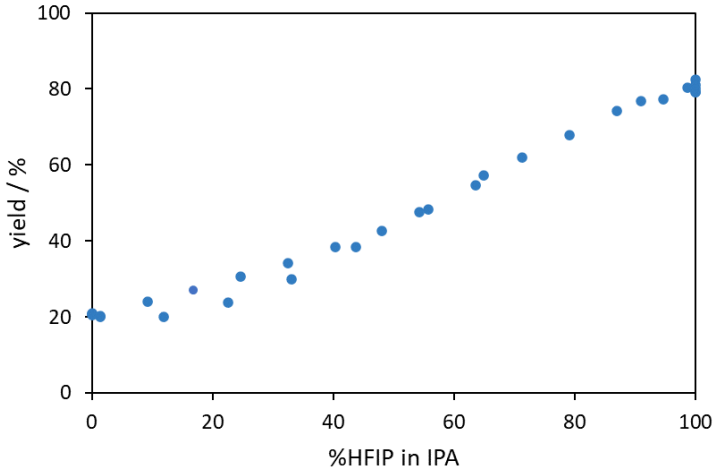


Figure 4.26. Bi-directional solvent ramping experiment results between IPA and HFIP performed at 220 °C and a cumulative flow rate of 0.2 mL min^{-1} for the reaction of **4.1d** to **4.2d**.

To further investigate the potential role of hydroxy hydrogen bonding on the reaction yield, a solvent ramp between acetonitrile and 50%v/v acetic acid in acetonitrile was performed (Fig. 4.27a). A relatively linear increase in yield was observed over this solvent ramp from 18% yield in acetonitrile, to 38% yield in 50%v/v acetic acid in acetonitrile. Comparison of this data to that for the first half of the ethylene glycol and 2-methyl THF ramp (Fig. 4.24a) affords a similar trend, demonstrating that the pKa of the solvent hydroxyl proton is not a key factor in the solvent effect on this reaction (pKa in water:[155] acetic acid, 4.8; ethylene glycol, 15.1). As expected, acetic acid also can react with the reaction product (phenol **4.2d**) to form the acylated product **4.8** (Scheme 4.6), the formation of which could also be monitored (uncalibrated) by the on-line HPLC set up (Fig. 4.27b).

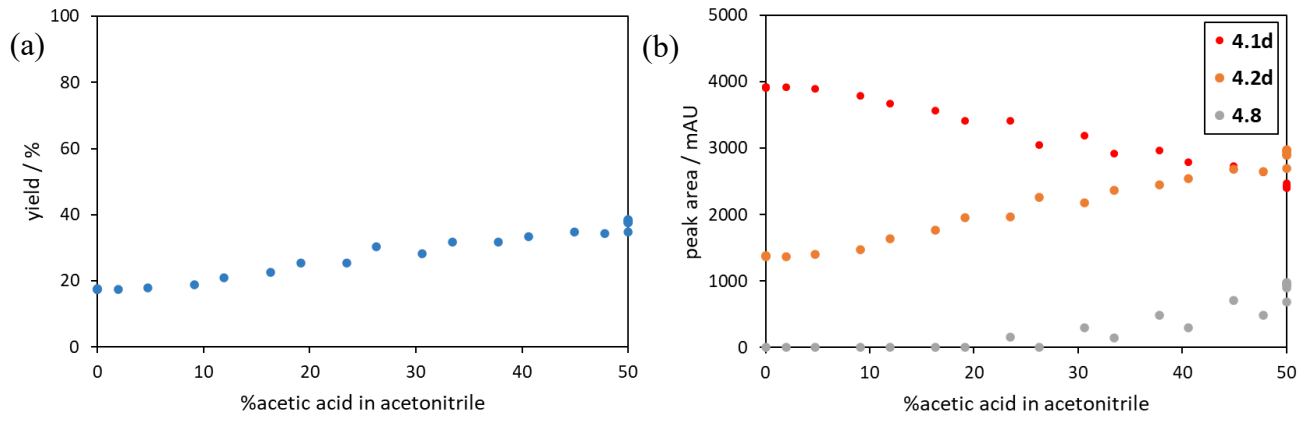
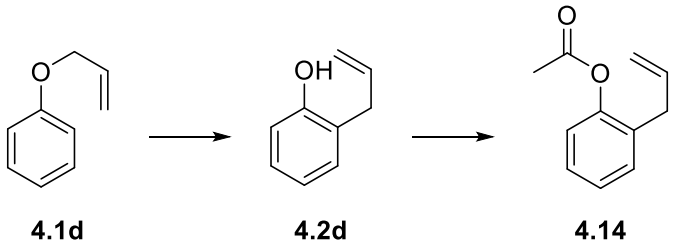


Figure 4.27. Bi-directional solvent ramping experiment results as: (a) yield of **4.2d**; and (b) UV absorption HPLC peak areas, between acetonitrile and 50%v/v acetic acid in acetonitrile performed at 220 °C and a cumulative flow rate of 0.2 mL min^{-1} for the reaction of **4.1d** to **4.2d**, including side product **4.8**.



Scheme 4.6. Side reaction to form acylated product **4.14** from the reaction of allyl ether **4.1d** in an acetonitrile-acetic acid mixture to form phenol **4.2d**.

6.4 Initial analysis

Combining all the solvent ramping data together affords a data set of 283 reaction yields from a wide range of solvent mixture reaction conditions (Fig. 4.28). Initial analysis consisted of utilising dielectric constants and an empirical polarity metric, $E_T(30)$, for pure solvents, to produce linear combinations of the respective metric for solvent mixtures (Table 4.6). These two metrics were chosen for initial correlation plots as values could be found for all the solvents utilised in the solvent ramps performed. Plotting the reaction yield against these metrics revealed some positive linear correlation for both dielectric constant ($R^2 = 0.5777$) and $E_T(30)$ ($R^2 = 0.6532$) (Fig. 4.29a and b, respectively). These trends reveal solvent polarity is somewhat important in affecting the yield of this reaction, but these factors do not fully describe the solvent effect on this reaction.

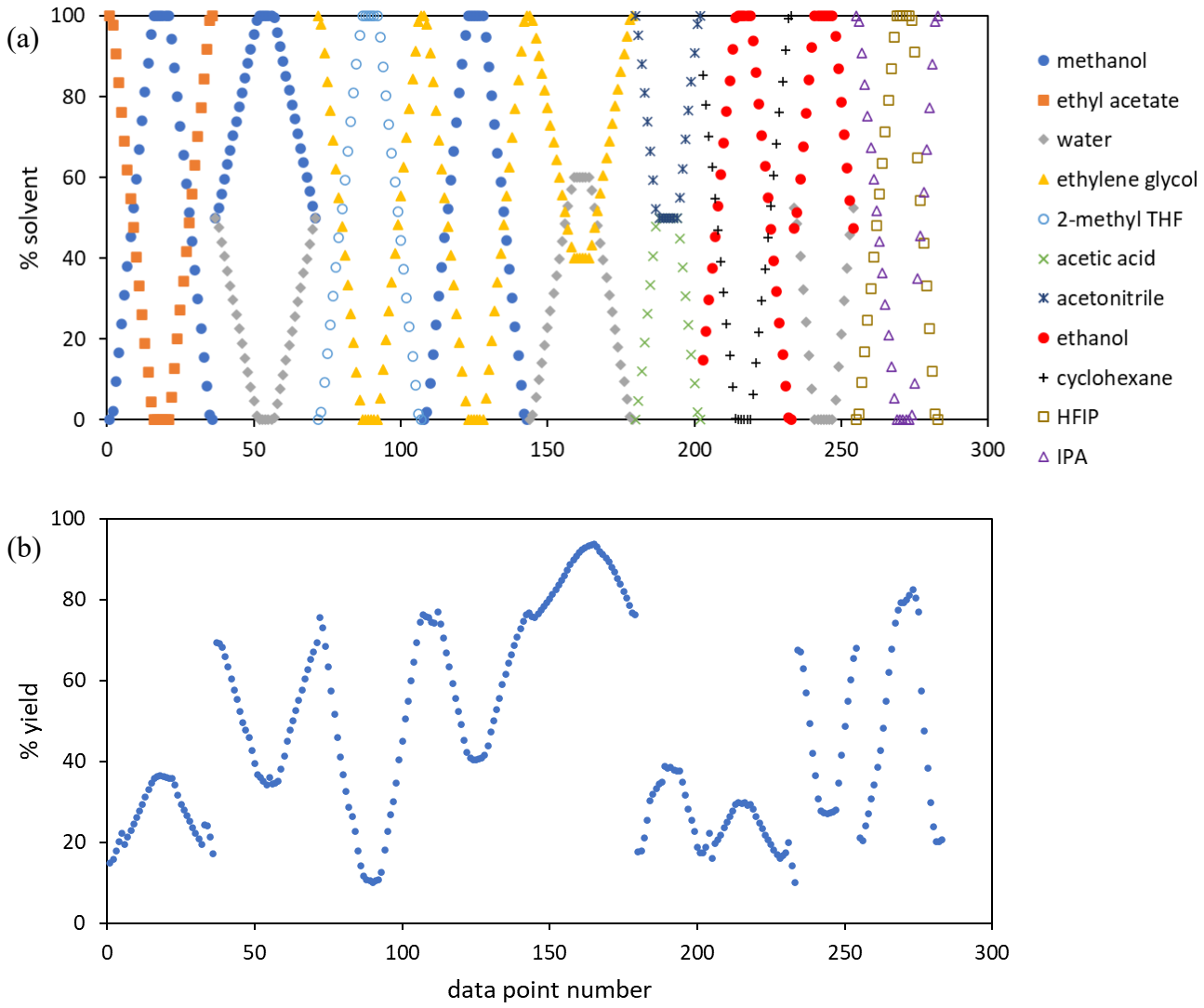


Figure 4.28. (a) a repeat of Fig. 4.20 for cross comparison; (b) all the solvent ramp yield data labelled by data point numbers.

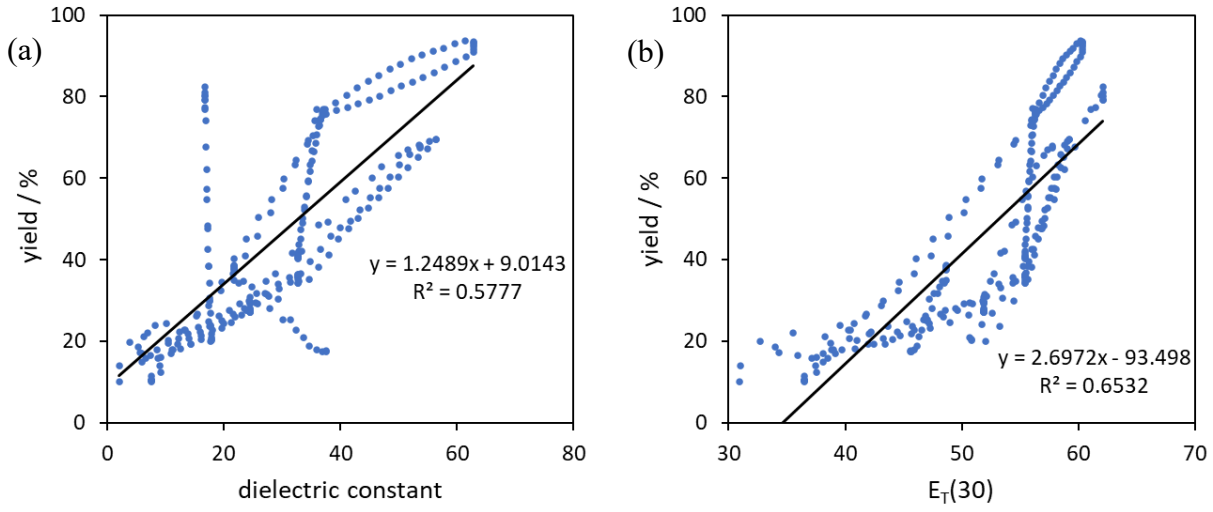


Figure 4.29. Linear correlation plots for reaction yield data collected across all solvent ramps described as correlated against: (a) dielectric constant; and (b) empirically derived Reichardt polarity metric $E_T(30)$.

For further analysis, more physical, theoretical, and empirical solvent properties can be selected from the literature, such as those accrued in Table 4.8, the meanings of which are explained and compared by Spange *et al.*.[151] Additional solvent descriptors could be generated computationally through Density Functional Theory (DFT) modelling or other computational methods such as the Python package RDKit.[156] Once the solvent descriptors are collected, a machine learning method, such as a ridge regressor or random forest regressor may be applied to discern which solvent properties are important, and to generate a predictive model for the solvent effect on this reaction.

Table 4.8. Solvents selected for solvent ramping experiments for the reaction of **4.1d** with attributed solvent properties compared in previous work by Spange *et al.*.[151] Red values are those not available in this data set, for which the value is taken from that for THF instead of 2-methyl THF. For a full description of the descriptor meanings see the original paper.[151]

Solvent	ε	α	β	π*	SA	SB	SP	SdP	N	n	f(n)	δ
cyclohexane	2.02	0	0	0	0	0.073	0.683	0	0.0093	1.426	0.2562	16.8
ethyl acetate	6.02	0	0.45	0.55	0	0.542	0.656	0.603	0.0102	1.372	0.2272	18.4
acetic acid	6.15	1.12	0.45	0.64	689	0.39	0.651	0.676	0.0175	1.369	0.2256	18.9
2-Me THF	7.58	0	0.45	0.58	0	0.584	0.7	0.768	0.0099	1.406	0.2456	19
HFIP	16.7	1.96	0	0.65	1.011	0.014	0.499	1.454	0.0095	1.275	0.1725	19.3
IPA	17.9	0.84	0.9	0.52	0.367	0.782	0.658	0.748	0.0133	1.384	0.2338	24.4
ethanol	24.5	0.86	0.75	0.54	0.4	0.658	0.633	0.783	0.0172	1.359	0.2202	26
methanol	32.7	0.98	0.66	0.6	0.605	0.545	0.608	0.904	0.0247	1.329	0.2065	29.3
ethylene glycol	37	0.9	0.52	0.92	0.717	0.534	0.777	0.91	0.0179	1.4318	0.2593	29.9
acetonitrile	37.5	0.19	0.4	0.75	0.044	0.286	0.645	0.974	0.019	1.344	0.2118	24.2
water	80.1	1.17	0.47	1.09	1.062	0.025	0.681	0.997	0.0554	1.333	0.2057	47.9

6.5 Ethanol-water ramp and deuterated ramp

A qualitative analysis of the solvent ramping data obtained suggested that the protic nature of solvents played an important role, which is separate to the higher polarity associated with these solvents; with alcohols and polyols generally affording high reaction yields. To investigate this effect further, an ethanol-D_2O ramp was implemented, the result of which could be compared to that obtained from ethanol-H_2O ramps. It was expected that a change from normal water to heavy water could lead to an observable kinetic isotope effect,[157,158] as it has previously been shown that D_2O has a ~4% shorter

hydrogen bond length than that of H_2O.[159] However, at 200 °C, the ramp containing D_2O overlapped very well with the H_2O ramp (Fig. 4.30), demonstrating the solvent effect was not dependent on the isotopic makeup of the water. Potentially to observe a change in hydrogen bonding characteristics, the ethanol in the ethanol-D_2O ramp must also be exchanged or d_6-ethanol, as proton-deuterium exchange could be occurring in the solvent mixture, however it could also be that simply other properties of these solvents produce the effect on reaction yield observed.

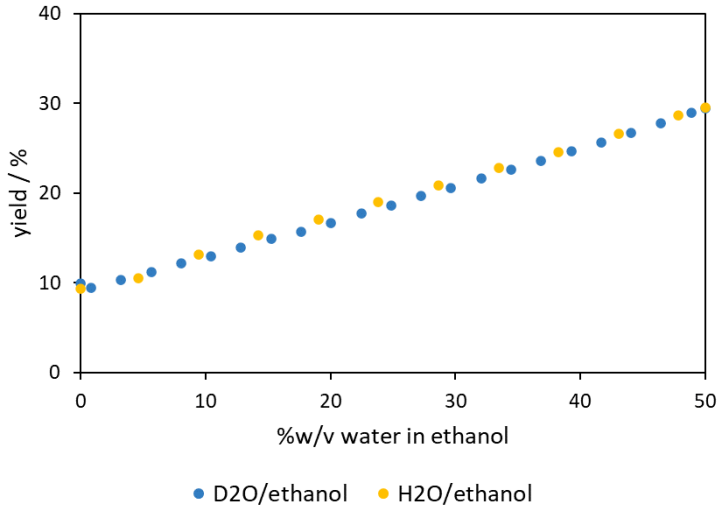


Figure 4.30. Solvent ramping experiment results between ethanol and 50%w/v water in ethanol performed at 200 °C and a cumulative flow rate of 0.2 mL min^{-1} for the reaction of **4.1d** to **4.2d** utilising: (a) light water (H_2O); and (b) heavy water (D_2O).

A preliminary examination of the variation in activation energy of the reaction with varying water-ethanol mixtures was performed utilising an ethanol-water solvent ramp at 200 °C (Fig. 4.30) and another at 220 °C (Fig. 4.22). A polynomial regression was used to fit ln(k) values for the solvent ramp data at each temperature, with fitting value R^2>0.99. These polynomial models were then used to produce ln(k) values for each temperature at 0, 10, 20, 30, 40, and 50 %w/v water in ethanol, which afforded approximate activation energies (E_a), entropy of activation ($\Delta S^{\ddagger}$), and enthalpy of activation ($\Delta H^{\ddagger}$) from low density Arrhenius and Eyring plots. These values can then be plotted against the %w/v water in ethanol to reveal polynomial dependencies on varying solvent makeup (Fig. 4.31). The results demonstrate a quadratic reduction in activation energy from 117.6 to 113.4 kJ mol^{-1} over the analysed

period (Fig. 4.31a), mirrored by the change in enthalpy of activation ($\Delta H^{\ddagger}$, black dots, Fig. 4.31b) from 113.6 to 109.4 kJ mol^{-1}. Interestingly, a more parabolic trend was observed for entropy of activation ($\Delta S^{\ddagger}$, red dots, Fig. 4.31b) between -53 – -48 J mol^{-1} K^{-1}, plausibly due to different solvent cage structures becoming dominant at different solvent makeups.

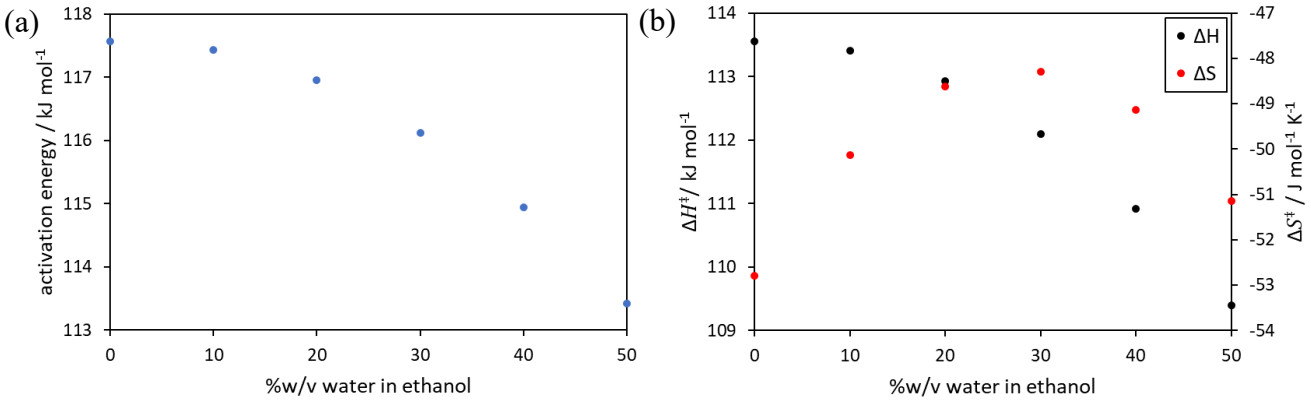


Figure 4.31. Data produced from ethanol-water solvent ramps performed at 200 and 220 °C and a cumulative flow rate of 0.2 mL min^{-1} for the reaction of **4.1d** to **4.2d** plotted as: (a) calculated activation energies (E_a) taken from Arrhenius plots; and (b) calculated enthalpy and entropy of activation taken from Eyring plots.

6.6 'One-pot' solvent ramp

The solvent ramping method can be combined with the 'one-pot' method described earlier in the chapter, demonstrating the continuous screening of two traditionally discrete, categorical parameters simultaneously (Fig. 4.32a). These data were collected from a solvent ramp between allylarylethers **4.1a-f** in ethanol and a solution of water containing no starting materials. The ramp was performed between 0 – 90 %w/v water in ethanol; it is worth noting that in this case, the change in solvent composition corresponds to a ten-fold dilution of the reactant concentrations. To confirm the insensitivity of the reaction system to this ten-fold dilution, a further solvent ramp was performed between ethanol and a 50%w/v water in ethanol solution, both containing allyl ethers **4.1a-f** (Fig. 4.32b). These reaction data from the different methods align well. This shows that the reaction is not only insensitive to dilution at these low concentrations, but also that the change in volume on solvent mixing

has a minimal effect under these conditions.

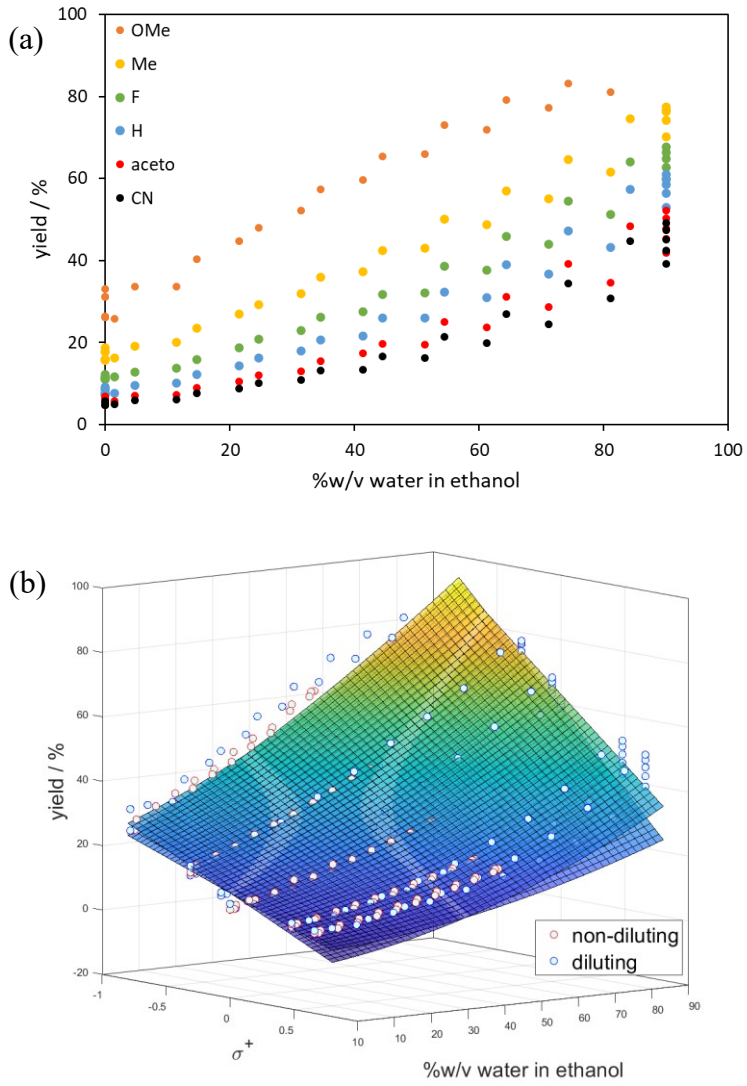


Figure 4.32. 'One-pot' solvent ramping experiment results for the reaction of allyl ethers **4.1a-f** to phenols **4.2a-f** performed at 200 °C and a cumulative flow rate of 0.2 mL min^{-1} for: (a) solvent ramp between **4.1a-f** dissolved in ethanol and a pure water solution; and (b) the former ramp and a solvent ramp between **4.1a-f** dissolved in both ethanol and a 50%w/v water in ethanol solution.

Reaction data collected by these 'one-pot' solvent ramping experiments can be used to assess the solvent dependency on the effect of substituent on the reaction, as shown earlier in the temperature ramping study (Fig. 4.14). A surface plot of the solvent effect on Hammett plots can be produced (Fig. 4.33a), however the change in Hammett plot gradient (ρ) with varying solvent ratio is more easily visualised on a simple two dimensional plot at three solvent ratios of an ethanol-water mixture (Fig. 4.33b). These data demonstrate a decreasing gradient (ρ) on increasing the percentage of water in ethanol for the

reactions. This effect, between ρ = -0.58 in ethanol to ρ = -0.46 in 80%w/v water in ethanol, is a stronger change in the effect of substituent than that seen over the temperature range monitored previously (-0.57 to -0.54).

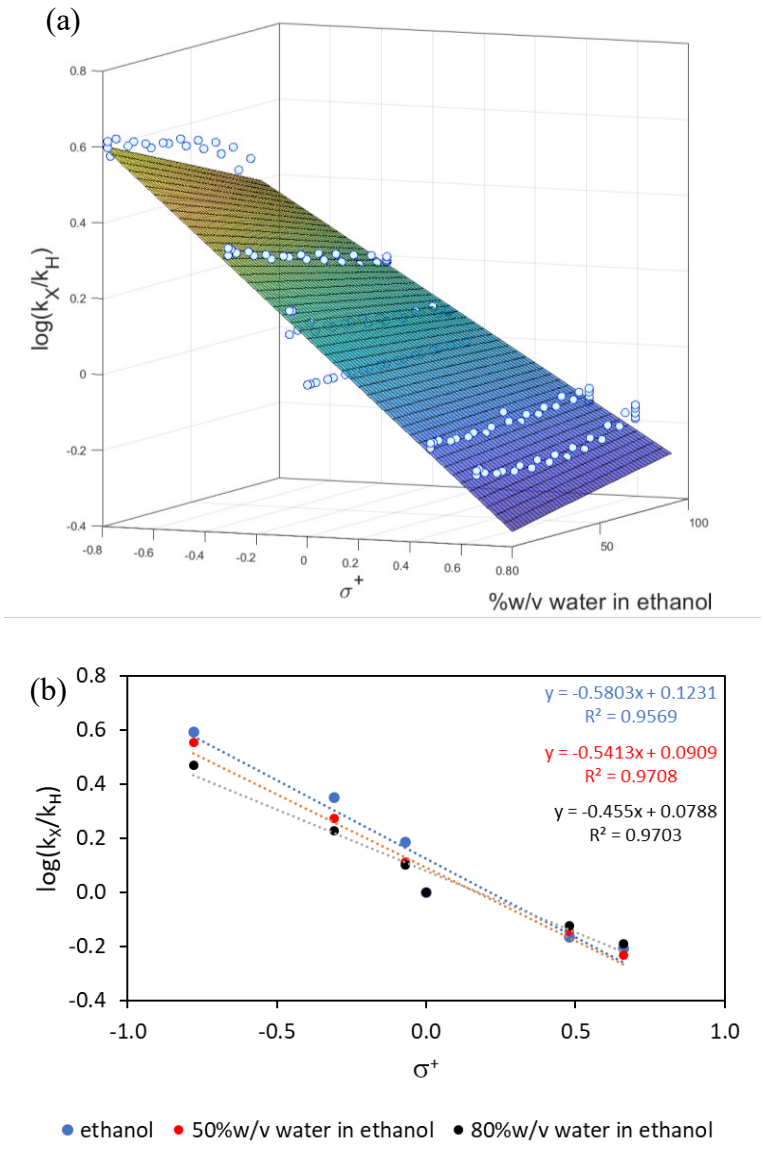


Figure 4.33. Hammett plot visualisations of 'One-pot' solvent ramping experiment results for the reaction of allyl ethers **4.1a-f** to phenols **4.2a-f** performed at 200 °C and a cumulative flow rate of 0.2 mL min^{-1} between **4.1a-f** dissolved in ethanol and a pure water solution as: (a) as surface plot; and (b) three selected solvent ratio Hammett plots.

7 Conclusions

The effects of traditionally discrete reaction parameters, such as the substituent on the reactant and the reaction solvent, were quantitatively investigated *via* novel methods incorporating transient flow to increase the efficiency of collecting reaction data. In this Chapter, the aromatic Claisen rearrangement proved a good test reaction on which to develop these methods.

The substituent effects were investigated by a 'one-pot' methodology in combination with transient flow methods for screening continuous reaction parameters (reaction time and temperature) to produce kinetic data. In just six hours, reaction data were collected for six aromatic Claisen rearrangement reactions over an 80 °C temperature range, affording accurate and efficient assessment of the effect on reaction rates of these parameters. This data facilitated the calculation of challenging fundamental kinetic parameters and the construction of a multivariate polynomial model for prediction of reaction rate constants for different reactants, based on their σ^+ parameter, under different temperatures, thus assessing synthetic feasibility of implementing this rearrangement. σ^+ values are widely available[146] or calculable[160] and thus this should prove a valuable tool to those assessing whether to include this reaction in a synthetic route. These 'one-pot' transient temperature ramps were performed over the supercritical point for ethanol, after which different solvent properties should affect the reaction; minimal change was observed over this point from data rich experimentation, calling into question any significant solvent polarity effect on the reaction.

A novel method was also developed to investigate solvent effects through transient flow methodology. The aromatic Claisen rearrangement has been widely reported to experience solvent effects based on solvent polarity, but little empirical evidence has been collected to investigate these effects. In this study, a solvent ramping method was applied to the aromatic Claisen rearrangement reaction of allylphenylether in a range of 11 solvents, which were combined in different pairings to gather continuous solvent effect data across a broad solvent space. This data demonstrated that the solvent

effect on this reaction is not solely polarity based, and that the protic nature of the solvent is likely to be a major contributing factor, concordant with the results seen over the supercritical limit of ethanol. Such hypothesis could be robustly tested utilising reaction data from more than 250 solvent mixtures, as well as potential use benchmarking commercial solvent modelling software such as COSMO-RS. This approach was also demonstrated in combination with the 'one-pot' method, analysing the effects of both substituent and solvent choice on the reaction simultaneously.

The methods described in this Chapter have been demonstrated for a unimolecular reaction, however extension to more complex reactions is likely also possible. The 'one-pot' method has been demonstrated in batch reactors on bimolecular reactions as competition experiments,[128,132,134–136] which would be simple to analyse utilising this flow method with minimal modification, limited only by analytical capabilities.[17,29,129,134] The solvent ramping method would require simply the use of more reactor inlet streams in order to investigate solvent effects on more complex bimolecular systems, and the use of an in-line dilution system prior to on-line HPLC analysis for UV absorbing solvents. This method would also greatly benefit from the use of a model-based design of experiments[161] framework for choosing which solvent ramps to perform and more quantitative, likely machine learning-based analysis of results in order to most efficiently utilise the data obtained.

Chapter 5: Conclusions and future work

Within this thesis, a variety of transient flow methods have been applied and developed. This work began with an explanation of transient flow as a reaction data collection technique and a comprehensive review of the literature in this field. Transient flow is found to be a varied innovative research area developing into a tool with a broad use for investigating chemical reactions, although yet to see widespread use.

A few key questions left unanswered by the literature thus far were targeted:

(i) What is the easiest method for collecting time series data in flow, without compromising accuracy?

(ii) Can the continuous reaction parameter space that can be investigated by transient flow methods be extended to provide efficient investigation of a more diverse reaction space? How can this data be best used?

(iii) How can we extend the benefits of transient flow to investigate traditionally discrete reaction parameters?

The first question was born out of the range of non-standardised methods used to collect residence time series data by transient flow in the literature. Residence time transient flow is the most common implementation of transient flow, however, the complexity and breadth of different methods can be off-putting to those first attempting to use these techniques.

In Chapter 2, three reactions of increasing complexity are investigated in two flow systems with different analytical techniques to provide a more comprehensive comparison between the easiest to implement residence time transient flow methods: RPO step, PO step, RPO linear flow rate ramp, and PO linear flow rate ramp. This work demonstrated the utility of RPO step changes as an easy, efficient, and accurate method which is quite general. However, if the analytical tool sample frequency is slow, or a particular range of short residence times is to be investigated, flow rate ramps may still be the best method to use.

In Chapter 3, the Knorr pyrazole synthesis was utilised as a model reaction in developing novel transient flow methods for investigating the continuous reaction parameter reactant stoichiometry. This new method revealed that this reaction – previously thought to have simple two-step kinetics – was more complex than first thought. A variety of transient flow methods were utilised to investigate the reaction kinetics including RPO step changes, reaction-stoichiometry ramps, additive concentration ramps, and multi-variate residence time-reactant stoichiometry ramps. The data collected by these methods allowed construction of a robust microkinetic model that accurately describing the reaction kinetics, including novel insights into product autocatalysis and the identification of an unexpected di-addition intermediate. Comparison of this fitted model for two differently substituted diketone reactants generated new insights into how the regioisomeric product ratio of an unsymmetric diketone reactant can be changed solely varying the reactant stoichiometry. This work has been published[97] and attracted interest from multiple computational groups due to the breadth and quality of the reaction data collected and the detail of the microkinetic model constructed. The results of these collaborations will be published in due course and demonstrate the impact of combining efficient data collection methods with computational methods.

Traditionally discrete reaction parameters have proven challenging to investigate in a data rich manner, especially when investigation of continuous reaction parameters is also desired. In Chapter 4, the aromatic Claisen rearrangement was chosen as an exemplar for the development of methods for investigating effects of *para*-substituents and solvents, because this reaction is known to be affected by these parameters. Substituent effect on the aromatic Claisen rearrangement reaction was investigated utilising a novel 'one-pot' transient flow method, by which six reactions were performed simultaneously over a transient temperature ramp analysed by on-line HPLC. This method efficiently produced reaction data on a discrete (substituent) and a continuous (temperature) reaction parameter simultaneously. The reaction data produced novel insights into the fundamental thermodynamic constants for the reaction series and allowed construction of a multivariate model to predict rate constants for any temperature or

substituent within the range investigated. This work was published[162] and has inspired further work within the group. Future work on 'one-pot' transient flow method development should focus on extending this method to more complex systems, including bimolecular competition reactions and heterogeneously catalysed reactions. Preliminary investigation of a multistep pericyclic reaction has started, with the vision of extracting kinetic constants out of multiple reaction steps in one temperature ramping experiment. This work was not described in this thesis, due to challenges in isolating intermediate products for quantification purposes, however this will be a valuable area for future investigation to continue, especially if extended to telescoped multistep reactions. The modification of the flow system to incorporate an evaporative light scattering detector (ELSD) to the on-line HPLC system would greatly facilitate study of such reactions through collection of quantitative concentration data without isolation and calibration of reaction species.

Solvent effects on the aromatic Claisen rearrangement have previously been described both in experimental and computational work, but a detailed empirical study has not been performed. This is a symptom of a wider challenge: solvent is a challenging parameter to investigate, often studied laboriously as a discrete variable. A novel solvent ramping method was developed at the end of Chapter 4. This is the subject of a patent,[163] and will likely form the core of a subsequent paper. Utilising this method solvent, a traditionally discrete reaction parameter, can be treated as a collection of continuous variables by ramping through different solvent mixtures with varying properties. This method was applied to the aromatic Claisen rearrangement reaction in 11 solvents, producing reaction data at over 250 different solvent conditions. This approach was also combined with the 'one-pot' method to investigate how such solvent effects might vary depending on reactant substituent.

To further develop the solvent ramping technique, future work should focus on three areas for maximum impact: (i) solvent parameterisation for machine learning based data analysis; (ii) extension to more complex chemical reactions and other chemical processes; and (iii) efficient reaction planning and

further automation. The first of these areas will allow the data collected to be best used to understand and predict solvent effects, and this could allow ‘greener’ solvent mixtures to replace unsustainable or undesirable solvents, such as NMP. The second area will demonstrate to the chemical sciences community the general utility of this method for different chemistries (bi-molecular reactions, heterogeneous reactions), investigation of more complex reaction outcomes such as solvent effects on selectivity, and extension to other unit operations such as extractions where this method will add value. This area will require physical modifications to be made to the flow system, such as increasing the number of input pumps, changing the type of reactor in the system, and utilising other analytical tools when necessary. The final area applies to all work conducted in this thesis. Further automation and efficient reaction planning will become essential as reaction data collection workflows are applied to a broader chemical space. This area will require the flow system to be better connected than it currently is, requiring some modules to be upgraded to facilitate communication and control. A robust control software will also need to be implemented or developed, allowing integration of model-based design of experiments and optimization algorithms. The more efficient planning of which experiments to perform combined with efficient data collection techniques, complimented by machine learning for the best use of the reaction data collected will transform synthetic chemistry into a predictable, data-driven science.

Chapter 6: Experimental

1 Introduction

This Chapter covers all experiments discussed throughout this thesis. These are arranged following the order in which the results are presented in the previous chapters, and cross referenced to the figure or section in which they were discussed. It is worth noting that although it may appear from reading this thesis that every experiment was successful, only approximately 10% of experiments performed during the course of the PhD research have been of sufficient quality and interest to be included in this thesis, with many other experiments failing in some manner or needing to be repeated.

All raw data and code for this thesis can be accessed on request at https://github.com/LindenSchrecker and found on the Imperial Data Repository DOI: 10.14469/hpc/13848.

2 Comparison of time series data collection in continuous flow

2.1 Flow system configuration 1

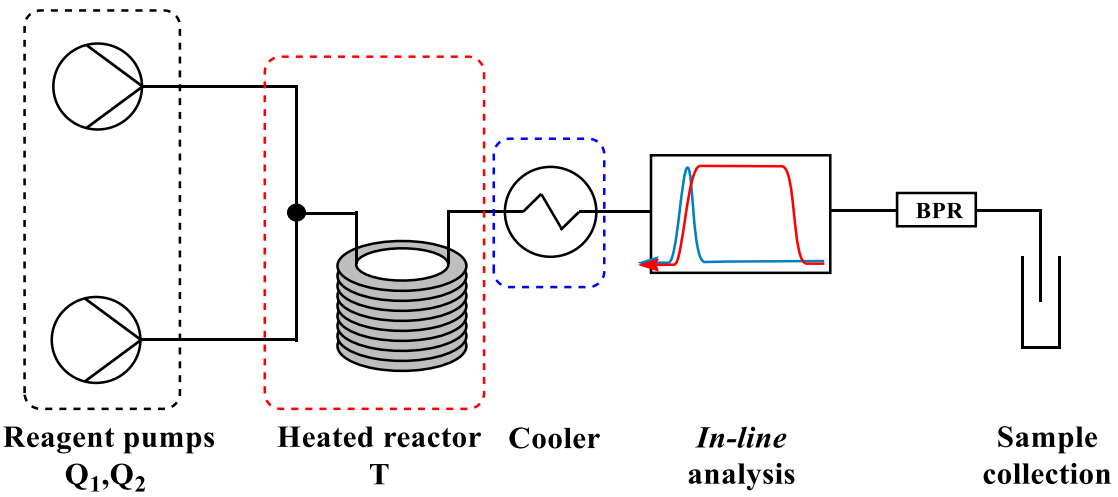


Figure 2.4. Schematic of the flow system for the control of individual flow rate (Q_1 and Q_2) and temperature (T), with in-line analytics.

2.1.1 Flow system overview

A flow system (Fig. 2.4) was constructed, prioritising the accurate control of parameters needed for transient flow methodology to be developed. The system consisted of reactant and solvent solutions

delivered from Duran bottles fitted with inlet tubing with in-line filters. The inlet tubing lines (1/8" OD, 2 mm ID PTFE, 1.6 mL and 1.2 mL respectively) were connected to two Gilson 305 HPLC pumps. The outlets of these pumps were connected to two 1 m lengths of stainless steel tubing ('SS1', 1/16" OD, 1mm ID) which fed into a Valco T-piece stainless steel mixer.

The mixer, including 0.38 m of each attached inlet line, is submerged in an oil bath, which is heated and stirred by a stirrer hotplate. The outlet of the mixer is connected to a 5.10 m tubular reactor constructed from SS1 tubing (4.13 mL internal volume), which is also submerged in the oil bath. A stainless steel HPLC style union was attached to the reactor outlet, just above the oil bath's surface, through an insulating PTFE sheet above the oil bath to a length of SS1 tubing (14 cm) which passes through a custom built cooling system consisting of an aluminium block mounted on a Peltier assembly.

The tubing is connected to the bottom fitting of the ReactIR flow cell (10 μL) and then a 10 cm length of 1 mm ID PTFE tubing connects the outlet of the flow cell to an Upchurch Scientific 250 psi BPR set at 8.1 bar. This is connected at the outlet to a further 15 cm length of 1 mm ID PTFE tubing, which can pass into a waste container or into a vial for collection.

2.1.2 Pumps

The pumps used are two Gilson 305 HPLC pumps, fitted with a 10 mL WSC and a 10 mL SC pump heads, respectively. These are connected by a GSIOC cable so that the pumps can control each other as a master/slave system through in-built Gilson firmware. In order to maintain the pumps in working order and confirm their accuracy, the check valves are cleaned and sonicated in methanol regularly, and the cumulative flow rate of the system is confirmed at different flow rates and at different times during experimentation.

2.1.3 Tubing and fittings

The pump inlet tubing is 1/8” OD, 2 mm ID PTFE tubing with a volume of 1.6 mL and 1.2 mL for pumps A and B respectively. The stainless steel tubing (‘SS1’) in the system is 1 mm ID, 1/16” OD from Thames Restek UK Ltd. and the T-piece is a VALCO T-piece mixer. The outlet of the back pressure regulator is connected to 1/16” OD, 1 mm ID PTFE tubing.

The fittings to the IR flow cell and connecting the BPR are ¼-28 flat-bottom flangeless ferrules. The inlet and outlet fittings to the Gilson pumps are standard Gilson 30X fittings. All other fittings are HPLC style fittings.

2.1.4 Heating and cooling

Heating is performed by an IKA Plate (RCT digital) stirrer hotplate with a silicon oil bath containing a magnetic stirrer bar and with a thermocouple attached for PID feedback control. Cooling is performed by a 60 W Peltier thermo-electric cooler module and heatsink assembly, procured from PiHut, with a custom cooling block milled to fit 1/16” tubing by the Advanced HackSpace, Imperial College London.

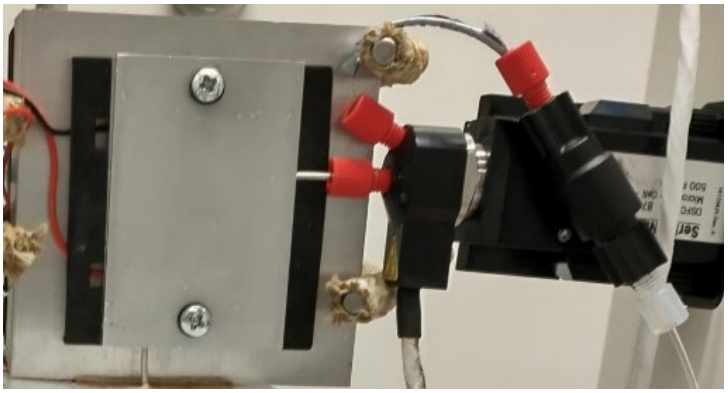


Figure 2.5: The cooling system used in the flow system consisting of a 60 W Peltier assembly connected to a custom aluminium block containing a cutting which fits to 1/16” stainless steel tubing. Insulation is used to cover the outside of the Peltier cooling side in order to improve the efficiency of the device by preventing direct heat transfer back across the heat junction.

2.1.5 *In-line* FTIR

The in-line IR spectroscopic data was collected using a Mettler Toledo ReactIR 15, equipped with a 10 μL DS Micro Flow Cell with a DComp (Diamond) probe tip. The spectrometer was set to collect spectra between 3000 cm^{-1} and 650 cm^{-1} using a resolution setting of 8 and a gain setting of 1x. A 15 second scan rate was employed in order to obtain good time resolution whilst maintain good signal to noise. Diagnostic peaks were identified for pyrazole **2.5/3.4a** and **3.4b** based on previous batch work and corroborated by individual injections and mixed injections of the reaction components, and by off-line HPLC. The optimal peaks were found in the 2nd derivative of the collected IR spectra as the height to a two point baseline. For **2.5/3.4a**: between 1508-1496 cm^{-1} to a two point baseline at 1514 and 1495 cm^{-1}; for **3.4b**: between 1508-1502 cm^{-1} to a two point baseline 1516-1495 cm^{-1}. These peaks were picked to allow maximum sensitivity for concentration of the pyrazole product whilst being independent of effects from other peaks corresponding to the reactants.

As described in Chapter 2, calibration of the relevant peaks was performed at the start of each experimental run by injection of known concentration samples ranging in concentration from 0.236 – 0.028 M (prepared in volumetric flasks via serial dilution of three independent stock solutions) into the IR flow cell with at least four point calibration for each experimental run**.**

2.1.6 System pressure

The back pressure regulator used was an Upchurch Scientific 250 psi BPR adjusted to 8.1 bar as measured for ethanol on the Vapourtec R series system. This is adequate pressure to keep all solvents used in this work in solution phase for the temperatures used.

2.2 Flow system configuration 2

2.2.1 Flow system overview

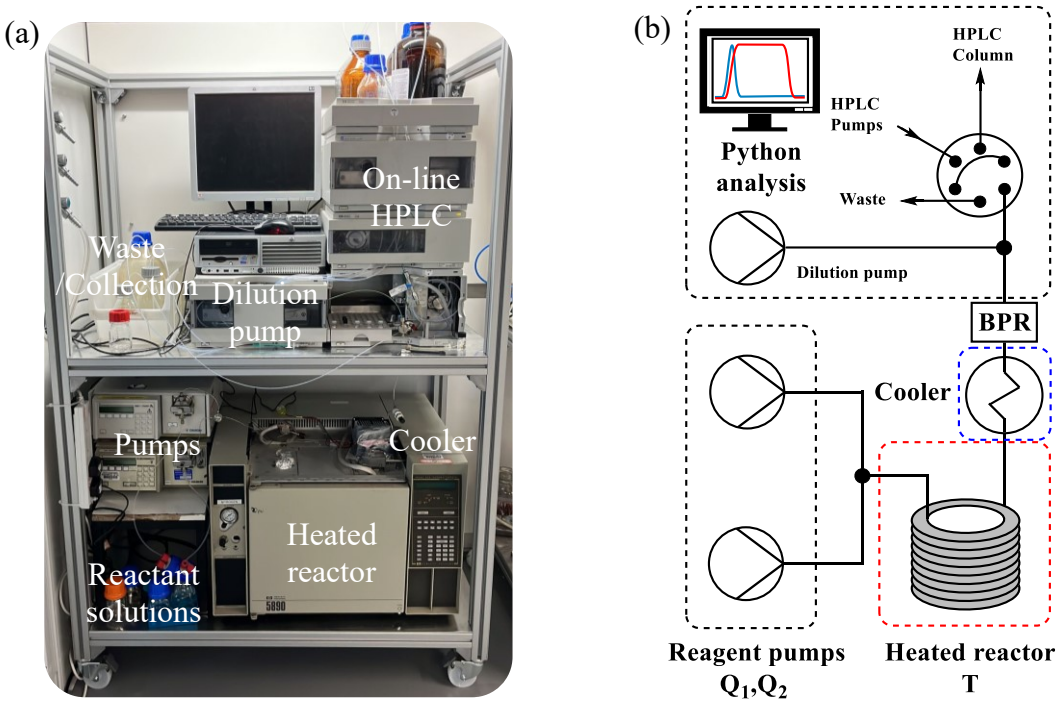


Figure 2.10. (a) the on-line HPLC flow system constructed (configuration 2); (b) a schematic representation of the fluidic path and key components of the on-line HPLC flow system.

This flow system is a modification of configuration 1, as such the following description focuses on the modifications made from configuration 1 and is not meant as a comprehensive description of the flow system.

Configuration 2 flow system (Fig. 2.10) was constructed in which reagent(s) and solvent(s) as solutions are delivered from Duran bottles fitted with inlet tubing with in-line filters. The inlet tubing lines (1/8" OD, 2 mm ID PTFE, 1.6 mL and 1.2 mL respectively) were connected to a Gilson 305 HPLC pump (pump A) and a Gilson 307 HPLC pump (pump B) respectively. The outlets of these pumps were connected to two stainless steel tubing (25 cm) which fed into a Valco T-piece stainless steel mixer.

The outlet of the mixer is connected to a 5.14 m length of stainless steel tubing ('SS1', 1 mm ID, 1/16" OD); the first 30 cm of which are outside of the GC oven (heated reactor length: 4.84 m, heated reactor volume: 3.92 mL). This is then connected by a stainless steel HPLC style union at the outlet of the GC

oven through an insulating PTFE sheet to a length of SS1 tubing (14 cm) which passes through a custom built cooling system consisting of an aluminium block and a Peltier assembly. The outlet of the cooling device is connected by a stainless steel HPLC style union to a 20 cm length of SS1 tubing into a VALCO variable pressure Back Pressure Regulator (BPR). The BPR outlet is connected to a 25 cm length of stainless steel tubing which connects to a VALCO T-piece stainless steel mixer. The other mixer fittings are connected to the inlet to the modified HPLC 6-port, 2-way injector valve and to the dilution pump of the HPLC setup.

2.2.2 Heating and cooling

Heating of the reactor is achieved by repurposing an HP 5890 Series II GC oven, using the inbuilt software/PID to allow accurate control over temperature ramping. Cooling is performed by a 60 W Peltier thermo-electric cooler module and heatsink assembly (PiHut) with a custom cooling block milled to fit 1/16" tubing by the Advanced HackSpace, Imperial College London.

2.2.3 On-line HPLC

On-line analysis was implemented by modifying the injector on an Agilent HP 1100 series HPLC. The fittings to the 6-port, 2-way injector valve were disconnected and reconnected as shown in the scheme above to allow a 0.6 μL sample loop to be continually filled from the reactor effluent in the resting valve position. When triggered by the Chemstation HPLC software the injector method switches the valve to its second position for 0.1 min, allowing the contents of the sample loop to be redirected by solvent from the Agilent HP 1100 series pumps into the column and subsequent detector.

2.2.4 On-line HPLC method for aromatic Claisen rearrangement of **2.6/4.1a**

The HPLC column used was a Restek Raptor C18 (2.7μm 50 mm x 2.1 mm) running an isocratic mixture of 40% acetonitrile in water. This method allowed injections every 4 minutes.

Table 6.1. Key parameters set for the HPLC method used in this example for on-line HPLC analysis.

Flow rate / mL min^{-1}	0.7
Stoptime / min	3.70
Posttime / min	0.29
Solvent A	H_2O
Solvent B	MeCN
DAD wavelength / nm	210

The Agilent 1100 Autosampler 1 automatically switches the valve at the beginning of the injector program. The inputted injector cycle is a "WAIT" command for 0.10 min and then a "VALVE MAINPASS" command.

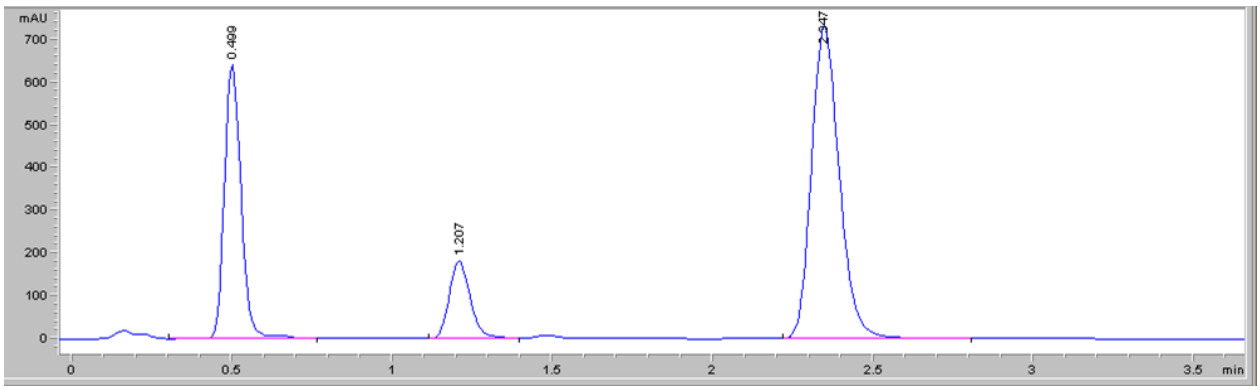


Figure 6.1. an example chromatogram obtained according to the HPLC method above for monitoring the reaction of *para*-methoxyphenyl allyl ether (**2.6/4.1a**).

Table 6.2. Substituents for *para*-methoxyphenyl allyl ether substrates and their corresponding retention times in the HPLC method in Figure 6.1.

compound	Retention time / min
2.6/4.1a	1.21
2.7/4.2a	0.49
ethyl benzene	2.34

These data were concatenated by a python script which was developed. This script can be found at https://github.com/LindenSchrecker.

2.3 Standard transient residence time experiments

2.3.1 Reverse Push Out step change (RPO step)

A standard RPO step is performed by programming the pumps to begin at 5 mL min^{-1} at a given %B ratio (flow rate ratio of pumps 1 and 2) for 3 minutes at which time the cumulative flow rate changes to 0.2 mL min^{-1} for a further 21 minutes. This can be directly linked to other transient flow rate experiments. Once all experiments in an experimental run are finished, the system is flushed with ethanol through both pumps for at least 10 reactor volumes.

Table 6.3. Pump flow rate method utilised for a standard RPO step change.

time / min	flow rate / mL min^{-1}
0	5
2.99	5
3	0.2
24.99	0.2

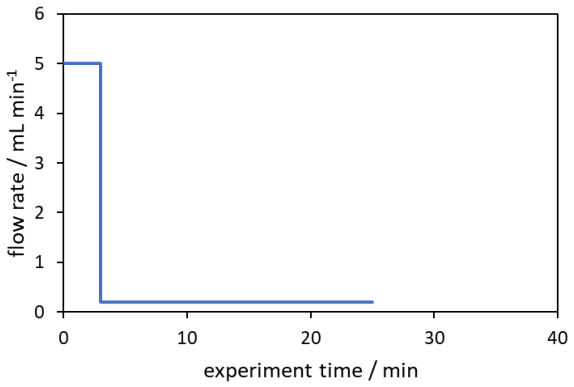


Figure 6.2. Cumulative volumetric flow rate method for a standard RPO step experiment.

2.3.2 Push Out step change (PO step)

A standard PO step is performed by programming the pumps to begin at 0.2 mL min^{-1} at a given %B ratio (flow rate ratio of pumps 1 and 2) for 22 minutes at which time the cumulative flow rate changes to 5 mL min^{-1} for a further 5 minutes.

Table 6.4. Pump flow rate method utilised for a standard PO step change.

time / min	flow rate / mL min^{-1}
0	0.2
21.99	0.2
22	5
25	5

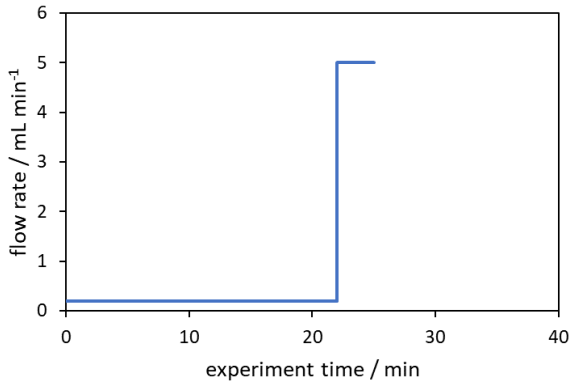


Figure 6.3. Cumulative volumetric flow rate method for a standard PO step experiment.

2.3.3 Linear Reverse Push Out flow rate ramp (RPO ramp)

A standard RPO ramp is performed by programming the pumps to begin at 5 mL min^{-1} at a given %B ratio (flow rate ratio of pumps 1 and 2) for 3 minutes before ramping the flow rate linearly over 10 minutes to 0.2 mL min^{-1} which was then maintained for a further 22 minutes.

Table 6.5. Pump flow rate method utilised for a standard RPO ramp.

time / min	flow rate / mL min^{-1}
0	5
3	5
13	0.2
35	0.2

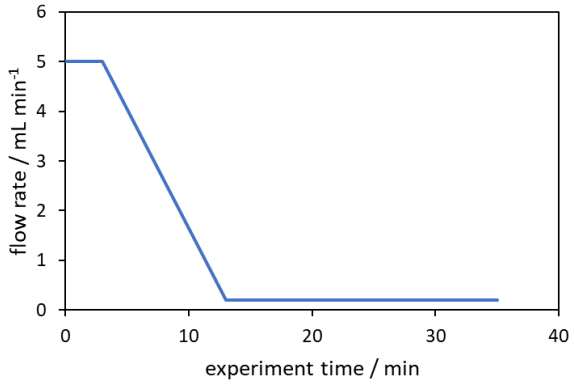


Figure 6.4. Cumulative volumetric flow rate method for a standard transient RPO ramp experiment.

2.3.4 Linear Push Out flow rate ramp (PO ramp)

A standard PO ramp is performed by programming the pumps to begin at 0.2 mL min^{-1} at a given %B ratio (flow rate ratio of pumps 1 and 2) for 22 minutes before ramping the flow rate linearly over 10 minutes to 5 mL min^{-1} which was then maintained for a further 3 minutes.

Table 6.6. Pump flow rate method utilised for a standard PO ramp.

time / min	flow rate / mL min^{-1}
0	0.2
22	0.2
32	5
35	5

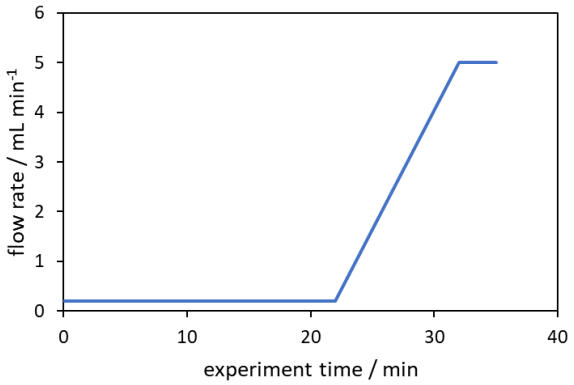


Figure 6.5. Cumulative volumetric flow rate method for a standard PO ramp experiment.

2.4 Compound synthesises and characterisation

In Chapter 2, all materials were purchased from commercial sources and used as received. Products of the reactions were synthesised for analytical method development and calibration as described in Sections 3 and 4 of this chapter.

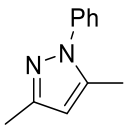
3 Discovery of an unexpectedly complex mechanism for the Knorr pyrazole synthesis

3.1 General compound synthesis and characterisation

Unless otherwise stated, materials were purchased from commercial sources and used as received without further purification. Automated flash column chromatography was performed using a Teledyne ISCO CombiFlash NextGen 100 system using pre-packed silica columns with a gradient of petroleum ethers/ethyl acetate.

^{1}H and ^{13}C NMR spectra were recorded on Bruker AVANCE III HD spectrometers (400 MHz and 500 MHz for ^{1}H NMR; 101 MHz and 126 MHz for ^{13}C NMR). ^{1}H NMR chemical shifts (δ_H) and ^{13}C NMR chemical shifts (δ_C) are quoted in parts per million (ppm) downfield of tetramethylsilane (TMS) and reported relative to residual solvent peaks ($CDCl_3$: δ_H = 7.26 ppm and δ_C = 77.16 ppm; CD_3OD: δ_H = 3.31 ppm and δ_C = 49.00 ppm).

3.1.1 3,5-dimethyl-1-phenyl-*1H*-pyrazole (**2.5/3.4a**)



2.5/3.4a

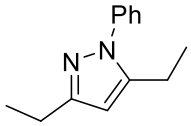
Acetyl acetone (0.102 g, 1 mmol) and ethanol (5 mL) were added to a 25 mL round bottomed flask containing a stirrer bar with a temperature probe and reflux condenser attached. Phenyl hydrazine (0.109 g, 1 mmol) was added to the reactor and the reaction was heated to 70 °C. After five hours the solvent was evaporated *in vacuo* to afford the *title compound* as an orange oil (0.140 g, 0.813 mmol, 81%).

^{1}H NMR (400 MHz, $CDCl_3$) δ 7.45–7.24 (5 H, m), 5.94 (1 H, s), 2.25 (3 H, s), 2.23 (3 H, d, J = 0.8 Hz).

^{13}C NMR (101 MHz, $CDCl_3$) δ 148.88q, 139.87q, 139.35q, 128.95, 127.19, 124.70, 106.90, 13.47, 12.32. These data are consistent with the reported literature values for NMR shifts.[164]

^{1}H NMR (400 MHz, CD_3OD) δ 7.55–7.35 (5 H, m), 6.07 (1 H, s), 2.26 (3 H, s), 2.24 (3 H, s). ^{13}C NMR (101 MHz, CD_3OD) δ 150.27q, 141.72q, 140.80q, 130.29, 129.07, 126.38, 107.77, 13.16, 12.10. HRMS (APCI+) found 173.1076 $C_{11}H_{13}N_2^+$ $[M+H]^+$ requires 173.1073.

3.1.2 3,5-diethyl-1-phenyl-*1H*-pyrazole (**3.4b**)

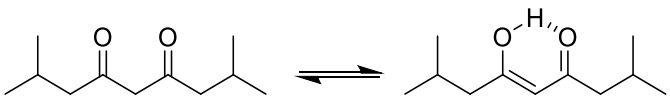


3.4b

Heptane-3,5-dione (0.126 g, 1 mmol) and ethanol (5 mL) were added to a 25 mL round bottomed flask containing a stirrer bar with a temperature probe and reflux condenser attached. Phenyl hydrazine (0.109 g, 1 mmol) was added to the reactor and the reaction was heated to 70 °C. After five hours the solvent was evaporated *in vacuo* to afford the *title compound* as an orange oil (0.150 g, 0.714 mmol, 71%).

^{1}H NMR (400 MHz, CD_3OD) δ 7.58–7.37 (5 H, m), 6.14 (1 H, s), 2.68–2.57 (4 H, m), 1.26 (3 H, t, J = 7.6 Hz), 1.17 (3 H, t, J = 7.6 Hz). ^{13}C NMR (101 MHz, CD_3OD) δ 156.39q, 147.95q, 140.91q, 130.32, 129.30, 126.88, 104.29, 22.18, 20.47, 14.41, 13.47. HRMS (APCI+) found 201.1376 $C_{13}H_{17}N_2^+$ $[M+H]^+$ requires 201.1386. These data are consistent with the reported literature values for NMR shifts.[165]

3.1.3 2,8-dimethylnonane-4,6-dione (**3.1d**)



3.1d **3.1d'**

Sodium hydride (60% in mineral oil, 0.4530 g, 11.3 mmol) was loaded into a 10 mL round bottomed flask containing a stirrer bar. The reactor was then filled with nitrogen gas, by use of a Schlenk line, and toluene (2 mL) was added. A mixture of ethyl *iso* valerate (0.6027 g, 4.63 mmol) and 4-methyl-2-

pentanone (0.4530 g, 4.63 mmol) was added via a manual syringe over 5 minutes at room temperature. The reaction was heated to 60 °C and left stirring for 18 hours. After 18 hours, the reaction mixture was diluted with diethyl ether (10 mL) and quenched with saturated ammonium chloride solution (10 mL) and then 1 M HCl (10 mL). The organic and aqueous layers were separated, and the aqueous layer washed with diethyl ether (2 x 10 mL). The organic layers were combined, washed with water (10 mL) and brine (10 mL) and dried over sodium sulphate. The mixture was then filtered and evaporated under reduced pressure to afford the *title compound* as a yellow oil (0.2992 g, 1.63 mmol, 35%).

The NMR spectra corresponds to a mixture of two tautomeric forms, represented below (**3.1d'** Fig. 6.6a and **3.1d** Fig. 6.6b), primarily resting as the keto-enol form (**3.1d'**) in a ratio of *circa.* 10:1.

3.1d': ^{1}H NMR (400 MHz, $CDCl_3$) δ 15.63 (1 H, s), 5.44 (1 H, s), 2.15–2.11 (4 H, m), 2.11–2.01 (2 H, m), 0.94 (12 H, d, J = 6.4 Hz).

3.1d: ^{1}H NMR (400 MHz, $CDCl_3$) δ 3.50 (2 H, s), 2.38 (2 H, d, J = 6.9 Hz), 2.15–2.11(?) (2 H, m), 0.91 (12 H, d, J = 6.6 Hz).

^{13}C NMR (101 MHz, $CDCl_3$) δ 193.99, 100.85, 47.71, 26.42, 22.65.

HRMS (APCI+) found 185.1518 $C_{11}H_{21}O_2^+$ $[M+H]^+$ requires 185.1542. No literature NMR spectra reported.

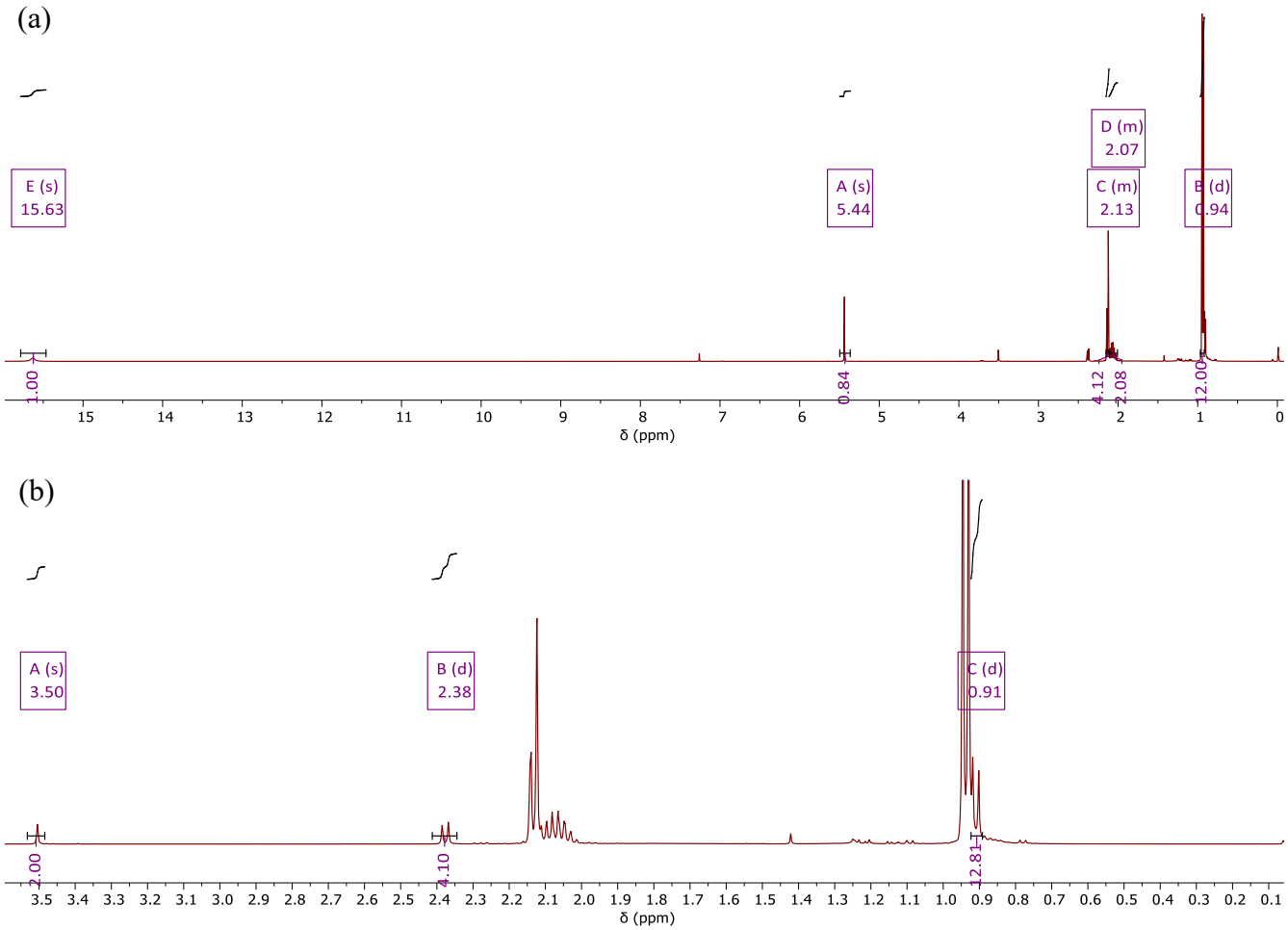
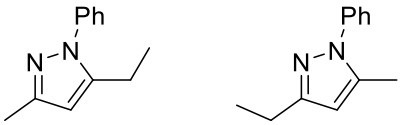


Figure 6.6. ^{1}H NMR spectra and enhanced ^{1}H NMR spectra for the mixture of tautomers **3.1d** (b) and **3.1d'** (a).

3.1.4 Regioisomeric mixture of 5-ethyl-3-methyl-1-phenyl-*1H*-pyrazole (**3.4f**) and 5-methyl-3-ethyl-1-phenyl-*1H*-pyrazole (**3.4f'**)



3.4f **3.4f'**

The regioisomeric mixture of pyrazole **3.4f** and **3.4f'** were synthesised as described in Chapter 3, Section 6. These compounds were characterised as a mixture: shifts in blue correspond to **3.4f**, shifts in red correspond to **3.4f'** and all other peaks correspond to overlapping peaks between both compounds. The corresponding peaks for each regioisomers were identified by relative integrations and assigned by selective nOe exciting at 7.44 ppm. This shift corresponds to a region containing phenyl proton signals of both regioisomers.

^{1}H NMR (400 MHz, $CDCl_3$) δ 7.48–6.73 (17.8 H, m), 6.02 (3.5 H, s), 2.68 (2.0 H, q, J = 7.6 Hz), 2.62 (5.0 H, qd, J = 7.6, 0.8 Hz), 2.31 (7.3 H, s), 2.29 (3.1 H, d, J = 0.8 Hz), 1.28 (3.0 H, t, J = 7.6 Hz), 1.18 (7.5 H, t, J = 7.6 Hz). No literature NMR spectra reported.

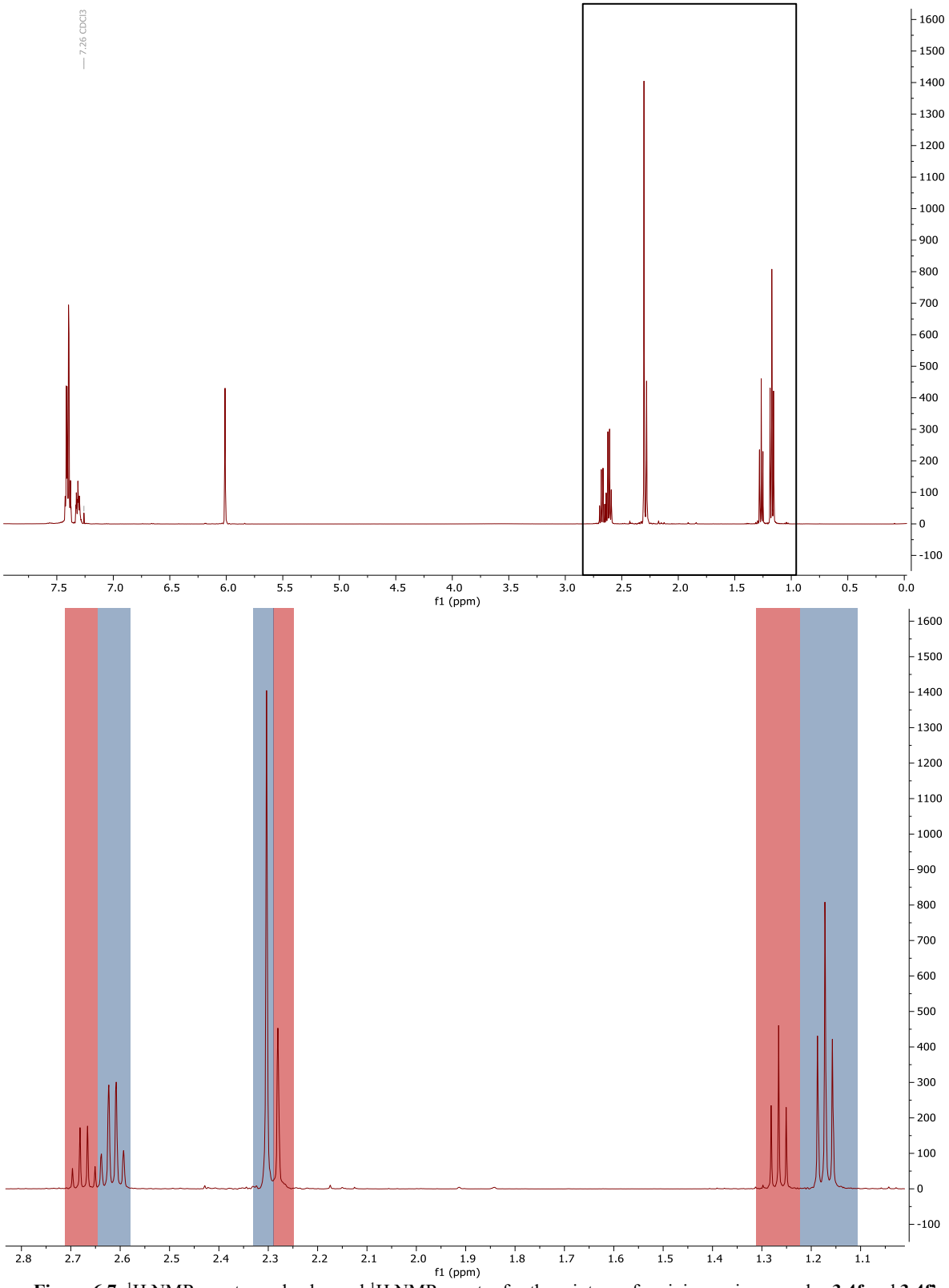


Figure 6.7. ^{1}H NMR spectra and enhanced ^{1}H NMR spectra for the mixture of regioisomeric pyrazoles **3.4f** and **3.4f'**.

^{13}C NMR (101 MHz, $CDCl_3$) δ 154.93, 148.83, 145.83, 139.96, 139.15, 129.07, 128.92, 128.90, 127.34, 127.10, 125.09, 124.69, 119.15, 112.05, 105.32, 104.79, 21.44, 19.68, 13.90, 13.52, 13.13, 12.39. HRMS (APCI+) found 187.1220 $C_{12}H_{15}N_2^+$ $[M+H]^+$ requires 187.1230.

3.2 Flow experiments

3.2.1 General flow experiment setup

The IR was calibrated by the method described in Chapter 2, Section 2.2.2. The pumps were then primed with absolute ethanol, the fluidic connection reconnected to the IR flow cell, and the system filled with absolute ethanol. The reactor was then heated to reaction temperature.

A solution of phenyl hydrazine in absolute ethanol and a solution of diketone in absolute ethanol were freshly prepared by weighing out the appropriate amount of the reagents into a volumetric flask and diluting with the requisite volume of absolute ethanol. The solutions were separately both rigorously mixed and transferred into bottles attached to the inlet lines for pump 1 and pump 2 respectively. The pumps were then run at 0.8 mL min^{-1} for two minutes each, in order to prime the inlet lines with the reagent solutions. The oil bath is allowed to warm to 70 °C and the Peltier assembly is turned on and allowed to equilibrate.

3.2.2 Standard transient residence time ramp experiment (General Method A)

A standard transient residence time ramp is performed by programming the Gilson pumps to begin at 5 mL min^{-1} at a given %B ratio (flow rate ratio of pumps 1 and 2) for 3 minutes at which time the cumulative flow rate changes to 0.2 mL min^{-1} for a further 21 minutes. This can be directly linked to other transient flow rate experiments. Once all experiments in an experimental run are finished, the system is flushed with ethanol through both pumps for at least 10 reactor volumes.

Table 6.7. Pump flow rate method utilised for General Method A.

time / min	flow rate / mL min^{-1}
0	5
2.99	5
3	0.2
24.99	0.2

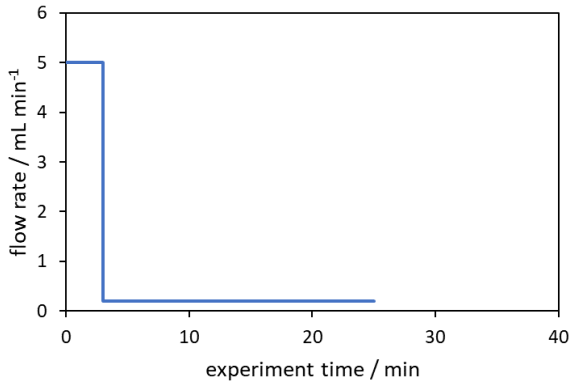


Figure 6.2. Cumulative volumetric flow rate method for a standard transient residence time ramp experiment (General Method A).

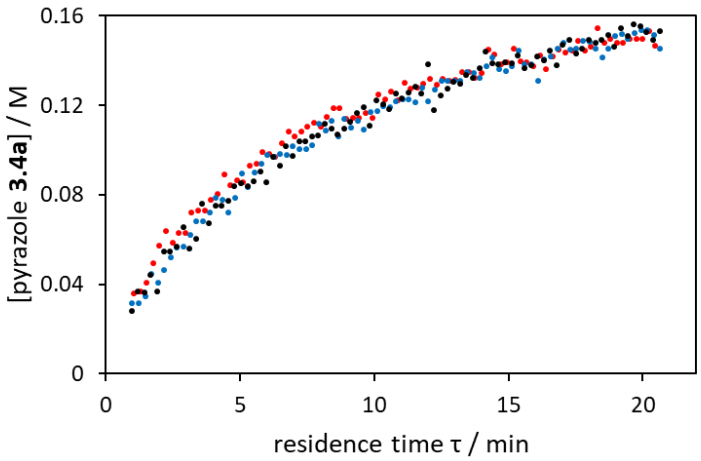


Figure 3.2. Repeatability of RPO method on the Knorr pyrazole synthesis of pyrazole **3.4a** from acetyl acetone and phenyl hydrazine at 70 °C, 0.2 M in ethanol across three repeated experiments.

3.2.3 Standard transient reactant stoichiometry ramp experiment (General Method B)

A standard transient reactant stoichiometry ramp is performed by programming the Gilson pumps to deliver a given cumulative flow rate at a given %B ratio (flow rate ratio of pumps 1 and 2) for 5-10 minutes. The %B is then set to ramp over a given time to the final %B ratio which is then held until a complete reactor volume has exited the reactor.

Table 6.8. Pump flow rate method utilised for General Method B.

time / min	flow rate / mL min^{-1}	%B
0	0.2	40
10		40
20		60
50	0.2	60

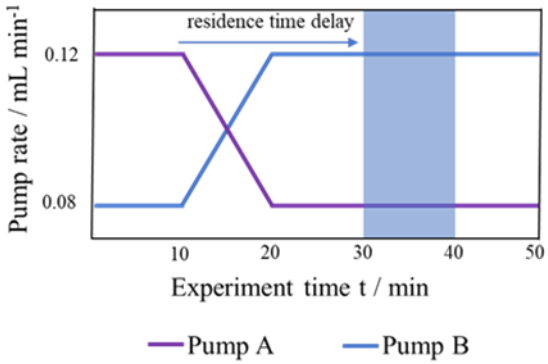


Figure 6.8. Cumulative volumetric flow rate method for a standard transient reactant stoichiometry ramp (General Method B).

As with the transient flow rate methodology, multiple different reactant stoichiometry ramps were performed, to confirm the robustness of the method and determine the most efficient method.

It was found that concentration ratios of **3.2**: **3.1a** from 0.24 M:0.16 M (40%B) to 0.16 M:0.24 M (60%B) could be investigated at the maximum residence time of 20.75 minutes in only 50 minutes of experiment time. The usage of material could also be limited to less than 1.5 reactor volumes of material by using ethanol as a carrying fluid to push the remainder of the reaction out of the reactor.

3.2.4 Standard transient bi-variate ramp experiment (General Method C)

A standard transient bi-variate ramp (residence time and reactant stoichiometry) is performed by programming the Gilson pumps to pump at a cumulative flow rate of 5 mL min-1 at a given %B ratio (flow rate ratio of pumps 1 and 2) for 5-10 minutes. The %B is then set to ramp over a given time to the final %B ratio which is then held until a complete reactor volume has exited the reactor.

Table 6.9. Pump flow rate method utilised for General Method C.

time / min	flow rate / mL min^{-1}	%B
0	5	40
3	5	40
3.82	5	60
3.83	0.2	60
27	0.2	60

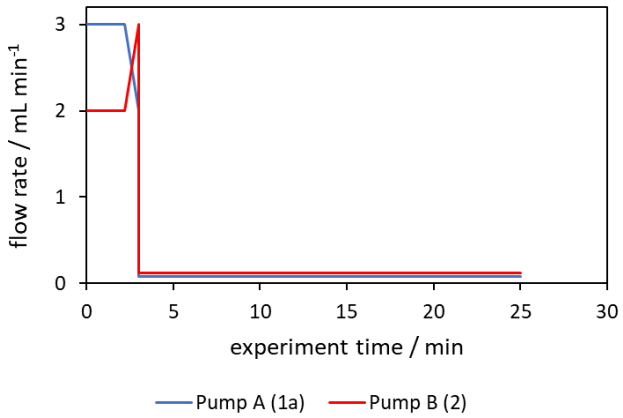


Figure 3.10. Cumulative volumetric flow rate method for a standard transient residence time-reactant stoichiometry ramp experiment performed over a residence time range between 0.8 – 20 minutes and a reactant stoichiometry ratio ([**3.1a**]/[**3.2**]) range between 1.5 – 0.8. (General Method C).

Reactor volume is 4.1347 mL (510 cm reactor length) therefore at a flow rate of 5 mL min^{-1} it takes 0.8269 min to prime. So for combined ramps we need to prime reactor at 5 mL min^{-1} as normal but at 40%B or 60%B for 3 min and then do a 0.82 min ramp from 40%B to 60%B or 60%B to 40%B which then can be flushed out over the next 23 min at 0.2 mL min^{-1}. (21.2 min max residence including dead volume).

3.2.5 Standard transient additive ramp experiment (General Method D)

A standard transient additive concentration ramp is performed using the three-pump system described in Fig. 3.12. Pump 1 is set to a fixed flow rate to pump an undoped reactant stream, while pump 2 and 3, containing a reactant stream and an additive doped reactant stream respectively, are connected by a GSIOC cable to be controlled by a program on the pump firmware. These pumps are set to ramp against one another while maintaining the same cumulative flow rate by the program described in table 6.10.

Table 6.10. Pump flow rate method utilised for General Method D.

time / min	cumulative flow rate / mL min^{-1}	Pump 1 flow rate / mL min^{-1}	Pump 2 flow rate / mL min^{-1}	Pump 3 flow rate / mL min^{-1}
0	1	0.5	0.5	0
10	1	0.5	0.5	0
30	1	0.5	0	0.5
40	1	0.5	0	0.5
60	1	0.5	0.5	0
70	1	0.5	0.5	0

This produces data for a bi-directional ramp as described in Fig. 3.13 as was repeated with different strength acidic and basic additives.

3.3 Combined experimental runs

3.3.1 Experimental run 1

General Method A was performed at 50%B using 0.4 M solutions of diketone **3.1a** and phenyl hydrazine. Then a series of steady state points were collected.

Table 6.11. Solutions produced for experimental run 1.

Compound	volume / mL	concentration / M	desired mass / g	actual mass / g	Pump
diketone **3.1a**	100	0.4	4.004	4.0018	B
phenyl hydrazine	100	0.4	4.328	4.3296	A

Table 6.12. Pump flow rate method utilised in experimental run 1 consisting of general method A.

time / min	flow rate / mL min^{-1}	%B
0	5	50
2.99	5	
3	0.2	
27	0.2	50

Manual steady state points were collected at 0.2, 0.4, 1, 2, and 5 mL min^{-1} after leaving the system to equilibrate at each of these flow rates.

These data were used in Fig. 3.2.

3.3.2 Experimental run 2

Three General Method A runs were performed linked together at 50, 40 and 60%B using 0.4 M solutions of diketone **3.1a** and phenyl hydrazine. Diluted versions of these 0.4 M solutions were then used for two further General Method A runs to collect same excess data.

Table 6.13. Solutions produced for experimental run 2.

Compound	volume / mL	concentration / M	desired mass / g	actual mass / g	Pump
diketone **3.1a**	50	0.4	2.002	2.0063	B
phenyl hydrazine	50	0.4	2.164	2.1640	A

Table 6.14. Pump flow rate method utilised in experimental run 2 consisting of three general method A experiments linked together.

time / min	flow rate / mL min^{-1}	%B
0	5	50
2.99	5	
3	0.2	
24.99	0.2	50
25	5	40
27.99	5	
28	0.2	
49.99	0.2	40
50	5	60
52.99	5	
53	0.2	
74.99	0.2	60

Same excess solutions were prepared as 14 mL solutions (the required volume for a single General Method A run is 10 mL): Using a digital pipette, to accurately dilute 10 mL of 0.4 M diketone **3.1a** and phenyl hydrazine stock solutions with 4 mL of ethanol (0.2863 and 0.2859 M respectively). A second set of same excess solution were prepared in the same manner but diluting 8 mL of 0.4 M diketone **3.1a** and phenyl hydrazine stock solutions with 6 mL of ethanol (0.2290 and 0.2287 M respectively).

General Method A was then run at 50%B for the first set of same excess solutions (0.29 M) and the second set of same excess solutions (0.23 M).

These data were used in Fig. 3.2, Fig. 3.3, Fig. 3.4, Fig. 3.17.

3.3.3 Experimental run 3

A General Method A was performed at 50%B using 0.2 M solutions of diketone **3.1a** and phenyl hydrazine. A modified version of General Method A was then performed using the same solutions in which tow step changes in cumulative flow rate were performed from 5 to 1 to 0.2 mL min^{-1}. Two more General Method A runs were performed using doped versions of these solution: a run in which 0.2 M pyrazole **3.1a** was included and a run in which both 0.2 M pyrazole **3.1a** and 0.4 M water were included. Doping experiments only (and only two of those).

Table 6.15. Solutions produced for experimental run 3.

Compound	volume / mL	concentration / M	desired mass / g	actual mass / g	Pump
diketone **1a**	100	0.2	2.002	2.0028	B
phenyl hydrazine	100	0.2	2.164	2.1648	A

Table 6.16. The first part of the pump flow rate method utilised in experimental run 3 consisting of three general method A experiments in separate runs.

time / min	flow rate / mL min^{-1}	%B
0	5	50
2.99	5	
3	0.2	
24.99	0.2	50

Table 6.17. The second part of the pump flow rate method utilised in experimental run 3 consisting of a modified version of general method A to investigate the "incubation period".

time / min	flow rate / mL min^{-1}	%B
0	5	50
2.99	5	
3	1	
9.99	1	
10	0.2	
32	0.2	50

To 25 mL of the 0.2 M phenyl hydrazine solution 0.8605 g (actually 0.8599 g) of pyrazole **3.4a** was added to produce a solution of 0.2 M phenyl hydrazine and 0.2 M pyrazole **3.4a.**

To 25 mL of the 0.2 M diketone **3.1a** solution 0.182 g of water was added to produce a solution of 0.2 M diketone **3.1a** and 0.4 M water.

These data were used in Fig. 3.4, Fig. 3.17.

3.3.4 Experimental run 4

Three General Method A runs were performed linked together at 50, 40 and 60%B using 0.4 M solutions of diketone **3.1b** and phenyl hydrazine. Diluted versions of these 0.4 M solutions were then used for two further General Method A runs to collect same excess data.

Table 6.18. Solutions produced for experimental run 4.

Compound	volume / mL	concentration / M	desired mass / g	actual mass / g	Pump
diketone **3.1b**	50	0.4	2.5634	2.5696	B
phenyl hydrazine	50	0.4	2.164	2.1617	A

Table 6.19. The first part of the pump flow rate method utilised in experimental run 4 consisting of three general method A experiments linked together.

time / min	flow rate / mL min^{-1}	%B
0	5	50
2.99	5	
3	0.2	
24.99	0.2	50
25	5	40
27.99	5	
28	0.2	
49.99	0.2	40
50	5	60
52.99	5	
53	0.2	
74.99	0.2	60

Same excess solutions were made as 14 mL solutions (the required volume for a single General Method A run is 10 mL). They were prepared using a digital pipette to accurately dilute 10 mL of 0.4 M diketone **3.1b** and phenyl hydrazine stock solutions with 4 mL of ethanol (0.2864 and 0.2856 M respectively). A second set of same excess solution were prepared in the same manner as 11.55 mL solutions. The second set diluted 6.6 mL of 0.4 M diketone **3.1b** and phenyl hydrazine stock solutions with 4.95 mL of ethanol respectively (0.2291 and 0.2285 M respectively) giving a similar dilution factor to those in Experimental run 2 for diketone **3.1a**.

General Method A was then run at 50%B for the first set of same excess solutions (0.29 M) and the second set of same excess solutions (0.23 M).

These data were used in Fig. 3.5, Fig. 3.17.

3.3.5 Experimental run 5

Three General Method A runs were performed linked together at 50, 40 and 60%B using 0.4 M solutions of diketone **3.1a** and phenyl hydrazine. These were also linked to three General Method B runs performed from 40 to 60%B at cumulative flow rates of 0.2, 0.3 and 0.4 mL min^{-1}. Subsequently two General Method C runs were performed linked together, the first from 40 to 60%B and the second from 60 to 40%B.

Table 6.20. Solutions produced for experimental run 5.

Compound	volume / mL	concentration / M	desired mass / g	actual mass / g	Pump
diketone **3.1a**	100	0.4	4.004	4.0015	B
phenyl hydrazine	100	0.4	4.328	4.3246	A

Table 6.21. The first part of the pump flow rate method utilised in experimental run 5 consisting of three general method A experiments and three general method B experiments linked together.

Program	time / min	flow rate / mL min^{-1}	%B
(3)	0	5	50
	2.99	5	
	3	0.2	
	24.99	0.2	50
	25	5	46
	27.99	5	
	28	0.2	
	49.99	0.2	46
	50	5	54
	52.99	5	
	53	0.2	
	74.99	0.2	54
	75		40
(4)	0	0.2	40
	10		40
	20		60
	49.99	0.2	60
	50	0.3	40
	60		40
	70		60
	94.99	0.3	60
	95	0.4	40
(5)	0	0.4	40
	5		40
	15		60
	30	0.4	60
TOTAL	**200 minutes**	**A: 45.6 mL**	**B: 48.1 mL**

Table 6.22. The second part of the pump flow rate method utilised in experimental run 5 consisting of two general method C experiments linked together.

Program	time / min	flow rate / mL min^{-1}	%B
(6)	0	5	40
	3	5	40
	3.82	5	60
	3.83	0.2	60
	26.99	0.2	60
	27	5	60
	30	5	60
	30.82	5	40
	30.83	0.2	40
	54	0.2	40

These data were used in Fig. 3.2, Fig. 3.6, Fig. 3.7, Fig. 3.8, Fig. 3.9, Fig. 3.11.

3.3.6 Experimental run 6

A General Method A was performed at 50%B using 0.4 M solutions of diketone **3.1b** and phenyl hydrazine. Then were two General Method B runs linked together were performed at a cumulative flow rate of 0.2 mL min^{-1} from 40 to 60%B and 60 to 40%B respectively. Another General Method B run was then performed at 0.4 mL min^{-1} from 40 to 60%B.

Table 6.23. Solutions produced for experimental run 6.

Compound	volume / mL	concentration / M	desired mass / g	actual mass / g	Pump
diketone **3.1b**	25	0.4	1.2817	1.2811	B
phenyl hydrazine	25	0.4	1.082	1.0797	A

Table 6.24. The second part of the pump flow rate method utilised in experimental run 6 consisting of two general method B experiments at 0.2 mL min^{-1} linked together.

time / min	flow rate / mL min^{-1}	%B
0	0.2	40
10		40
30		60
60		60
80		40
110	0.2	40

Table 6.25. The third part of the pump flow rate method utilised in experimental run 6 consisting of one general method B experiment at 0.4 mL min^{-1}.

time / min	flow rate / mL min^{-1}	%B
0	0.4	40
5		40
15		60
30	0.4	60

These data were used in Fig. 3.9.

3.3.7 Experimental run 7

General Method D was performed five times at 70 °C utilising different additives. The pump solution were as described in Table 6.26.

Table 6.26. Solutions produced for experimental run 7.

Additive of experiment	Pump number	Solution volume / mL	[3.1a]		[3.2]		[additive]	
			M	g	M	g	mol%	g
AcOH	1	100			0.4	4.327		
	2	50	0.4	2.004				
	3	50	0.4	2.003			20	0.2467
NaOEt	1	100			0.4	4.327		
	2	50	0.4	2.006				
	3	50	0.4	2.003			10	0.1493
NaOEt	1	50	0.4	2.006				
	2	50			0.4	2.166		
	3	50			0.4	2.167	10	0.1490
TEA	1	50	0.4	2.001				
	2	100			0.4	4.327		
	3	50			0.4	2.163	20	0.4132
DIPEA	1	50	0.4	2.001				
	2	50			0.4	2.165		
	3	50			0.4	2.166	20	0.5228
DBU	1	50	0.4	2.006				
	2	50			0.4	2.165		
	3	25			0.4	1.080	10	0.1686

3.4 HPLC-MS methods and experiments

LC-MS analysis was performed using an Agilent 1260 Infinity II instrument, a diode array UV-Vis Detector and an InfinityLab LC/MSD mass spectrometer, performing positive ES-API MS.

3.4.1 Initial intermediate identification method for R = Me

An initial vial reaction was performed, by mixing 6 equivalents of phenyl hydrazine and 1 equivalent of diketone **3.1a** in a neat solution, as well as subsequent samples collected from reactant stoichiometry ramps and residence time ramps for diketone **3.1a** were analysed using an Agilent Zorbax SB-C18 column (50 mm x 4.6 mm x 3.5 µm) at 40 °C with acetonitrile (solvent A) and 20 mM aqueous ammonium formate (solvent B). Beginning at 60%B for 0.5 min, followed by a 2.5 min ramp to 95%B, then a 2 minute isocratic hold before returning to the initial conditions.

This method clearly showed separate peaks with m/z values corresponding to di-addition intermediate **3.5a** (3.181 min) and pyrazole **3.4a** (2.077 min) in the 6 equivalent neat excess experiment:

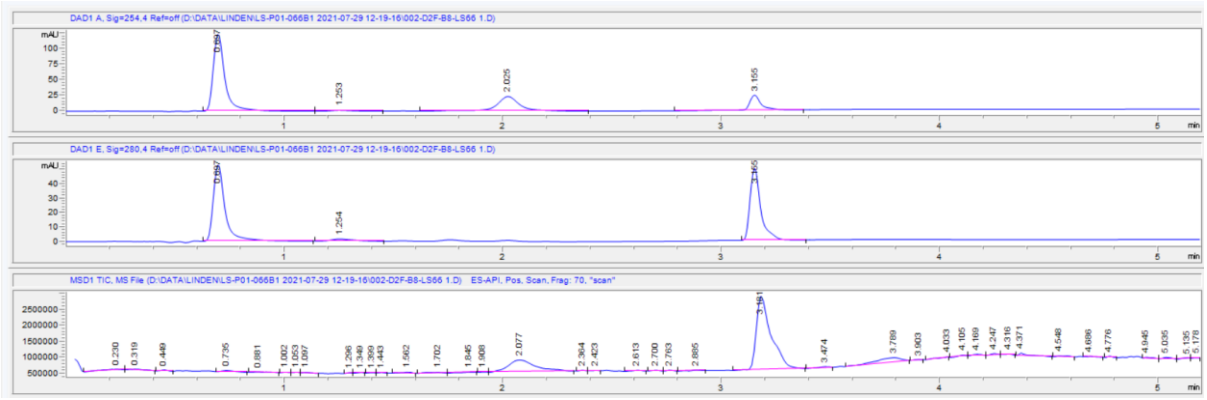


Figure 6.9. Separation and identification of di-addition intermediate **3.5a** using LC-MS on a neat reaction at room temperature between 1 equivalent of diketone **1a** and 6 equivalents of phenyl hydrazine. The figure consists of the diode array trace at 254 nm and 280 nm, and the TIC (total ion chromatogram) from the mass spectrometer.

In subsequent experimental runs without such extreme excesses, peaks with m/z values corresponding to mono-addition intermediate **3.3a** (1.735 min), di-addition intermediate **3.5a** (2.087 min) and pyrazole **3.4a** (3.215 min) could be clearly identified. For example, at the end of transient ramp at 0.2 mL min^{-1} and 60%B:

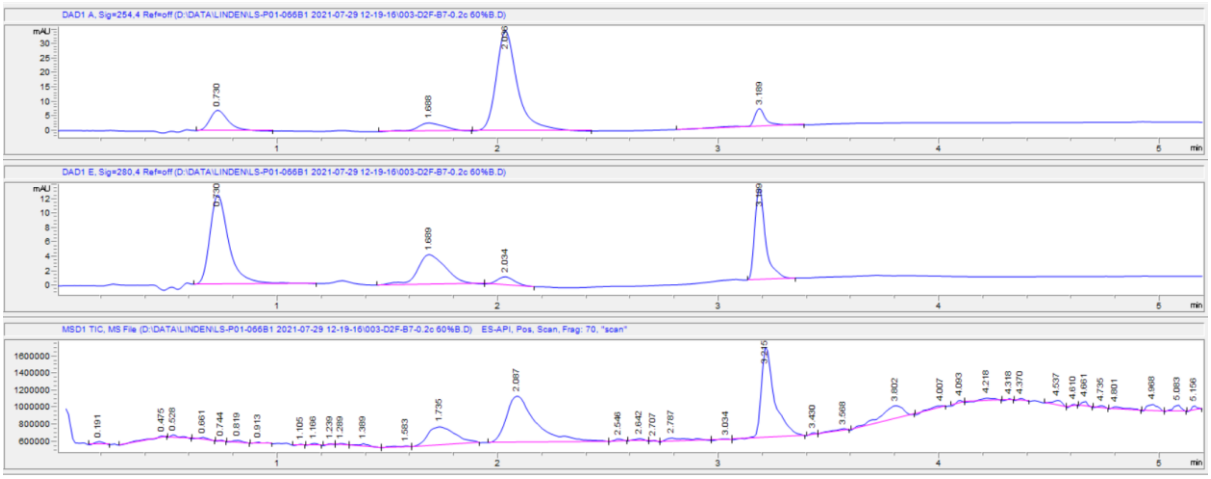


Figure 6.10. Separation and identification of mono-addition intermediate **3.3a** and di-addition intermediate **3.5a** using LC-MS used in a variety of experimental runs for the reaction of diketone **3.1a** and phenyl hydrazine. The figure consists of the diode array trace at 254 nm and 280 nm, and the TIC from the mass spectrometer.

3.4.2 Method for identification of unsymmetric diketone reaction intermediates

The reactions performed using a 0.4 M stock solution of hexane-2,4-dione **1f** and 0.4 M stock solution of phenyl hydrazine at 70 °C and a cumulative flow rate of 0.2 mL min^{-1} at 40 and 60%B respectively were analysed using an Agilent Zorbax SB-C18 (50 mm x 4.6 mm x 3.5 µm) column at 40 °C with acetonitrile (solvent A) and 20 mM aqueous ammonium formate (solvent B). Beginning at 50%B for 0.5 min, followed by a 3 min ramp to 65%B, then a 0.5 minute isocratic hold, followed by a 1 min ramp to 95%B, then a 0.5 min isocratic hold before returning to the initial conditions.

This method allowed separation of peaks with m/z values corresponding to mono-addition intermediate **3.3f** (1.298 min), di-addition intermediate **3.5f** (3.760 min) and either or both pyrazole products **3.4f**/**3.4f'** as one peak (1.496 min) despite further attempts to separate the regioisomeric pyrazoles using LC-MS.

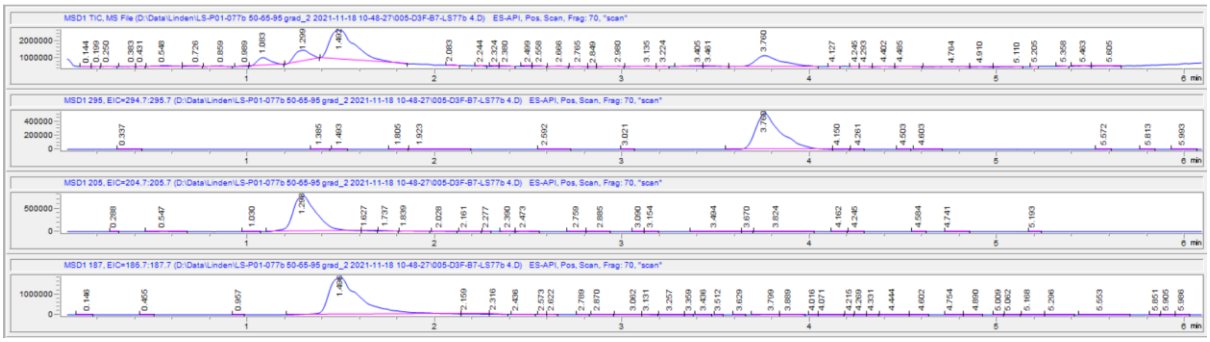


Figure 6.11. Separation and identification of mono-addition intermediate **3.3f** and di-addition intermediate **3.5f** using LC-MS while attempting to separate regioisomeric pyrazoles **3.4f** and **3.4f'** for the reaction of diketone **3.1f** and phenyl hydrazine. The figure consists of the TIC from the mass spectrometer, followed by the EIC (extracted ion chromatogram) for the di-addition intermediate **3.5f** (m/z = 295.2), mono-addition intermediate **3.3f** (m/z = 205.2) and pyrazole products **3.4f**/**3.4f'** (m/z = 187.2).

After removing the solvent from the reactions using a Smart Evaporator, it was found the extract ion chromatograms for intermediates **3.3f** and **3.5f** disappeared as the intermediates relaxed to product and starting materials:

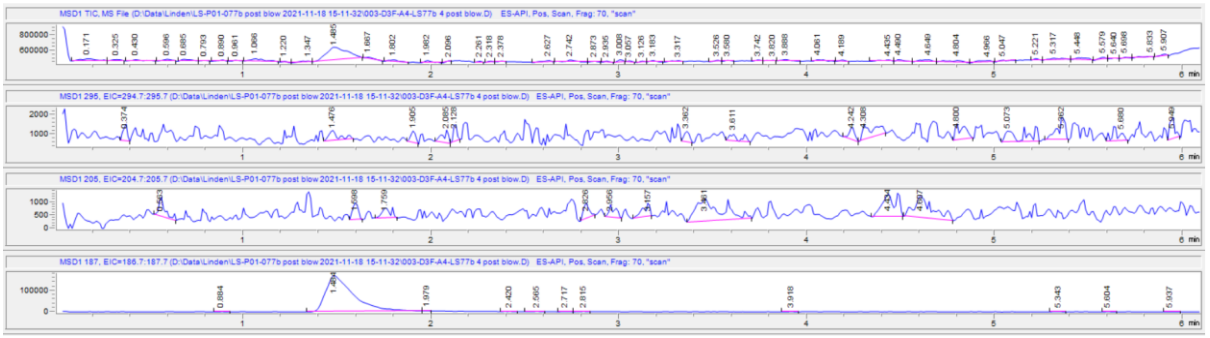


Figure 6.12. Separation and identification of mono-addition intermediate **3.3f** and di-addition intermediate **3.5f** using LC-MS while attempting to separate regioisomeric pyrazoles **3.4f** and **3.4f'** for the reaction of diketone **3.1f** and phenyl hydrazine analysed after concentration by removal of reactant solvent *in vacuo*. The figure consists of the TIC from the mass spectrometer, followed by the EIC (extracted ion chromatogram) for the di-addition intermediate **3.5f** (m/z = 295.2), mono-addition intermediate **3.3f** (m/z = 205.2) and pyrazole products **3.4f**/**3.4f'** (m/z = 187.2).

3.4.3 Intermediate identification method for range of alkyl substituents

Vial reactions performed at 0.2 M in ethanol at room temperature between phenyl hydrazine and a range of diketones sampled at 10 minutes were analysed using a Phenomenex Gemini NX-C18 (50 mm x 2.0 mm x 3.0 µm) column at 40 °C with acetonitrile (solvent A) and 20 mM aqueous ammonium formate

(solvent B). Beginning at 65%B for 0.5 min, followed by a 3 min ramp to 95%B, then a 2 minute isocratic hold before returning to the initial conditions.

This method allowed identification of the presence of separate peaks with m/z values corresponding to mono-addition intermediate **3.3**, di-addition intermediate **3.5** and pyrazole **3.4** across the range of alkyl substituents. All peaks were present in R =Me, Et and ^{t}Bu (**a**,**b**,**d**), peaks for mono-addition intermediate **3.3** and pyrazole **3.4** were present when R = ^{i}Pr (**c**) and no peaks were identified corresponding to any intermediates or products when R = ^{t}Bu (**e**) as identified by extracted ion chromatograms.

3.5 NMR experiments

3.5.1 Lack of interaction between diketone **3.1a** and pyrazole **3.4a**

^{1}H NMR spectra taken of diketone **3.1a**, pyrazole **3.4a**, and a combination of both together in CD_3OD showed no interaction was happening between the two species in solution and thus that both a tandem acid-base catalysed mechanism using a diketone and a pyrazole was plausible.

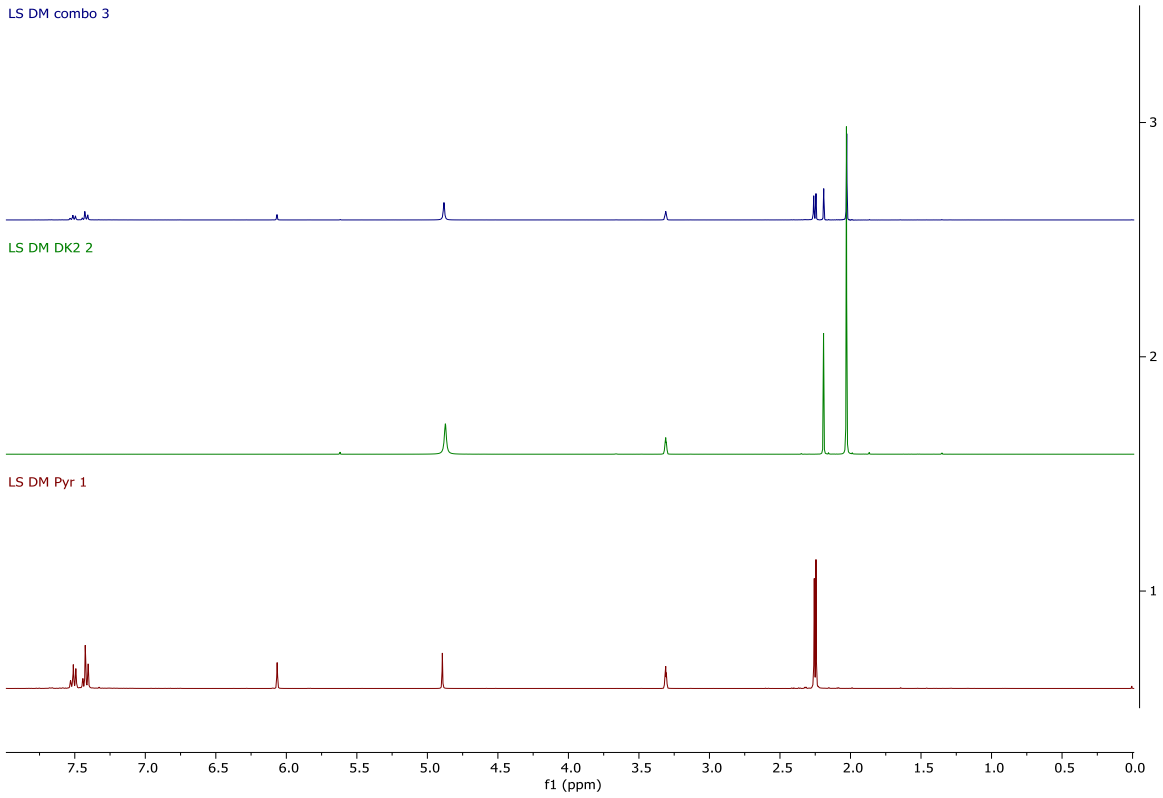


Figure 6.13. ^{1}H NMR spectra of a combination of diketone **3.1a** and pyrazole **3.4a** in CD_3OD with comparative spectra for diketone **3.1a** and pyrazole **3.4a** all taken after the samples were allowed to equilibrate in CD_3OD.

3.5.2 Major regioisomer identification

^{1}H NMR was performed on the regioisomeric mixtures of pyrazoles **3.4f** and **3.4f'** produced from the different excess reactions of phenyl hydrazine with unsymmetric diketone **3.1f** in a ratio of 1.5:1. These experiments produced different ratios of pyrazoles **3.4f** and **3.4f'** but did not allow us to identify which isomer was which. The shift of the phenyl protons in the pyrazole products were then be used as the centre for excitation for selective excitation nOe (Chapter 3, Fig. 3.21b). Selective excitation at 7.44 ppm revealed enhancement of the same signals in both samples as expected and only one of each signal

for the methyl and ethyl signals as desired. The enhanced peaks are those which are closest to the excited phenyl protons and therefore correspond to the alkyl group which sits on the same side as the phenyl ring. Enhancement of the neighbouring ethyl CH_2 environment in pyrazole **3.4f** was 0.7%, with the corresponding ethyl CH_3 enhanced by 0.1% and that of the neighbouring CH_3 in pyrazole **3.4f'** was 0.5%. As a comparison, enhancement of the 4 position proton on the pyrazole ring was 0.1% and all other environments from the alkyl groups the opposite side of the pyrazole ring were less than 0.1%.

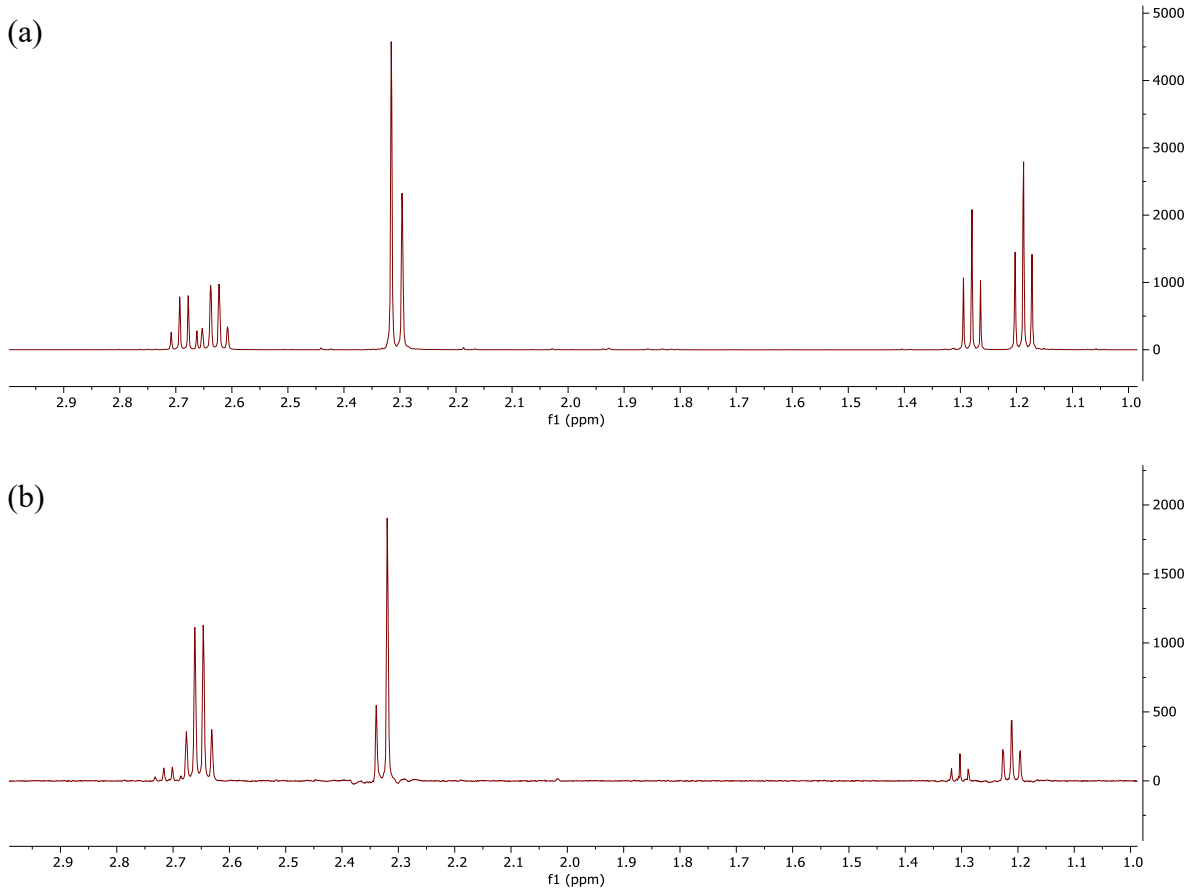


Figure 6.14. ^1H NMR (a) and selective excitation nOe (b) spectra in $CDCl_3$ of the isolated product mixture of the reaction of 1 equivalent of diketone **3.1f** and 1.5 equivalents of phenyl hydrazine.

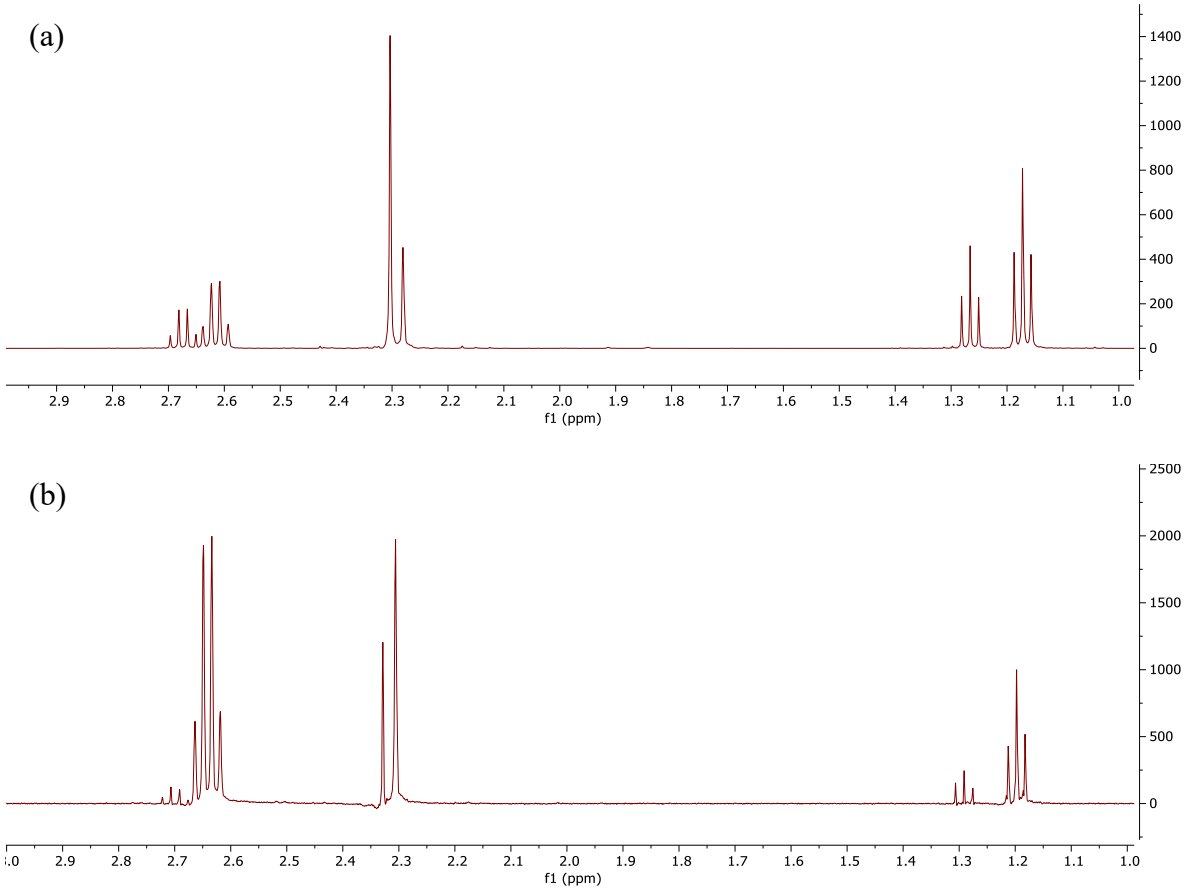


Figure 6.15. ^{1}H NMR (a) and selective excitation nOe (b) spectra in $CDCl_3$ of the isolated product mixture of the reaction of 1.5 equivalents of diketone **3.1f** and 1 equivalent of phenyl hydrazine.

3.6 MATLAB Surface plotting

3D visualisation and microkinetic model response surface generation was performed in MATLAB R2021b. The response surface was generated by creating a function containing the reactions and series of ODEs as used in Berkeley Madonna which takes time, reaction component concentrations and kinetic rate constants as in put parameters. The kinetic parameters are then inputted and the function solved using ode45 (a solver for coupled ODEs) for a range of starting concentrations of diketone **3.1** and phenyl hydrazine from [**3.1**]/[**3.2**] = 0.66 to 1.5 in intervals of 0.02 at a time resolution of 0.0021 minutes. This could then be plotted using the function surf. It is worth noting that ODE solver ode45 solves coupled ODEs in a different manner to Rosenbrock (stiff) as used in Berkeley Madonna and thus acts as another method of showing the solver independent nature of our microkinetic model solution. The collected data was plotted in series over this surface using the function plot3 to generate the

graphs shown in Fig. 3.11, 3.19, 6.15, and 6.16. All code used is available at https://github.com/LindenSchrecker.

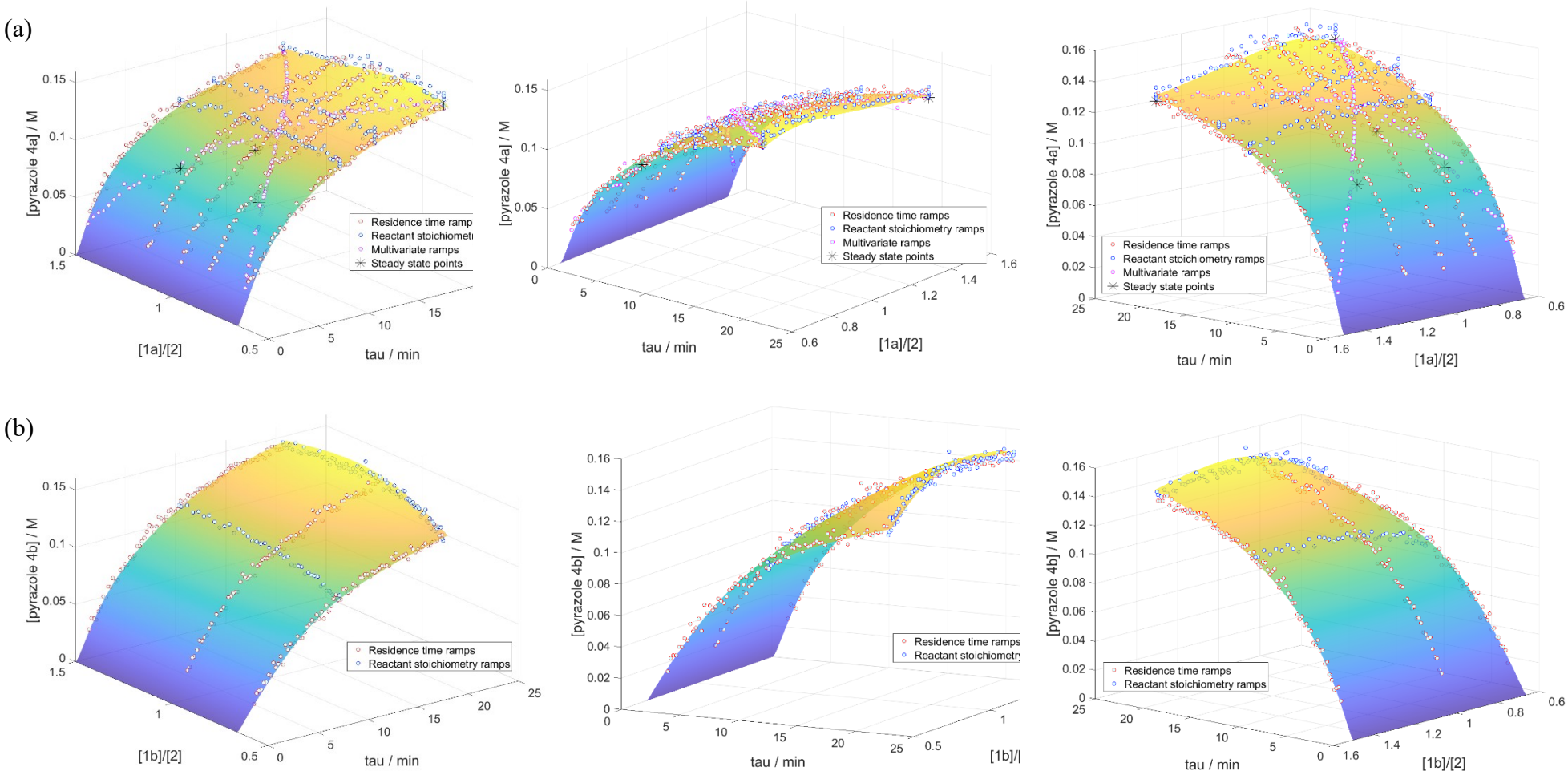


Figure 6.16. Multiple angles of the 3D visualised response surfaces for the reaction of phenyl hydrazine with (a) diketone **3.1a**; (b) diketone **3.1b**.

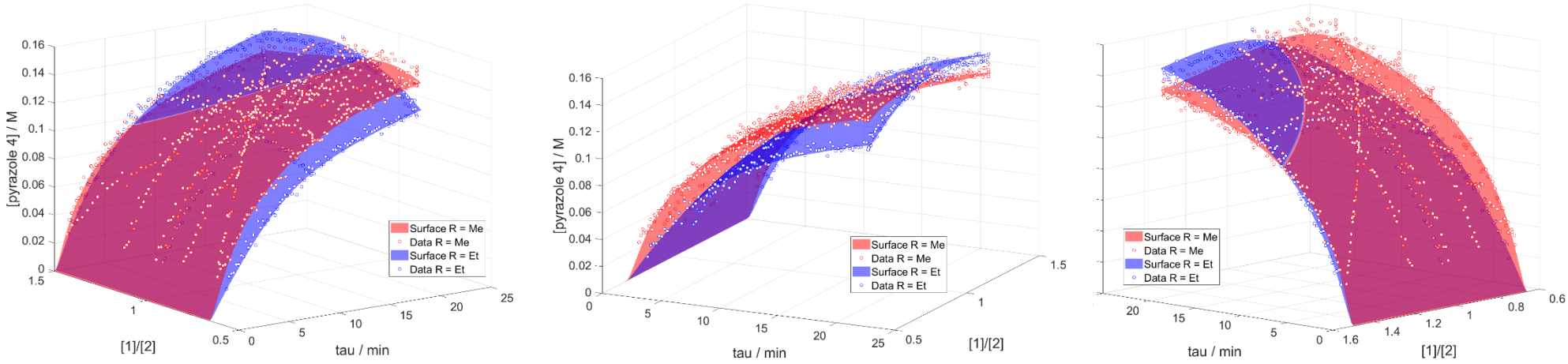


Figure 6.17. Multiple angles of the 3D visualised interaction plot of surfaces for diketone **3.1a** and **3.1b**.

4 Investigation of traditionally discrete reaction parameters

4.1 Synthesis methods and characterisation

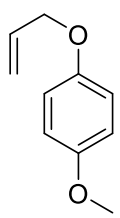
4.1.1 General Methods

Unless otherwise stated, materials were purchased from commercial sources and used as received without further purification. Acetone was dried over 3 Å molecular sieves in a solvent purification system. Automated flash column chromatography was performed using a Teledyne ISCO CombiFlash NextGen 100 system using pre-packed silica columns with a gradient of petroleum ethers/ethyl acetate. Microwave heating was performed in a Biotage Initiator microwave reactor at high absorption level.

^{1}H and ^{13}C NMR spectra were recorded on Bruker AVANCE III HD spectrometers (400 MHz for ^{1}H NMR; 101 MHz for ^{13}C NMR). ^{1}H NMR chemical shifts (δ_H) and ^{13}C NMR chemical shifts (δ_C) are quoted in parts per million (ppm) downfield of tetramethylsilane (TMS) and reported relative to residual solvent peaks ($CDCl_3$: δ_H = 7.26 ppm and δ_C = 77.16 ppm).

No unexpected or unusually high safety hazard were encountered.

4.1.2 Synthesis of 4-methoxy phenyl ally ether (**2.6/4.1a**)

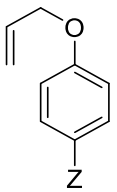


In a 500 mL RB flask fitted with a reflux condenser, a solution of 4-methoxyphenol (10.1 g, 81.4 mmol) in acetone (250 mL) was stirred at 300 rpm. Potassium carbonate (22.3 g, 161 mmol) was added in batches and the solution was heated to 60 °C under nitrogen and left to stir for 20 minutes. Allyl bromide

(9.80 g, 81.0 mmol) was then added, and the solution was heated to reflux (66 °C) and left to stir for 4 hours. After cooling to ambient temperature, the solution was filtered through celite and evaporated *in vacuo*. The residue was purified by automated column chromatography in 10% ethyl acetate in petroleum ether. This produced the desired product as a colourless oil (9.05 g, 44.8 mmol, 55%).

^{1}H NMR (400 MHz, $CDCl_3$) δ 6.93 – 6.78 (m, 4H), 6.23 – 5.89 (m, 1H), 5.58 – 5.13 (m, 2H), 4.65 – 4.35 (m, 2H), 3.77 (s, 3H). ^{13}C NMR (101 MHz, $CDCl_3$) δ 153.97, 152.81, 133.70, 117.58, 115.78, 114.67, 69.58, 55.78. These data are consistent with the reported literature values for NMR shifts.[166]

4.1.3 Synthesis of starting materials in medium throughput (**4.1b, 4.1c, 4.1e-h**)



The precursors were prepared in parallel using a Reactarray Barnstead RAR-010A reaction station equipped with 10 x 25 mL reactors that are fitted individually with reflux condensers. Each reactor was flushed with N_2 and charged with a cross-shaped stirrer, potassium carbonate (2.50 g, 18.1 mmol), the requisite phenol starting material (approximately 6 mmol., see table 6.27 for quantities) and dry acetone (20 mL). The reaction mixtures were subsequently stirred with gentle heating at 30 °C for 20 minutes in order to ensure deprotonation of the phenol. Allyl bromide (1.13 g, 9.34 mmol) was added to each reactor *via* a pipette, and the reaction mixtures were left stirring at 30 °C for 18 hours. After cooling, the solutions were filtered through celite into falcon tubes and the acetone was removed using a nitrogen blow down evaporator. This produced the desired products as listed below in Table 6.27.

Table 6.27. Values for the medium throughput synthesis of para substituted phenyl allyl ether **4.1**.

Compound	Z	MW of phenol / g mol^{-1}	mass of phenol / g	mass of 1x / g	isolated yield / %	Description
4.1b	Me	108.14	0.655	0.656	73	orange oil
4.1c	F	112.10	0.336	0.360	79	colourless oil
4.1e	$C(O)CH_3$	136.15	0.817	0.956	91	colourless oil
4.1f	CN	119.12	0.752	0.705	70	white solid
4.1g	NHAc	151.16	0.907	0.915	80	white solid
4.1h	Br	173.01	1.03	1.09	87	colourless oil

4.1b (Z = Me):

^{1}H NMR (400 MHz, $CDCl_3$) δ 7.08 (d, *J* = 8.2 Hz, 2H), 6.83 (d, *J* = 8.2 Hz, 2H), 6.23 – 5.94 (m, 1H), 5.56 – 5.13 (m, 2H), 4.62 – 4.39 (m, 2H), 2.29 (s, 3H). ^{13}C NMR (101 MHz, $CDCl_3$) δ 156.59, 133.66, 130.18, 130.00, 117.65, 114.71, 69.02, 20.61. These data are consistent with the reported literature values.[116]

4.1c (Z = F):

^{1}H NMR (400 MHz, $CDCl_3$) δ 7.06 – 6.81 (m, 4H), 6.17 – 5.94 (m, 1H), 5.67 – 5.09 (m, 2H), 4.58 – 4.47 (m, 2H). ^{13}C NMR (101 MHz, $CDCl_3$) δ 157.43 (d, *J* = 238.4 Hz), 154.82, 133.31, 117.91, 115.96 (d, *J* = 12.7 Hz), 115.81 (d, *J* = 2.5 Hz), 69.56. These data are consistent with the reported literature values.[116]

4.1e (Z = $C(O)CH_3$):

^{1}H NMR (400 MHz, $CDCl_3$) δ 7.92 (d, *J* = 8.3 Hz, 2H), 6.94 (d, *J* = 8.3 Hz, 2H), 6.19 – 5.95 (m, 1H), 5.50 – 5.25 (m, 2H), 4.64 – 4.56 (m, 2H), 2.55 (s, 3H). ^{13}C NMR (101 MHz, $CDCl_3$) δ 196.91, 162.59, 132.60, 130.69, 130.54, 118.34, 114.50, 69.00, 26.49. These data are consistent with the reported literature values.[167]

4.1f (Z = CN):

^{1}H NMR (400 MHz, $CDCl_3$) δ 7.57 (d, *J* = 8.3 Hz, 2H), 6.95 (d, *J* = 8.3 Hz, 2H), 6.10 – 5.95 (m, 1H),

5.49 – 5.27 (m, 2H), 4.63 – 4.53 (m, 2H). ^{13}C NMR (101 MHz, $CDCl_3$) δ 161.93, 134.07, 132.16, 119.31, 118.61, 115.55, 104.17, 69.10. Melting point: 44 – 46 °C (lit.[168] 41 – 42 °C). These data are consistent with the reported literature values for NMR shifts.[168]

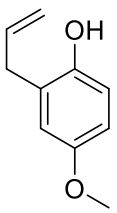
4.1g (Z = NHAc):

^{1}H NMR (400 MHz, $CDCl_3$) δ 7.42 – 7.33 (m, 2H), 7.19 (s, 1H), 6.91 – 6.81 (m, 2H), 6.15 – 5.95 (m, 1H), 5.46 – 5.23 (m, 2H), 4.54 – 4.47 (m, 2H), 2.15 (s, 3H). ^{13}C NMR (101 MHz, $CDCl_3$) δ 168.33, 155.57, 133.36, 131.21, 121.96, 117.86, 115.18, 69.22, 24.52. Melting point: 95 – 97 °C (lit.[169] 94 – 95 °C). These data are consistent with the reported literature values for NMR shifts.[169]

4.1h (Z = Br):

^{1}H NMR (400 MHz, $CDCl_3$) δ 7.37 (d, *J* = 8.3 Hz, 2H), 6.80 (d, *J* = 8.3 Hz, 2H), 6.10 – 5.96 (m, 1H), 5.46 – 5.25 (m, 2H), 4.54 – 4.48 (m, 2H). ^{13}C NMR (101 MHz, $CDCl_3$) δ 157.80, 132.98, 132.37, 118.08, 116.68, 113.12, 69.12. These data are consistent with the reported literature values.[170]

4.1.4 Synthesis of 2-allyl-4-methoxy phenol (**2.7/4.2a**)

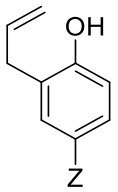


4-Methoxy phenyl allyl ether (**2.6/4.1a**, 1.60 g, 9.75 mmol) was added to a 0.5 – 2 mL microwave vial with a stirrer. The vial was subjected to microwave heating at 200 °C for 40 min. After cooling to room temperature, the crude product formed was dissolved in petroleum ether (10 mL) and extracted into a 2.5 M NaOH solution (2 x 5 mL). The combined aqueous layers were washed with petroleum ether (2 x 5 mL) before re-acidifying - with conc. HCl (6 mL) to pH 2. The acidified aqueous layer was extracted with ethyl acetate (3 x 10 mL). The combined ethyl acetate washes were diluted with petroleum ether (40 mL) and filtered through a silica plug. The organic mixture was dried over magnesium sulfate,

filtered and evaporated *in vacuo* to produce the desired product as a pale yellow oil (1.33 g, 8.11 mmol, 83%).

^{1}H NMR (400 MHz, $CDCl_3$) δ 6.81 – 6.60 (m, 3H), 6.13 – 5.90 (m, 1H), 5.20 – 5.09 (m, 2H), 4.55 (br s, 1H), 3.76 (s, 3H), 3.45 – 3.29 (m, 2H). ^{13}C NMR (101 MHz, $CDCl_3$) δ 153.92, 148.10, 136.28, 126.54, 116.73, 116.64, 116.06, 112.76, 55.86, 35.50. These data are consistent with the reported literature values.[171]

4.1.5 Synthesis of other aromatic Claisen products (**4.2b-h**)



4.2d-f:

200 μL of each allyl ethers (**4.1d-f**) were dissolved in 9 mL ethanol and 5 mL of water using a pipette in quantities listed below in Table 6.28. The solutions were then pumped through the flow system at 0.2 mL min^{-1} at 220 °C (16 min residence time). Prior to each experiment, the system was primed with the reaction solution for 2 min at 1 mL min^{-1} and the reactor was heated to 220 °C. The reaction solution was pumped at 0.2 mL min^{-1} at 70 bar for 23 min.[1] The reactor effluent was then collected for 70 min with addition of ethanol to the inlet at 35 min. After each experiment the system was then flushed with ethanol. Each solution was evaporated to half volume *in vacuo* to remove the ethanol. The resultant solution was dissolved in DCM (10 mL) and 2.5 M NaOH (10 mL) was added. The separated aqueous solution was acidified with 2 M HCl (15 – 25 mL) and washed with DCM (10 mL). The DCM was evaporated *in vacuo* to afford the desired products.

[1] The time taken for solution to pass from the mixer to the outlet of the system.

4.2b:

Attempts to produce 2b (Z = Me) by the above method failed to furnish clean products even after flash column chromatography, as the product either appeared to either remain on the column (silica or alumina) or degrade. Hence, the Claisen rearrangement of 1b (0.281 g) was performed in flow, by dissolving the precursor in DMF (10 mL) and subjected to heating at 240 °C using the flow system for 4 hours (recirculatory mode, 0.5 mL min^{-1}). Diethyl ether (20 mL) was then added, and the resultant solution was washed with saturated lithium chloride solution (5 x 20 mL). The diethyl ether was then evaporated to give the desired product as a pale yellow oil (0.205 g, 1.38 mmol, 73%)

4.2c and **4.2g**:

200 µL of allyl ether **4.1c** or **4.1g** were dissolved in ethanol (20 mL) in quantities listed below in Table 6.28. The reaction solution was subjected to heating at 250 °C using the flow system for 1 hours (recirculatory mode, 0.5 mL min^{-1}). The ethanolic solution is then collected and evaporated *in vacuo*. The residue is dissolved in DCM (10 mL) and 2.5 M NaOH (10 mL) was added. The separated aqueous solution was acidified with 2 M HCl (25 mL) and washed with DCM (10 mL). The DCM was evaporated *in vacuo* to afford the desired products.

Table 6.28. Values for the medium throughput synthesis of aromatic Claisen products **4.2**.

Compound	Z	mw of SM / g mol^{-1}	mass of 4.1 / g	mass of 4.2 / g	isolated yield / %	Description
4.2b	Me	148.09	0.281	0.205	73	Orange oil
4.2c	F	152.06	0.055	0.049	89	Orange oil
4.2d	H	134.07	0.283	0.116	41	Colourless oil
4.2e	$C(O)CH_3$	176.08	0.313	0.157	50	White solid
4.2f	CN	159.07	0.166	0.132	80	White solid
4.2g	NHAc	191.09	0.182	0.164	95	White solid
4.2h	Br	211.98	0.418	0.197	47	White solid

4.2b (Z = Me):

^{1}H NMR (400 MHz, $CDCl_3$) δ 6.99 – 6.88 (m, 2H), 6.77 – 6.66 (m, 1H), 6.16 – 5.94 (m, 1H), 5.31 – 5.08 (m, 2H), 4.86 (s, 1H), 3.43 – 3.34 (m, 2H), 2.27 (s, 3H). ^{13}C NMR (101 MHz, $CDCl_3$) δ 151.96, 136.68, 131.10, 130.25, 128.38, 125.14, 116.47, 115.79, 35.29, 20.61. These data are consistent with the reported literature values for NMR shifts.[171]

4.2c (Z = F):

^{1}H NMR (400 MHz, $CDCl_3$) δ 7.05 – 6.65 (m, 3H), 6.08 – 5.90 (m, 1H), 5.26 – 5.09 (m, 2H), 4.76 (br s, 1H), 3.43 – 3.33 (m, 2H). ^{13}C NMR (101 MHz, $CDCl_3$) δ 158.49, 156.12, 150.09, 135.67, 127.02, 117.21, 116.92, 116.74, 116.69, 116.65, 116.38, 116.30, 116.24, 116.01, 114.19, 113.96, 35.14. NB: some of the ^{13}C shifts are doublets caused by coupling to ^{19}F. These data are consistent with the reported literature values for NMR shifts.[172]

4.2d (Z = H):

^{1}H NMR (400 MHz, $CDCl_3$) δ 7.19 – 7.07 (m, 2H), 6.94 – 6.86 (m, 1H), 6.86 – 6.78 (m, 1H), 6.11 – 5.96 (m, 1H), 5.21 – 5.12 (m, 2H), 4.96 (br s, 1H), 3.51 – 3.29 (m, 2H). ^{13}C NMR (101 MHz, $CDCl_3$) δ 154.23, 136.52, 130.58, 128.05, 125.40, 121.10, 116.63, 115.95, 35.27. These data are consistent with the reported literature values for NMR shifts.[80]

4.2e (Z = $C(O)CH_3$):

^{1}H NMR (400 MHz, $CDCl_3$) δ 7.85 – 7.75 (m, 2H), 6.97 – 6.84 (m, 1H), 6.09 – 5.94 (m, 1H), 5.23 – 5.07 (m, 2H), 3.52 – 3.40 (m, 2H), 2.57 (s, 3H). ^{13}C NMR (101 MHz, $CDCl_3$) δ 198.25, 159.37, 135.86, 131.52, 130.13, 129.38, 126.08, 116.99, 115.64, 34.83, 26.45. Melting point: 113 – 114 °C (lit.[173] 115 – 116 °C). These data are consistent with the reported literature values for NMR shifts.[173]

4.2f (Z = CN):

^{1}H NMR (400 MHz, $CDCl_3$) δ 7.48 – 7.40 (m, 1H), 7.18 – 6.79 (m, 2H), 6.10 – 5.89 (m, 1H), 5.34 – 5.09 (m, 2H), 3.46 – 3.37 (m, 2H). ^{13}C NMR (101 MHz, $CDCl_3$) δ 158.07, 134.93, 134.65, 132.55,

130.59, 117.98, 116.65, 104.43, 34.61. Melting point: 80 – 82 °C (lit.[122] 83 – 84 °C). These data are consistent with the reported literature values for NMR shifts.[171]

4.2g (Z = NHAc):

^{1}H NMR (400 MHz, $CDCl_3$) δ 7.25 – 7.17 (m, 2H), 7.10 (br s, 1H), 6.81 – 6.69 (m, 1H), 6.07 – 5.90 (m, 1H), 5.19 – 5.11 (m, 2H), 3.48 – 3.31 (m, 2H), 2.14 (s, 3H). ^{13}C NMR (101 MHz, $CDCl_3$) δ 168.53, 151.36, 136.22, 130.85, 126.15, 123.09, 120.60, 116.83, 116.23, 35.16, 24.48. Melting point: 94 – 96 °C (lit.[79] 88 – 90 °C). No literature values have been reported for NMR shifts.

4.2h (Z = Br):

^{1}H NMR (400 MHz, $CDCl_3$) δ 7.32 – 7.17 (m, 2H), 6.75 – 6.64 (m, 1H), 6.09 – 5.85 (m, 1H), 5.29 – 5.08 (m, 2H), 4.93 (br s, 1H), 3.42 – 3.31 (m, 2H). ^{13}C NMR (101 MHz, $CDCl_3$) δ 153.37, 135.60, 133.12, 130.72, 127.78, 117.67, 117.35, 113.03, 34.95. Melting point: 58 – 60 °C (lit.[79] 58 – 60 °C). These data are consistent with the reported literature values for NMR shifts.[170]

4.2 On-line HPLC methods

4.2.1 Method 1: analysis of the reaction of **2.6**/**4.1a**

The on-line HPLC method utilised for analysis of the reaction of **2.6**/**4.1a** over different residence time ramps was the same as seen in Section 2.2.4.

4.2.2 Method 2: analysis method for 'one-pot' method

This on-line HPLC method was used for analysis of all aromatic Claisen rearrangement reactions performed in ethanol. This includes the time and temperature ramps for the reaction of **4.1d** on its own, all the 'one-pot' experiments, and the test substrate reactions.

The column used was a Restek Raptor C18 2.7 μm 50 mm x 2.1 mm running a gradient method in water

and acetonitrile as described in Table 6.29. In the method, the time after the gradient allowed the column to re-equilibrate to a steady state pressure before the following injection. This method allowed injections every 6.5 minutes.

Table 6.29. Key parameters set for the HPLC method used in this work for on-line HPLC analysis.

Flow rate / mL min^{-1}	0.7
Stoptime / min	5.75
Posttime / min	0.29
Solvent A	H_2O
Solvent B	MeCN
DAD wavelength / nm	210

Time / min	**%B**
0	25
1.2	30
3.5	50
3.51	60
3.85	60
3.86	25

The Agilent 1100 Autosampler 1 automatically switches the valve at the beginning of the injector program. The inputted injector cycle is a "WAIT" command for 0.10 min and then a "VALVE MAINPASS" command.

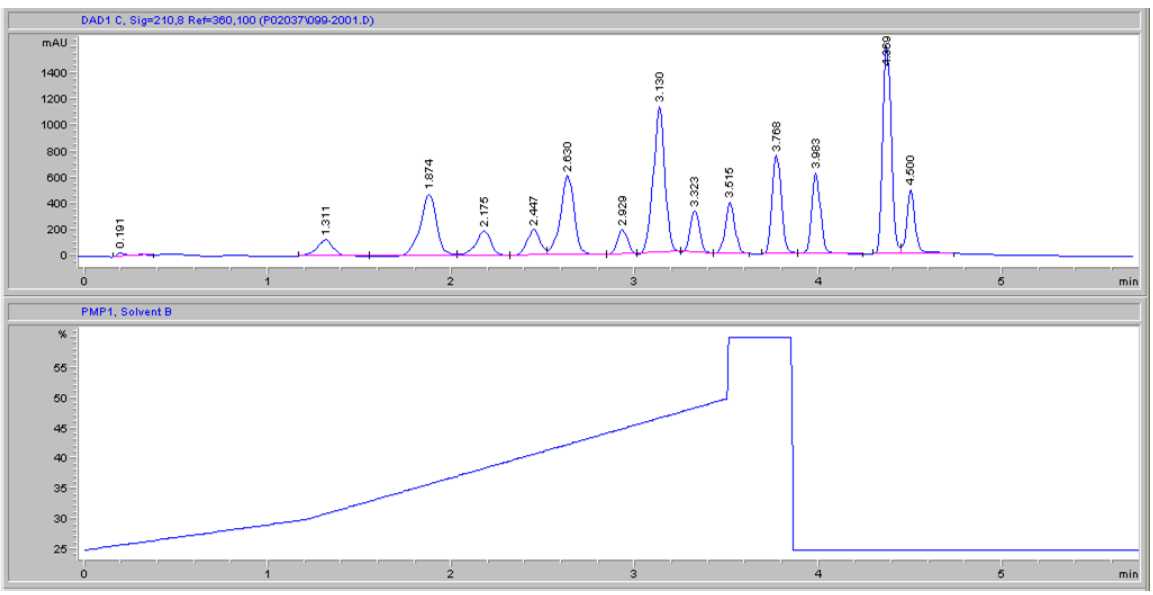


Figure 6.18. An example chromatogram of a "one-pot" method using the HPLC method discussed above. The lower diagram shows a diagrammatic representation of the HPLC method.

Table 6.30. Substituents for phenyl allyl ether substrates and their corresponding retention times in the HPLC method in Figure 6.18.

4.1/4.2	Z	Retention time of 4.1/ min	Retention time of 4.2/ min
a	*p*-MeO	3.52	1.87
b	*p*-Me	4.50	3.32
c	*p*-F	3.98	2.93
d	H	3.77	2.45
e	*p*-C(O)CH_3	2.63	1.31
f	*p*-CN	3.13	2.18
-	ethyl benzene	4.39	

4.2.3 Method 3: analysis method for reaction of **4.1d** for solvent ramps

The HPLC column used was a Restek Raptor C18 (2.7μm 50 mm x 2.1 mm) running an isocratic mixture of 40% acetonitrile in water. This method allowed injections every 2 minutes.

Table 6.31. Key parameters set for the HPLC method used in this example for on-line HPLC analysis.

Flow rate / mL min^{-1}	0.7
Stoptime / min	3.00
Posttime / min	0.29
Solvent A	H_2O
Solvent B	MeCN
DAD wavelength / nm	210

The Agilent 1100 Autosampler 1 automatically switches the valve at the beginning of the injector program. The inputted injector cycle is a “WAIT” command for 0.10 min and then a “VALVE MAINPASS” command.

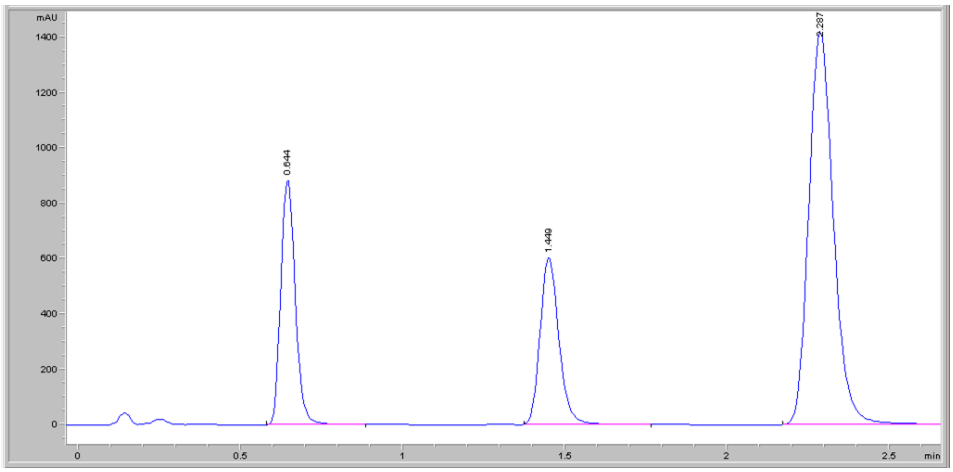


Figure 6.19. an example chromatogram obtained according to the HPLC method above for monitoring the reaction of allylphenylether (**4.1d**).

Table 6.32. Substituents for phenyl allyl ether substrates and their corresponding retention times in the HPLC method in Figure 6.19

compound	Retention time / min
allylphenylether	1.45
ortho-allylphenol	0.64
ethyl benzene	2.30

These data were concatenated by a python script which was developed. This script can be found at https://github.com/LindenSchrecker.

4.3 Transient flow experimental work

4.3.1 Solution preparation for flow experiments

Solutions were made for the flow experiments by pipetting 40 µL of ethyl benzene (as an internal standard) into a vial and noting the mass. This was then tared and the process repeated in the same vial with 30 µL of the given allyl phenyl ether **4.1** desired for the experiment. This was further repeated for the 'one-pot' experiments with further iterations was further allyl phenyl ethers.

The content of this vial was then washed into a volumetric flask (100 mL) with absolute ethanol, which

was then made up to 100 mL with the addition of absolute ethanol. This solution was mixed thoroughly by inversions and then filtered through a PTFE syringe filter (25 mm diameter, 0.45 μm pore) into a Duran bottle which had been carefully washed and dried to avoid particles being present. The solution was then attached to an inlet line on the flow system as described above.

5

4.3.2 Transient temperature ramp method

The data shown in Figures 4.6, 4.7, 4.9, 4.10, 4.14, 4.15, 4.16, and 4.17 were collected via transient temperature ramps. These were performed by priming the system at 2 mL min^{-1} for 4 minutes whilst heating the reactor to the desired initial temperature, controlled by the GC oven. The flow rate was then 10 lowered to 0.2 mL min^{-1} and a temperature ramp was programmed into the GC oven and executed. This ramp varied in timings and temperatures but in general began with a 30 minute hold at the initial temperature, then a ramp at a rate of 0.5 °C min^{-1} to achieve the final temperature which was then maintained for a further 30 minutes.

15 In order to confirm a lack of hysteresis in the system (differences in results from the order in which they are collected and how the conditions are implemented) temperature ramps were executed, in which in the same experimental run a ramp up to a temperature was followed by a ramp down over the same temperature range. These showed good consistency at a ramp rate of 0.5 °C min^{-1} whereas at a faster ramp rate of 1 °C min^{-1} this was not the case, as previously discussed by Jensen *et al.*.[15] Thus 0.5 °C 20 min^{-1} was chosen as a good ramp rate for accuracy and data density.

The rate of ramping was also important for the analysis of our data. We calculated the average temperature that each sample experienced in the reactor and used this value as the temperature of reaction in the Arrhenius plots. If the ramp rate were too high this could cause issues due to the exponential 25 dependency of the Arrhenius relationship on temperature. At a ramp rate of 0.5 °C min^{-1} each sample

experienced a temperature range of 10 °C.

On-line HPLC analysis was performed utilising on-line HPLC method 2, producing a data point every 6.5 minutes. These data were concatenated by a python script which was developed. This script can be found at https://github.com/LindenSchrecker.

4.4 Solvent ramping method

4.4.1 Solvent ramping method: single substrate

Multiple solutions were prepared containing **4.1** and **4.3** in known and equal quantities dissolved in different solvents or solvent mixtures. These were prepared either as 50 mL or 100 mL solution in volumetric flasks. Two of these solutions were attached to the inlet lines of the flow system and both pumps were primed for at least 3 minutes at 2 mL min^{-1}. The flow rate was decreased to 0.2 mL min^{-1} and the reactor temperature raised to 220 °C at 100 bar. A ramp was then controlled between the flow rate of the two pumps by the Gilson firmware either as a 25 minute ramp or 50 min ramp as described in tables 6.31 and 6.32.

Table 6.33. A standard 25 minute bi-directional solvent ramping pump method at 0.2 mL min^{-1}.

Experimental time / min	Cumulative flow rate / mL min^{-1}	%B (% of flow rate provided by pump B)
0	0.2	0
15	0.2	0
40	0.2	100
65	0.2	100
90	0.2	0
130	0.2	0

Table 6.34. A standard 50 minute bi-directional solvent ramping pump method at 0.2 mL min^{-1}.

Experimental time / min	Cumulative flow rate / mL min^{-1}	%B (% of flow rate provided by pump B)
0	0.2	0
20	0.2	0
70	0.2	100
90	0.2	100
140	0.2	0
180	0.2	0

Solvent ramps were performed in this manner between a range of different solutions having different solvent or solvent mixtures as described in Chapter 4, Section 6.

The HPLC samples, collected utilising on-line HPLC method 3, are then automatically analysed using a python script, which allows each sample to be assigned a time stamp and for the peak areas of **4.1**, **4.2**, and **4.3** to picked and collated. This data can then be stored as a csv file or visualised as seen in figure 4. The data series represented are for a bidirectional ramp in solvent composition to confirm that the data at each solvent composition is independent of the ramp direction (hysteresis).

4.4.2 Solvent ramping method for one-pot

A solution was prepared containing **4.1a–f** and **4.3** in known quantities (as listed in Table 6.33) dissolved in absolute ethanol in a 100 mL volumetric flask. This solution was attached to the A pump inlet line of the flow system and a solution of filtered distilled water was attached to the B pump inlet line. Both pumps were primed for at least 3 minutes at 2 mL min^{-1}. The flow rate was dropped to 0.2 mL min^{-1} and the reactor temperature raised to 200 °C at 100 bar. A ramp was then controlled between the flow rate of the two pumps by the Gilson firmware as described in the below Table 6.35.

Table 6.35. An example of the quantities of *para*-substituted phenyl allyl ethers (**4.1**) compounds used for the 'one-pot' solvent ramp experiment.

Compound	Mass / mg
4.1a	32.7
4.1b	28.0
4.1c	20.0
4.1d	28.8
4.1e	32.0
4.1f	25.7
4.3	34.8

Table 6.36. A 60 minute flow rate ramp utilised to study the 'one-pot' experiment over an ethanol-water ramp, leading to ten-fold dilution of the reactant solution.

Experimental time / min	Cumulative flow rate / mL min^{-1}	%B (% of flow rate provide by pump B)
0	0.2	0
30	0.2	0
90	0.2	90
120	0.2	90

The HPLC samples, collected utilising on-line HPLC method 2, were then automatically analysed using a python script which allows each sample to be assigned a time stamp and for the peak areas of **4.1a-f**, **4.2a-f**, and **4.3** to be picked and collated. This data can then be stored as a csv file or visualised as the yield of each reaction *vs.* w/v% water in ethanol.

The output of the above method is a series of data points for the % yield of all six chemical reactions across a spectrum of the ratios of solvent or solvent mixtures. The method allows, for the first time, for the data relating to multiple reactions to be collected in a continuous manner and in bulk.

References

(1) National Academy of Sciences, N. A. of E. and I. of M. Ensuring the Integrity, Accessibility, and Stewardship of Research Data in the Digital Age. *Ensuring Integrity, Access. Steward. Res. Data Digit. Age* **2009**. https://doi.org/10.17226/12615.

(2) Bordawekar, S.; Chanda, A.; Daly, A. M.; Garrett, A. W.; Higgins, J. P.; LaPack, M. A.; Maloney, T. D.; Morgado, J.; Mukherjee, S.; Orr, J. D.; et al. Industry Perspectives on Process Analytical Technology: Tools and Applications in API Manufacturing. *Organic Process Research and Development*. 2015, pp 1174–1185. https://doi.org/10.1021/acs.oprd.5b00088.

(3) Shevlin, M. Practical High-Throughput Experimentation for Chemists. *ACS Med. Chem. Lett.* **2017**, *8* (6), 601–607. https://doi.org/10.1021/acsmedchemlett.7b00165.

(4) Hartman, R. L.; McMullen, J. P.; Jensen, K. F. Deciding Whether To Go with the Flow: Evaluating the Merits of Flow Reactors for Synthesis. *Angew. Chemie Int. Ed.* **2011**, *50* (33), 7502–7519. https://doi.org/10.1002/ANIE.201004637.

(5) Plutschack, M. B.; Pieber, B.; Gilmore, K.; Seeberger, P. H. The Hitchhiker's Guide to Flow Chemistry. *Chemical Reviews*. 2017, pp 11796–11893. https://doi.org/10.1021/acs.chemrev.7b00183.

(6) Taylor, C. J.; Manson, J. A.; Clemens, G.; Taylor, B. A.; Chamberlain, T. W.; Bourne, R. A. Modern Advancements in Continuous-Flow Aided Kinetic Analysis. *React. Chem. Eng.* **2022**, *7* (5), 1037–1046. https://doi.org/10.1039/D1RE00467K.

(7) Schmidt, O. P.; Dechert-Schmitt, A. M.; Garnsey, M. R.; Wisniewska, H. M.; Blackmond, D. G. Kinetic Analysis of Catalytic Organic Reactions Using a Temperature Scanning Protocol. *ChemCatChem* **2019**, *11* (16), 3808–3813. https://doi.org/10.1002/cctc.201900560.

(8) Schmidt, O. P.; Blackmond, D. G. Temperature-Scanning Reaction Protocol Offers Insights into Activation Parameters in the Buchwald-Hartwig Pd-Catalyzed Amination of Aryl Halides. *ACS Catal.* **2020**, *10* (15), 8926–8932. https://doi.org/10.1021/acscatal.0c01929.

(9) Hone, C. A.; Kappe, C. O. Towards the Standardization of Flow Chemistry Protocols for Organic Reactions. *Chem. - Methods* **2021**, *1* (11), 454–467. https://doi.org/10.1002/CMTD.202100059.

(10) Ładosz, A.; Kuhnle, C.; Jensen, K. F. Characterization of Reaction Enthalpy and Kinetics in a Microscale Flow Platform. *React. Chem. Eng.* **2020**, *5* (11), 2115–2122. https://doi.org/10.1039/D0RE00304B.

(11) Gibson, Q. H. Stopped-Flow Apparatus for the Study of Rapid Reactions. *Discuss. Faraday Soc.* **1954**, *17*, 137–139. https://doi.org/10.1039/DF9541700137.

(12) Levenspiel, O. *Chemical Reaction Engineering, 3rd Edition*; 1998.

(13) Konermann, L. Monitoring Reaction Kinetics in Solution by Continuous-Flow Methods: The Effects of Convection and Molecular Diffusion under Laminar Flow Conditions. *J. Phys. Chem. A* **1999**, *103* (36), 7210–7216. https://doi.org/10.1021/JP9908350.

(14) Trojanowicz, M. Flow Chemistry vs. Flow Analysis. *Talanta* **2016**, *146*, 621–640. https://doi.org/10.1016/j.talanta.2015.07.043.

(15) Florit, F.; Nambiar, A. M. K.; Breen, C. P.; Jamison, T. F.; Jensen, K. F. Design of Dynamic Trajectories for Efficient and Data-Rich Exploration of Flow Reaction Design Spaces. *React. Chem. Eng.* **2021**, *6* (12), 2306–2314. https://doi.org/10.1039/D1RE00350J.

(16) Minnich, C.; Hardy, S.; Krämer, S. Stopping the Babylonian Confusion: An Updated Nomenclature for Process Analyzers in PAT Applications. *Chemie-Ingenieur-Technik* **2016**, *88* (6), 694–697. https://doi.org/10.1002/cite.201500188.

(17) Gomez, M. V.; de la Hoz, A. NMR Reaction Monitoring in Flow Synthesis. *Beilstein J. Org. Chem.* **2017**, *13* (1), 285–300. https://doi.org/10.3762/bjoc.13.31.

(18) Giraudeau, P.; Felpin, F. X. Flow Reactors Integrated with In-Line Monitoring Using Benchtop NMR Spectroscopy. *React. Chem. Eng.* **2018**, *3*

(4), 399–413. https://doi.org/10.1039/c8re00083b.

(19) Perro, A.; Lebourdon, G.; Henry, S.; Lecomte, S.; Servant, L.; Marre, S. Combining Microfluidics and FT-IR Spectroscopy: Towards Spatially Resolved Information on Chemical Processes. *Reaction Chemistry and Engineering*. Royal Society of Chemistry December 1, 2016, pp 577–594. https://doi.org/10.1039/c6re00127k.

(20) Ley, S. V; Ingham, R. J.; O'Brien, M.; Browne, D. L. Camera-Enabled Techniques for Organic Synthesis. *Beilstein Journal of Organic Chemistry*. Beilstein-Institut May 31, 2013, pp 1051–1072. https://doi.org/10.3762/bjoc.9.118.

(21) Yue, J.; Schouten, J. C.; Alexander Nijhuis, T. Integration of Microreactors with Spectroscopic Detection for Online Reaction Monitoring and Catalyst Characterization. *Ind. Eng. Chem. Res.* **2012**, *51* (45), 14583–14609. https://doi.org/10.1021/ie301258j.

(22) Baumann, M. Integrating Continuous Flow Synthesis with In-Line Analysis and Data Generation. *Org. Biomol. Chem.* **2018**, *16* (33), 5946–5954. https://doi.org/10.1039/C8OB01437J.

(23) Rodriguez-Zubiri, M.; Felpin, F. O.-X. Analytical Tools Integrated in Continuous-Flow Reactors: Which One for What? *Org. Process Res. Dev.* **2022**, *26* (6), 1766–1793. https://doi.org/10.1021/ACS.OPRD.2C00102.

(24) Biancolillo, A.; Marini, F. Chemometric Methods for Spectroscopy-Based Pharmaceutical Analysis. *Front. Chem.* **2018**, *6* (NOV), 1–14. https://doi.org/10.3389/fchem.2018.00576.

(25) Swartz, M. HPLC Detectors: A Brief Review. *Journal of Liquid Chromatography and Related Technologies*. 2010, pp 1130–1150. https://doi.org/10.1080/10826076.2010.484356.

(26) Christensen, M.; Adedeji, F.; Grosser, S.; Zawatzky, K.; Ji, Y.; Liu, J.; Jurica, J. A.; Naber, J. R.; Hein, J. E. Development of an Automated Kinetic Profiling System with Online HPLC for Reaction Optimization. *React. Chem. Eng.* **2019**, *4* (9), 1555–1558. https://doi.org/10.1039/c9re00086k.

(27) Parrott, A. J.; Bourne, R. A.; Akien, G. R.; Irvine, D. J.; Poliakoff, M. Self-Optimizing Continuous Reactions in Supercritical Carbon Dioxide. *Angew. Chemie - Int. Ed.* **2011**, *50* (16), 3788–3792. https://doi.org/10.1002/anie.201100412.

(28) Herck, J. Van; Abeysekera, I.; Buckinx, A.-L.; Cai, K.; Hooker, J.; Thakur, K.; Reydt, E. Van de; Voorter, P.-J.; Wyers, D.; Junkers, T. Operator-Independent High-Throughput Polymerization Screening Based on Automated Inline NMR and Online SEC. *Digit. Discov.* **2022**, *1* (4), 519–526. https://doi.org/10.1039/D2DD00035K.

(29) Bhati, C.; Minocha, N.; Purohit, D.; Kumar, S.; Makhija, M.; Saini, S.; Kaushik, D.; Pandey, P. High Performance Liquid Chromatography: Recent Patents and Advancement. *Biomed. Pharmacol. J.* **2022**, *15* (2), 729–746. https://doi.org/10.13005/BPJ/2411.

(30) Haas, C. P.; Lübbesmeyer, M.; Jin, E. H.; McDonald, M. A.; Koscher, B. A.; Guimond, N.; Di Rocco, L.; Kayser, H.; Leweke, S.; Niedenführ, S.; et al. Open-Source Chromatographic Data Analysis for Reaction Optimization and Screening. *ACS Cent. Sci.* **2023**, *9* (2), 307–317. https://doi.org/10.1021/acscentsci.2c01042.

(31) Valera, F. E.; Quaranta, M.; Moran, A.; Blacker, J.; Armstrong, A.; Cabral, J. T.; Blackmond, D. G. The Flow's the Thing…Or Is It? Assessing the Merits of Homogeneous Reactions in Flask and Flow. *Angew. Chemie Int. Ed.* **2010**, *49* (14), 2478–2485. https://doi.org/10.1002/anie.200906095.

(32) Gomez, M. V.; Verputten, H. H. J.; Díaz-Ortíz, A.; Moreno, A.; De La Hoz, A.; Velders, A. H. On-Line Monitoring of a Microwave-Assisted Chemical Reaction by Nanolitre NMR-Spectroscopy. *Chem. Commun.* **2010**, *46* (25), 4514–4516. https://doi.org/10.1039/B924936B.

(33) Drelinkiewicz, D.; Alston, S. T.; Durand, T.; Whitby, R. J. The Switch-off Method: Rapid Investigation of Flow Photochemical Reactions. *React. Chem. Eng.* **2023**. https://doi.org/10.1039/d3re00261f.

(34) Vandekerckhove, B.; Piens, N.; Metten, B.; Stevens, C. V.; Heugebaert, T. S. A. Practical Ferrioxalate Actinometry for the Determination of Photon Fluxes in Production-Oriented Photoflow Reactors. *Org. Process Res. Dev.* **2022**. https://doi.org/10.1021/ACS.OPRD.2C00079.

(35) Müller, S. T. R.; Murat, A.; Maillos, D.; Lesimple, P.; Hellier, P.; Wirth, T. Rapid Generation and Safe Use of Carbenes Enabled by a Novel Flow Protocol with In-Line IR Spectroscopy. *Chem. - A Eur. J.* **2015**, *21* (19), 7016–7020. https://doi.org/10.1002/chem.201500416.

(36) Rütti, D. P.; Moser, M.; Georg, A. G.; Spier, E. S.; Meier, D. M. Kinetic Data for Continuous Processes from Liquid-Liquid Loop Reactor Experiments. *Chemie-Ingenieur-Technik* **2021**, *93* (8), 1267–1272. https://doi.org/10.1002/CITE.202100005.

(37) Sullivan, R. J.; Newman, S. G. Reaction Cycling for Kinetic Analysis in Flow. *J. Org. Chem.* **2020**, *85* (8), 5464–5474. https://doi.org/10.1021/ACS.JOC.0C00216/ASSET/IMAGES/LARGE/JO0C00216_0007.JPEG.

(38) Zhang, C.; Zhang, J.; Luo, G. Kinetics Determination of Fast Exothermic Reactions with Infrared Thermography in a Microreactor. *J. Flow Chem.* **2020**, *10* (1), 219–226. https://doi.org/10.1007/s41981-019-00071-8.

(39) Mozharov, S.; Nordon, A.; Littlejohn, D.; Wiles, C.; Watts, P.; Dallin, P.; Girkin, J. M. Improved Method for Kinetic Studies in Microreactors Using Flow Manipulation and Noninvasive Raman Spectrometry. *J. Am. Chem. Soc.* **2011**, *133* (10), 3601–3608. https://doi.org/10.1021/ja1102234.

(40) Durand, T.; Henry, C.; Bolien, D.; Harrowven, D. C.; Bloodworth, S.; Franck, X.; Whitby, R. J. Thermolysis of 1,3-Dioxin-4-Ones: Fast Generation of Kinetic Data Using in-Line Analysis under Flow. *React. Chem. Eng.* **2016**, *1* (1), 82–89. https://doi.org/10.1039/c5re00007f.

(41) Haas, C. P.; Biesenroth, S.; Buckenmaier, S.; Van De Goor, T.; Tallarek, U. Automated Generation of Photochemical Reaction Data by Transient Flow Experiments Coupled with Online HPLC Analysis. *React. Chem. Eng.* **2020**, *5* (5), 912–920. https://doi.org/10.1039/d0re00066c.

(42) Haven, J. J.; Vandenbergh, J.; Junkers, T. Watching Polymers Grow: Real Time Monitoring of Polymerizations via an on-Line ESI-MS/Microreactor Coupling. *Chem. Commun.* **2015**, *51* (22), 4611–4614. https://doi.org/10.1039/c4cc10426a.

(43) Haven, J. J.; Zaquen, N.; Rubens, M.; Junkers, T. The Kinetics of N-Butyl Acrylate Radical Polymerization Revealed in a Single Experiment by Real Time On-Line Mass Spectrometry Monitoring. *Macromol. React. Eng.* **2017**, *11* (4), 1–12. https://doi.org/10.1002/mren.201700016.

(44) Parkinson, S.; Hondow, N. S.; Conteh, J. S.; Bourne, R. A.; Warren, N. J. All-Aqueous Continuous-Flow RAFT Dispersion Polymerisation for Efficient Preparation of Diblock Copolymer Spheres, Worms and Vesicles. *React. Chem. Eng.* **2019**, *4* (5), 852–861. https://doi.org/10.1039/C8RE00211H.

(45) Knox, S. T.; Parkinson, S.; Stone, R.; Warren, N. J. Benchtop Flow-NMR for Rapid Online Monitoring of RAFT and Free Radical Polymerisation in Batch and Continuous Reactors. *Polym. Chem.* **2019**, *10* (35), 4774–4778. https://doi.org/10.1039/c9py00982e.

(46) Herck, J. Van; Junkers, T. Rapid Kinetic Screening via Transient Timesweep Experiments in Continuous Flow Reactors. *Chem. - Methods* **2022**, *2* (1), e202100090. https://doi.org/10.1002/CMTD.202100090.

(47) Schwolow, S.; Braun, F.; Rädle, M.; Kockmann, N.; Röder, T. Fast and Efficient Acquisition of Kinetic Data in Microreactors Using In-Line Raman Analysis. *Org. Process Res. Dev.* **2015**, *19* (9), 1286–1292. https://doi.org/10.1021/acs.oprd.5b00184.

(48) Hone, C. A.; Holmes, N.; Akien, G. R.; Bourne, R. A.; Muller, F. L. Rapid Multistep Kinetic Model Generation from Transient Flow Data. *React. Chem. Eng.* **2017**, *2* (2), 103–108. https://doi.org/10.1039/c6re00109b.

(49) Moore, J. S.; Jensen, K. F. "Batch" Kinetics in Flow: Online IR Analysis and Continuous Control. *Angew. Chemie Int. Ed.* **2014**, *53* (2), 470–473. https://doi.org/10.1002/ANIE.201306468.

(50) Taylor, N. G.; Reis, M. H.; Varner, T. P.; Rapp, J. L.; Sarabia, A.; Leibfarth, F. A. A Dual Initiator Approach for Oxygen Tolerant RAFT

Polymerization. *Polym. Chem.* **2022**, *13* (33), 4798–4808. https://doi.org/10.1039/d2py00603k.

(51) Kleijwegt, R. J. T.; Doruiter, S. Y.; Winkenwerder, W.; van der Schaaf, J. Investigating Tertiary Amine Alkylation/Benzylation Kinetics with Ramp-Flow in a Plug-Flow Reactor Using in-Line 1H NMR Spectroscopy. *Chem. Eng. Res. Des.* **2021**, *168*, 317–326. https://doi.org/10.1016/J.CHERD.2021.02.021.

(52) Reizman, B. J.; Jensen, K. F. An Automated Continuous-Flow Platform for the Estimation of Multistep Reaction Kinetics. *Org. Process Res. Dev.* **2012**, *16* (11), 1770–1782. https://doi.org/10.1021/op3001838.

(53) Taylor, C. J.; Booth, M.; Manson, J. A.; Willis, M. J.; Clemens, G.; Taylor, B. A.; Chamberlain, T. W.; Bourne, R. A. Rapid, Automated Determination of Reaction Models and Kinetic Parameters. *Chem. Eng. J.* **2021**, *413* (June 2020), 127017. https://doi.org/10.1016/j.cej.2020.127017.

(54) Ringborg, R. H.; Toftgaard Pedersen, A.; Woodley, J. M. Automated Determination of Oxygen-Dependent Enzyme Kinetics in a Tube-in-Tube Flow Reactor. *ChemCatChem* **2017**, *9* (17), 3285–3288. https://doi.org/10.1002/CCTC.201700811.

(55) Duan, X.; Tu, J.; Teixeira, A. R.; Sang, L.; Jensen, K. F.; Zhang, J. An Automated Flow Platform for Accurate Determination of Gas–Liquid–Solid Reaction Kinetics. *React. Chem. Eng.* **2020**, *5* (9), 1751–1758. https://doi.org/10.1039/D0RE00191K.

(56) Schaber, S. D.; Born, S. C.; Jensen, K. F.; Barton, P. I. Design, Execution, and Analysis of Time-Varying Experiments for Model Discrimination and Parameter Estimation in Microreactors. *Org. Process Res. Dev.* **2014**, *18* (11), 1461–1467. https://doi.org/10.1021/OP500179R/SUPPL_FILE/OP500179R_SI_001.PDF.

(57) Moore, J. S.; Smith, C. D.; Jensen, K. F. Kinetics Analysis and Automated Online Screening of Aminocarbonylation of Aryl Halides in Flow. *React. Chem. Eng.* **2016**, *1* (3), 272–279. https://doi.org/10.1039/C6RE00007J.

(58) Aroh, K. C.; Jensen, K. F. Efficient Kinetic Experiments in Continuous Flow Microreactors. *React. Chem. Eng.* **2018**, *3* (1), 94–101. https://doi.org/10.1039/c7re00163k.

(59) McMullen, J. P.; Jensen, K. F. Rapid Determination of Reaction Kinetics with an Automated Microfluidic System. *Org. Process Res. Dev.* **2011**, *15* (2), 398–407. https://doi.org/10.1021/op100300p.

(60) Sagmeister, P.; Poms, J.; Williams, J. D.; Kappe, C. O. Multivariate Analysis of Inline Benchtop NMR Data Enables Rapid Optimization of a Complex Nitration in Flow. *React. Chem. Eng.* **2020**, *5* (4), 677–684. https://doi.org/10.1039/D0RE00048E.

(61) Waldron, C.; Pankajakshan, A.; Quaglio, M.; Cao, E.; Galvanin, F.; Gavriilidis, A. An Autonomous Microreactor Platform for the Rapid Identification of Kinetic Models. *React. Chem. Eng.* **2019**, *4* (9), 1623–1636. https://doi.org/10.1039/c8re00345a.

(62) Waldron, C.; Pankajakshan, A.; Quaglio, M.; Cao, E.; Galvanin, F.; Gavriilidis, A. Model-Based Design of Transient Flow Experiments for the Identification of Kinetic Parameters. *React. Chem. Eng.* **2020**, *5* (1), 112–123. https://doi.org/10.1039/c9re00342h.

(63) Gomez, M. V.; Rodriguez, A. M.; De La Hoz, A.; Jimenez-Marquez, F.; Fratila, R. M.; Barneveld, P. A.; Velders, A. H. Determination of Kinetic Parameters within a Single Nonisothermal On-Flow Experiment by Nanoliter NMR Spectroscopy. *Anal. Chem.* **2015**, *87* (20), 10547–10555. https://doi.org/10.1021/acs.analchem.5b02811.

(64) Williams, P. J. H.; Killeen, C.; Chagunda, I. C.; Henderson, B.; Donnecke, S.; Munro, W.; Sidhu, J.; Kraft, D.; Harrington, D. A.; Mcindoe, J. S. Continuous Addition Kinetic Elucidation: Catalyst and Reactant Order, Rate Constant, and Poisoning from a Single Experiment. **2022**. https://doi.org/10.26434/CHEMRXIV-2022-52G7Z.

(65) Meissner, M. P.; Nordblad, M.; Woodley, J. M. Online Measurement of Oxygen-Dependent Enzyme Reaction Kinetics. *ChemBioChem* **2018**, *19* (1), 106–113. https://doi.org/10.1002/CBIC.201700577.

(66) O'Neal, E. J.; Lee, C. H.; Brathwaite, J.; Jensen, K. F. Continuous Nanofiltration and Recycle of an Asymmetric Ketone Hydrogenation Catalyst. *ACS Catal.* **2015**, *5* (4), 2615–2622. https://doi.org/10.1021/acscatal.5b00149.

(67) Wyvratt, B. M.; McMullen, J. P.; Grosser, S. T. Multidimensional Dynamic Experiments for Data-Rich Process Development of Reactions in Flow. *React. Chem. Eng.* **2019**, *4* (9), 1637–1645. https://doi.org/10.1039/c9re00078j.

(68) McMullen, J. P.; Wyvratt, B. M. Automated Optimization under Dynamic Flow Conditions. *React. Chem. Eng.* **2022**, *8* (1), 137–151. https://doi.org/10.1039/d2re00256f.

(69) Sagmeister, P.; Schiller, C.; Weiss, P.; Silber, K.; Knoll, S.; Horn, M.; Hone, C. A.; Williams, J.; Kappe, C. O. Accelerating Reaction Modeling Using Dynamic Flow Experiments, Part 1: Design Space Exploration. *React. Chem. Eng.* **2023**. https://doi.org/10.1039/D3RE00243H.

(70) Echtermeyer, A.; Amar, Y.; Zakrzewski, J.; Lapkin, A. Self-Optimisation and Model-Based Design of Experiments for Developing a C-H Activation Flow Process. In *Food, Pharmaceutical and Bioengineering Division 2017 - Core Programming Area at the 2017 AIChE Annual Meeting*; AIChE, 2017; Vol. 2, pp 747–760. https://doi.org/10.3762/bjoc.13.18.

(71) Pankajakshan, A.; Waldron, C.; Quaglio, M.; Gavriilidis, A.; Galvanin, F. A Multi-Objective Optimal Experimental Design Framework for Enhancing the Efficiency of Online Model Identification Platforms. *Engineering* **2019**, *5* (6), 1049–1059. https://doi.org/10.1016/J.ENG.2019.10.003.

(72) Folch, J. P.; Zhang, S.; Lee, R. M.; Shafei, B.; Walz, D.; Tsay, C.; van der Wilk, M.; Misener, R. SnAKe: Bayesian Optimization with Pathwise Exploration. **2022**. https://doi.org/10.48550/arxiv.2202.00060.

(73) Schwalbe, T.; Autze, V.; Kursawe, A.; Sahin, K. System and Method for Determining Optimal Reaction Parameters Using Continuously Running Process. WO2004092908, 2004.

(74) Asprey, S. P.; Wojciechowski, B. W.; Rice, N. M.; Dorcas, A. Applications of Temperature Scanning in Kinetic Investigations: The Hydrolysis of Acetic Anhydride. *Chem. Eng. Sci.* **1996**, *51* (20), 4681–4692. https://doi.org/10.1016/0009-2509(96)00306-5.

(75) Zogg, A.; Stoessel, F.; Fischer, U.; Hungerbühler, K. Isothermal Reaction Calorimetry as a Tool for Kinetic Analysis. *Thermochim. Acta* **2004**, *419* (1–2), 1–17. https://doi.org/10.1016/j.tca.2004.01.015.

(76) Satchell, D. P. N.; Wassef, W. N.; Bhatti, Z. A. The Kinetics and Mechanism of the Mineral Acid-Catalysed Hydrolysis of Carboxylic Acid Anhydrides in Water and in Dioxane - Water Mixtures. Application of the Excess Acidity Function to These Systems. *J. Chem. Soc. Perkin Trans. 2* **1993**, *2* (12), 2373–2379. https://doi.org/10.1039/p29930002373.

(77) Bunton, C. A.; Fuller, N. A.; Perry, S. G.; Shiner, V. J. The Hydrolysis of Carboxylic Anhydrides. Part III.* Reactions in Initially Neutral Solution. *J. Chem. Soc.* **1963**, *44* (2), 3028–3036. https://doi.org/10.1039/jr9630002918.

(78) Poh, J.-S.; Browne, D. L.; Ley, S. V. A Multistep Continuous Flow Synthesis Machine for the Preparation of Pyrazoles via a Metal-Free Amine-Redox Process. *React. Chem. Eng.* **2016**, *1* (1), 101–105. https://doi.org/10.1039/C5RE00082C.

(79) White, W. N.; Gwynn, D.; Schlitt, R.; Girard, C.; Fife, W. The Ortho-Claisen Rearrangement. I. The Effect of Substituents on the Rearrangement of Allyl p-X-Phenyl Ethers. *J. Am. Chem. Soc.* **1958**, *80* (13), 3271–3277. https://doi.org/10.1021/JA01546A023/ASSET/JA01546A023.FP.PNG_V03.

(80) Kobayashi, H.; Driessen, B.; Van Osch, D. J. G. P.; Talla, A.; Ookawara, S.; Noël, T.; Hessel, V. The Impact of Novel Process Windows on the Claisen Rearrangement. *Tetrahedron* **2013**, *69* (14), 2885–2890. https://doi.org/10.1016/j.tet.2013.02.038.

(81) Dymond, J. H.; Malhotra, R. The Tait Equation: 100 Years On. *Int. J. Thermophys.* **1988**, *9* (6), 941–951. https://doi.org/10.1007/BF01133262/METRICS.

(82) Fustero, S.; S Anchez-Rosell, M.; Barrio, P.; Sim On-Fuentes, A. From 2000 to Mid-2010: A Fruitful Decade for the Synthesis of Pyrazoles. *Chem. Rev* **2011**, *111*, 6984–7034. https://doi.org/10.1021/cr2000459.

(83) Ansari, A.; Ali, A.; Asif, M.; Shamsuzzaman. Review: Biologically Active Pyrazole Derivatives. *New J. Chem.* **2016**, *41* (1), 16–41. https://doi.org/10.1039/c6nj03181a.

(84) Das, A.; Ishitani, H.; Kobayashi, S. Toward Continuous-Flow Synthesis of Biologically Interesting Pyrazole Derivatives. *Adv. Synth. Catal.* **2019**, *361* (22), 5127–5132. https://doi.org/10.1002/adsc.201900954.

(85) Zhang, X.; Kang, J.; Niu, P.; Wu, J.; Yu, W.; Chang, J. I2-Mediated Oxidative C-N Bond Formation for Metal-Free One-Pot Synthesis of Di-, Tri-, and Tetrasubstituted Pyrazoles from α,β-Unsaturated Aldehydes/Ketones and Hydrazines. *J. Org. Chem.* **2014**, *79* (21), 10170–10178. https://doi.org/10.1021/jo501844x.

(86) Deng, X.; Mani, N. S. Reaction of N-Monosubstituted Hydrazones with Nitroolefins: A Novel Regioselective Pyrazole Synthesis. *Org. Lett.* **2006**, *8* (16), 3505–3508. https://doi.org/10.1021/OL061226V.

(87) Muzalevskiy, V. M.; Rulev, A. Y.; Romanov, A. R.; Kondrashov, E. V.; Ushakov, I. A.; Chertkov, V. A.; Nenajdenko, V. G. Selective, Metal-Free Approach to 3- or 5-CF_3-Pyrazoles: Solvent Switchable Reaction of CF_3-Ynones with Hydrazines. *J. Org. Chem.* **2017**, *82* (14), 7200–7214. https://doi.org/10.1021/acs.joc.7b00774.

(88) Tinarelli, A.; Righi, P.; Rosini, G.; Andreotti, D.; Profeta, R.; Spada, S. Regioselective Synthesis of 1,3,5- and 1,3,4,5-Substituted Pyrazoles via Acylation of N-Boc-N-Substituted Hydrazones. *Tetrahedron* **2011**, *67* (3), 612–617. https://doi.org/10.1016/j.tet.2010.11.057.

(89) Fan, X. W.; Lei, T.; Zhou, C.; Meng, Q. Y.; Chen, B.; Tung, C. H.; Wu, L. Z. Radical Addition of Hydrazones by α-Bromo Ketones to Prepare 1,3,5-Trisubstituted Pyrazoles via Visible Light Catalysis. *J. Org. Chem.* **2016**, *81* (16), 7127–7133. https://doi.org/10.1021/acs.joc.6b00992.

(90) Duan, L.; Zhou, H.; Gu, Y.; Gong, P.; Qin, M. The Use of Enaminones and Enamines as Effective Synthons for MSA-Catalyzed Regioselective Synthesis of 1,3,4-Tri- And 1,3,4,5-Tetrasubstituted Pyrazoles. *New J. Chem.* **2019**, *43* (41), 16131–16137. https://doi.org/10.1039/c9nj03701b.

(91) Singh, S. K.; Srinivasa Reddy, M.; Shivaramakrishna, S.; Kavitha, D.; Vasudev, R.; Babu, J. M.; Sivalakshmidevi, A.; Rao, Y. K. Modified Reaction Conditions to Achieve High Regioselectivity in the Two Component Synthesis of 1,5-Diarylpyrazoles. *Tetrahedron Lett.* **2004**, *45* (41), 7679–7682. https://doi.org/10.1016/J.TETLET.2004.08.100.

(92) Norris, T.; Colon-Cruz, R.; Ripin, D. H. B. New Hydroxy-Pyrazoline Intermediates, Subtle Regio-Selectivity and Relative Reaction Rate Variations Observed during Acid Catalyzed and Neutral Pyrazole Cyclization. *Org. Biomol. Chem.* **2005**, *3* (10), 1844–1849. https://doi.org/10.1039/b500413f.

(93) Singh, S. P.; Kumar, D.; Batra, H.; Naithani, R.; Rozas, I.; Elguero, J. The Reaction between Hydrazines and β-Dicarbonyl Compounds: Proposal for a Mechanism. *Can. J. Chem.* **2000**, *78* (8), 1109–1120. https://doi.org/10.1139/v00-104.

(94) Singh, S. P.; Kumar, V.; Aggarwal, R.; Elguero, J. The Reaction of Aryl and Heteroarylhydrazines with Aryl-Trifluoromethyl β-Diketones. *J. Heterocycl. Chem.* **2006**, *43* (4), 1003–1014. https://doi.org/10.1002/JHET.5570430428.

(95) Sloop, J. C.; Lechner, B.; Washington, G.; Bumgardner, C. L.; Loehle, W. D.; Creasy, W. Pyrazole Formation: Examination of Kinetics, Substituent Effects, and Mechanistic Pathways. *Int. J. Chem. Kinet.* **2008**, *40* (7), 370–383. https://doi.org/10.1002/kin.20316.

(96) Selivanov, S. I.; Golodova, K. G.; Ershov, B. A. NMR Studies of Formation Mechanisms of Heterocycles. IV. Carbon-13 NMR of Intermediates in the Reaction of 1,3-Diketones with Hydrazine. *Zhurnal Org. Khimii* **1986**, *22* (10), 2073–2081.

(97) Schrecker, L.; Dickhaut, J.; Holtze, C.; Staehle, P.; Vranceanu, M.; Hellgardt, K.; Hii, K. K. Discovery of Unexpectedly Complex Reaction Pathways for the Knorr Pyrazole Synthesis via Transient Flow. *React. Chem. Eng.* **2023**, *8* (1), 41–46. https://doi.org/10.1039/d2re00271j.

(98) Schrecker, L. MRes Dissertation: “Understanding the Knorr Pyrazole Synthesis : A Data-Led Approach.” *Imp. MRes Diss.* **2020**.

(99) Burés, J. Variable Time Normalization Analysis: General Graphical Elucidation of Reaction Orders from Concentration Profiles. *Angew. Chemie - Int. Ed.* **2016**, *55* (52), 16084–16087. https://doi.org/10.1002/anie.201609757.

(100) Zelenin, K. N.; Malov, M. Y.; Bezhan, I. P.; Khrustalev, V. A.; Yakimovich, S. I. Structure of Bis (Acylhydrazones) of 1,3-Dioxo Compounds. *Chemistry of Heterocyclic Compounds*. 1985, pp 713–714. https://doi.org/10.1007/BF00515087.

(101) Zelenin, K. N.; Malov, M. Y.; Yakimovich, S. I. Reaction of 3,3-Dimethyl-2,4-Pentanedione with Phenylhydrazine. *Zhurnal Org. Khimii* **1986**, No. 5, 1096–1097.

(102) Berkeley Madonna https://berkeley-madonna.myshopify.com/ (accessed Feb 17, 2022).

(103) Hoffmann, R. W. Allylic 1,3-Strain as a Controlling Factor in Stereoselective Transformations. *Chem. Rev.* **1989**, *89* (8), 1841–1860. https://doi.org/10.1021/cr00098a009.

(104) Fustero, S.; Román, R.; Sanz-Cervera, J. F.; Simón-Fuentes, A.; Cuñat, A. C.; Villanova, S.; Murguía, M. Improved Regioselectivity in Pyrazole Formation through the Use of Fluorinated Alcohols as Solvents: Synthesis and Biological Activity of Fluorinated Tebufenpyrad Analogs. *J. Org. Chem.* **2008**, *73* (9), 3523–3529. https://doi.org/10.1021/jo800251g.

(105) Tu, Z.; Stuyver, T.; Coley, C. W. Predictive Chemistry: Machine Learning for Reaction Deployment, Reaction Development, and Reaction Discovery. *Chem. Sci.* **2022**, *14* (2), 226–244. https://doi.org/10.1039/d2sc05089g.

(106) Mennen, S. M.; Alhambra, C.; Allen, C. L.; Barberis, M.; Berritt, S.; Brandt, T. A.; Campbell, A. D.; Castañón, J.; Cherney, A. H.; Christensen, M.; et al. The Evolution of High-Throughput Experimentation in Pharmaceutical Development and Perspectives on the Future. *Org. Process Res. Dev.* **2019**, *23* (6), 1213–1242. https://doi.org/10.1021/ACS.OPRD.9B00140/ASSET/IMAGES/LARGE/OP-2019-00140K_0023.JPEG.

(107) Cortés-Borda, D.; Wimmer, E.; Gouilleux, B.; Barré, E.; Oger, N.; Goulamaly, L.; Peault, L.; Charrier, B.; Truchet, C.; Giraudeau, P.; et al. An Autonomous Self-Optimizing Flow Reactor for the Synthesis of Natural Product Carpanone. *J. Org. Chem.* **2018**, *83* (23), 14286–14289. https://doi.org/10.1021/acs.joc.8b01821.

(108) Perera, D.; Tucker, J. W.; Brahmbhatt, S.; Helal, C. J.; Chong, A.; Farrell, W.; Richardson, P.; Sach, N. W. A Platform for Automated Nanomole-Scale Reaction Screening and Micromole-Scale Synthesis in Flow. *Science (80-.).* **2018**, *359* (6374), 429–434. https://doi.org/10.1126/science.aap9112.

(109) Sagmeister, P.; Lebl, R.; Castillo, I.; Rehrl, J.; Kruisz, J.; Sipek, M.; Horn, M.; Sacher, S.; Cantillo, D.; Williams, J. D.; et al. Advanced Real-Time Process Analytics for Multistep Synthesis in Continuous Flow**. *Angew. Chemie - Int. Ed.* **2021**, *60* (15), 8139–8148. https://doi.org/10.1002/anie.202016007.

(110) Breslow, R. Hydrophobic Effects on Simple Organic Reactions in Water. *Acc. Chem. Res.* **1991**, *24* (6), 159–164. https://doi.org/10.1021/AR00006A001/ASSET/AR00006A001.FP.PNG_V03.

(111) Dyson, P. J.; Jessop, P. G. Solvent Effects in Catalysis: Rational Improvements of Catalysts via Manipulation of Solvent Interactions. *Catal. Sci. Technol.* **2016**, *6* (10), 3302–3316. https://doi.org/10.1039/C5CY02197A.

(112) Diorazio, L. J.; Hose, D. R. J.; Adlington, N. K. Toward a More Holistic Framework for Solvent Selection. *Org. Process Res. Dev.* **2016**, *20* (4), 760–773. https://doi.org/10.1021/acs.oprd.6b00015.

(113) Alder, C. M.; Hayler, J. D.; Henderson, R. K.; Redman, A. M.; Shukla, L.; Shuster, L. E.; Sneddon, H. F. Updating and Further Expanding GSK’s Solvent Sustainability Guide †. *Green Chem.* **2016**, *18*, 3879. https://doi.org/10.1039/c6gc00611f.

(114) Bryan, M. C.; Dunn, P. J.; Entwistle, D.; Gallou, F.; Koenig, S. G.; Hayler, J. D.; Hickey, M. R.; Hughes, S.; Kopach, M. E.; Moine, G.; et al.

Key Green Chemistry Research Areas from a Pharmaceutical Manufacturers' Perspective Revisited. *Green Chem.* **2018**, *20* (22), 5082–5103. https://doi.org/10.1039/C8GC01276H.

(115) Srinivasadesikan, V.; Dai, J. K.; Lee, S. L. Quantum Mechanistic Insights on Aryl Propargyl Ether Claisen Rearrangement. *Org. Biomol. Chem.* **2014**, *12* (24), 4163–4171. https://doi.org/10.1039/C4OB00388H.

(116) Pincock, A. L.; Pincock, J. A.; Stefanova, R. Substituent Effects on the Rate Constants for the Photo-Claisen Rearrangement of Allyl Aryl Ethers. *J. Am. Chem. Soc.* **2002**, *124* (33), 9768–9778. https://doi.org/10.1021/JA011981Y/SUPPL_FILE/JA011981Y_S.PDF.

(117) Lin, Y. L.; Cheng, J. Y.; Chu, Y. H. Microwave-Accelerated Claisen Rearrangement in Bicyclic Imidazolium [b-3C-Im][NTf2] Ionic Liquid. *Tetrahedron* **2007**, *63* (45), 10949–10957. https://doi.org/10.1016/J.TET.2007.08.060.

(118) Debnath, S.; Mondal, S. A Computational (DFT) Study on Aza-Claisen Rearrangement: Effect of Temperature, Solvent and Substitution on Activation Barrier. *Comput. Theor. Chem.* **2014**, *1046*, 42–48. https://doi.org/10.1016/J.COMPTC.2014.07.010.

(119) Acevedo, O.; Armacost, K. Claisen Rearrangements: Insight into Solvent Effects and "on Water" Reactivity from QM/MM Simulations. *J. Am. Chem. Soc.* **2010**, *132* (6), 1966–1975. https://doi.org/10.1021/JA908680C/ASSET/IMAGES/LARGE/JA-2009-08680C_0005.JPEG.

(120) Claisen, L. Über Umlagerung von Phenol-Allyläthern in C-Allyl-Phenole. *Berichte der Dtsch. Chem. Gesellschaft* **1912**, *45* (3), 3157–3166. https://doi.org/10.1002/CBER.19120450348.

(121) Castro, A. M. M. Claisen Rearrangement over the Past Nine Decades. *Chem. Rev.* **2004**, *104* (6), 2939–3002. https://doi.org/10.1021/cr020703u.

(122) Goering, H. L.; Jacobson, R. R. A Kinetic Study of the Ortho-Claisen Rearrangement. *J. Am. Chem. Soc.* **1958**, *80* (13), 3277–3285. https://doi.org/10.1021/ja01546a024.

(123) White, W. N.; Fife, W. K. The Ortho-Claisen Rearrangement. IV. The Rearrangement of X-Cinnamyl p-Tolyl Ethers. *J. Am. Chem. Soc.* **1961**, *83* (18), 3846–3853. https://doi.org/10.1021/JA01479A026/ASSET/JA01479A026.FP.PNG_V03.

(124) White, W. N.; Slater, C. D. The Ortho-Claisen Rearrangement. V. The Products of Rearrangement of Allyl m-X-Phenyl Ethers. *J. Org. Chem.* **1961**, *26* (10), 3631–3638. https://doi.org/10.1021/JO01068A004/ASSET/JO01068A004.FP.PNG_V03.

(125) White, W. N.; Slater, C. D. The Ortho-Claisen Rearrangement. VI. The Rates of Rearrangement of Allyl m-X-Phenyl Ethers to 2-Allyl-5-X-Phenols. *J. Org. Chem.* **1962**, *27* (8), 2908–2914. https://doi.org/10.1021/JO01055A045/ASSET/JO01055A045.FP.PNG_V03.

(126) White, W. N.; Wolfarth, E. F. The Ortho-Claisen Rearrangement. VII. The Rearrangement of Allyl p-Tolyl-2,6-D2 Ether. *J. Org. Chem.* **1961**, *26* (9), 3509–3510. https://doi.org/10.1021/JO01067A603/ASSET/JO01067A603.FP.PNG_V03.

(127) Baumgartner, L. M.; Dennis, J. M.; White, N. A.; Buchwald, S. L.; Jensen, K. F. Use of a Droplet Platform to Optimize Pd-Catalyzed C-N Coupling Reactions Promoted by Organic Bases. *Org. Process Res. Dev.* **2019**, *23* (8), 1594–1601. https://doi.org/10.1021/acs.oprd.9b00236.

(128) Yau, H. M.; Croft, A. K.; Harper, J. B. "One-Pot" Hammett Plots: A General Method for the Rapid Acquisition of Relative Rate Data. *Chem. Commun.* **2012**, *48* (71), 8937–8939. https://doi.org/10.1039/c2cc34074g.

(129) Yau, H. M.; Haines, R. S.; Harper, J. B. A Robust, "One-Pot" Method for Acquiring Kinetic Data for Hammett Plots Used to Demonstrate Transmission of Substituent Effects in Reactions of Aromatic Ethyl Esters. *J. Chem. Educ.* **2015**, *92* (3), 538–542. https://doi.org/10.1021/ed400701m.

(130) Fiori, K. W.; Bois, J. Du. Catalytic Intermolecular Amination of C - H Bonds : Method Development and Mechanistic Insights. *J. Am. Chem. Soc.* **2007**, *129* (3), 562–568.

(131) Mack, J. B. C.; Bedell, T. A.; Deluca, R. J.; Hone, G. A. B.; Roizen, J. L.; Cox, C. T.; Sorensen, E. J.; Bois, J. Du. Rhodium-Catalyzed C − H Amination: A Case Study of Selectivity in C − H Functionalization Reactions. *J. Chem. Educ.* **2018**, *95*, 2243–2248.

https://doi.org/10.1021/acs.jchemed.7b00697.

(132) Mullins, R. J.; Vedernikov, A.; Viswanathan, R. Competition Experiments as a Means of Evaluating Linear Free Energy Relationships. An Experiment for the Advanced Undergraduate Organic Chemistry Lab. *J. Chem. Educ.* **2004**, *81* (9), 1357–1361. https://doi.org/10.1021/ed081p1357.

(133) Lu, J.; Paci, I.; Leitch, D. C. A Broadly Applicable Quantitative Relative Reactivity Model for Nucleophilic Aromatic Substitution (SNAr) Using Simple Descriptors. *Chem. Sci.* **2022**, *13* (43), 12681–12695. https://doi.org/10.1039/D2SC04041G.

(134) Ballard, M.; Bown, M.; James, S.; Yang, Q. NMR Studies of Mixed Amines. *Energy Procedia* **2011**, *4*, 291–298. https://doi.org/10.1016/J.EGYPRO.2011.01.054.

(135) Bartolo, N. D.; Woerpel, K. A. Mechanistic Insight into Additions of Allylic Grignard Reagents to Carbonyl Compounds. *J. Org. Chem.* **2018**, *83* (17), 10197–10206. https://doi.org/10.1021/ACS.JOC.8B01430/ASSET/IMAGES/MEDIUM/JO-2018-014306_0019.GIF.

(136) Holm, T. Use of Competition Kinetics with Fast Reactions of Grignard Reagents. *J. Org. Chem.* **2000**, *65* (4), 1188–1192. https://doi.org/10.1021/JO991777H/ASSET/IMAGES/LARGE/JO991777HF00001.JPEG.

(137) Williamson, A. XLV . Theory of Ætherification. *Philisophical Mag.* **1850**, *37* (251), 350–356. https://doi.org/10.1080/14786445008646627.

(138) Brown, H. C.; Okamoto, Y. Electrophilic Substituent Constants. *J. Am. Chem. Soc.* **1958**, *80* (18), 4979–4987. https://doi.org/10.1021/JA01551A055/ASSET/JA01551A055.FP.PNG_V03.

(139) McDaniel, D. H.; Brown, H. C. An Extended Table of Hammett Substituent Constants Based on the Ionization of Substituted Benzoic Acids. *J. Org. Chem.* **1958**, *23* (3), 420–427. https://doi.org/10.1021/JO01097A026/ASSET/JO01097A026.FP.PNG_V03.

(140) Bulk Modulus and Fluid Elasticities https://www.engineeringtoolbox.com/bulk-modulus-elasticity-d_585.html (accessed Feb 16, 2024).

(141) Liquids - Volumetric Expansion Coefficients https://www.engineeringtoolbox.com/cubical-expansion-coefficients-d_1262.html (accessed Feb 16, 2024).

(142) Lu, J.; Boughner, E. C.; Liotta, C. L.; Eckert, C. A. Nearcritical and Supercritical Ethanol as a Benign Solvent: Polarity and Hydrogen-Bonding. *Fluid Phase Equilib.* **2002**, *198* (1), 37–49. https://doi.org/10.1016/S0378-3812(01)00754-3.

(143) Bazaev, A. R.; Abdulagatov, I. M.; Bazaev, E. A.; Abdurashidova, A. PVT Measurements for Pure Ethanol in the Near-Critical and Supercritical Regions. *Int. J. Thermophys.* **2007**, *28* (1), 194–219. https://doi.org/10.1007/S10765-007-0158-2/METRICS.

(144) Hammett, L. P. The Effect of Structure upon the Reactions of Organic Compounds. Temperature and Solvent Influences. *J. Am. Chem. Soc.* **1937**, *59* (1), 96–103. https://doi.org/10.1063/1.1749914.

(145) Jaffé, H. A REEXAMINATION OF THE HAMMETT EQUATION. *Chem. Rev.* **1953**, *53* (2), 191–261.

(146) Hansch, C.; Leo, A.; Taft, R. W. A Survey of Hammett Substituent Constants and Resonance and Field Parameters. *Chem. Rev* **1991**, *91*, 165–195.

(147) Exner, O. Determination of the Isokinetic Temperature. *Nature* **1970**, *227* (5256), 366–367. https://doi.org/10.1038/227366a0.

(148) Papa, D.; Schwenk, E.; Whitman, B. Reductions with Nickel-Aluminum Alloy and Aqueous Alkali. *J. Org. Chem.* **1942**, *7* (6), 587–590. https://doi.org/10.1021/jo01200a017.

(149) Alder, C. M.; Gray, M.; Huff, C. A.; Manning, C. O.; Preston, A.; Rushworth, P.; Shuster, L. E.; Watson, R. J.; Wheelhouse, K. M. P.; Williams, G. D.; et al. Multigram Synthesis of Tetrasubstituted Dihydrobenzofuran GSK973 Enabled by High-Throughput Experimentation and a Claisen Rearrangement in Flow. *Cite This Org. Process Res. Dev* **2022**, *2022*, 379. https://doi.org/10.1021/acs.oprd.1c00422.

(150) Dielectric Constants of Common Solvents https://depts.washington.edu/eooptic/linkfiles/dielectric_chart%5B1%5D.pdf (accessed Oct 26,

2023).

(151) Spange, S.; Weiß, N.; Schmidt, C. H.; Schreiter, K. Reappraisal of Empirical Solvent Polarity Scales for Organic Solvents. *Chemistry–Methods* **2021**, *1* (1), 42–60. https://doi.org/10.1002/cmtd.202000039.

(152) Aycock, D. F. Solvent Applications of 2-Methyltetrahydrofuran in Organometallic and Biphasic Reactions. *Org. Process Res. Dev.* **2007**, *11* (1), 156–159. https://doi.org/10.1021/op060155c.

(153) Bégué, J. P.; Bonnet-Delpon, D.; Crousse, B. Fluorinated Alcohols: A New Medium for Selective and Clean Reaction. *Synlett* **2004**, No. 1, 18–29. https://doi.org/10.1055/s-2003-44973.

(154) Motiwala, H. F.; Armaly, A. M.; Cacioppo, J. G.; Coombs, T. C.; Koehn, K. R. K.; Norwood, V. M.; Aubé, J. HFIP in Organic Synthesis. *Chem. Rev.* **2022**, *122* (15), 12544–12747. https://doi.org/10.1021/acs.chemrev.1c00749.

(155) Serjeant, E. P.; Dempsey, B. *Ionisation Constants of Organic Acids in Aqueous Solution*, IUPAC Chem.; International Union of Pure and Applied Chemistry (IUPAC), 1979.

(156) RDKit https://www.rdkit.org/ (accessed Nov 6, 2023).

(157) Bunton, C. A.; Shiner, V. J. Isotope Effects in Deuterium Oxide Solution. Part II. Reaction Rates in Acid, Alkaline and Neutral Solution, Involving Only Secondary Solvent Effects. *J. Am. Chem. Soc.* **1961**, *83* (15), 3207–3214. https://doi.org/10.1021/ja01476a010.

(158) Kresge, A. J. Session II: Theory and Interpretation of Isotope Effects. (B) Isotope Effects in H 2 0-D 2 0 Mixtures. *Pure Appl. Chem.* **1964**, *8* (3–4), 521–524. https://doi.org/10.1351/pac196408030521.

(159) Soper, A. K.; Benmore, C. J. Quantum Differences between Heavy and Light Water. *Phys. Rev. Lett.* **2008**, *101* (6), 1–4. https://doi.org/10.1103/PhysRevLett.101.065502.

(160) Bragato, M.; Von Rudorff, G. F.; Von Lilienfeld, O. A. Data Enhanced Hammett-Equation: Reaction Barriers in Chemical Space. *Chem. Sci.* **2020**, *11* (43), 11859–11868. https://doi.org/10.1039/D0SC04235H.

(161) Franceschini, G.; Macchietto, S. Model-Based Design of Experiments for Parameter Precision: State of the Art. *Chem. Eng. Sci.* **2008**, *63* (19), 4846–4872. https://doi.org/10.1016/j.ces.2007.11.034.

(162) Schrecker, L.; Dickhaut, J.; Holtze, C.; Staehle, P.; Wieja, A.; Hellgardt, K.; Hii, K. K. An Efficient Multiparameter Method for the Collection of Chemical Reaction Data via 'One-Pot' Transient Flow. *React. Chem. Eng.* **2023**, *8* (12), 3196–3202. https://doi.org/10.1039/d3re00439b.

(163) Schrecker, L.; Hellgardt, K.; Hii, K. K. (Mimi); Dickhaut, J.; Holtze, C.; Wieja, A. GB2315116.0 SOLVENT SCREENING METHOD. *GB Pat.* **2023**, No. GB2315116.

(164) Tan, G.; Yang, Y.; Chu, C.; Zhu, H.; Roesky, H. W. Cu24O24Si8R8: Organic Soluble 56-Membered Copper(I) Siloxane Cage and Its Use in Homogeneous Catalysis. *J. Am. Chem. Soc.* **2010**, *132* (35), 12231–12233. https://doi.org/10.1021/ja1056104.

(165) Armstrong, A.; Jones, L. H.; Knight, J. D.; Kelsey, R. D. Oxaziridine-Mediated Amination of Primary Amines: Scope and Application to a One-Pot Pyrazole Synthesis. *Org. Lett.* **2005**, *7* (4), 713–716. https://doi.org/10.1021/ol0474507.

(166) Noda, H.; Motokura, K.; Miyaji, A.; Baba, T. Efficient Allylation of Nucleophiles Catalyzed by a Bifunctional Heterogeneous Palladium Complex-Tertiary Amine System. *Adv. Synth. Catal.* **2013**, *355* (5), 973–980. https://doi.org/10.1002/ADSC.201300063.

(167) Mao, Y.; Liu, Y.; Hu, Y.; Wang, L.; Zhang, S.; Wang, W. Pd-Catalyzed Debenzylation and Deallylation of Ethers and Esters with Sodium Hydride. *ACS Catal.* **2018**, *8* (4), 3016–3020. https://doi.org/10.1021/ACSCATAL.8B00185/ASSET/IMAGES/LARGE/CS-2018-00185F_0005.JPEG.

(168) Hemming, D. S.; Talbot, E. P.; Steel, P. G. A Mild Copper Catalyzed Method for the Selective Deprotection of Aryl Allyl Ethers. *Tetrahedron*

Lett. **2017**, *58* (1), 17–20. https://doi.org/10.1016/J.TETLET.2016.11.084.

(169) Schmidt, B.; Wolf, F. Synthesis of Phenylpropanoids via Matsuda-Heck Coupling of Arene Diazonium Salts. *J. Org. Chem.* **2017**, *82* (8), 4386–4395. https://doi.org/10.1021/ACS.JOC.7B00447/SUPPL_FILE/JO7B00447_SI_001.PDF.

(170) Bujok, R.; Bieniek, M.; Masnyk, M.; Michrowska, A.; Sarosiek, A.; Stępowska, H.; Arlt, D.; Grela, K. Ortho- and Para-Substituted Hoveyda-Grubbs Carbenes. An Improved Synthesis of Highly Efficient Metathesis Initiators. *J. Org. Chem.* **2004**, *69* (20), 6894–6896. https://doi.org/10.1021/JO049222W/SUPPL_FILE/JO049222WSI20040823_015531.PDF.

(171) Schlüter, J.; Blazejak, M.; Hintermann, L. Aluminum-Catalyzed Hydroalkoxylation at Elevated Temperatures: Fast and Simple Access to Coumarans and Other Oxygen Heterocycles. *ChemCatChem* **2013**, *5* (11), 3309–3315. https://doi.org/10.1002/CCTC.201300182.

(172) Hutt, J. T.; Wolfe, J. P. Synthesis of 2,3-Dihydrobenzofurans via the Palladium Catalyzed Carboalkoxylation of 2-Allylphenols. *Org. Chem. Front.* **2016**, *3* (10), 1314–1318. https://doi.org/10.1039/C6QO00215C.

(173) Oh, Y.; Jang, Y. J.; Jeon, M.; Kim, H. S.; Kwak, J. H.; Chung, K. H.; Pyo, S.; Jung, Y. H.; Kim, I. S. Total Synthesis and Anti-Inflammatory Evaluation of Penchinone A and Its Structural Analogues. *J. Org. Chem.* **2017**, *82* (21), 11566–11572. https://doi.org/10.1021/ACS.JOC.7B02212/SUPPL_FILE/JO7B02212_SI_001.PDF.